

Calcination behavior of lumpy limestones from different origins

Dissertation

zur Erlangung des akademischen Grades

Doktoringenieur

(Dr.-Ing)

vorgelegt von

M.Tech. Purna Chandra Gourisankar Sandaka

geb. am 15.06.1981

in Ichapurm, Andhra Pradesh, India

genehmigt durch die

Der Fakultät für Verfahrens- und Systemtechnik
der Otto-von-Guericke-Universität Magdeburg

Gutachter:

Prof. Dr.-Ing. Eckehard Specht
Institute of Fluid Dynamics and Thermodynamics,
Universität Magdeburg, Germany.

Prof. rer. nat. Albrecht Wolter
Institute für Nichtmetallische Werkstoffe,
Technische Universität Clausthal.

Dr. Thomas Schwertmann
Process Engineering,
Rheinkalk GmbH.

Preface

This dissertation is submitted to Otto von Guericke University, Magdeburg for the degree of Doctor of Philosophy. The research described herein was conducted under the supervision of **Prof. Eckehard Specht** between July 2009 and October 2015. To the best of my knowledge, this work is original, except where suitable references are made to previous works. Neither this, nor any substantially similar dissertation has been submitted for degree, diploma or qualification at any other university or institution.

Gourisankar Sandaka
Magdeburg, 03.11.2015

Acknowledgement

I would like to show my gratitude for those, who so generously contributed to the work presented in this thesis.

Special mention goes to my enthusiastic supervisor **Prof. Dr.- Ing. E. Specht** for providing me the opportunity to work with him and pursue a doctoral degree. He has been supportive since the days I began working on Lime calcination; Prof. Specht continuously encouraged me to finish this work successfully. His strong motivation and trust enriched my confidence levels helped me to complete my PhD. His friendly way of handling the research students has broken the communication barriers.

Dr.-Ing H. Woche provided his valuable guidance during the gravimetric experiments. I would like to thank **Dr.-Ing. Janan Al-Karawi**, especially for his valuable support along with all the lab technicians who continuously supported me for the experimental part of the work. I would love to thank our secretary **Frau Hasemann** for her continuous support for the administration part of the work. I would like to personally thank all my colleagues for their encouragement and understanding.

I feel immense pleasure in saluting the Otto von Guericke University, Magdeburg for giving me a great opportunity to pursue the research study in Germany. I would like to acknowledge the financial support provided by the Graduiertenkolleg (GKMM) through the German Research Foundation (DFG).

Dr. -Ing. Ashok is a great mentor and a best friend of mine. His unconditional support has been essential all these years, through which my motivation towards the research has been enhanced. His continuous support for both personal and professional life during the tenure of my work is invaluable. I would have missed a lot if I didn't meet him. Priya always encouraged me to complete the dissertation. I got lot of inspiration from her. One word thank you is not sufficient to my dearest friend **Dr. -Ing. Thirumalesha**, who motivated me to pursue research in Germany and with whom I always share best moments of my life. **Dr. -Ing. Koti** who is always with me from the day we first met, who stands as an example of a friend and I learned a lot from him. I would say, one of the best persons I have ever seen.

Finally, I would like to express my sincere thanks to every individual German citizen for contributing either directly or indirectly. During my stay in Germany, I learned self-discipline, punctuality and time management from the fellow citizens of Germany. Similarly, I would like to thank my home country and Indian Institute of Technology Madras. Further, I extend my sincere thanks to my dearest (colleague) friends Nadine, Haido, Tino, Pavan, Aina, Nyein Nyein and Gourav. I had wonderful time with Nadine and Tino in office for the whole tenure. We shared best time with Bassem, Sabariman and Aina during experimental time. I cannot stay without thanking Bassem for his friendly nature and supportive behavior during experiments. I also personally thank all my Indian friends Sukumar, Santosh, Krishna, Niranjana, Narasimha Madhav, Mitra, Deepthi, Sai, Latha, Maya and especially the duo “Ramya & Prithvi” in Magdeburg.

I have an amazing family, unique in many ways, and their support has been unconditional all these years. Especially, I thank my parents, who are the reason for my existence and establishment. I would like to thank my brother **Ravi**, Sisters **Syamili and Sravani** for their continuous encouragement and support. I specially thank my Uncle and Aunt whose wish to see me as a Doctor Engineer. The best gift so far I have received in my **life** is my **wife Harita** and I would be grateful to her for exceptional love and immense support. She supported her best for completing the thesis. Her efforts are incredible and I absolutely find no words to express my feelings towards her.

Abstract

It is known that limestone from different origins decomposed at same kiln conditions produce totally different quality of product (hard burnt or soft burnt). It infers that the process parameters required (to adjust) for the production of desired quality of lime cannot be prejudged. The main focus of current research work is to understand the calcination behavior by determining the material properties from limestone of different origins based on thermogravimetric experiments and mathematical models. Limestone decomposition experiments from different origins have been conducted at temperatures ranging from 850 to 1200°C. The particles are decomposed in air or pure CO₂ gas. Cylindrical particles of size range from 14 mm to 33 mm have been used for the decomposition.

A quasi-stationary model has been developed to predict the front temperature and also the conversion profiles numerically. By using the experimental data and the model predications, the material properties and calcination parameters have been estimated.

In addition to the quasi-stationary model, transient model has also been developed for the particle undergoing decomposition. Fully explicit forward in time and central in space (FTCS) finite difference scheme is used to discretize the governing heat transfer equation with variable source term (represents the reaction enthalpy). MATLAB code has been used to solve one dimensional finite difference discretized form of the governing equation with variable source term and temperature dependent properties. Using this model, pre heating of the lime particle (core temperature, before the particle attains the calcination temperature) as well as the post heating (core reaching the ambient temperature, after the complete conversion) can be predicted.

Gas diffusion from the reaction front to the surface of the particle is assumed as a stationary process for both the quasi-stationary and transient models. Stefan flow model is applied for the flow of CO₂ gas in the lime pores when the experiment is conducted in the air environment and Darcy flow model is applied for the pore diffusion when the experiment is conducted in pure CO₂ environment. In the latter case by using the Darcy

flow model, high pressure gradients responsible for the bulk flow of gas through the pores to the ambient can be well predicted.

In addition to the above mentioned models, a special method has been developed to determine the lime thermal conductivity. By using the measured core temperature, slope of the measured conversion profile and by solving the quasi-stationary fourth order radiation heat equation along with the Fourier heat conduction equation, the thermal conductivity variation with conversion degree has been determined. In this case, it is not necessary to consider the mass transport.

The limestone decomposition process is influenced by many parameters. The thermal properties include density, specific heat capacity, thermal conductivity of lime and limestone. In addition, several other properties enthalpy of reaction, emissivity of furnace wall and lime particle, porosity and pore size of lime, equilibrium decomposition temperature are also to be known. Influence of most important parameters on the decomposition (of a single particle) has been inspected. Sensitivity of the calcination parameters and material properties on the decomposition in a normal industrial shaft kiln has also been investigated. In addition to the limestone decomposition, favorable conditions for the recarbonation reaction and also the influence of number of cycles on recarbonation of lime have also been studied.

Thermal conductivity of lime from different origins is in the range from 0.3 to 0.85 $\text{Wm}^{-1}\text{K}^{-1}$. Decomposition is up to 30% sensitive to thermal conductivity for the particles of size range 20 mm and up to 80% sensitive to larger particles (100 mm diameter). Reaction coefficient influences significantly the decomposition temperature rather the calcination time. Diffusion coefficient plays significant role for the lime decomposition at lower kiln gas temperatures.

Zusammenfassung

Es ist bekannt, dass Kalkstein von verschiedener Herkunft, der bei gleichen Bedingungen des Ofens zersetzt wird, Produkte völlig unterschiedlicher Qualität liefert (Hartbrand oder Weichbrand). Daraus lässt sich ableiten, dass die erforderlichen Prozessparameter, um eine gewünschte Qualität zu erreichen, nicht voraus gesagt werden können. Der Fokus der aktuellen Forschungsarbeit liegt darin, das Verhalten der Kalzinierung zu verstehen, indem die Stoffeigenschaften von Kalkstein verschiedener Herkunft mit Hilfe von thermogravimetrischen Experimenten und mathematischen Modellen ermittelt werden. Experimente zur Zersetzung von Kalkstein verschiedener Herkunft wurden bei Temperaturen von 850 bis 1200°C durchgeführt. Die Partikel wurden in Luft oder reinem CO₂-Gas zersetzt. Zylindrische Partikel mit einer Größenverteilung von 14 bis 33 mm wurden für die Zersetzung verwendet.

Ein quasi-stationäres Modell wurde entwickelt um den Verlauf der Temperatur der Reaktionsfront und der Umwandlung numerisch vorausszusagen. Unter Verwendung der experimentellen Daten und der Modellvoraussagen wurden die Stoffeigenschaften und die Kalzinationsparameter ermittelt.

Zusätzlich wurde ein instationäres mathematisches Modell für den Zersetzungsverlauf entwickelt. Das FTCS-Verfahren (Forward-Time Central-Space) mit der Finite-Differenzen-Methode wird verwendet, um Fouriersche Differentialgleichung mit dem variablen Quellterm zu diskretisieren (bildet die Reaktionsenthalpie ab). Ein MATLAB-Code wurde verwendet, um die eindimensionale Differentialgleichung in diskretisierter Form mit variablen Quelltermen und temperaturabhängigen Stoffwerten zu lösen. Unter Verwendung dieses Modells kann das Aufheizen (Kerntemperatur, bevor Partikel Kalzinierungstemperatur erreichen) und das Nachheizen (wenn der Kern nach der Kalzinierung wieder die Umgebungstemperatur erreicht) von Kalkpartikeln vorausgesagt werden.

Die Gas-Diffusion von der reagierenden Oberfläche des Partikels wird für beide Modelle, das quasi-stationäre und das Übergangsmodell, als ein stationärer Prozess vorausgesetzt. Das Modell des Stefan-Stroms wird für die Diffusion des CO₂-Gases in den Kalkporen

verwendet, wenn die Zersetzung bei Umgebungsluftbedingungen durchgeführt wurde. Im Fall der Zersetzung in reinem CO₂-Gas wurde das Modell von Darcy angenommen.

Im diesem Fall, sind hohe Druckgradienten verantwortlich für den Massenstrom des Gases durch die Poren in die Umgebung und können gut vorausgesagt werden.

Zusätzlich wurde eine spezielle Methode entwickelt, um die Wärmeleitfähigkeit von Kalk zu bestimmen. Unter Verwendung der gemessenen Kerntemperatur, dem Gradienten des gemessenen Umsetzungsprofils und durch Lösen der Wärmestrahlungsgleichung und der Fourier-Wärmeleitungsgleichung, wurde die Veränderung der Wärmeleitfähigkeit mit dem Umsetzungsgrad bestimmt.

Die Kalksteinzersetzung wird durch viele Parameter beeinflusst. Die thermischen Eigenschaften beinhalten Dichte, spezifische Wärmekapazität und Wärmeleitfähigkeit von Kalk und Kalkstein. Außerdem müssen auch weitere Eigenschaften, wie Reaktionsenthalpie, Emissionsgrad der Ofenwand und des Kalkpartikels, Porosität und Porengröße des Kalks und Zersetzungstemperatur im Gleichgewicht bekannt sein. Die wichtigsten Einflussparameter auf die Zersetzung (eines einzelnen Partikels) wurden untersucht. Die Empfindlichkeit der Kalzinationsparameter und Materialeigenschaften auf die Zersetzung in einem Kalkschachtofen wurde ebenfalls untersucht. Zusätzlich zu der Kalksteinzersetzung, wurden auch die günstigsten Bedingungen für die Recarbonisierungsreaktion und auch der Einfluss der Anzahl der Zyklen auf die Recarbonisierung des Kalks studiert.

Die Wärmeleitfähigkeit von Kalk verschiedener Herkunft liegt im Bereich von 0,3 bis 0,85 Wm⁻¹K⁻¹. Die Zersetzung wird bis zu 30% von der Wärmeleitfähigkeit für Partikel mit einer Größe von 20 mm und bis zu 80% für größere Partikel (100 mm Durchmesser) beeinflusst. Der Reaktionskoeffizient beeinflusst die Zersetzungstemperatur signifikant weniger als die Kalzinierungszeit. Der Diffusionskoeffizient spielt eine wesentliche Rolle bei der Kalkzersetzung bei geringeren Ofengastemperaturen.

Nomenclatures

A	area	$[m^2]$
c_p	specific heat capacity	$[kJ/kg/K]$
d	particle diameter	$[m]$
D_P	pore diffusion coefficient	$[m^2/s]$
h	height of cylinder	$[m]$
Δh_{CO_2}	reaction enthalpy regarding to CO_2	$[kJ/kg]$
$\Delta \tilde{H}_R, \Delta H$	molar reaction enthalpy	$[kJ/mol]$
\bar{J}	net mass flux	$[kg/m^2/s]$
k	reaction coefficient	$[m/s]$
K_{CO_2}	density of CO_2 in limestone	$[kg/m^3]$
L	length	$[m]$
\dot{m}	mass flux	$[kg/m^2/s]$
\dot{m}_v	mass rate of CO_2 per unit volume	$[kg/s/m^3]$
\dot{M}	mass flow rate	$[kg/s]$
P	Total pressure,	$[Pa]$
p	partial pressure of CO_2 gas	$[Pa]$
\dot{q}	heat flux	$[W/m^2]$
\dot{Q}	heat flow rate	$[W]$
r	radius	$[m]$
Δr	element size	$[m]$
\tilde{R}	the universal molar gas constant	$[J/mol/K]$
R_{CO_2}	gas constant for CO_2	$[J/kg/K]$
R_D	diffusion resistance	$[1/s]$
R_k	chemical reaction resistance	$[1/s]$
R_α	resistance to heat transfer	$[1/s]$
R_β	mass transfer resistance	$[1/s]$
R_λ	resistance to thermal conductivity	$[1/s]$
t	time	$[s]$
T	temperature	$[^\circ C]$ or $[K]$
Δt	time step	$[s]$
V	volume	$[m^3]$

w	velocity	[m/s]
X	conversion degree	[-]
y_{CO_2}	mass fraction of CO ₂ in limestone	[kg/kg]

Greek symbols

α	heat transfer coefficient	[W/m ² /K]
β	mass transfer coefficient	[m/s]
ε	emissivity	[-]
κ	permeability	[m ²]
λ	thermal conductivity coefficient	[W/m/K]
μ	dynamic viscosity	[Pa s]
ρ	density	[kg/m ³]
σ	Stefan-Boltzmann constant	[W/m ² /K ⁴]
τ	tortuosity	[-]
ν	kinematic viscosity	[m ² /s]
ψ	void fraction	[-]
Ω_ϕ	sensitivity for the parameter ϕ	[-]

Subscripts

A	area
amb	ambient
conv	convection
D	diffusion
eff	effective
eq	equilibrium
F	furnace
f	front
g	gas
mix	mixture
s	surface

Dimensionless number

Nu	Nusselt number
Pr	Prandtl number
Re	Reynolds number
Sc	Schmidt number
Sh	Sherwood number

Contents

Preface	ii
Acknowledgement	iii
Abstract	v
Zusammenfassung	vii
1 Introduction	1
1.1 Overview and Motivation	1
1.2 Applications of limestone	3
1.2.1 Ground calcium carbonate (GCC)	3
1.2.2 Fine/ultrafine ground	4
1.2.3 Crushed stone.....	5
1.2.4 Large or Massive stone	6
1.3 Applications of Lime.....	6
1.4 Characterization of limestone and lime	8
1.4.1 Limestone	8
1.4.2 Lime Production	10
1.4.3 Lime quality.....	10
2 Literature Review	17
2.1 Introduction	17
2.2 Rate limiting resistances	17
2.3 Various models and experimental study of lime decomposition.....	18
2.4 Specific heat capacities of Limestone and Lime	22
2.5 Reaction enthalpy.....	24
2.6 Equilibrium pressure	25
2.7 Reaction rate coefficient	28
2.8 Thermal conductivity of limestone and lime	30
2.9 Lime Density with burning time	32
2.10 Porosity	34
2.11 Emissivity	35
2.12 Tortuosity.....	36
2.13 Permeability	37
2.14 Conclusions and Summary.....	37

3	Thermo gravimetric experiments	39
3.1	Experimental Method.....	39
3.2	Experimental Measurements	41
3.2.1	Temperature and conversion profiles	41
3.2.2	Experiments at different ambient temperatures	42
3.2.3	Experimental profiles reproducibility	43
3.2.4	Experiments with samples from different origins.....	45
3.2.5	Experiments with samples of different size	46
4	Decomposition Models and Experimental comparisons	49
4.1	Limestone quasi stationary decomposition model	49
4.2	Radiative heat transfer	53
4.2.1	Effective emissivity	53
4.2.2	Estimating the furnace wall emissivity	53
4.3	Convective heat and mass transfer coefficient	59
4.4	Stationary Diffusion and convective diffusion inside the lime layer	61
4.5	Measurement of pore size	63
4.6	Determination of thermal conductivity	64
4.7	Simulations with quasi-stationary model	66
4.8	Start time and conversion begin time	67
4.9	Simulations with quasi stationary model	67
4.9.1	Sample D	67
4.9.2	Sample 1mu1	70
4.10	Transient Model for lime decomposition process	73
4.10.1	One dimensional approach	73
4.10.2	Heat conduction equation.....	74
4.11	Simulations with transient model.....	77
4.11.1	Sample D.....	77
4.11.2	Sample 1mu1	80
4.12	Comparison between the models with measured profiles	81
4.13	Effect of Gas Temperature on the calcination.....	83
4.13.1	Gas Temperature	83
4.13.2	Furnace Temperature.....	83
4.13.3	Effect of Gas Temperature	84
4.14	Determination of decomposition temperature	86

5	Influence of the parameters on calcination.....	87
5.1	Introduction.....	87
5.2	Influence of thermal conductivity	88
5.3	Influence of reaction coefficient	89
5.4	Influence of tortuosity	91
5.5	Influence of mass transfer coefficient	92
5.6	Equilibrium Temperature	93
5.7	Enthalpy of reaction	94
5.8	Conclusions.....	94
6	Sensitivity of parameters in industrial shaft kilns	97
6.1	Introduction.....	97
6.2	Determination of heat and mass transfer coefficients for the kiln.....	98
6.3	Gas properties	100
6.4	System of equations	103
6.5	Definition of Sensitivity.....	105
6.6	Sensitivity of various parameters	106
6.6.1	Heat transfer coefficient.....	106
6.6.2	Thermal conductivity.....	107
6.6.3	Reaction coefficient	109
6.6.4	Diffusion coefficient.....	110
6.7	Mass transfer coefficient	111
6.8	Analysis and discussion	111
7	Lime decomposition in CO₂ atmosphere	113
7.1	Introduction.....	113
7.2	Determination of properties	114
7.2.1	Sample T.....	114
7.2.2	Sample F2-IV.....	116
7.3	Summary.....	117

8	Recarbonation of lime	119
8.1	Introduction.....	119
8.2	Historical background and Literature review.....	119
8.3	Experimental setup.....	122
8.3.1	Reaction with lime particles	123
8.3.2	Reaction with Lime milk	124
8.4	Carbonation at higher temperatures	125
8.5	Influence of Temperature.....	126
8.5.1	Influence of particle size.....	128
8.5.2	Influence of number of cycles	129
8.6	Summary.....	130
9	Material properties	131
9.1	Introduction.....	131
9.2	Experiments at different temperatures	131
9.2.1	Sample 1mu1 decomposed at (950°C).....	131
9.2.2	Sample 1mu1 at 1050 °C.....	133
9.3	Experiments with different particle sizes	134
9.4	Simulations and comparisons for the sample KN1	136
9.4.1	Sample KN1 with 14.4 mm (Small particle)	136
9.4.2	Sample KN1 with 24.5 mm (Medium particle)	137
9.4.3	Sample KN1 with 32.2 mm (Big particle).....	138
9.5	Material properties and parameters for various Limestone.....	139
	Appendix.....	153
	List of Publications	183
	List of Master Thesis Supervised	184
	Curriculum Vitae	185

Chapter 1

Introduction

1.1 Overview and Motivation

Lime is an important raw material in various industries. Lime is generally produced in shaft kilns or rotary kilns. Lime is used in different forms in wide range of Industries for various purposes. These applications are described in detail in the next section.

The principal users of lime are:

- steel (lowering slag melting temperature) ~ 35 %
- environment (desulfurization, water cleaning) ~ 20 %
- building ~ 10 %
- chemistry ~ 8 %
- roads ~ 10 %
- paper/pcc ~ 7 %
- nonferrous metals ~ 3 %
- agriculture (soil conditioner) ~ 3 %
- sugar ~ 4 % .

Quality of the product Lime is the major aspect of the process. Soft burnt lime (lime produced under controlled conditions, such as at relatively lower temperatures) is generally highly reactive and has significant usage in certain industries such as steel industry. Whereas hard burnt lime (lime produced at high temperatures) is less reactive in nature and has its applications in some other branches of industry such as building industry. This is because the calcination process at higher temperatures causes sintering of the product (lime), which in turn reduces the internal surface area available for the reaction. So it is essential to understand the temperature distributions in the lime kiln in

order to assure the better quality of the lime. Burning lime or decomposition of limestone is an endothermic process, in which the kinetics of the burning process strongly depends on temperatures. In principle, to regulate or to optimize the lime burning process, the temperature and the concentration (conversion) profiles in the kilns must be determined. However, with burning lime in shaft kilns, practical determinations of these parameters are very difficult. For example, the measurements of the kiln temperatures by using thermocouples have to undergo two major problems. Firstly, due to high temperature in the firing zone, common thermocouples (e.g., Ni-Cr/Ni) are often damaged; therefore, highly expensive thermocouples (e.g., Pt-Rh/Pt) are required. Secondly, due to the movements of solid bed with dust creation, thermocouples can also be damaged during measurements. So it is very difficult or almost impossible to insert thermo elements inside such kilns. In this case, simulations got significant place in this process to model the temperature and the lime burning profiles. In addition to that, same lime kiln with the same operating conditions can produce totally different qualities of lime when Limestone from different origins is used as raw material. This scenario notifies that the calcination process significantly depends on the origin of limestone, in other words it can be said that it depends on material properties of limestone in a particular quarry. Calcination is a complex process as it involves five sub processes namely heat transfer from the ambient to the surface of the solid, conduction heat transfer inside the oxide region, chemical reaction at the reaction front, diffusion of the CO₂ inside the porous oxide region and mass transfer of CO₂ from the surface to the ambient. Lime Calcination is a high temperature endothermic decomposition reaction. Heat of reaction depends on the origin of the limestone as specific heat capacity of the stone depends on the origin. The typical range of heat of reaction can vary in the range of 158-172 kJ/mol [1].

It is very essential to understand and to analyze the behavior of the lime at the micro scale (single lime particle level) in order to achieve a good level of understanding about the industrial scale (macro level) calcination process. A thorough knowledge of the calcination at a single particle level can provide a great insight which there by handy to analyze a real time calcination process in industrial kilns. Temperature profiles within the particle during calcination provide information that how high the core temperature of particle is raised during decomposition reaction. This could in turn describe the quality of the product lime whether it is hard burned or soft burned.

This study mainly focuses on modeling of the single lime particle to investigate the temperature profiles inside the particle during calcination and also to study the decomposition behavior with the help of the laboratory scale thermogravimetric single particle decomposition experiments. Current work also concentrates on discovering the material properties of the limestone of different origins as well as other important parameters such as reaction coefficient and also the tortuosity of lime. By knowing the material properties of lime and also the influence of other important process parameters which govern the decomposition process, it is possible to provide necessary guidelines to lime industry for their calcination process regarding the process parameters to be used to achieve necessary quality of lime (product). Experiments have also been conducted with different size particles to cross verify the material properties and other parameters. Few limestone samples are also decomposed in the CO₂ gas environment. Material properties predicted in these cases are compared with experiments conducted in normal conditions.

1.2 Applications of limestone

Limestone products can be further classified into following types based on the crystal type, the way of formation and also on the composition basis.

1.2.1 Ground calcium carbonate (GCC)

GCC generally refers to calcium carbonate with calcite crystal structure. It's mostly of the pure form. GCC formations are formed by very slow natural precipitations. Applications of GCC are as follows [2],[3]

- A.) **Agriculture:** It's used to stabilize the acidity of the soil by increasing the pH of soil. GCC improves the crop yields and minimizes use of fertilizer. It is used mostly in cultivating mushroom forms.
- B.) **Feed:** High purity limestone with low levels of acid insoluble components is used as calcium supplement in poultry, pigs and cattle. Limestone intake helps strengthen the shells and results in proper egg formation.
- C.) **Filler:** Used as solid aggregate filler in Asphalt Filler and also as filler for strengthening the latex backing of rugs and carpets.
- D.) **Ceramics:** In low fired bodies, Limestone is used in very small quantities as a filler to reduce fired shrinkage. It is also used as flux in ceramic glazes.

- E.) **Mining:** Powdered limestone is used as a dust suppressant in coal mines and helps provide passive fire protection and prevent explosions underground.
- F.) **Pre cast concrete and Synthetic Floor tiles:** It improves the concrete density, surface finish and physical properties. Limestone powder typically used in plasticized PVC and plastisols.
- G.) **Water treatment:** It is used to adjust the pH of the acid waters in lakes and reservoirs.

1.2.2 Fine/ultrafine ground

- A.) **Adhesives & Sealants:** Limestone (GCC) is used as a filler and viscosity control additive in sealants, joint fillers, grouts and ceramic tile adhesives (CTA's). Sometimes GCC can constitute up to 80% of the formulation.
- B.) **Food:** GCC is used as an inexpensive dietary calcium supplement and antacid. Food grade Calcium carbonate (E170) is added to all brown and white flour products in the UK.
- C.) **Household Products:** Polishing and cleaning products often use limestone as a mild abrasive or inert binder. Finely ground limestone will not scratch glass, ceramics or steel surfaces.
- D.) **Paper:** Fine grades of GCC are used extensively in paper manufacturing. Consistent particle sizing and color are essential. As an alkali material it reduces acidity of paper, improving the durability of printed material.
- E.) **Paints:** GCC is used as functional filler and pigment extender in a variety of coatings including decorative paints, industrial coatings, road-marking paints, protective coatings, textured finishes, plasters and wood finishes.
- F.) **Pharmaceuticals:** Calcium carbonate is used as inert filler in tablets and as base carrier for veterinary products.
- G.) **Plastics:** GCC is widely used as functional filler in plastic products, comprising up to 25% of the volume, adding density, improving rheology and reducing cost. GCC is often blended or "coated" with additives such as stearates to aid bonding within the plastic.

H.) **Rubber:** GCC is useful as an extender and in controlling the flow properties of products which are to be molded or extruded.

1.2.3 Crushed stone

Aggregates

A.) **Concrete:** Concrete is a composite construction material, composed of cement, aggregate (generally a coarse aggregate made from crushed rocks such as limestone, or granite, plus a fine aggregate such as sand), water and chemical admixtures.

Landscaping: Decorative limestone aggregates, chippings and grits are used as roof chippings, in landscaping projects such as cycling ways and footpaths, driveways and car parks as well as for ground cover in gardens and rockeries. It is also used as fill or base in the construction of the roads

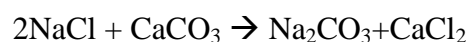
Chemical stone

A.) **Flue Gas Desulphurisation:** Limestone is used to neutralize and remove acids (sulphur dioxide) present in the flue gases of power generating facilities, and is used in flue gas desulphurisation (FGD) at coal fired power plants and municipal waste-to-energy plants.

B.) **Glass Manufacture:** Most commercial glasses consist essentially of silica together with soda (Na_2O) and lime (CaO), the lime being partly replaced by magnesia (MgO) depending on the application. Lime is introduced into the glass melt as limestone (CaCO_3) and magnesia by adding dolomite [$\text{CaMg}(\text{CO}_3)_2$].

C.) **Iron Smelting:** In iron and steel manufacture limestone is used to remove impurities (usually in the form of silica or sand) from the molten iron in the blast furnace to form a substance known as slag which is easily removed.

D.) **Soda Industry:** Solvay Ammonia process or Ammonia-soda process is one of the major Industrial processes where brine solution is treated with limestone to make soda ash.

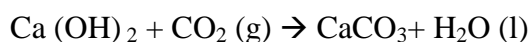


1.2.4 Large or Massive stone

- A.) **Building and Walling Stone:** Limestone is still used as walling stone in house builds and municipal buildings. Random screened limestone is still used for traditional dry stone walling.
- B.) **Monumental Stone:** Limestone blocks and polished panels are decorative and tasteful choice for architects and builders. The highest grade is monumental stone. This is a very uniform limestone with few surface imperfections. These properties make it ideal for carving and limestone of this class can hold very fine detail when used in sculpture, headstones, plaques, or ornamental features.
- C.) **Paving Stones:** Limestone paving is popular because of its very hard wearing properties, and its lightly textured surface making it is perfect for applications where a flat surface is essential.

1.3 Applications of Lime

- A.) **Steel Industry:** The most modern and important application of lime is its ability to form solutions with silicates. Nearly 40% of the lime produced worldwide is used in Steel and Iron Industry. It is used as a flux to remove Phosphorous, silicon and Sulphur impurities. Generally ores of Iron are rocks contain mainly oxides and silicates. Lime is mixed with ore and the mixture is melted, lime reacts with silicates and forms slag. This slag is immiscible with molten Iron and it is drained and separated. Approximately it needs 80 kg of Lime for a metric ton of Iron. Lime also used in the production of other metals. It is used to remove silicates from Alumina before it gets reduced to Aluminum metal.
- B.) **Metal extraction Industry:** Lime is also used in the recovery of several other metals such as gold, silver, copper, mercury, zinc and nickel.
- C.) **Construction Industry:** One of the oldest applications of lime is its ability to react with CO_2 to form Carbonate. Lime is mixed with sand and water and the mixture is called mortar. It is used to bind bricks, blocks and stones together. At room temperature re-carbonization is very slow in nature. Slacked lime ($\text{Ca}(\text{OH})_2$) is relatively faster to react with lime to give limestone and water. However this reaction even takes several years for the completion.

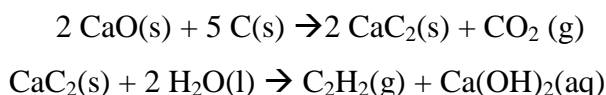


Lime plaster and Portland cement are also lime based products used in the construction Industry.

D.) **Paper and pulp Industry:** Because Lime is highly alkaline; it dissolves the lignin in wood that binds the fibers together. Precipitated calcium carbonate (PCC) is often used as filler and for coating in the paper manufacturing process.

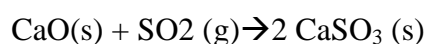
E.) **Sugar Industry:** In the sugar refining process, lime makes coagulation with plant material and allowing it to be more easily separated from the sugar syrup.

F.) **Chemical Industry:** It is important material in the manufacture of chemicals. Lime is heated together with coke to form calcium carbide which in turn reacts with water to form Acetylene. Acetylene is one of the important fuels for welding and also it is starting material for making several other organic compounds.

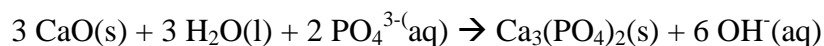


G.) **Pollution control:**

Lime is used in the stack gas scrubbers to remove SO₂ emissions from the effluents. Lime reacts with sulfur dioxide to form solid calcium sulfite.



Lime is added to sewage to remove phosphates



H.) **Water treatment:** Lime is used in the pretreatment of water to soften, to decrease the acidity and to clear drinking water.

I.) **Tannery:** Lime is used to remove hair and plump the hides in the leather tanning process.

1.4 Characterization of limestone and lime

1.4.1 Limestone

The main component of limestone is calcium carbonate (CaCO_3), which is formed by the compaction of the remains of coral animals and plants on the bottoms of oceans. It can be a soft white substance (chalk) through to a very hard substance (marble). Most commercial limestone deposits are a brownish rock. The chemical composition and bulk density of typical limestone are shown in the literature for the limestone types they have used in their research [4]

Chemical composition (%)	Cretaceous limestone		Jurassic limestone		Devonian limestone			Marble
	Langelsheim	Lägerdorf	Blaustein	Regensbug	Winterberg	Stromberg	Diez	Cercos
CaO	52.47	54.24	55.70	55.11	54.29	55.41	55.51	55.34
MgO	0.30	0.260	0.190	0.400	0.39	0.43	0.400	0.59
SiO ₂	4.68	1.860	0.240	0.340	1.83	0.26	0.100	0.08
Fe ₂ O ₃	0.24	0.080	0.032	0.090	0.21	0.06	0.010	0.05
Al ₂ O ₃	0.63	0.27	0.043	0.12	0.08	0.13	0.013	0.01
K ₂ O	0.08	0.046	0.007	0.017	0.02	-	0.005	0.004
Na ₂ O	0.03	0.041	0.013	0.018	0.01	-	0.013	0.01
BaO	0.01	0.01	0.012	0.011	0.02	-	0.008	0.01
SrO	0.03	0.036	0.004	0.005	0.02	-	0.009	0.01
Mn _x O _y	0.03	0.016	0.013	0.024	0.02	0.02	0.011	0.004
SO ₃	0.05	0.055	-	0.043	0	-	-	-
Weight loss (CO ₂)	41.50	42.81	43.51	43.62	43.05	43.78	43.54	43.97
Density (g cm ⁻³)	2.51	2.57	2.61	2.68	2.68	2.69	2.70	2.71

Molar mass: CaCO_3 100g/mol; CaO 56g/mol; MgO 40.3g/mol; CO₂ 44g/mol.

Table 1.1: Chemical composition and bulk density of typical limestone

The chemical composition analysis has been carried out for some of the limestone types used in the current research and the results are tabulated in the below table 1.4-2. The RFA analysis has been carried out with the help of Dr. Thomas Schwertmann, Lhoist Western Europe, Rheinkalk GmbH, Germany. The calcium carbonate content is in the range from 91% for the limestone 1mu1 and 99% for the stone B. The bulk density ranges from 2.1 g/cc for F2-iv to 2.75 g/cc for limestone B and BL0607.

Chemical composition (%)	B	T	1mu1	12mu3	5Tz	15x	F1-iii	F2-iv	BL0607
CaO	55.19	55.02	50.78	51.62	53.43	52.45	54.99	54.26	55.10
MgO	0.43	0.52	0.72	0.58	1.52	0.73	0.51	1.04	0.37
SiO ₂	0.20	0.38	4.22	3.6	0.41	2.17	0.16	0.5	0.07
Fe ₂ O ₃	0.05	0.1	0.42	0.36	0.47	0.78	0.05	0.2	0.02
Al ₂ O ₃	0.1	0.19	1.53	1.17	0.2	0.6	0.09	0.2	0.06
K ₂ O	0	0.02	0.51	0.37	0	0.17	0	0.02	0
Na ₂ O	0.02	0.02	0.05	0.04	0.04	0.04	0.03	0.04	0.02
Mn _X O _Y	0	0.02	0	0	0	0	0	0	0
SO ₃	0.04	0.05	0.07	0.24	0.41	0.13	0.11	0.13	0.02
Weight loss (CO ₂) (%)	43.78	43.75	40.64	41.14	43.59	41.96	43.71	43.72	43.65
Density (g cm ⁻³)	2.75	2.69	2.68	2.72	2.19	2.63	2.22	2.11	2.73

Table 1.2: Chemical composition and bulk density of limestone used in current research

1.4.2 Lime Production

World production of lime grew steadily from just under 60 million metric tonnes (mmt) in 1960 to a peak of almost 140 mmt in 1989 [3]. The early 2000s recession led to a drop in production to 116 mmt in 2002. Published estimates of the global production of quicklime suggest that the total is approximately 117 mmt in 2003. As per the statistics reported from international lime association (ILA) based on the U.S. Geological survey 2015 [5][6], the world lime production for the year 2014 has been reached to 350 mmt for the year 2014. China tops with 230 mmt that is with 65% of the total world production. United states and India produces 19 and 16 mmt takes second and third position respectively. Germany produces 6.8 mmt which is 2 percent of the total world production. Italy, Turkey and France fall in the places next to Germany whereas Vietnam, Slovenia and South Africa are in the last three positions for the production of lime.

1.4.3 Lime quality

Reactivity

The quality or the reactivity of the product Lime is the most important criteria in the industry. The lower the decomposition temperature is held during the decomposition of limestone, the higher will be the lime reactivity. The lime reactivity is detected by the velocity of temperature increase of the water-lime-slurry, after the 150 g lime powder of grain size of 0-3 mm was dosed into 600 ml distilled water of 20°C [7]. From the slaking-curve, which indicates the temperature increase of the slurry due to the hydration reaction of lime, a parameter t_{60} can be read out, which means after this time the slurry temperature will increase from 20 up to 60°C (see DIN EN 459-2 2002). When t_{60} is shorter than 2 min, then the lime is said to be soft-burnt. In Figure 1-1, measurements are showed for three different limes. From the index t_{60} , the three limes with different reactivity are differentiated as soft, middle or hard-burnt.

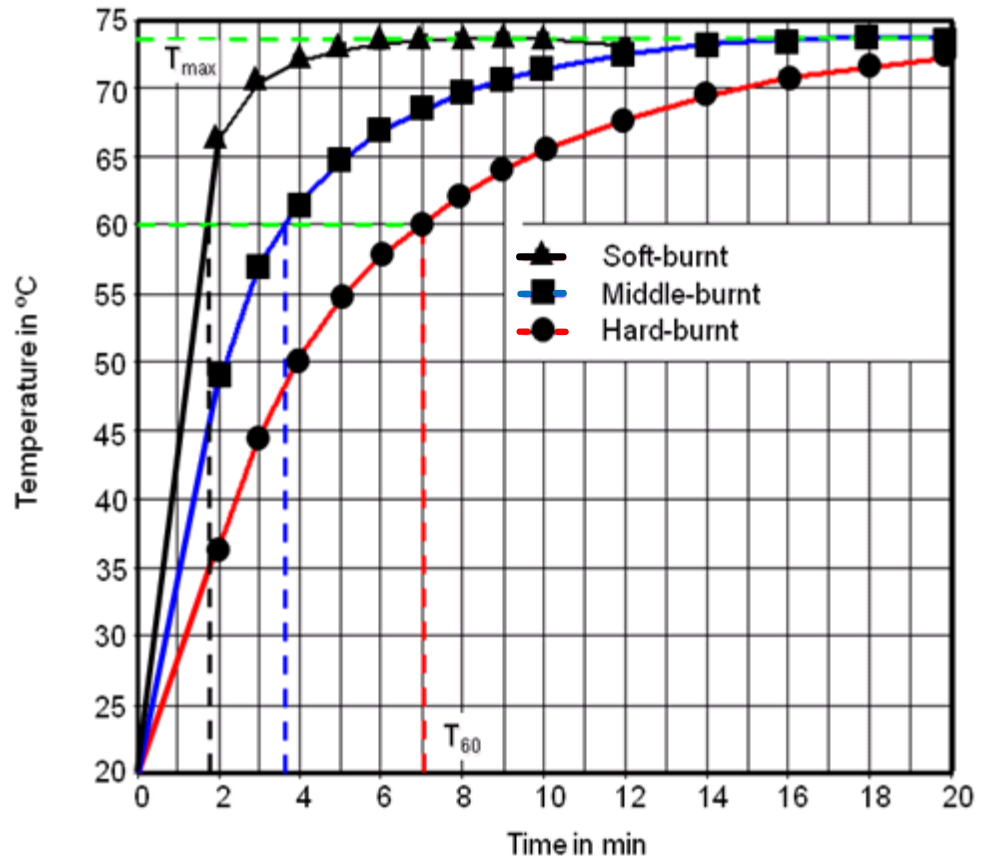
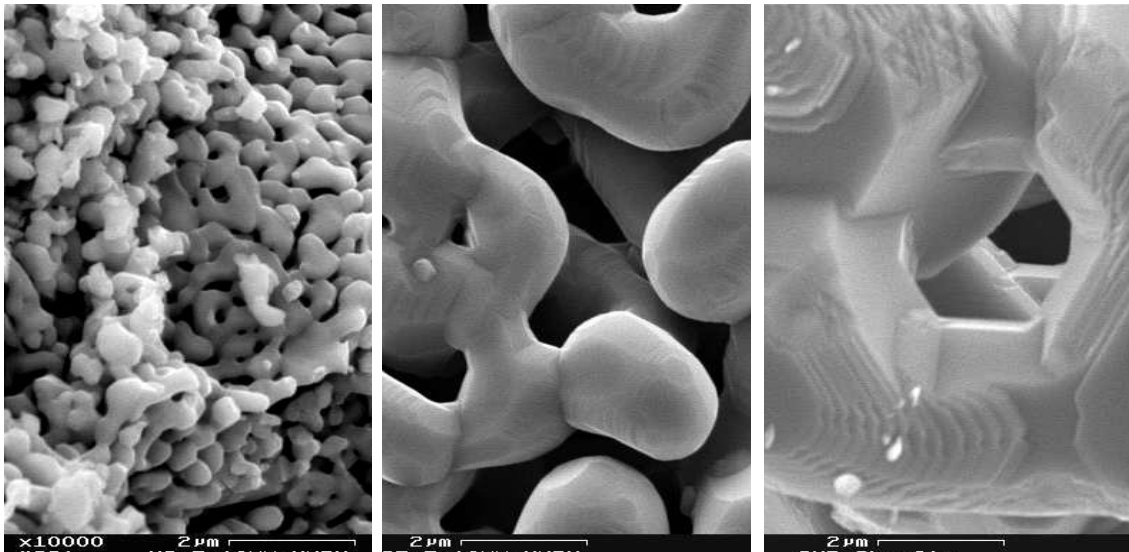


Figure 1-1: Measurement of lime reactivity, (Modified from T. Schwertmann 2007 [8])

The t_{60} -value is correlated with specific surface area of lime (for example BET-surface area), or the porosity of the lime. The higher the temperature at the end of burning, the smaller will be the specific surface and the porosity; hence the t_{60} -value will be larger. This is decided by the development of the crystal structure or the sintering effect in the lime. Under Scanning Electronic Microscope (SEM), limes of different reactivity have different crystal structure and pores system, which is showed in Figure 1-2.



	Soft-burnt	Middle –burnt	Hard-burnt
[g/cm ³]	1.65	2.0	2.4
[m ² /g]	2.33	2.03	0.52

Figure 1-2: SEM pictures of three different qualities of lime [9]

From the t_{60} -value, sometimes also called R-value is calculated with:

$$R = \frac{\Delta T}{\Delta t} = \frac{60 - 20}{t_{60}} = \frac{40}{t_{60}} \cdot \frac{^{\circ}\text{C}}{\text{min}} \quad (1.4-1)$$

The R-values with Annular Shaft Kilns are mostly about 20, namely $t_{60} = 2$ min, but it happens sometimes as well, that the R-value is smaller than 17 or larger than 30. To characterize the lime reactivity in steel works, a so called index Coarse Grain Titration is used.

The influence of the oxide shell temperature on the mean pore diameter is shown in Figure 1-3.

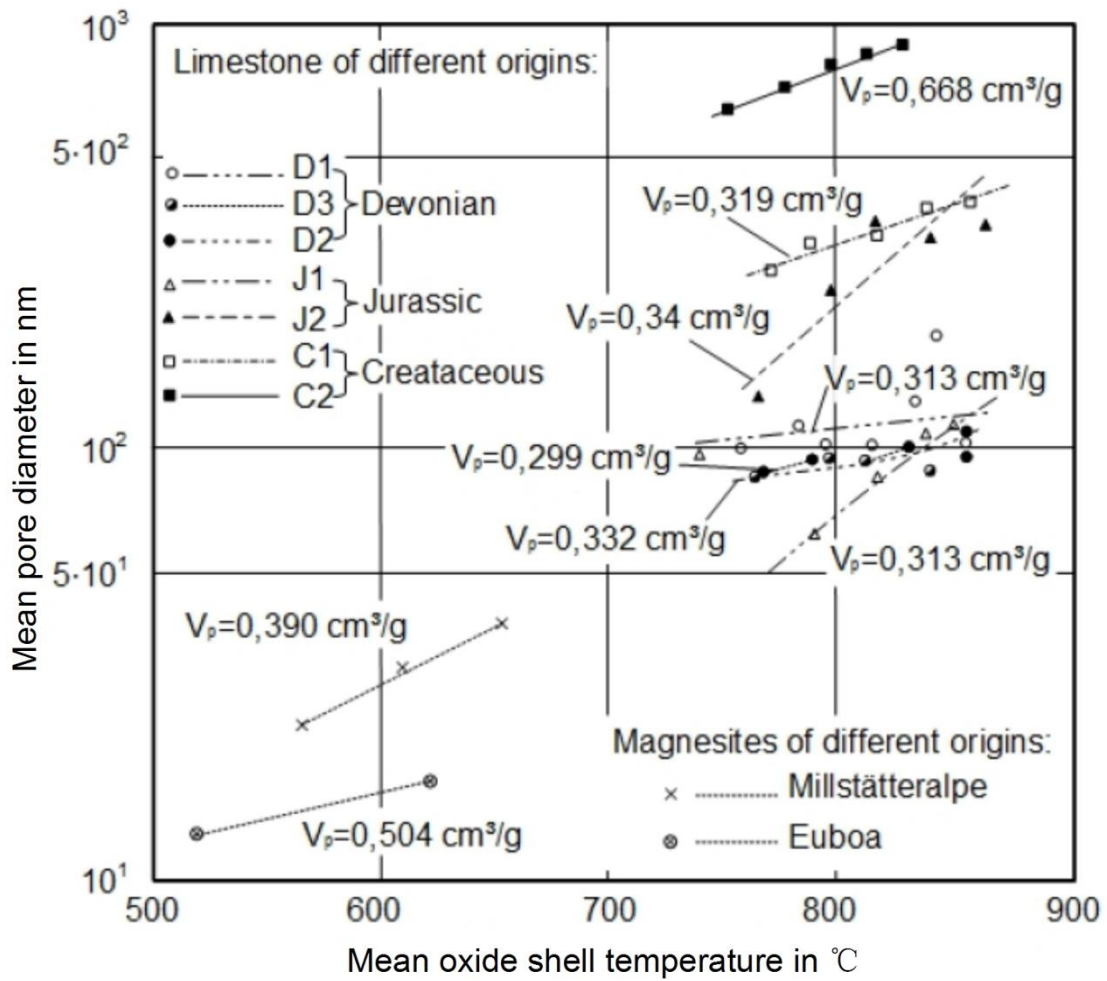


Figure 1-3: The influence of the oxide shell temperature on the mean pore diameter (Kainer et al. 1986 [10])

The influence of the calcination temperature and heat treatment time on the pore size is presented with Figure 1-4 and Figure 1-5. With increasing calcination temperature and time, the pore surface and pore volume decrease and the average pore size increases.

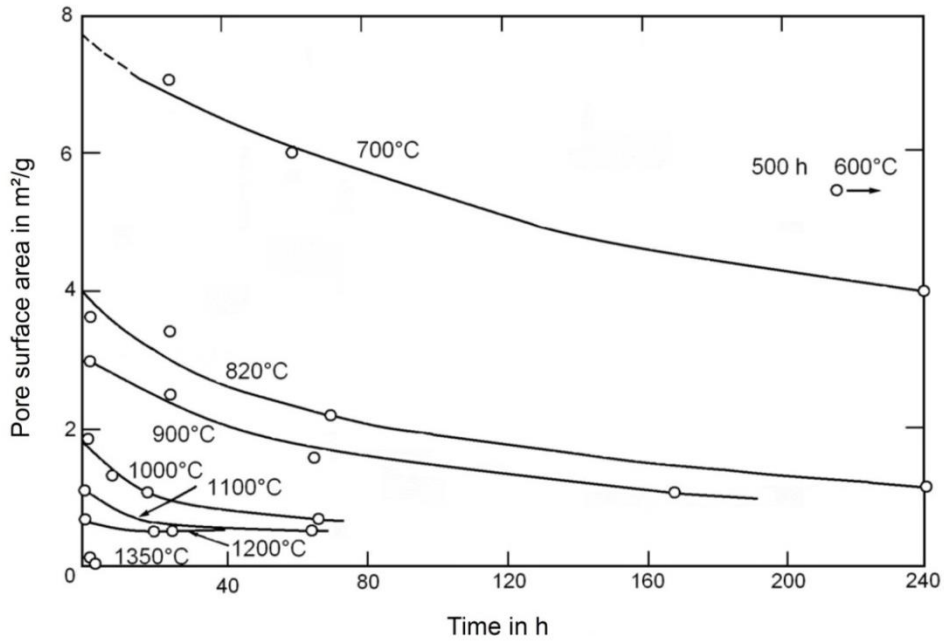


Figure 1-4: Effects of heat treatment time and temperature on pore surface area of burnt lime (Turkdogan et al. 1973 [11])

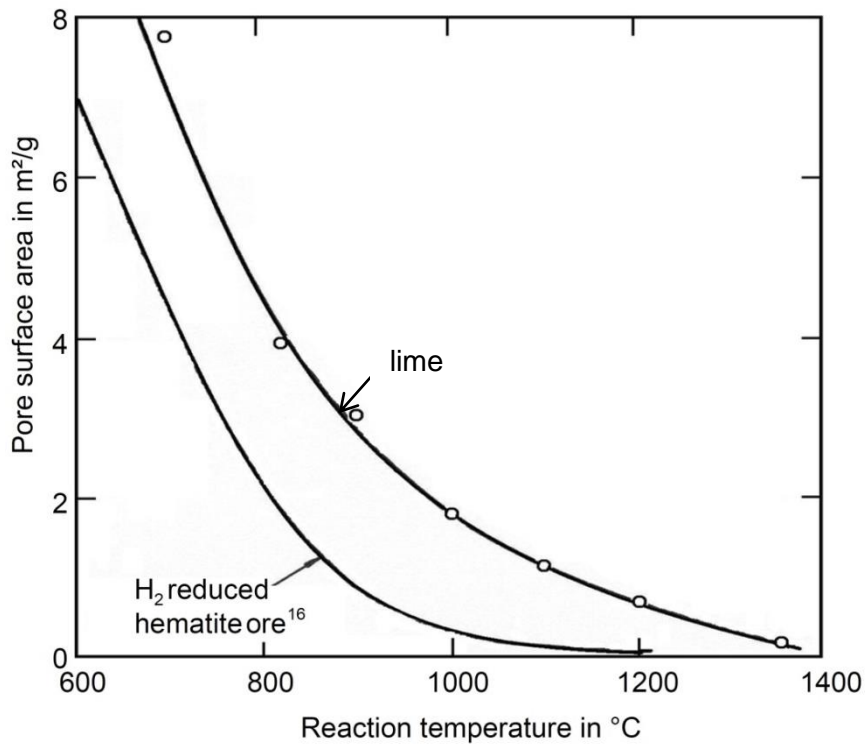


Figure 1-5: Pore surface area of burnt lime (extrapolated to zero heat treatment time) compared with that of porous iron formed by H₂-reduction of porous hematite ore. (Turkdogan et al. 1973 [11])

Residual CO₂ in lime

A further measure for the quality is the residual CO₂ in the lime. This is the unreacted, non-decomposed calcite CaCO₃. The residual CO₂ content is described by the mass of unreacted CO₂ relative to the mass of produced lime and it can be calculated with the formula below:

$$y_{\text{res. CO}_2} = \frac{\dot{M}_{\text{CO}_2} - \dot{M}_{\text{CO}_2\text{R}}}{\dot{M}_{\text{LS}} - \dot{M}_{\text{CO}_2\text{R}}}$$

The initial mass of CO₂ in the limestone is described by

$\dot{M}_{\text{CO}_2} = y_{\text{CO}_2} \cdot \dot{M}_{\text{LS}}$, is the carbon dioxide content in limestone and y_{CO_2} is the CO₂ content in the limestone. The conversion degree is defined as the mass of the reacted carbon dioxide relative to the carbon dioxide content in limestone. The conversion degree is defined as the mass of the reacted carbon dioxide relative to the carbon dioxide content in limestone:

$$\eta = \frac{\dot{M}_{\text{CO}_2\text{R}}}{\dot{M}_{\text{CO}_2}}$$

From above equations the relation between conversion degree and residual CO₂ content is obtained:

$$\eta = \frac{y_{\text{CO}_2} - y_{\text{res. CO}_2}}{(1 - y_{\text{res. CO}_2}) \cdot y_{\text{CO}_2}}$$

or

$$\text{residual- CO}_2 \text{ - content} = \frac{1}{\frac{1}{y_{\text{CO}_2}} - \eta} - \frac{1}{\frac{1}{y_{\text{CO}_2} \cdot \eta} - 1}$$

For a carbon dioxide content in limestone of 0.42 and residual CO₂ content of 0.01 the conversion degree is 0.986.

Chapter 2

Literature Review

2.1 Introduction

Several authors have been investigating the lime decomposition process for more than hundred years. In the very beginning of 20th century, the interest towards the research on calcination process has been accelerated. Several people started working on the calcination process intensively across the globe. Thermo gravimetric analysis experiments (TGA) are the most common method to investigate and to get a good overview of the process. Thermogravimetric Analysis is a technique in which the mass of a substance is monitored as a function of temperature or time as the sample specimen is subjected to a controlled temperature program in a controlled atmosphere.

High temperature endothermic topo chemical solid decomposition reaction has to overcome a series of resistances. These resistances include heat transfer resistance (R_a) to the surface of the particle, conduction heat transfer resistance (R_λ) from the surface to the reaction front, chemical reaction resistance (R_k), diffusion resistance (R_D) in the porous product layer and finally the mass transfer resistance (R_β) to CO_2 from the surface to the ambient. The order of these resistances is schematically represented and explained in Chapter 4.

2.2 Rate limiting resistances

Wallace A. Gilke (1926) [12], conducted decomposition experiments of the limestone of size 4 to 6 mesh to through 200 mesh screening, at temperatures ranging from 700 to 1000 °C. Samples were placed in small porcelain crucibles in a 4x4 inch Hoskins electric furnace and heated at different constant temperatures for different intervals of time. He concluded that the rate of calcination under the atmospheric pressure of carbon dioxide is only 40% of that of the calcination carried out at normal atmospheric

conditions. The results obtained for such a small particle sizes (0.07 – 4 mm) cannot be applicable to macro size (relatively much bigger real stones) stones those undergo real time calcination in industrial kilns.

Calcination behavior and the rate limiting resistances of the decomposition process vary with shape and the size of the reacting particle [C.C. Furnace (1931)], [13]. Furnace et al. worked with particles of equivalent spherical diameter of 2.5 to 8.5 cm. They mentioned that the major driving force to the reaction is the equilibrium carbon dioxide pressure of calcium carbonate; however the limiting factor at higher temperature is the heat transfer resistance. It's also been observed that no significant change in calcination rate has been identified though the concentration of CO₂ in the furnace has been raised from 0% to 50% either at low or at high temperature runs. This observation is totally in contradiction with the results obtained by Wallace A. Gilke (1926) et al., where they mentioned that calcination is only 40% in the atmosphere of CO₂. Campbell et al. (1969) [14], concluded that the heat and mass transfer determine the rate of calcination and chemical process at the front is of no importance. Chemical reaction and the mass transport in the particle porous system were reported as the main limiting factors of the calcination for the experiments conducted by F. Garcia Labiano (2002) [15], with particle size 0.4- 2mm and in the CO₂ concentrations ranging from 0-80%. As per Patil et al. (2004) [16], temperature gradient in the pellet is small and the heat supply alone is the rate controlling step. In large particles of about 10 mm size, heat and mass transfer are the rate controlling steps [P.C. Okonkwo et al. (2012) [17]]. Rate limiting mechanism need not necessarily be a single or a combination of a couple of resistances together. It depends on the size, shape of the particle and also depends on the experimental conditions. It's likely to be combination of all these five resistances in a real time industrial decomposition process.

2.3 Various models and experimental study of lime decomposition

Most of the research has been carried out to understand the rate of calcination and the limiting factors on the decomposition process till 1960s. Later some experimental study has been carried out in the late 1960s to measure the thermal conductivity of porous

lime and the diffusion coefficient of carbon dioxide through it [Campbell et al. (1969) [14]]. They have conducted several experiments to measure the thermal conductivity and diffusion coefficients of porous lime with various porosities. Thermal conductivity values ranging from 0.3 – 0.65 W/m K while the porosity of lime varying from 0.8 – 0.6 and the molecular diffusion coefficient in porous lime with porosity 0.5, tortuosity 9 and at 950 °C is measured as 9.4×10^{-6} . They determined that the Knudsen diffusivity is the dominant mechanism, and molecular pore diffusion is not important. Material properties can be determined with the help of the temperature and decomposition curves obtained by properly designed and installed experimental setup [Kainer et al. (1986), [10]]. Kainer et al. proposed a method to determine reaction coefficient, pore diffusion coefficient and thermal conductivity of limestone of various origins. During the decomposition process, due to the release of CO₂ gas at the front, pore evolves and depending on the pore size, Knudsen diffusion or Fick's diffusion can take place. The effective diffusion coefficient proposed D_{eff}^p can take care of both of these diffusion mechanisms.

Grain model was applied for cylindrical pellets of 11.95 mm diameter and 28 mm length by M S Murthy et al. (1994) [18], with transient heat and mass transfer equations assuming spherical grains. TGA experiments are conducted in the temperature range 750-860°C, they have used convective heat transfer correlation $Nu = 0.59(GrPr)^{0.25}$ (Weise, 1935 [19]; Saunders, 1936 [20]) and the bulk diffusion coefficient for CO₂-air mixture was calculated using Chapman –Enskog equation and the mass transfer coefficient for free convection was found from correlation proposed by Mathers et al.(1957) , $Nu^1 = 2 + 0.59(GrPr)^{0.25}$. They added pure metallic powder to the reactant and also they used black coated pellets to alter the decomposition kinetics. Additives increased the rate of calcination. Activation energy obtained with this model is 42kcal/mol. But they could not explain the mechanism of calcination or the role played by the additives.

Khinast et al. (1995) [21], used random pore model for their experimental study to investigate the calcination behavior of micro meter particle size. Experiments and model calculations have shown that the reaction surface area and its evolution can be described by random pore model. Shrinking core model with surface reaction rate controlling mechanism is used by IrfanAr and GülsenDogu (2000) [22] and they studied the calcination behavior of 10 different limestone samples taken from different regions of Turkey with thermo gravimetric analysis (TGA) technique. They have used possibly smaller sample sizes of approximately 1 mm in size in order to minimize the inter particle

heat and mass transfer. CO₂ which arises from decomposition of CaCO₃ was swept away by the nitrogen stream. Therefore its equilibrium partial pressure was not reached and there was no film resistance. They have reported that activation energy of the calcination is 40-50 kcal/gmol or 167-209 kJ/mol and the porosity of the product lime is in a wide range 0.32-0.51.

Authors	Activation energies of calcination	
	kcal /g mole	kJ/g mole
M S Murthy et all (1994) [18]	42	175.56
IrfanAr and GülsenDogu (2000) [22]	40-50	167.2-209
K. Muazu et all (2011) [23]	29.9	122

Table 2.1: Activation energy of calcination reported in literature

Equivalent diffusivity for the limestone particles of size in the range of 2-4 mm was measured by Jian Yun Xie (2002) [24]. This equivalent diffusivity is a combination of Knudsen and molecular diffusion. This is same as the equivalent diffusivity proposed by Kainer et al. [10]. Halikia et al. (2001) [25] used four different isothermal methods and found that the phase boundary controlled reaction model found to better fit the experimental results. They have conducted several TGA experiments in the temperature range between 637°C and 865°C with different samples weights 14.9 g and 19.3g in nitrogen atmosphere. They have given a kinetic model equation for the isothermal decomposition of CaCO₃ in temperatures varying between 637 and 750°C as $1 - (1 - \alpha)^{1/2} = kt$ where α is fraction reacted, k is a reaction coefficient and t is the time and this reaction kinetics varied for different experimental conditions. Patil et al. (2004) [16], applied grain model for spherical particles and solved the unsteady state diffusion reaction equations under external pressure pulsations. They have compared their numerical model results with the experiments conducted by earlier authors. They observed significant improvements in the conversion time under pulsating pressure conditions. H.Mikulcic et al. (2011) [26] [27], have developed numerical model for calcination process which includes effect of temperature, decomposition pressure, diffusion and pore efficiency. But experiments are conducted with 5-10 μ m particles. Their analysis and results cannot be used in real time scenario where relatively large

stones undergo calcination and the rate controlling mechanism significantly depends on the size of the particles.

K. Muazu et al. (2011) [23], tried to find the rate equation and found that the first order reaction kinetics best fit with the limestone they have studied. They conducted experiments at three different temperatures 900, 1000 and 1200 °C and also determined the activation energy and frequency factors as 122 kJ/mol/K and 2.943 respectively.

Calcination behavior of Ukpilla limestone found in the central region of the Nigeria was studied by P.C. Okonkwo et al. (2012) [17]. They concluded that the diffusivity and mass transfer coefficients decrease with increase in calcination temperature and the thermal conductivity increases with increase in temperature. They also reported that reactivity of lime decreases with increase in calcination temperature. They have conducted experiments with different particle size, ranging from 100 mesh size to 10 mm particle size. They have proposed a correlation for pore diffusivity as $D = A+B (T-830^{\circ}\text{C})$ where $A = 0.83 \text{ cm}^2\text{s}^{-1}$ and $B = 0.00021 \text{ cm}^2\text{s}^{-1} \text{ }^{\circ}\text{C}^{-1}$. From this equation for a normal reaction temperature of 900°C, Diffusivity can be computed as $8 \times 10^{-5} \text{ m}^2\text{s}^{-1}$.

Hill and Winter (1956) [28] conducted experiments with calcium carbonate and identified the thermal dissociation pressures of CaCO_3 . They have tabulated the equilibrium dissociation pressures of CO_2 at different temperatures ranging from 449 – 904 °C and found that equilibrium pressure corresponds to 1 atm of CO_2 is in between 898 and 904 °C.

E.H. Baker (1961) [29] , has studied the calcium oxide and carbon dioxide equilibrium at wide range of pressures up to 300 atm., and observed that the equilibrium dissociation temperature corresponds to 1 bar CO_2 pressure is 902 °C. They used 100 mesh size samples for their high pressure experiments.

All the research mentioned above deals with limestone powder or micron size particles. Most of them concentrated on finding out the reaction coefficient and focused on calcination reaction kinetics. But the reaction constant determined, cannot be used if the surface area of the particle is unknown. Below section delineate the models proposed for lumped pieces of limestone with a definite shape.

2.4 Specific heat capacities of Limestone and Lime

The data in the literature for the specific heat capacity of Limestone and Lime, especially the dependency with temperature is very rare. Even though few literatures is available, the reference for the origin of the stone is not clearly mentioned and also how these values are measured or how these heat capacities are computed is not known.

Silva et al. in 2009 [1], [30] studied the dependence of the specific heat capacity of limestone and lime on the temperature. They have used Pegasus 404 Differential Scanning Calorimeter from the manufacturer Netzsch in an atmosphere of Argon from ambient temperature up to 1300°C. The specific heat capacities of the four different kinds of limestone are presented in dependence on the temperature in Figure 2-1. The curves present the real values from the three different measurements. The specific heat capacity is shown only up to 650°C. The specific heat capacity increases with the temperature. The deviation among the four different kinds of limestone is only about $\pm 0.05 \text{ J/g/K}$. The line in the figure presents the values given in the handbooks of material properties Barin, Knacke [1973] [31] and Landolt, Börnstein [2002] [32]. The specific heat capacity can be approximated in the range $T > 293 \text{ K}$ by:

$$c_p(T) = c_p(T_0) \cdot (T/T_0)^n \quad (2-1)$$

with $T_0 = 473 \text{ K}$, $c_p(T_0) = 1.0 \text{ J/g/K}$. The exponent n varies slightly according to the kind of limestone, but can be averaged as $n = 0.30$.

Therewith follows the correlation for the mean specific heat capacity:

$$\bar{c}_p(T) = \frac{1}{T-T_0} \cdot \int_{T_0}^T c_p(T) \cdot dT = \frac{c_p(T_0)}{n+1} \cdot \frac{(T/T_0)^{n+1} - 1}{T/T_0 - 1} \quad (2-2)$$

Average values of the measured specific heat capacities of lime of different origins also presented in Figure 2-2. It can be seen that, specific heat capacity varies from lime to lime. For most of the stones it falls in the range from 0.85 to 0.95 J/g/K at least in the range of calcination temperatures 800 to 1000°C. From these two figures it can be clearly seen that specific heat capacity of lime and limestone is not the same for all stones. It can

vary with origin and also with the temperature. As enthalpy of reaction has direct dependence with the specific heat capacities, so different possible specific heat capacities must be considered to compute the enthalpy of reaction.

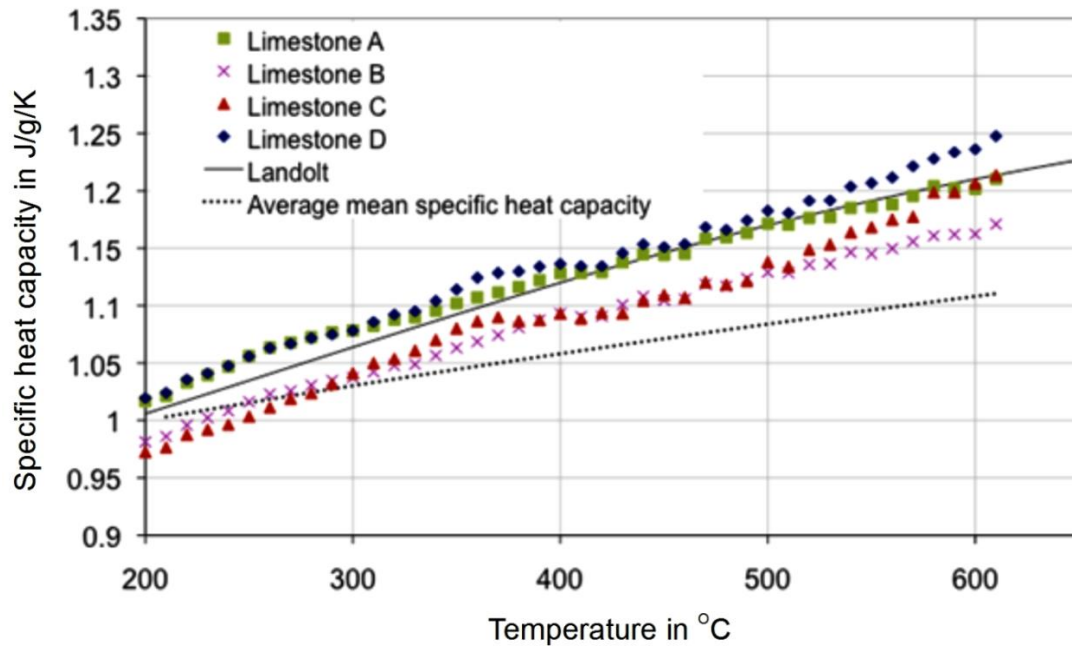


Figure 2-1: Average values of the real specific heat capacity of limestone of different origin vs. temperature (Silva et al. 2009 [1])

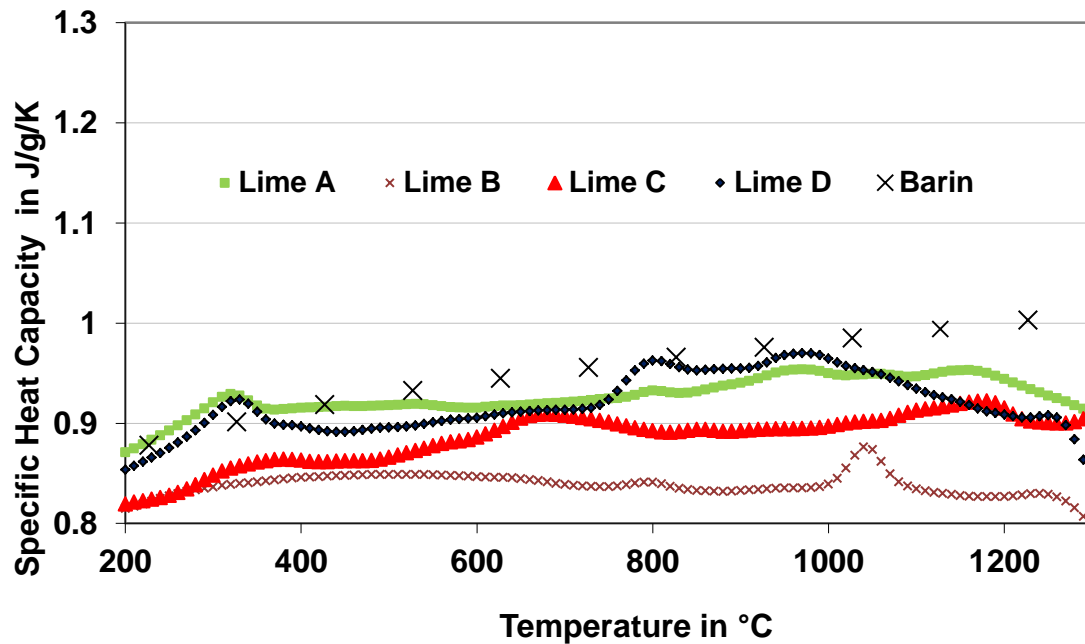


Figure 2-2: Average values of the real specific heat capacity of lime of different origin vs. temperature (Silva et al. 2009 [1])

2.5 Reaction enthalpy

The reaction enthalpy is temperature dependent, which is caused by the difference of the specific heat capacities of educts and products. This relation can be obtained by applying Hess's law:

If the limestone is decomposed at T_0 , then the products CaO and CO₂ have to be heated up to the temperature T. If the limestone is decomposed at the temperature T, then CaCO₃ has to be heated up before form T_0 to T. This result in

$$\Delta h_{CaCO_3}(T_0) + (y_{CaO} \cdot c_{CaO} + y_{CO_2} \cdot c_{P,CO_2}) \cdot (T - T_0) = c_{CaCO_3} \cdot (T - T_0) + \Delta h_{CaCO_3}(T) \quad (2-3)$$

where T is reaction temperature in K,

T_0 a reference temperature in K,

y_{CaO} the mass fraction of CaO in CaCO₃,

y_{CO_2} the mass fraction of CO₂ in CaCO₃,

c_{CaO} the mean specific heat capacity of CaO between T_0 and T,

c_{P,CO_2} the mean specific heat capacity of CO₂ at constant pressure between T_0 and T, and

c_{CaCO_3} the mean specific heat capacity of CaCO₃ between T_0 and T.

From the above equation follows for the difference between the reaction enthalpies at different temperatures:

$$\Delta h_{CaCO_3}(T) = \Delta h_{CaCO_3}(T_0) + (y_{CaO} \cdot c_{CaO} + y_{CO_2} \cdot c_{P,CO_2} - c_{CaCO_3}) \cdot (T - T_0) \quad (2-4)$$

Specific heat capacity of CO₂ is computed from the above equation 2-2 with $c_p(298K) = 0.85 \text{ kJ}/(\text{kg} \cdot \text{K})$, $n = 0.34$ [33]. From Figure 2-1, the mean value of specific heat capacity for limestone is $1.1 \text{ kJ}/\text{kg}/\text{K}$ and for the lime, C_p is independent of temperature (Figure 2-2) and it is varied in between 0.8 and 0.9, so it can be considered as $0.85 \text{ kJ}/\text{kg}/\text{K}$ as average value.

From these values the molar reaction enthalpy at 900°C can be obtained as $168 \text{ kJ}/\text{mol}$. However specific heat capacities of lime and limestone are not constants, so minimum

and maximum values of heat capacities of lime and limestone (0.82, 0.92, 1.10, 1.17 J/g/K) and the mean specific heat capacity of CO₂ (1.09 J/g/K) is inserted in the equation (2-4) to identify the possible range of enthalpy of reaction. The decomposition enthalpies at 900 °C are found to be between 1570 and 1690 J/g CaCO₃ for the possible range of specific heat capacities. Due to such a possible variation of enthalpy of reaction, it is very essential to study the influence of reaction enthalpy on calcination process.

2.6 Equilibrium pressure

The temperature corresponds to 1 bar of CO₂ pressure is measured and reported by several authors. Arrhenius approach is written as below, which can be used to determine the equilibrium pressure

$$p_{eq} = p_{eq0} \cdot \exp\left(\frac{-\Delta\tilde{H}_R}{\tilde{R} \cdot T}\right) \quad (2-5)$$

where $\Delta\tilde{H}_R$ is the molar reaction enthalpy, 168 kJ/mol at 900°C,

\tilde{R} the universal molar gas constant, 8.314 J/(mol·K),

T the reaction temperature, K, and

p_{eq0} is the pre-exponential coefficient, or frequency factor, Kainer [10] has taken 4×10^{12} pa. According to the above equation (2-5), the temperature corresponds to p_{eq} of 1 bar is 881°C.

Source	Decomposition Temperature at 1bar
Hill and Winter [28]	898-904
Pott [34]	892
Riesenfeld [35]	910
Johnston [36]	898
Marc and Simek [37]	898
Southard and Royster[38]	894
Baker [29]	902
Hills [14]	903
Boynton [39]	898

Table 2.2: Decomposition temperature measured in pure CO₂ according to various authors.

There is no standard decomposition/equilibrium temperature has been reported in the literature. The value ranges from 865-920°C. The discrepancies in the results are thus to be attributed either to the fact that equilibrium conditions were not attained or to the presence of water vapor or of some other impurity capable of developing pressure [36]. A summary of some chronologically reported temperature decomposition values, which are considered reliable, is given in Table 2-2.

Silva et al. [1] studied the decomposition temperature of the limestone with the use of a Simultaneous Setaram TG-DTA 92 apparatus and tabulated the equilibrium temperature of limestone from different parts of the world and it is shown in Table 2-3.

Material	Average Decomposition
	Temperature / °C
Limestone A (Brazil)	907
Limestone B (Brazil)	910
Limestone C (Germany)	908
Limestone D (Germany)	908
Chalky Limestone (Italy)	917
Crystalline Limestone (Italy)	917
Limestone (Greece)	923
Limestone (Austria)	919
Limestone (Mexico)	911
Limestone (Oman)	923
Limestone (China)	920
Limestone (Bulgaria)	910
Limestone (Jamaica)	911
Marble	920
Cement raw meal	907
Dolomite	907
Clay Powder Type A	899
Clay Powder Type B	848

Table 2.3: Equilibrium temperatures reported by (Silva et al. 2009 [1])

Cheng et al. [40] have studied the calcination behavior and proposed a method to determine the material properties (λ , D_p and k) of lumped pieces of limestone with shrinking core model. They have considered all the five resistances (mentioned in the previous chapter) for their model. They have assumed constant reaction front temperature during the calcination period, especially when the conversion degree lies in between 0.1 and 0.9. All these five resistances and the equilibrium pressure which are functions of front temperature are also become constant for the constant ambient conditions such as constant ambient temperature and at constant atmospheric pressure. With this, an analytical method has been developed where two linear equations are formulated with all these resistances as slopes and intercepts to the straight lines formed with these equations.

However in general the calcination (reaction front) temperature is not constant and it slightly varies during the reaction. The assumption of constant front temperature after 10% conversion and until 90% is not necessarily true with all the limestone and at all possible ambient temperatures. Some stones undergo calcination to much higher degree (up to 20%) during the pre-heating of the core and some stones calcinate to much lower

than 10%. Also this pre calcination (calcination happens before the core of the particle reaches to the calcination temperature) conversion degree depends highly on the ambient temperature maintained and to some extent on the origin of the stone. Similarly, the post heating need not necessarily begins after 90% conversion. It can begin soon after complete conversion for certain type of stones and at certain experimental conditions.

Apart from, even in the calcination zone, front temperature is not constant which varies up to 10-15 °C; this is equivalent to 10-15% of the total temperature change of the particle in the interested calcination temperature domain (800 – 1000 °C). Because of this significant change in front temperature, the resistances formulated by Cheng et al. which are functions of front temperature are not really constants and hence, with the linear equations proposed, we end up with curves (because of varying slope) instead of straight lines. Hence this method is not accurate and even it is very difficult to use this method to determine the thermo physical properties (λ , D_p and k).

2.7 Reaction rate coefficient

Kainer [10] computed the reaction coefficients based on the equation

$$\dot{M}_{CO_2} = \frac{k \cdot (p_{eq} - p_f)}{R_{CO_2} \cdot T_f} \cdot A_f \quad (2-6)$$

Where \dot{M}_{CO_2} is the rate of CO₂ evolving at the front in kg/s

k is the reaction coefficient in $m \ s^{-1}$

R_{CO_2} is the individual gas constant for CO_{2 gas}, 189 J/kg/mole

T_f , p_f , A_f are the temperature, partial pressure and surface area at the reaction front respectively. From the analysis and measurements of Silva et al., the equilibrium temperature ranges between 907-920°C. But for most of the stones it is around 910°C. In this thesis, 910 °C has been considered as most possible dissociation temperature for major varieties of limestone. Further calculations and hence reaction coefficients have been determined considering this temperature as the dissociation temperature. When equilibrium temperature is fixed to 910 °C, the pre exponential or frequency factor in the

equation 2.1 has been changed from 4.10^7 bars to $1.744.10^7$ bars. This causes a significant change in the reaction rate coefficients those are previously reported in the literature. So the reaction coefficients determined in this thesis would be different from any of the previously reported values in the literature.

Temperature depends exponentially on the equilibrium pressure as shown in the equation 2-5 in the previous section. So a small change in dissociation temperature has exponential change in equilibrium pressure. In the above equation 2.2, reaction rate coefficient k is multiplied with the difference of equilibrium pressure and the front pressure. Hence there is a significant change in reaction coefficient with a change in dissociation temperature in order to keep the rate of CO_2 flow constant. Based on the equilibrium relation 2-5, several authors computed reaction coefficients. These coefficients have been determined in different units by different authors. Cheng et al. [40] have compared the reaction rate coefficients for limestone of different origin. Figure 2-3, show the reaction rate coefficients of various limestone reported by Cheng et al. Though there is a variation of the reaction coefficients for limestone of different origins, but on overall, the coefficients falls in the range of 0.002-0.01 m/s and the average value can be taken as 0.005 which is common to most of the limestone. However all these coefficients are computed based on the dissociation temperature of 880°C corresponds to 1 bar CO_2 pressure. In this dissertation reaction coefficients are computed considering the dissociation temperature of 910°C and hence to achieve more appropriate values for the reaction coefficients of different origins.

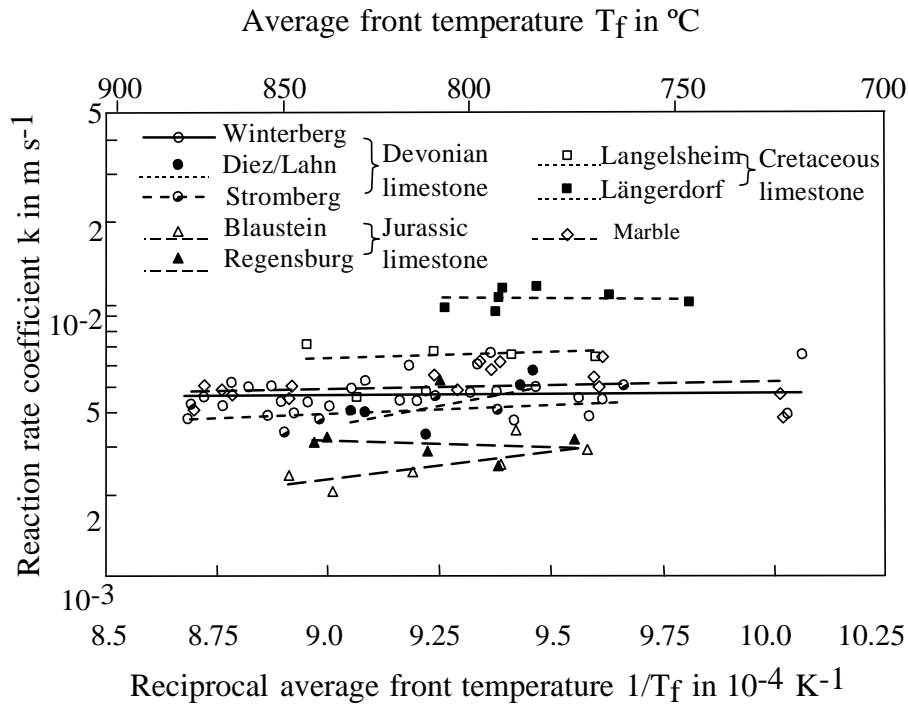


Figure 2-3: Reaction rate coefficients of various types of limestone. [Cheng et al. [40]]

2.8 Thermal conductivity of limestone and lime

In the literature very few attempts have been made to study the thermal conductivities of limestone. Silva [1] conducted several experiments with a laser-flash apparatus from NETZSCH (Model: LFA 427). Thermal diffusivities of limestone and lime are measured up to the temperature ranges of 600°C and 1300°C respectively. From the experimental data of the specific heat capacity and thermal diffusivity of limestone and lime of different origins, the thermal conductivities were determined and are plotted in the Figure 2-4.

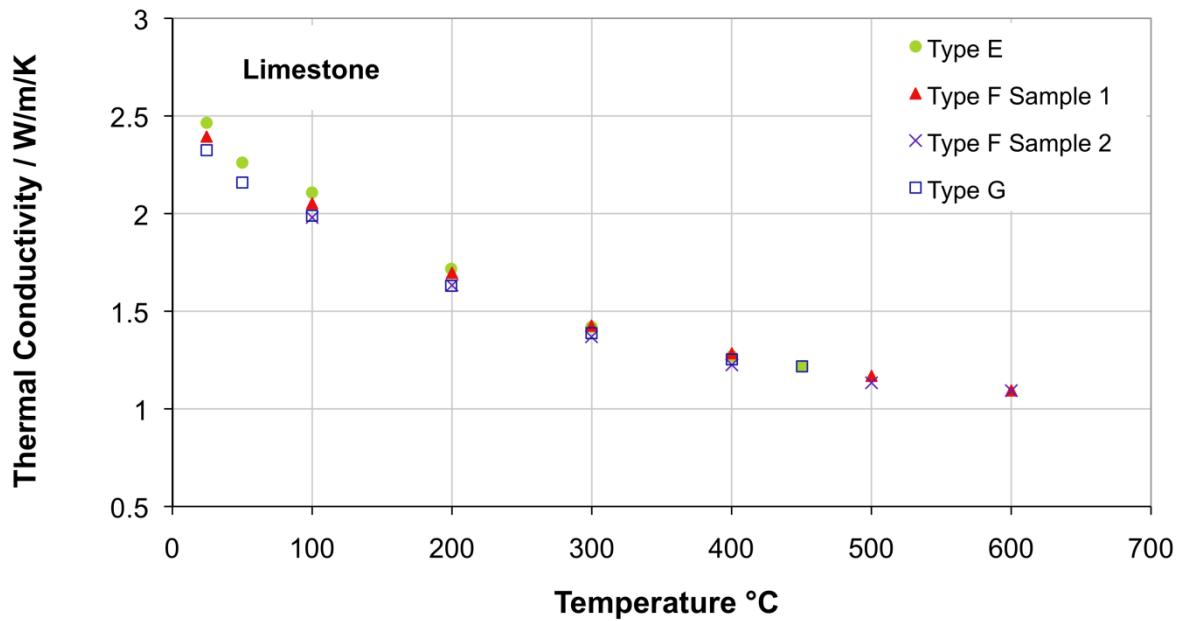


Figure 2-4: Variation of thermal conductivity with temperature for different limestone (Silva 2009 [1])

From the above data of thermal conductivity dependence on temperature an approximation has been developed by the same author as described in below equation and the same approximation has been used in the current research to determine the dependency of thermal conductivity of limestone with temperature.

$$\lambda(T) = A + \frac{B}{301 + T}$$

where λ is the thermal conductivity (W/m/K), $A= 0.33$, $B= 672.36$ and T the desired temperature given in °C.

Below Figure shows the measured thermal conductivity variation for lime with respect to temperature for four different limes.

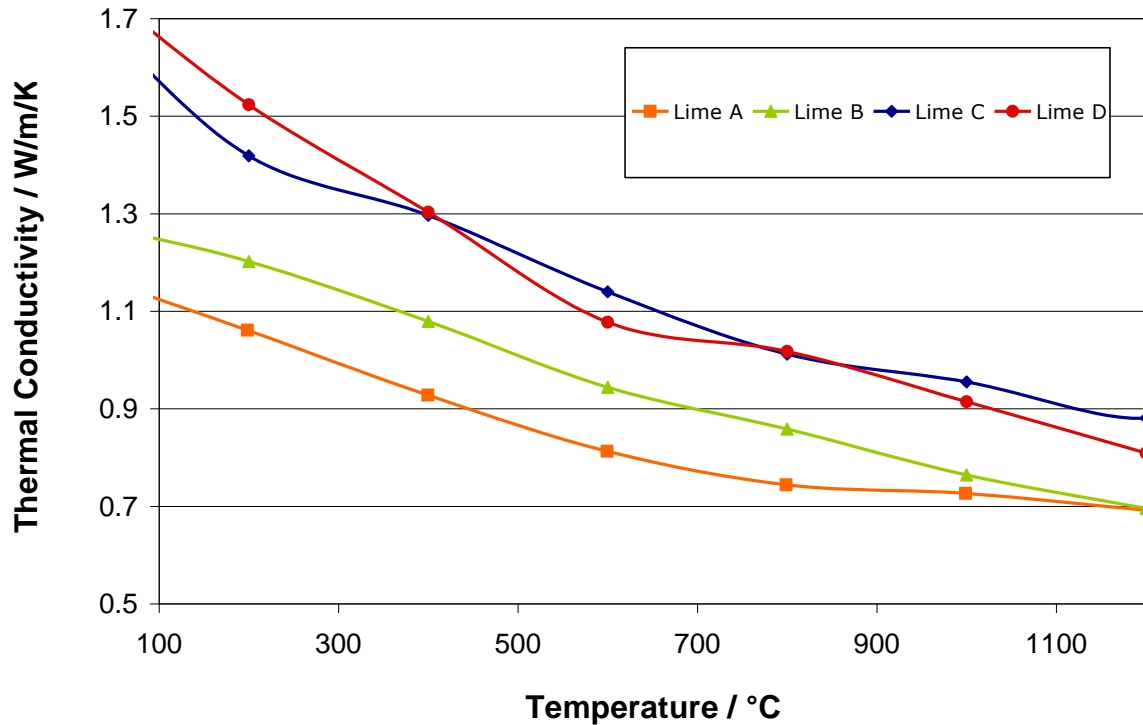


Figure 2-5: Variation of thermal conductivity with temperature for different lime (Silva[1])

From the above Figure 2-5, it can be inferred that the lime conductivity depends on the origin of lime and it also depends significantly with temperature. Turkdogan [11] reported the thermal conductivity of burnt lime as 0.52 W/mK. The value is determined based on the decomposition experiments conducted with the Michigan limestone with 9% porosity and with a density of 2470 kg/m³ at a furnace temperature between 800 to 1200°C. The value is much lower compared with the values measured by Silva [1]. Current research focusses on determining the thermal conductivity of lime from different origins.

2.9 Lime Density with burning time

Wolter et al. conducted calcination experiments at different temperatures and the lime produced is then burned for different times. The variation of densities of lime samples have been plotted in the below Figure 2-6. From the figure it can be inferred that, the density is independent of the duration, however density is found to be high when the calcination is carried out at higher temperatures. This shows that, higher temperatures

cause sintering (shrinking of the solid) which in turn results in increase of the bulk density. Figure 2-7 shows the variation of density with calcination temperature for four different limes.

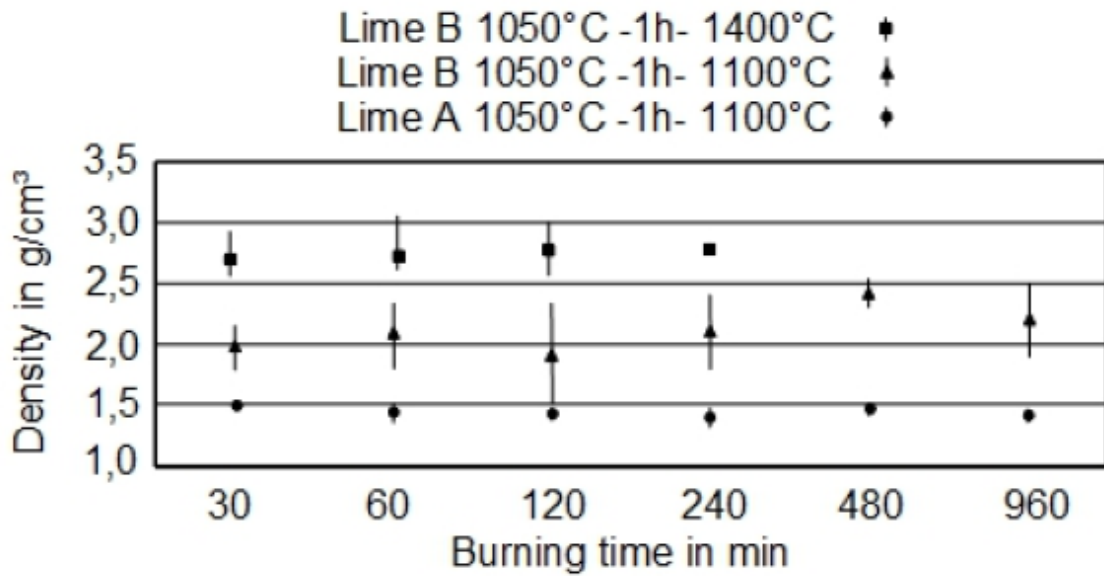


Figure 2-6: Density of lime in dependence on the burning time (Wolter [41])

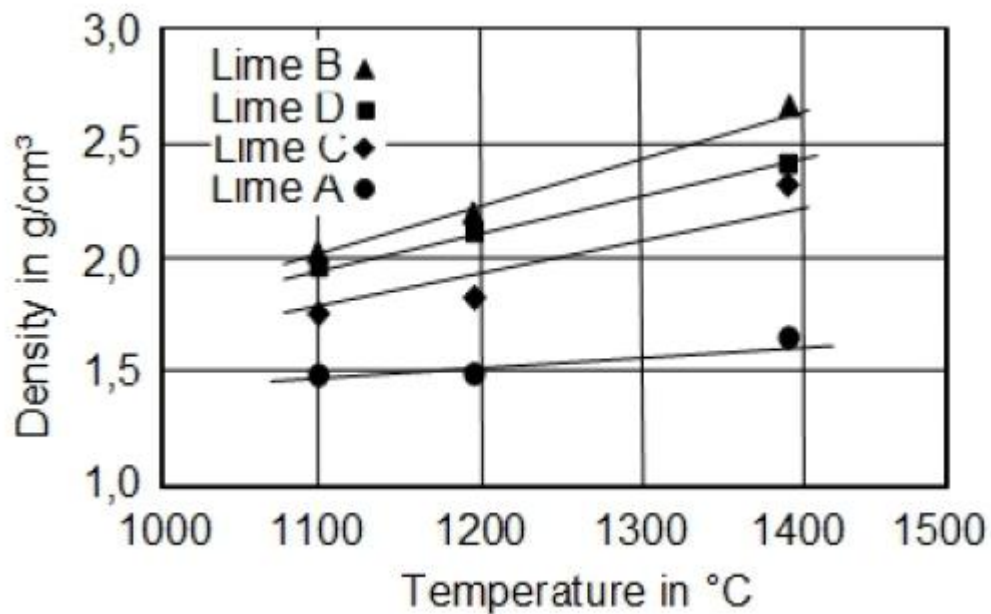


Figure 2-7: Increasing of lime density with burning temperature (Wolter [41])

2.10 Porosity

Figure 2-8 shows the variation of porosity with respect to burning temperature for the same lime experimented by Wolter et al. for measuring the density shown in the above Figures 2-6 and 2-7.

Like density, porosity also doesn't depend on the burning time. The Lime A which has low density has higher porosity of 0.6 and the lime C with high density exhibits low porosity of 0.4. This experiment shows the porosity of lime can vary from 0.4 to 0.6. For a given limestone with a density 2700 kg m^{-3} , assuming 100% calcium carbonate the bulk density of lime can be computed as 1512 kgm^{-3} as shown below.

$$\rho_{\text{bulk}} = \frac{m_{\text{CaO}}}{m_{\text{CaCO}_3}} \cdot \rho_{\text{S, CaCO}_3} = \frac{M_{\text{CaO}}}{M_{\text{CaCO}_3}} \cdot \rho_{\text{S, CaCO}_3} = \frac{56}{100} \cdot 2700 = 1512 \text{ kgm}^{-3} .$$

The porosity of lime under this ideal case is given by $\varepsilon = 1 - \frac{\rho_{\text{bulk}}}{\rho_{\text{solid}}} = 1 - \frac{1512}{3360} = 0.55$. It is

shown as dotted line in the Figure 2-8.

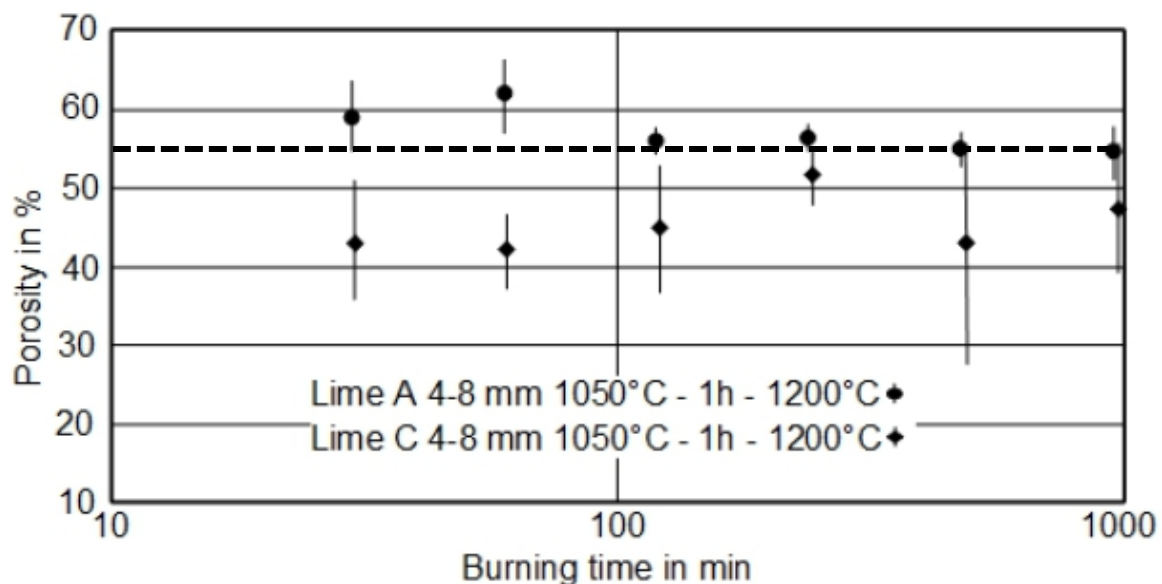


Figure 2-8: Porosity of two different limes (Wolter [41])

2.11 Emissivity

Emissivity of lime and limestone is measured by very few researchers in the literature. Hild K and Mitt K. [1932] [42] have measured the lime emissivity as 0.23 at 900°C. Hills [43] has used the value 0.27 at 832 °C for calculating the effective heat transfer coefficient. W.Lipinski and A. Steinfeld [2003] [44] used emissivity of lime as 0.41 for wavelength below cut off wavelength and 0.59 for wave lengths above cut off values. It is not clear that what exactly cut off wavelength means. Bauer [45] measured the spectral and overall emissivity of lime and it is shown in the below Figures 2-9 and 2-10 respectively.

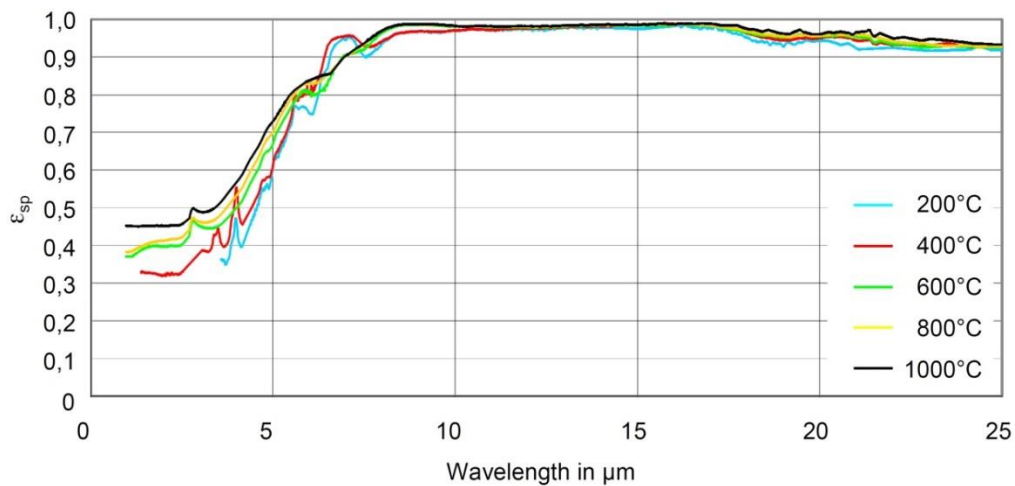


Figure 2-9: Spectral emissivity of a pure lime [45]

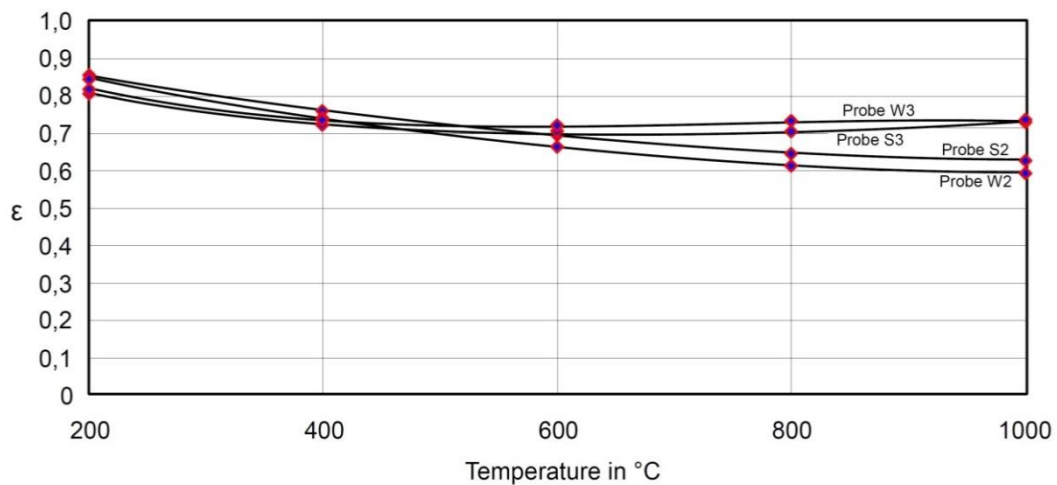


Figure 2-10: Emissivity of a lime from literature [45]

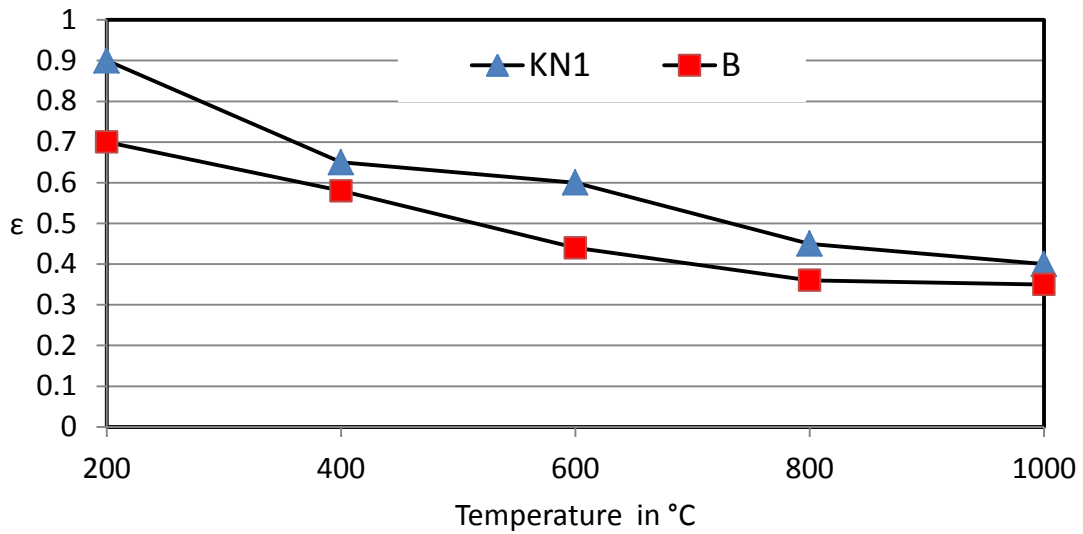


Figure 2-11: Emissivity of lime used in the present work [45]

Figure 2-11 shows the emissivity measurement analysis has been carried out for the couple of limestone samples used in the current study with the help from Prof. Bauer from the University of Düsseldorf. For these samples emissivity is found to be varied from 0.4 to 0.35 at higher temperatures.

2.12 Tortuosity

During the calcination the evacuation of CO_2 gas causes the evolution of pores in the calcium oxide region. Tortuosity is defined as the length of such pore to the real distance between the ends of the pore. Generally these pores can be assumed as a curved tube, where the length of this curve is much higher than real distance between two of its ends. Tortuosity (τ) can be defined as

$$\tau = \frac{C}{L}$$

Where C is the total length of the pore and L is the distance between its ends. This parameter is important in defining the pore diffusion solids. Very few authors discussed

about this parameters in the literature. Campbell et al. (1969) [14] have assumed τ as 1.5 for their model and found good agreement with the diffusion experiments conducted by them. T. Rajeswararao [46] has determined the value of τ as approximately 2. They have conducted the experiments with carbonate and oxide solid pellets to determine the effective diffusivities. Saiterfield C. N. and Sherwood T. K., [47] in their book on “Role of Diffusion in catalysis” mentioned the τ can be approximately regarded as 2 in the oxide layer. Hills 1968 [43] also used τ as 2. M.S. Murthy [18] 1994, also used its value as 2. Current research focusses on detrermining this Tortuosity value for limes of different origin.

2.13 Permeability

Permeability coefficient has been used by many researchers to describe the Darcy flow in the porous structure of the lime layer. However there is no standard value for the lime layer was found in the literature. Radilla et al. [48] measured the permeability values for the Lavoux limestones and they found it is in the range from $0.2 \cdot 10^{-12} \text{ m}^2$ to $0.3 \cdot 10^{-12} \text{ m}^2$. Takkinen et al. [49] used it as $1 \cdot 10^{-10} \text{ m}^2$ for their calculations. Lech [50] measured permeability of oxide layer for various limestone and found that it is in the order of 10^{-15} m^2 . In the present work, model predicted permeability has been used with Darcy model for the decomposition analysis of limestone in CO_2 environment.

2.14 Conclusions and Summary

Several researches over the decades have been working with lime calcination process. Various methods and models have been proposed and applied for the solid decomposition process. However, the objective for each and every researcher is not one and the same. Few researchers concentrated only on the kinetics and ignored the heat and mass transfer effects. Many of these researchers worked with decomposing micro meter size lime particles where they applied particle model or grain model and didn't attempt to study the conduction and diffusion effects inside the particles which take place in real time decomposition process in lime industries. Relatively very few literature have been found

for the relatively large particle decomposition process and they studied the properties such as reactivity, conductivity and diffusivity, but the equilibrium decomposition pressure that they have taken for their models is not convincing and hence the properties measured cannot be correct. Various parameters for the calcination process such as reaction coefficient, thermal conductivity, diffusion coefficient, mass transfer coefficient, tortuosity, porosity, permeability and other important parameters from various authors have been reviewed and reported in this chapter. Apart, Stefan flow effect which occurs during high temperature calcination is not considered by any of the earlier authors.

Present work mainly focuses on the study of the lime decomposition process for the relatively large size particles where all the five possible resistances mentioned in the previous section are significant. The effect and the influence of these resistances on the decomposition process have been studied. During high temperature decomposition process, due to high pressure gradient between the reaction front and the surface of the particle, there would be additional flow of CO₂ gas takes place in addition to the expected molecular diffusion, which can be termed as Stefan flow. The effect of this Stefan flow has been incorporated along with the molecular diffusion coefficient proposed by earlier authors. Determination of the thermo physical material properties of the lime from different origins is one of the main goals of this thesis. Sensitivity of the process parameters or resistances on the particle size has been studied.

Chapter 3

Thermo gravimetric experiments

3.1 Experimental Method

The experimental setup for conducting the thermo gravimetric experiments is shown schematically in the Figure 3-1. This laboratory kiln is 120 cm in length and its diameter is 8 cm. This column can be electrically heated up to 1200 °C. With this equipment, calcination reaction can be carried out up to maximum of temperature of 1200°C. In order to have well-defined flow conditions around the specimen, air is introduced from the bottom of the furnace with a known volumetric flow rate. This air is passed through a bed of solid particles to ensure a proper distribution of the air flow. There exists a control system to adjust the airflow rate as required. This air flow takes away the CO₂ released during the decomposition reaction and accumulated around the specimen. This continuous flow of air maintains the atmospheric conditions around the specimen. Using the electrical heating system, a constant and fixed temperature can be maintained inside the column. Desired constant temperature in the column is ensured before the particle is inserted into the column.

Limestone is drilled in to desired cylinders of 14 to 33 mm in diameter and minimum length is ensured to have at least four times the diameter. A hole of 1 mm in diameter is drilled at the center of this specimen to a depth of 2-3 cm to insert a thermocouple later during the experiment. The cylindrical particle (specimen) is hanged with a weight balance to measure the weight loss during the decomposition process. A thermocouple installed at the center of the cylinder records the core temperature. During the experiment the weight loss as well as the core temperature is simultaneously recorded. Top and bottom parts of the specimen are sealed with inert material as shown in the Figure 3-2, in order to ensure the heat transfer to occur only in the radial direction. There are two other thermocouples also installed in the furnace to measure the electric coil temperature and also the bed temperature.

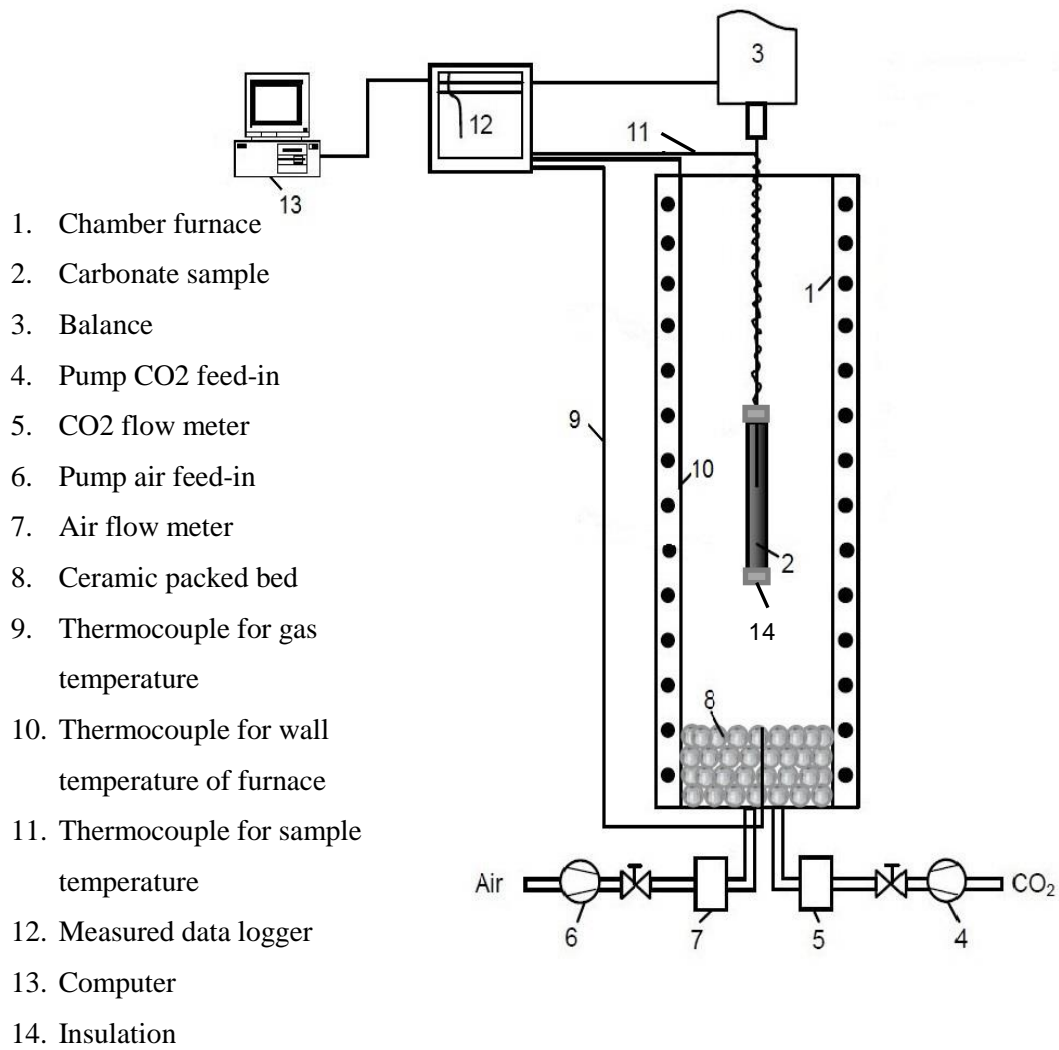


Figure 3-1: Schematic diagram of the experimental setup



Figure 3-2: Insulated specimen at top and bottom

3.2 Experimental Measurements

3.2.1 Temperature and conversion profiles

During the experiment, core temperature and the weight loss are measured simultaneously. Conversion degree has been calculated from the measured weight loss. Conversion degree at any given time is defined as the extent of CO₂ gas that already left from the limestone to the total amount of CO₂ gas that initially exists in the reactant limestone. At the end of the calcination reaction, limestone totally converts into lime (CaO) and hence conversion degree would be equal to one.

In Figure 3-3, the blue dotted curve shows the core temperature variation with respect to the time for the limestone sample named F2-i, when the experiment is conducted in the ambient temperature at 1050 °C. It can be seen that initially the core temperature rises rapidly till it reaches decomposition temperature before the calcination begins. This initial heating period is called preheating (represented as zone 1 in the figure). This specimen took approximately 7 minutes for the core temperature to reach 900 °C and attain a steady phase. During the calcination reaction, the curve maintains a steady temperature level (decomposition temperature) shown as zone 2 in the below figure and after the reaction is completed, the particle temperature suddenly rises and reaches to the ambient temperature. This phase of heating is termed as post heating and it represented as zone 3. Once the post heating is completed, it maintains constant temperature equilibrium with the ambient temperature which is represented as zone 4 in the figure. The pre and post heating time periods are very less compared to the time taken for the intermediate calcination period.

The green curve (line- dotted curve) shows the conversion degree (right Y-axis), based on the weight loss measured during the limestone decomposition with time on the X-axis. By comparing these two curves, it can be seen that approximately 20% of the conversion has been completed in the first 7 minutes of the calcination i.e. during the preheating period. This is because surface reaches decomposition temperature much earlier and certain degree of reaction takes place at the surface of the particle even before the core reaches the decomposition temperature. Once the full-fledged reaction has established at the

exterior of the particle, further heat transfer to the interior of the particle is not possible as the enthalpy of reaction is many times greater than the internal energy and the heat supplied is fully utilized as enthalpy of reaction and hence a steady core temperature has been maintained till the end of calcination.

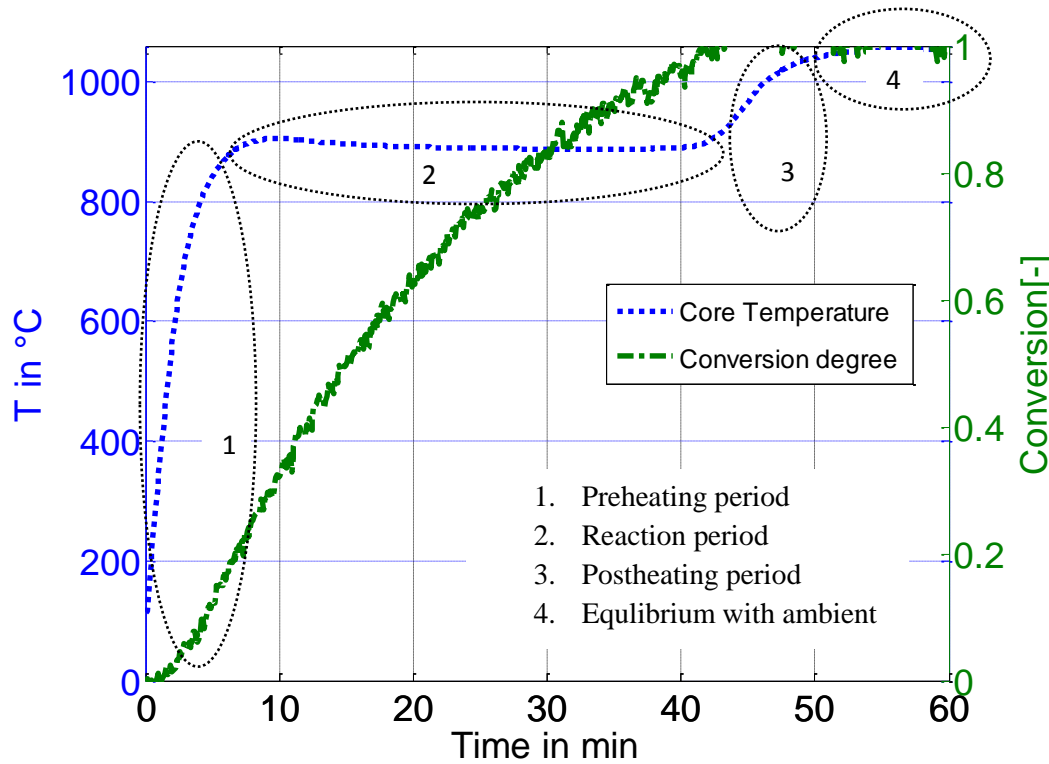


Figure 3-3: Temperature profile for the Limestone sample F2-i

3.2.2 Experiments at different ambient temperatures

Rate of calcination reaction is mainly driven by the ambient temperature. At high temperatures the equilibrium partial pressure of CO_2 is higher and decomposition takes place at higher temperatures but at faster rate. Experiments have been conducted with several samples and at different ambient temperatures. The measurement of the calcination behavior of samples at three different temperatures have been demonstrated in the below paragraphs.

Figure 3-4 (a) and (b) show the comparison of temperature and conversion profiles for the limestone F1-iii at three different ambient temperatures 1061, 955 and 900°C respectively. Time for calcination for these three cases are 60, 120 and 180 minutes respectively. The calcination time can be perceived from either of the temperature or conversion profiles, whereas calcination temperature and the difference in the decomposition temperature can be clearly seen in the temperature profile (Figure 3-4 (a)). From this Figure3-4 (a) , calcination temperatures can be approximately depicted as 915, 875 and 860°C for the decomposition experiments carried out at 1061, 955 and 900°C respectively.

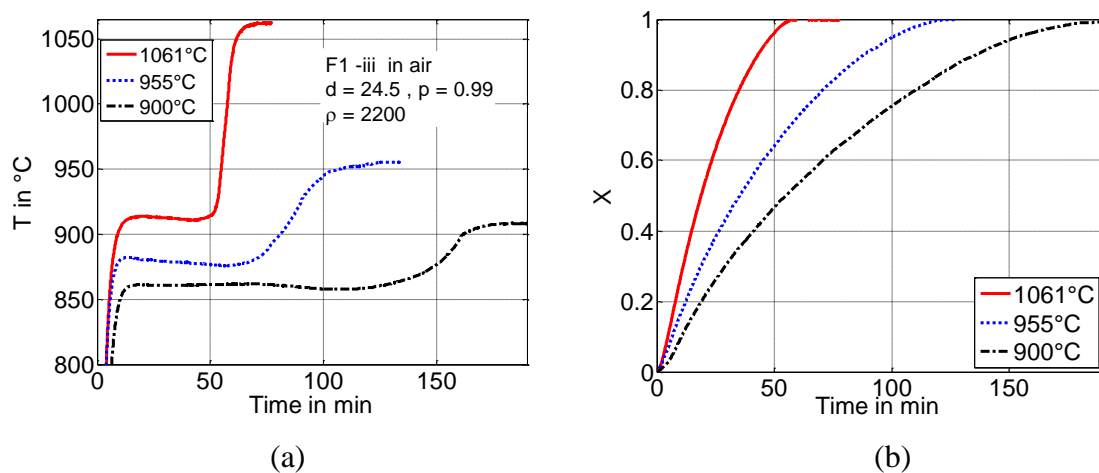


Figure 3-4 Comparison of temperature (a) and conversion (b) profiles of sample F1-iii at three different temperatures

3.2.3 Experimental profiles reproducibility

As the analysis is based on the core temperature variation especially during the calcination phase, entire analysis and further determination of material properties depends on the shape and behavior of the reaction zone of the curve. A difference in core temperature variation and the behavior of the curve is explained based on the material properties and the ambient experimental conditions. So it has been taken care to attain the most accurate profiles by minimizing the possible experimental errors. To ensure the

accuracy of the measured decomposition profiles, few experiments have been repeated with the sample from the same stone and at the same experimental conditions. Almost the same profiles have been reproduced in these cases. Below Figure 3-5 is an example of reproducibility.

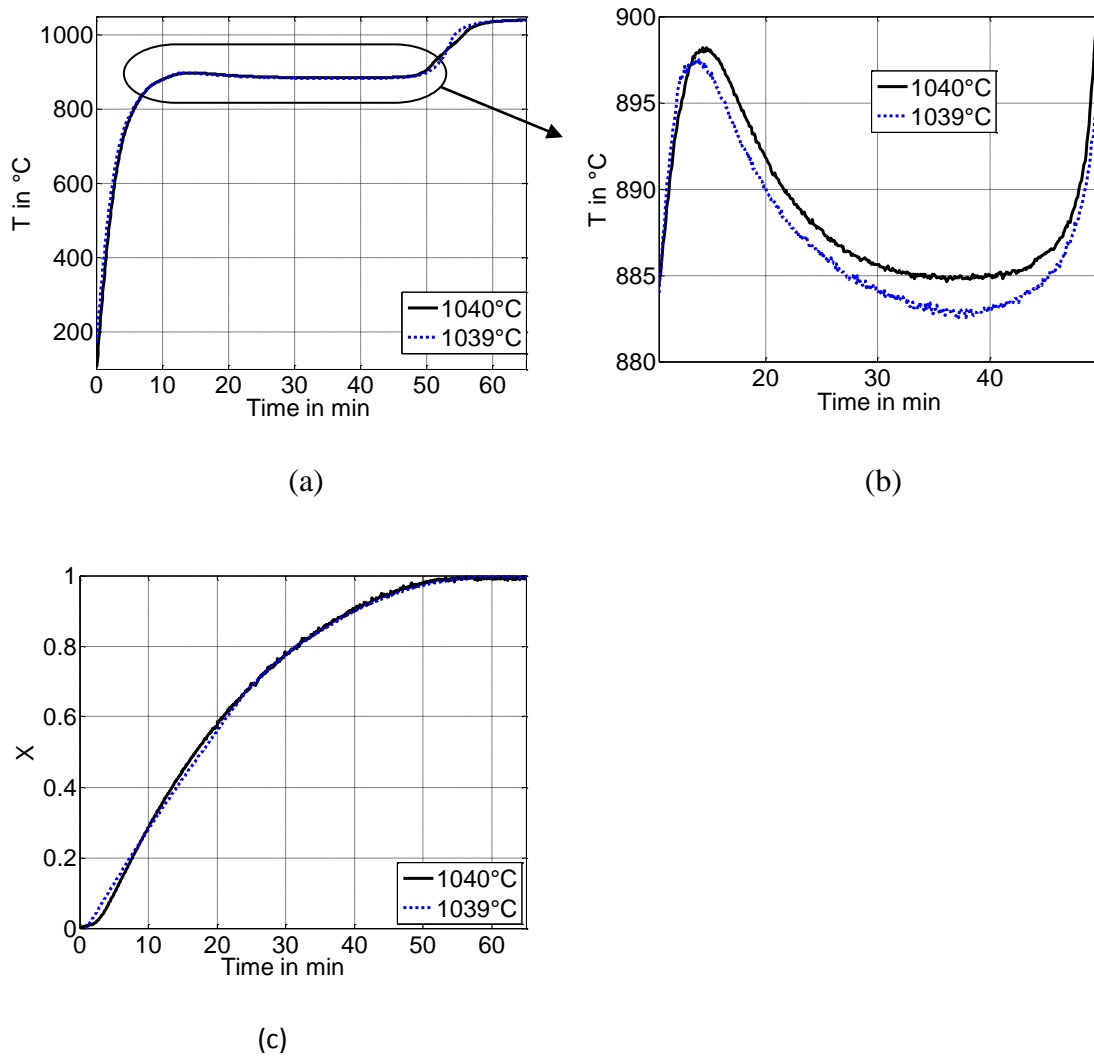


Figure 3-5 : Compares the temperature (a),(b) and conversion (c) profile for the experiment conducted and repeated at the same temperature for the sample 8mu2

Figure 3-5 (a) compares the temperature profile of the experiment conducted and repeated at the same temperature for the sample 8mu2. First time experiment is conducted at 1040°C and the same experiment is repeated. (Expected to maintain the same ambient temperature, but could not achieve exactly the same temperature, but maintained at 1039°C). However these two profiles are assumed to be at same conditions. From this

Figure it is clearly seen that, these profiles are exactly matching except that around 1K difference in temperature has been noticed when the experiment is repeated. Such a minute change in measurements are not necessarily to be considered. Figure 3-5 (b) compares the conversion profiles for this experiment. The conversion profiles measured for both the times are matching.

3.2.4 Experiments with samples from different origins

Limestone physical and thermal properties change from one stone to another and with stone from different origins. This difference in properties causes difference in calcination behavior and hence the different patterns in temperature and conversion profiles. In this section, variations in calcination behavior for limestone of different origins have been studied. Even though the experimental conditions are the same for all the five different samples decomposed, a significant change is observed in the temperature and conversion profiles as shown in the below Figure 3-6. In the Figure 3.6 (a), the temperature profiles of these samples are shown. Figure 3-6 (b) shows the close view of the reaction part of the complete core temperature profiles. In this Figure, it is clearly observed that the samples KN1 and D decompose at relatively high temperature (between 910-920°C) and needs longer time for the calcination. For other samples 1mu1, A and F2-i, though the reaction temperature level appears to be lower (between 885-900°C), but a difference in shape of the curve can be clearly observed. These differences can be explained based on the material properties for these samples. Figure 3-6 (C) compares the measured conversion profiles for these five different samples. It can be clearly seen that the extent of conversion is quite different for different samples in spite of all these samples are decomposed at the same conditions. For example at 20 min time, sample A shows 75% conversion, whereas the sample 1mu1 shows 70% conversion. However decomposition degree of other three samples are only around 60%. It can also be observed that the samples A and 1mu1 required only 40 minutes for complete decomposition whereas other three samples took approximately 60 minutes for complete calcination. In the next chapters mathematical models have been developed to study the variation in this calcination behavior and explained these discrepancies based on the thermo physical properties of the respective limestone.

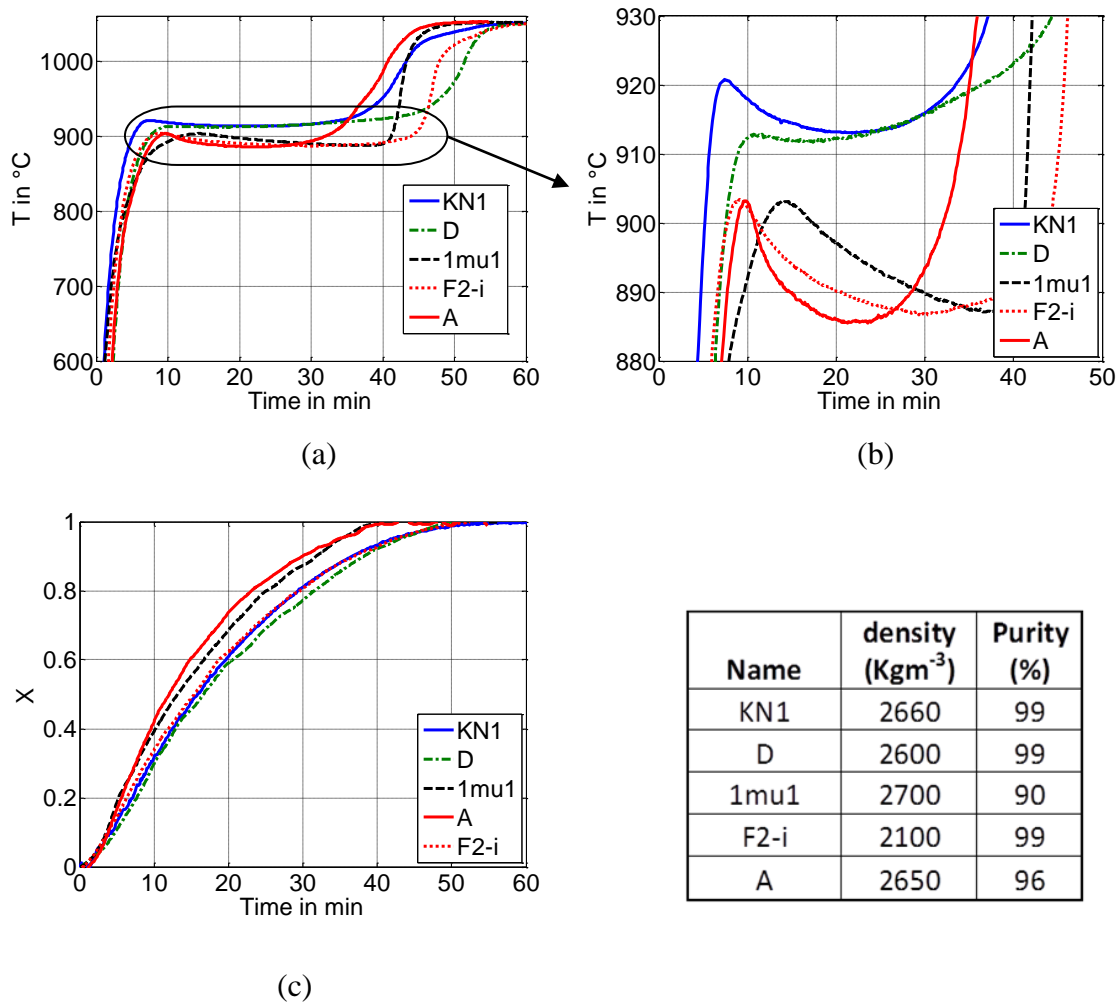


Figure 3-6 : Comparison of temperature profiles of different samples at same conditions

3.2.5 Experiments with samples of different size

Experiments have been conducted with samples of different size. Experimentally measured temperature and conversion profiles have been compared for the same stone at two different cylindrical diameters. Limestone sample D has been cut in to two cylinders with diameters 24.5 mm and 32.4 mm. These two samples have been decomposed at the same experimental conditions and at same ambient temperature 1050 °C. Figure 3-7 compares the temperature (a) and conversion (c) profiles respectively. As expected, larger particle took longer calcination time (80 minutes) and the smaller one took shorter time (50 minutes) respectively. However the calcination temperature is almost the same for these two samples. In the close view profile (b), it can be seen that smaller particle

reaches the peak in 10 minutes whereas the bigger particle takes 15 minutes. This difference is because bigger particle needs longer duration for the pre heating. But the calcination temperature for both of these samples is in between 910-920 °C and also the same trend has been noticed.

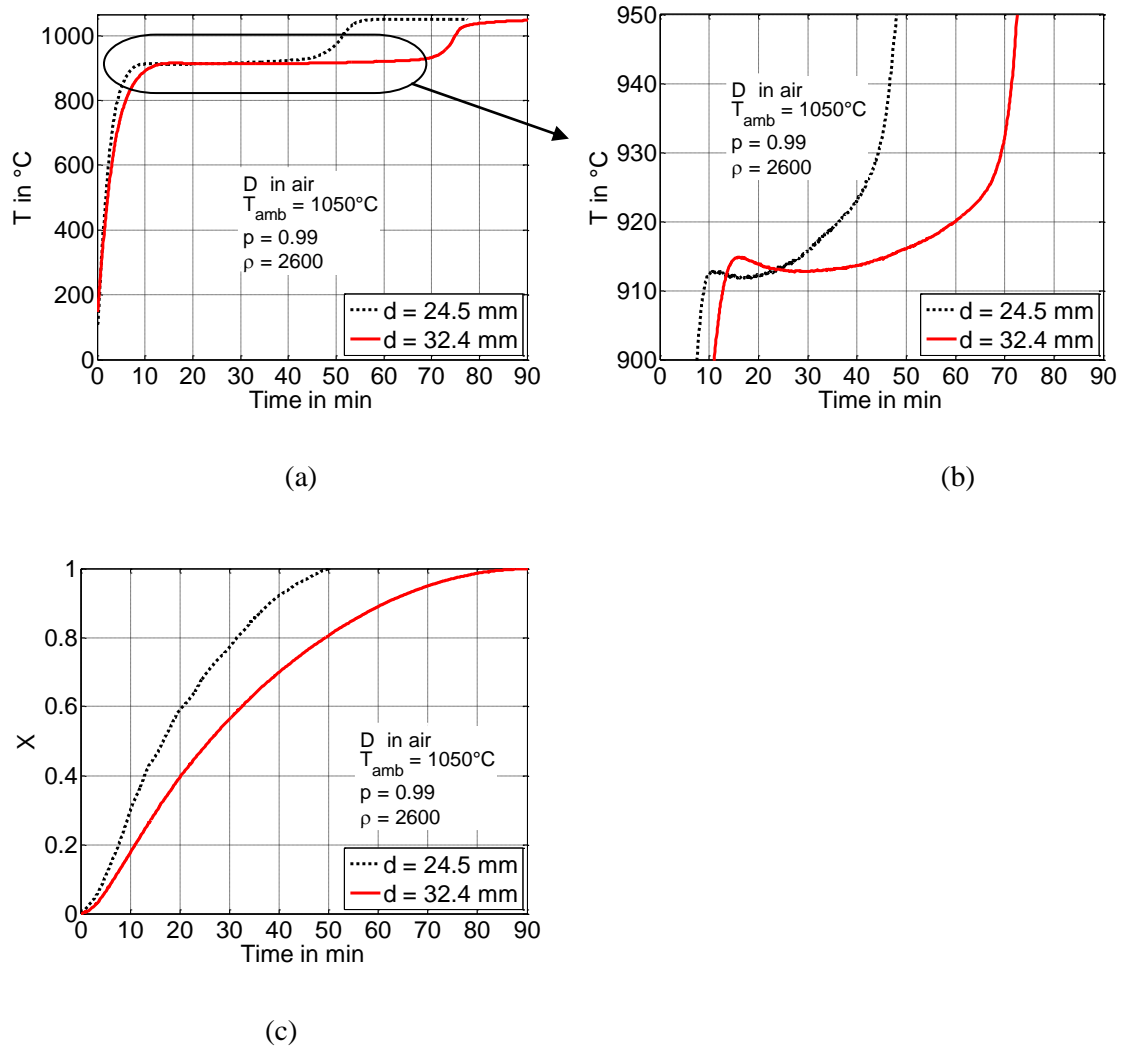
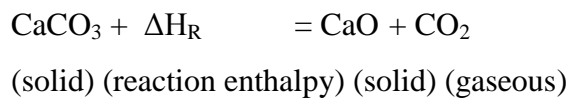


Figure 3-7: Comparison of temperature (a) and conversion (c) profiles for the sample D at different particle size

Decomposition Models and Experimental comparisons

4.1 Limestone quasi stationary decomposition model

The decomposition of limestone is an endothermic topochemical reaction described as follows



The calcination process can be explained by using a partially decomposed piece of carbonate. Calcination profiles of CO₂ partial pressure and temperature are shown in Figure 4-1. The specimen comprises a dense carbonate core surrounded by a porous oxide layer. In the calcination reactor at temperature T_g heat is transferred by radiation and convection (symbolized by α) to the solid surface at a temperature of T_s. By means of thermal conduction (λ) heat penetrates through the porous oxide layer to reach the reaction front, where the temperature is T_f. As the reaction enthalpy is many times greater than the internal energy, the heat flowing further into the core is negligible during reaction. Therefore, the core temperature is only slightly lower than the front temperature. Once heat is supplied, the chemical reaction (k) then takes place, for which driving force is the deviation of CO₂ partial pressure from the equilibrium (p_{eq}- p_f). The released CO₂ diffuses (D_p) through the porous oxide layer to the surface and finally passes by convection (β) to the surroundings where the CO₂ partial pressure p_g exists. The four physical transport processes and the chemical kinetics involved are therefore interconnected. In order to determine the decomposition of a single limestone particle, a one-dimensional shrinking core model was established by Kainer et al. [3], which is based on the assumptions of an ideal sample geometry (sphere, cylinder or plate), a pseudo steady state condition and constant material properties. A system of heat and mass

balance equations, which are used to calculate the decomposition of limestone, are given as follows

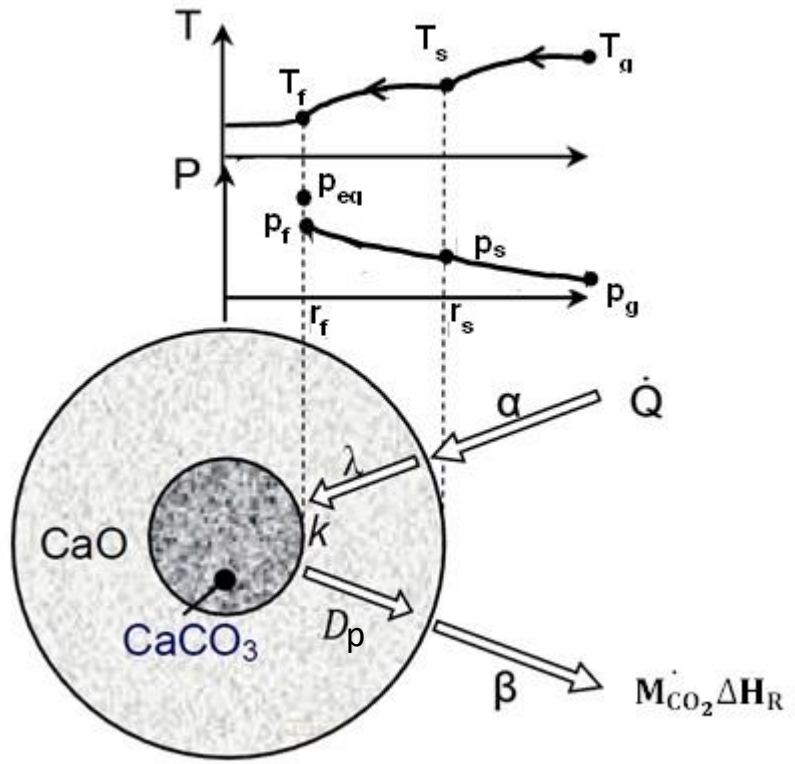


Figure 4-1: Decomposition model of cylindrical limestone particle

Radiation and convection heat transfer from the kiln wall to the surface of the particle is given by

$$\dot{Q} = (\sigma \cdot \epsilon \cdot (T_F^4 - T_s^4) - \alpha_{\text{conv}} \cdot (T_s - T_g)) \cdot 2\pi r_s L \quad (4.1-1)$$

The heat balance equation (e.g., for cylinder) is obtained by heat conduction from the particle surface through the lime layer to the reaction front.

$$\dot{Q} = \frac{2\pi L \lambda \cdot (T_s - T_f)}{\ln\left(\frac{r_s}{r_f}\right)} \quad (4.1-2)$$

The heat flow rate and mass flow rate of CO₂ are related by

$$\dot{Q} = \dot{M}_{\text{CO}_2} \cdot \Delta H \quad (4.1-3)$$

The dependence of equilibrium pressure upon the front temperature is described as

$$p_{\text{eq}} = p_{\text{eq}0} \cdot \exp\left(\frac{-\Delta\tilde{H}_R}{\tilde{R} \cdot T_f}\right) \quad (4.1-4)$$

where $\Delta\tilde{H}_R$ is the molar reaction enthalpy, 164 kJ/mol at 900°C,

\tilde{R} the universal molar gas constant, 8.314 J/(mol·K),

T_f is the reaction front temperature, K, and

$p_{\text{eq}0}$ is the pre-exponential coefficient, or frequency factor, 1.7441×10^7 bar.

For the reaction at the front, the reaction rate is proportional to the deviation of partial pressure at the front to that of the equilibrium pressure

$$\dot{M}_{\text{CO}_2} = \frac{k \cdot (p_{\text{eq}} - p_f)}{R_{\text{CO}_2} \cdot T_f} \cdot 2\pi r_f L \quad (4.1-5)$$

The rate of diffusion of CO₂ in the porous oxide layer is given by

$$\dot{M}_{\text{CO}_2} = \frac{P \cdot D_p}{R_{\text{CO}_2} \cdot T_f} \cdot \frac{2\pi L}{\ln\left(\frac{r_s}{r_f}\right)} \cdot \ln\left(\frac{P - p_s}{P - p_f}\right) \quad (4.1-6)$$

Where D_p is the pore diffusion coefficient, for a solid with porosity ψ and tortuosity τ and at a higher temperature T , it can be written as below

$$D_p = D_{\text{CO}_2\text{-air}} \cdot \left(\frac{T}{T_0} \right)^{1.77} \cdot \frac{\Psi}{\tau} \quad (4.1-7)$$

$D_{\text{CO}_2\text{-air}}$ is the binary diffusion coefficient for CO₂ in air atmosphere at room temperature T_0 .

The above equation (4.6) is obtained by combining the molecular diffusion and bulk flow together. The derivation of the above equation is explained in the next section 4.3.

The Diffusion of CO₂ from the surface of the particle to the ambient environment is written as

$$\dot{M}_{\text{CO}_2} = \frac{\beta \cdot (p_s - p_g)}{R_{\text{CO}_2} \cdot T_f} \cdot 2\pi r_s L \quad (4.1-8)$$

The mass flux of CO₂ can be expressed as the product of CO₂ concentration to the rate at which the core shrinks and the front area.

$$\dot{M}_{\text{CO}_2} = -K_{\text{CO}_2} \cdot \frac{dr_f}{dt} \cdot 2\pi r_f L \quad (4.1-9)$$

where K_{CO_2} is the fraction of CO₂ in limestone, e.g. 1190 kgCO₂/m³ for a pure limestone with a density of about 2700 kg/m³.

The conversion degree X is defined as the ratio of the total mass of reacted CO₂ to the mass of CO₂ content in the limestone

$$X = \frac{M_{\text{CO}_2(R)}}{M_{\text{CO}_2(t=0)}} \quad (4.1-10)$$

It can be defined in another way related to the moving front with time dependency as

$$X = \frac{M_{\text{CO}_2(t=0)} - M_{\text{CO}_2(t=0)}}{M_{\text{CO}_2(t=0)}} = 1 - \left(\frac{r_f}{r_s} \right)^2 \quad (4.1-11)$$

Combining equations 4.9 and 4.11, we get

$$\dot{M}_{\text{CO}_2} = -K_{\text{CO}_2} \cdot \frac{dX}{dt} \cdot \pi r_s^2 L \quad (4.1-12)$$

The above system of algebraic equations have been solved simultaneously for the unknown parameters (T_f , T_s , X , r_f , \dot{M}_{CO_2} , \dot{Q} , p_f and p_s).

4.2 Radiative heat transfer

4.2.1 Effective emissivity

Cylindrical limestone particle is hanged inside the tube furnace during decomposition. Radiative heat transfer from the inner wall of the tube furnace to the surface of the specimen which is hanged at the center of the furnace is considered as the case of ‘radiative heat transfer between the two concentric cylinders’.

Assuming the limestone particle as cylinder 1 and tube furnace as cylinder 2, the effective emissivity is given by

$$\varepsilon = \frac{1}{\frac{1}{\varepsilon_1} + \frac{A_1}{A_2} \left(\frac{1}{\varepsilon_2} - 1 \right)} . \quad (4.2-1)$$

Where ε_1 , ε_2 , A_1 and A_2 are emissivity and surface areas of lime and the tube furnace respectively. When the limestone specimen is suddenly exposed to the furnace at very high temperatures (temperature much higher than decomposition temperature), the time for reaction to begin on the surface of the particle is much smaller compared to total time of decomposition, hence the inner cylinder emissivity can be assumed as emissivity of lime itself.

4.2.2 Estimating the furnace wall emissivity

In order to predict the radiation heat transfer to the particle as accurate as possible which is very important and plays a significant role in modeling the complete calcination behavior, it is essential to study the emissivity of the tube furnace (used for decomposition experiments) accurately. To study the emissivity of the furnace wall, experiments have been conducted with steel cylinders of two different diameters as shown in the Figure 4-2. Steel cylinder 1 is 24.5 mm in diameter with 130 mm in length and steel cylinder 2 is 44.5 mm in diameter with 200 mm in length. Steel cylinder 2 is approximately double the diameter compared to the small steel cylinder. So steel cylinder 1 is termed as small cylinder and the steel cylinder 2 is termed as big cylinder in further discussion. Length to diameter ratio for both of these cylinders has been chosen to be

greater than 4, so that one dimensional heat transfer analysis can be applied without loss of desirable accuracy. In addition to this, top and bottom surfaces of both of these cylinders have been insulated during heating or cooling for further accuracy. The emissivity of these steel cylinders has been determined in the first place in order to determine the furnace wall emissivity. A hole of diameter 1 mm is drilled at the center for these two cylinders till the middle point (in the axial direction) and thermocouple is inserted through this hole.

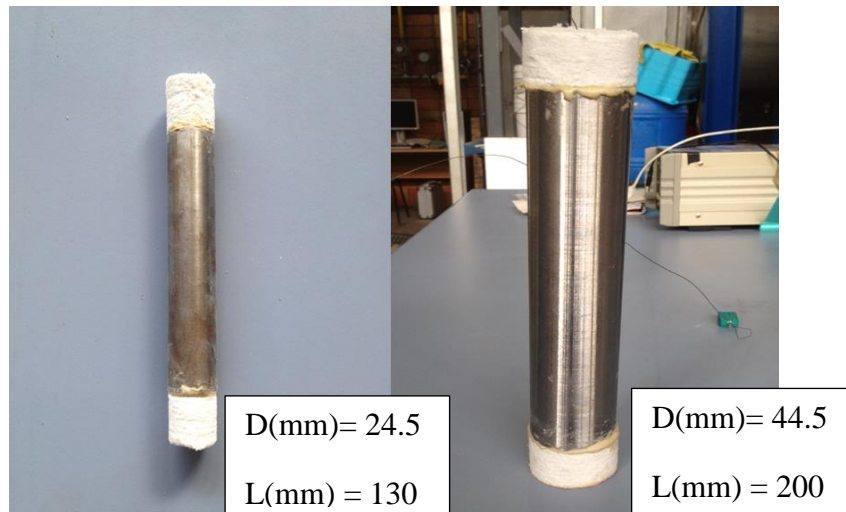


Figure 4-2 Small and big steel cylinders with insulations

These cylinders have been hanged inside the tube furnace (for which emissivity has to be estimated) which is maintained at a constant temperature of 600°C.

The thermocouple inserted at the center of the steel cylinder measures the increase in the core temperature. This temperature profile has been regarded as heating curve in further discussion. When the core reaches the ambient temperature (600°C in this case) that means when it reaches the steady state, the cylinder has been taken outside from the furnace and again the decrease in temperature of the core when the cylinder is suddenly exposed to the room temperature has been recorded. This temperature profile has been regarded as the cooling curve in the following paragraphs.

These steel cylinders have been heated and cooled several times and the core temperature profiles in these cases have been recorded. After first heating, the surface of the steel cylinder slightly oxidizes on the surface and turns to brownish in color and results in relatively rough surface texture. This causes change in emissivity of the surface.

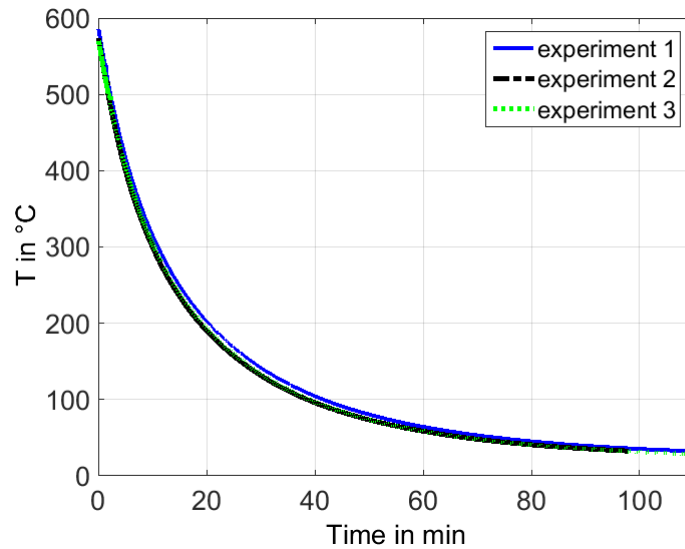


Figure 4-3 Natural convective core temperature profiles of small steel cylinder

The above Figure 4-3 shows the core temperature profiles of the small steel cylinder when it is exposed to natural convection cooling at room temperature. Blue curve shows the cooling profile when the cylinder is only one time heated to 600°C. Black and Green dotted curves show the cooling profiles of the same cylinder when it was heated 2nd and 3rd time. Initially the smooth and shiny surfaced cylinder has lower emissivity causes relatively slow cooling rate but for the later surface emissivity slightly changes and hence the 2nd and 3rd curves show much faster cooling profiles. These black and green curves show the emissivity is slightly increased and reaches to a constant value after 3rd heating. However the differences are not so clearly visible in the above Figure 4-3.

By solving the one dimensional unsteady state heat conduction equation in cylindrical coordinates (Equation 4.2-2) with proper initial (Equation 4.2-3) and boundary conditions (Equation 4.2-4 and 4.2-5) and with an approximate natural convection heat transfer coefficient for this case, similar cooling core temperature profiles can be predicted as in shown the Figure 4-4. It compares the experimentally measured and predicted temperature profiles of this steel cylinder. Using this model comparison, emissivity of the steel cylinder can be estimated.

$$\frac{\partial T}{\partial t} = \frac{\lambda}{\rho \cdot c_p} \cdot \left(\frac{\partial^2 T}{\partial r^2} + \frac{1}{r} \frac{\partial T}{\partial r} \right) \quad (4.2-2)$$

$$T \text{ (at all nodal points)} = 600 \text{ }^\circ\text{C} \quad (4.2-3)$$

$$-\lambda \cdot \frac{\partial T}{\partial r} = \left(\sigma \cdot \epsilon \cdot (T_S^4 - T_g^4) + \alpha_{\text{conv}} \cdot (T_S - T_g) \right) \cdot 2\pi r_s L \quad (4.2-4)$$

$$-\lambda \cdot \frac{\partial T}{\partial r} = 0 \quad (4.2-5)$$

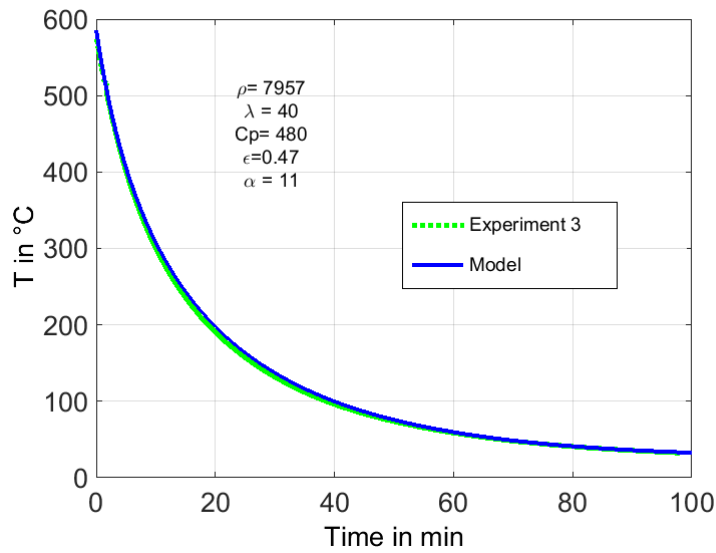


Figure 4-4 : Measured and predicted core temperature profiles of small steel cylinder

In the same way cooling experiments were carried out with same steel material but one with the bigger diameter. The resultant cooling curves are shown in the below Figure 4-5. From this Figure it can be clearly seen that, second and third cooling, results in almost matching curves when the emissivity reaches to a constant value.

One dimensional unsteady state heat conduction equation in cylindrical coordinates has been solved in this case as well to compare the measured profile and there by to find out the emissivity. Figure 4 -6 shows the measured and predicted cooling profiles for the big steel cylinder. Using this comparison emissivity of the steel cylinder can be determined.

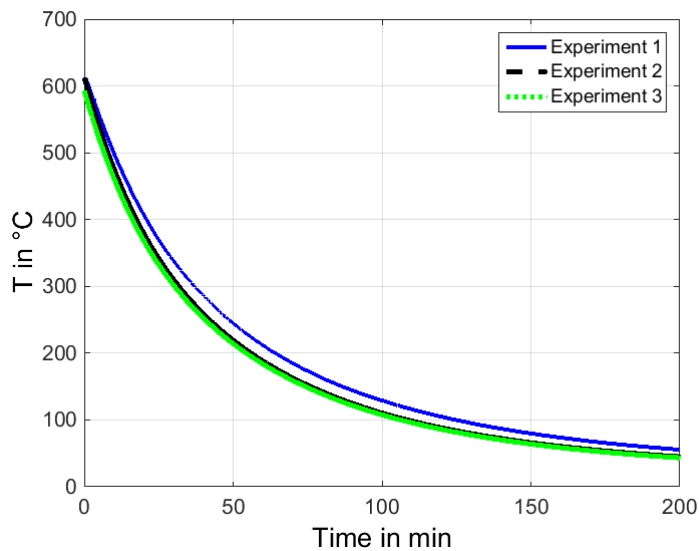


Figure 4-5 :Natural convective core temperature profiles of big steel cylinder

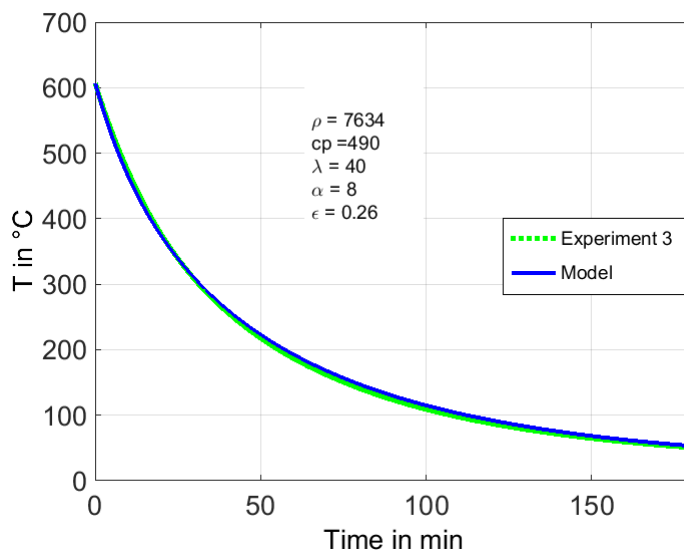


Figure 4-6 :Measured and predicted core temperature profiles of big steel cylinder

With the help of the cooling curves, emissivity of steel cylinder is found to be in the range from 0.26 to 0.47.

Below Figure 4-7 show the measured and predicted core temperature profiles for the small cylinder and Figure 4-8 shows the same for the big steel cylinder respectively when they are inserted in to the hot furnace maintained at 600 °C.

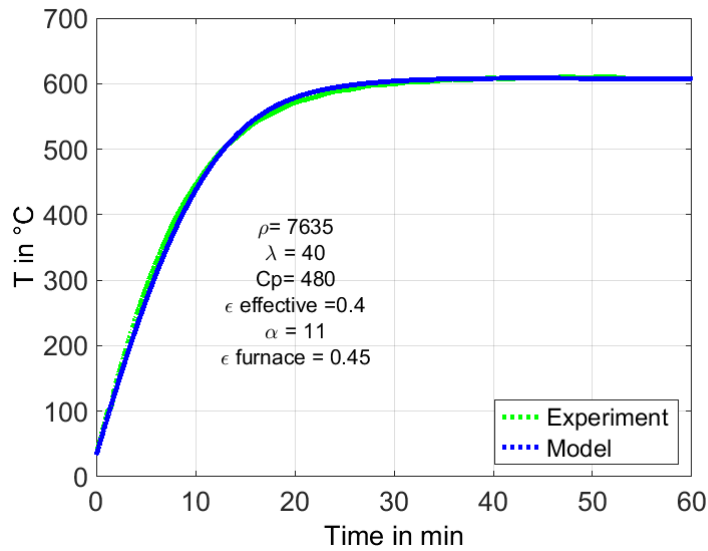


Figure 4-7 : Measured and predicted core temperature profiles of small steel cylinder

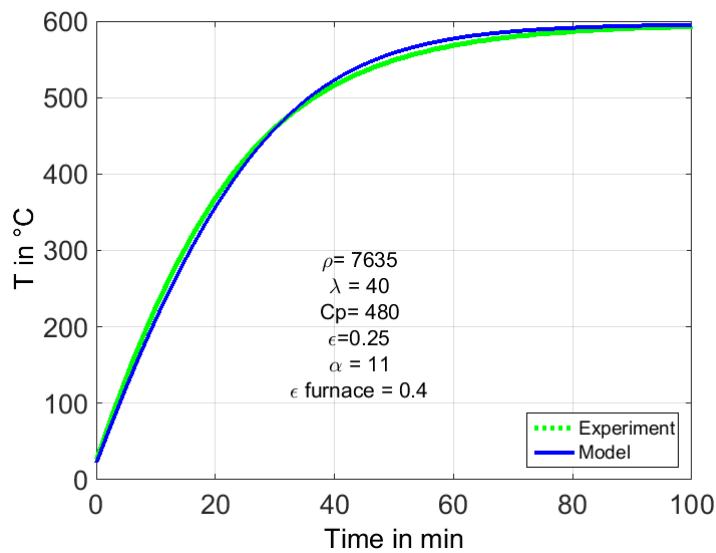


Figure 4-8 : Measured and predicted core temperature profiles of big steel cylinder

The radiative heat transfer from the furnace wall to the steel cylinder depends on the effective emissivity of the furnace inner wall and the emissivity of the steel cylinder. Steel cylinder emissivity is already predicted by using the cooling curves. From the heating curves of Figures 4-6 and 4-7, the effective emissivity is estimated. Once the effective and steel cylinder emissivities are known, the furnace emissivity is calculated by

$$\epsilon_{\text{furnace}} = \frac{1}{\left(\frac{1}{\epsilon_{\text{effective}}} - \frac{1}{\epsilon_{\text{steel}}} \right) \cdot \frac{A_{\text{furnace}}}{A_{\text{steel}}} + 1} \quad (4.2-6)$$

With the above equation furnace emissivity has been calculated as 0.4 with the big steel cylinder and 0.45 with the small cylinder. So furnace wall emissivity is estimated to be in the range from 0.4 to 0.45.

4.3 Convective heat and mass transfer coefficient

The heat transfer coefficient for the air flowing from the bottom of the furnace tube is computed with below Nusselt number correlation. This air in turn cools the sample which is heated by the radiation heat transfer from the walls of the furnace.

$$\text{Nu} = 0.644 * (\text{Re})^{0.5} (\text{Pr})^{1/3}$$

In the above equation the Nusselt number is defined as

$$\text{Nu} = \frac{\alpha \cdot d}{\lambda_g}, \text{ where } \lambda_g \text{ is the thermal conductivity of air.}$$

The Reynolds number $\text{Re} = \frac{w \cdot d}{\nu}$. ν is the kinematic viscosity of air.

In both Nusselt and Reynolds numbers, length of the cylindrical particle has been considered as characteristic dimension for calculating the Reynolds number.

Gas velocity at higher temperatures is calculated by

$$w = w_{STP} \cdot \frac{\rho_{STP}}{\rho} \text{ and the velocity at STP is given by } w_{STP} = \frac{V_{STP}}{A_F} .$$

For the given gas velocity, convective mass transfer coefficient can be computed using the Sherwood number correlation for a laminar flow in a pipe.

$$Sh = 0.644 * (Re)^{0.5} (Sc)^{1/3} .$$

In the above equation Sherwood Number is defined as

$$Sh = \frac{\beta \cdot d}{D_{CO_2-air}} , \text{ where } \beta \text{ is the mass transfer coefficient, } d \text{ is the characteristic dimension}$$

same as used in Reynolds number. The diffusivity of the CO₂ in air, D_{CO_2-Air} can be approximated with $D_o = 0.16 \cdot 10^{-4} \text{ m}^2/\text{s}$ and $n_D = 1.77$. So at higher temperatures D_{CO_2-Air} is given by [51]

$$D = D_o \cdot \left(\frac{T}{T_o} \right)^{n_D+1} .$$

Below table illustrates the heat and mass transfer coefficients for different gas temperatures [48] [53][54] in the range from 300 to 900°C for air flow rate of 7m³/hr in a tube furnace of diameter 8 cm.

T(°C)	kin.visc (m ² s ⁻¹) (.10 ⁻⁵)	Velocity (ms ⁻¹)	Dco ₂ - air (m ² s ⁻¹) (.10 ⁻⁵)	Re	Sc	Sh	β (ms ⁻¹)	λ (Wm ⁻¹ K ⁻¹)	Nu	α (Wm ⁻² K ⁻¹)
300	5	0.78	5.5	1711	0.82	25	0.014	0.043	24	10
400	6	0.922	7.4	1530	0.81	23	0.017	0.049	22	11
500	8	1.063	9.6	1392	0.80	22	0.021	0.054	21	12
600	9	1.205	11.9	1285	0.79	21	0.025	0.059	20	12
700	10	1.347	14.5	1200	0.77	20	0.030	0.064	20	13
900	20	1.701	22.0	1044	0.74	19	0.041	0.076	18	14

Table 4.1 : Probable values of heat transfer coefficients (**α**) and mass transfer coefficients (**β**) at different temperatures in the tube furnace.

4.4 Stationary Diffusion and convective diffusion inside the lime layer

During the reaction CO₂ gas releases at the reaction front surface. This released gas diffuses through the pores of the lime layer and leaves at the surface of the particle to the ambient environment. This diffusion process can be explained by Fick's law of diffusion, which is written for CO₂ gas diffusion in one spatial dimension as

$$\bar{J}_{D,CO_2} = -D_{CO_2} \frac{\partial \phi}{\partial x} \quad (4.4-1)$$

Where \bar{J}_{D,CO_2} , the mass flow rate of CO₂ diffusing per unit area, ϕ is the mass density of CO₂ and $\phi = p_{CO_2}/RT$,

$\frac{\partial \phi}{\partial x}$ is the density gradient and D_{CO_2} is the Diffusivity coefficient for CO_2 in air.

The above Fick's law defines only the mass diffusion of species which results in concentration gradient of species. In addition to the molecular or mass diffusion, there is additional flow of species takes place because of continuous evolvment of chemical species (CO_2 gas) at the interface due to chemical reaction. This additional flow is referred as Stefan flow.

So the total flux which is combination of mass diffusive flux and Stefan flow (bulk flow) is written as

$$\bar{J} = y_{CO_2} \bar{J} + \bar{J}_{D,CO_2} \quad (4.4-2)$$

Where y_{CO_2} is the fraction of CO_2 which can also be written as p_{CO_2}/P where p_{CO_2} is the partial pressure of CO_2 and P is the total pressure and for the uni molecular diffusion process (only CO_2), the net flux \bar{J} is same as \bar{J}_{CO_2} . Hence the above equation (4.5-2) can be re written as

$$\bar{J}_{CO_2} = y_{CO_2} \bar{J}_{CO_2} + \bar{J}_{D,CO_2} \quad (4.4-3)$$

The above equation can be simplified to the below form for cylinder of radius r by substituting equation 4.5-1 in the above equation

$$\bar{J}_{CO_2} = \frac{-D_{CO_2}}{R_{CO_2} T} \cdot \left(\frac{1}{1 - \frac{p_{CO_2}}{P}} \right) \cdot \frac{dp_{CO_2}}{dr} \quad (4.4-4)$$

Where R_{CO_2} is individual gas constant for CO_2 gas in J/kg/K.

The above equation (4.5-4) written for mass rate instead of mass rate flux and integrating for net mass rate from the reaction front at partial pressure p_f to the partial pressure at surface of the particle p_s , the above equation can be simplified to equation 4.5-5

$$\dot{M}_{CO_2} = \frac{P \cdot D_p}{R_{CO_2} \cdot T_f} \cdot \frac{2\pi L}{\ln\left(\frac{r_s}{r_f}\right)} \cdot \ln\left(\frac{P - p_s}{P - p_f}\right) \quad (4.1-6)$$

But the diffusion equation in its general form can be written as below

$$\dot{M}_{\text{CO}_2} = \frac{D_p^{\text{eff}}}{R_{\text{CO}_2} \cdot T_f} \cdot \frac{-2\pi L}{\ln\left(\frac{r_s}{r_f}\right)} \cdot (p_s - p_f) \quad (4.4-5)$$

The above equation accounts for the pore diffusion inside the lime layer and also for the CO₂ gas flow that is due to bulk flow (Stefan flow). So the diffusion coefficient in the above equation (4.5-5) is termed as effective diffusion coefficient. By comparing the above two equations (4.1-6) and (4.5-5), the relation between the effective diffusion coefficient and pore diffusion coefficient for CO₂ is determined as

$$D_p^{\text{eff}} = \frac{-D_p P \ln\left(\frac{P - p_s}{P - p_f}\right)}{p_s - p_f} \quad (4.4-6)$$

4.5 Measurement of pore size

It is important to know the mean pore size of the lime particle in order to use the appropriate diffusion model. Figure 1.4-3 from the Literature shows the mean pore size of various limestone samples with respect to oxide shell temperature. As it is clear from the Figure, the mean pore size of the particle varies from 10 nm to the 1 micro m and also the diffusion mechanism varies with pore size, in this research pore size measurements for the lime particles used in this work have been conducted. Quadrachrome Poremaster, automatic pore size analyzer has been used to measure the pore size. For the analysis two different limestones one with density around 2000 kg m⁻³ and the other with 2700 kg m⁻³ have been decomposed for the porosity measurement. The results show that for the high density sample pore size is in the range from 20 to 80 micro meters and for the low density sample, the range is 30 to 80 micro meter. From these two observations, the pore size is in the micro meter range and Fickian diffusion model can describe the pore diffusion mechanism.

4.6 Determination of thermal conductivity

By using the above discussed quasi-stationary and Transient models, the parameters conductivity, reaction coefficient, tortuosity of lime can be determined. In this case, heat transfer, chemical reaction and mass transport have to be considered and needs to be modelled together. There exists a slight influence of each of the parameter on others. For example, thermal conductivity determined is dependent on reaction coefficient, tortuosity and other parameters to an extent.

So a special method is developed to determine the thermal conductivity using the measured core temperature and slope of the measured conversion profiles as discussed below.

The front temperature T_f from the measured core temperature profile and slope of the conversion profile $\frac{dX}{dt}$ have been substituted in equations 4.1-2 and 4.1-12 respectively for the different conversion degrees. The three below equations

$$\dot{Q} = (\sigma \cdot \epsilon \cdot (T_F^4 - T_s^4) - \alpha_{conv} \cdot (T_s - T_g)) \cdot 2\pi r_s L \quad (4.6-1)$$

$$\dot{Q} = \frac{2\pi L \lambda \cdot (T_s - T_f)}{\ln\left(\frac{r_s}{r_f}\right)} \quad (4.6-2)$$

$$\dot{M}_{CO_2} = -K_{CO_2} \cdot \frac{dX}{dt} \cdot \pi r_s^2 L \quad (4.6-3)$$

have been solved simultaneously for the unknown variables thermal conductivity (λ) and the surface temperature (T_s). This method is independent of mass transport mechanism. It is based only on the heat transfer to the particle and the weight loss measured.

The above mentioned method is applied to Limestone sample D with diameter 25mm and density of 2600 kg m^{-3} . The bulk density is calculated based on the measured weight of cylindrical particle and its dimensions. It has been decomposed in the tube furnace which was maintained at a temperature of 1050°C . From the weight loss during decomposition, it was found that it contains 99 % calcite. So its purity is mentioned as 99% in further

discussion. Below Figure 4-9 (a), (b) shows the measured core temperature profile for this sample in full view and in close view respectively. Figure 4-9 (c) shows the measured conversion profile for the same sample. In Figure 4-9 (b), it can be clearly observed that the variation of core temperature during the decomposition reaction. Hence this portion of temperature profile has been considered as front temperature profile for the analysis of determining the thermal conductivity.

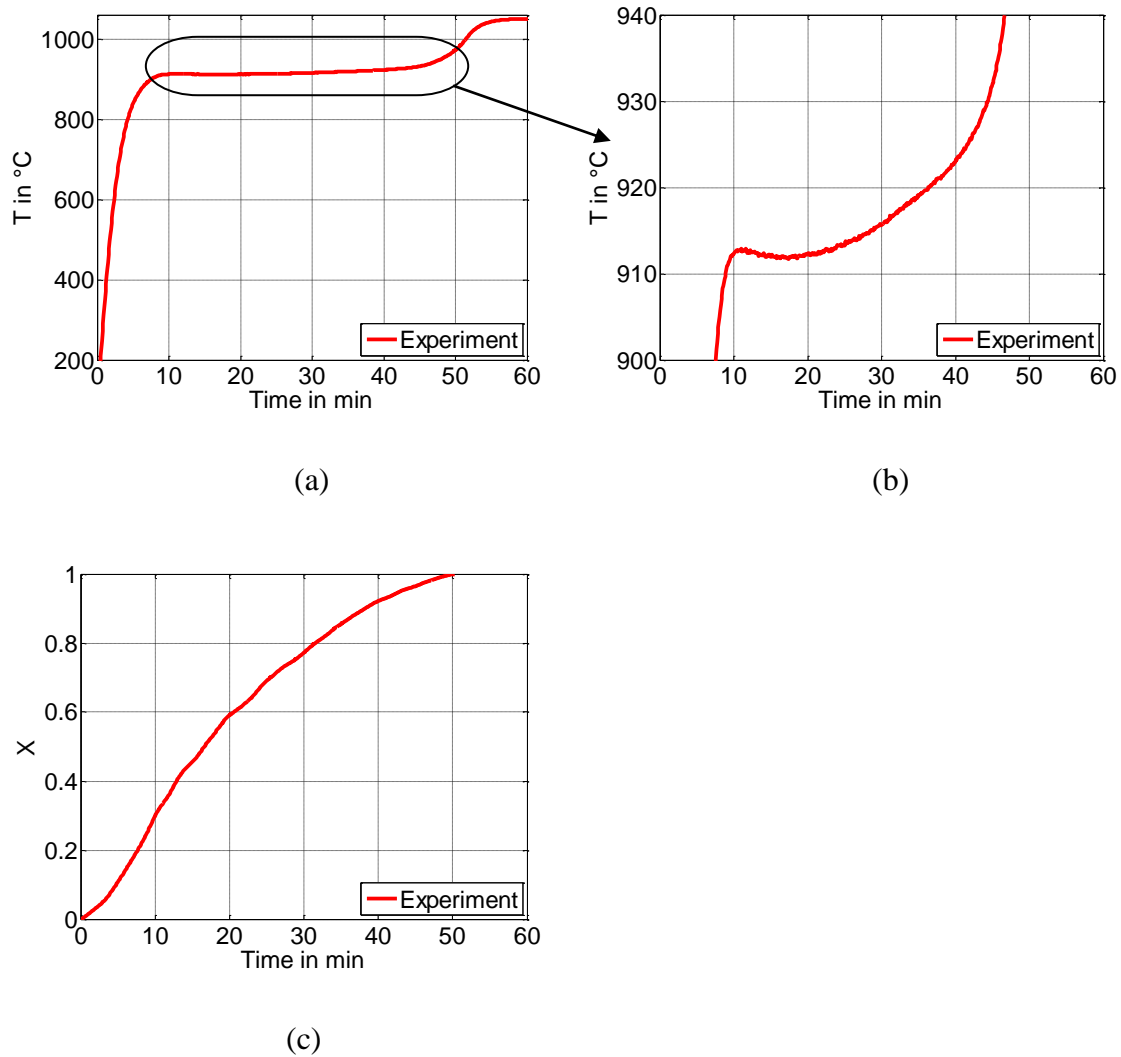


Figure 4-9: Measured temperature (a), (b) and conversion (c) profiles for the sample D

By using the front temperature at different conversion degree and the variation of slope of the conversion degree, the above mentioned equations have been solved to determine the thermal conductivity.

Figure 4-10 (a) shows the measured core temperature as a function of measured conversion degree. It can be clearly seen from this figure that till conversion reaches to 0.35, core temperature is continuously increases and also the core temperature raises with higher gradient after 80% conversion degree is completed. So, for this sample it has been considered that the core temperature as front temperature in the range of conversion degree from 0.35 to 0.8. So in this zone, thermal conductivity has been determined and it is plotted in Figure 4-10 (b) at three different effective emissivities. The thermal conductivity is found to be varying between 0.45-0.55 when the emissivity is 0.6 and conductivity increases with decreasing emissivity. Conductivity determined is very sensitive to the front temperature, and a very small errors in the experimental measurements show a considerable amount of changes in the conductivity.

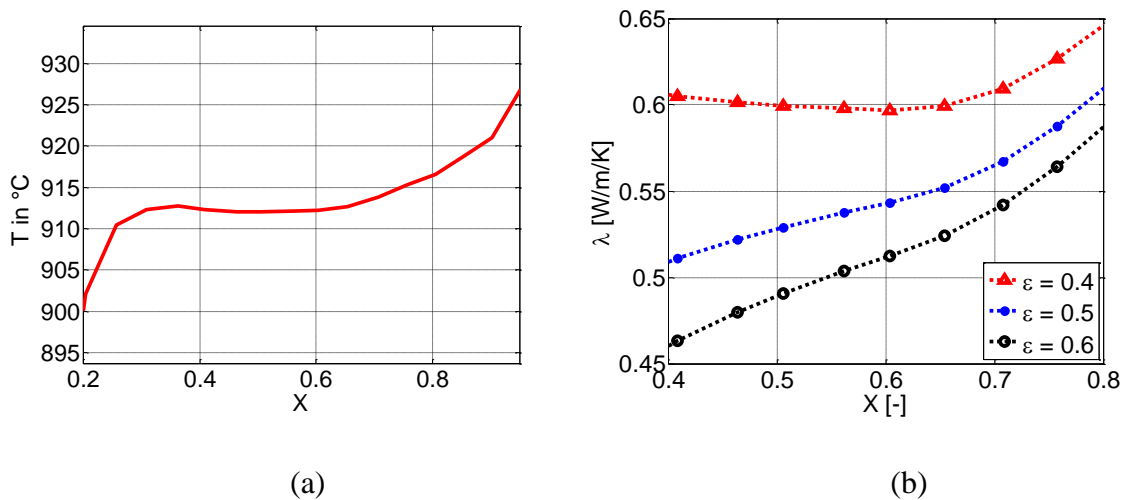


Figure 4-10: (a) Variation of core temperature with conversion degree
(b) Variation of thermal conductivity (λ) with conversion degree

4.7 Simulations with quasi-stationary model

In this section, a couple of decomposition experiments have been considered and the quasi stationary model has been applied to simulate the measured temperature and conversion profiles. These predicted profiles have been compared with the experimentally measured profiles in order to determine the material properties and also the calcination parameters.

4.8 Start time and conversion begin time

When the particle at room temperature suddenly suspended in the tube furnace at higher temperature, the surface of the particle reaches to the ambient (extreme high) temperature very quickly and calcination begins at the surface of the particle, whereas for the core of the particle it takes few minutes to reach to the reaction temperature. Because of this phenomenon we can see certain conversion degree during pre-heating of the core. For the below sample D, it approximately took 8 min for the core to reach 910 °C and during this time 22% of the conversion already completed. This early conversion cannot be predicted by the stationary model. So the beginning of the calcination is given as 22% conversion from the start time of 8 min to the MATLAB program. But these initial values of conversion degree and the beginning time to input to the MATLAB program change with type of sample and also the ambient calcination temperature maintained.

4.9 Simulations with quasi stationary model

4.9.1 Sample D

Limestone sample D which was described in the previous section has been considered here as well to explain the determination of material properties based on quasi stationary model. The entire system of algebraic equations 4.1-1 to 4.1-12 (mentioned in the above section 4.1) are simultaneously solved to investigate the important parameters such as front temperature T_f , Surface Temperature T_s , front and surface partial pressures of CO_2 P_f and P_s respectively in addition to the material properties thermal conductivity, tortuosity, chemical reaction coefficient etc. With the above pseudo stationary model, only the reaction phase of the entire decomposition process can be estimated. The preheating and post heating parts of the temperature profile (as shown in Figure 3-3) cannot be determined. However, a reasonable temperature profile for the reaction phase of the measured curve would be enough to predict the calcination behavior with the model proposed.

Experimentally measured core temperature and conversion profiles are compared and fitted with the profiles predicted by the pseudo stationary model equations as shown in the Figure 4-11. The red continuous curves in the above Figure 4-11 shows the experimentally measured core temperature (a), (b) and conversion (c) profiles whereas the blue dotted curves shows predicted temperature and conversion profiles of the quasi stationary model. The predicted temperature is compared with the calcination reaction zone (part) of the measured temperature profile as shown in the close view of temperature profile (b) because quasi stationary model can predict only the reaction part of entire decomposition temperature profile.

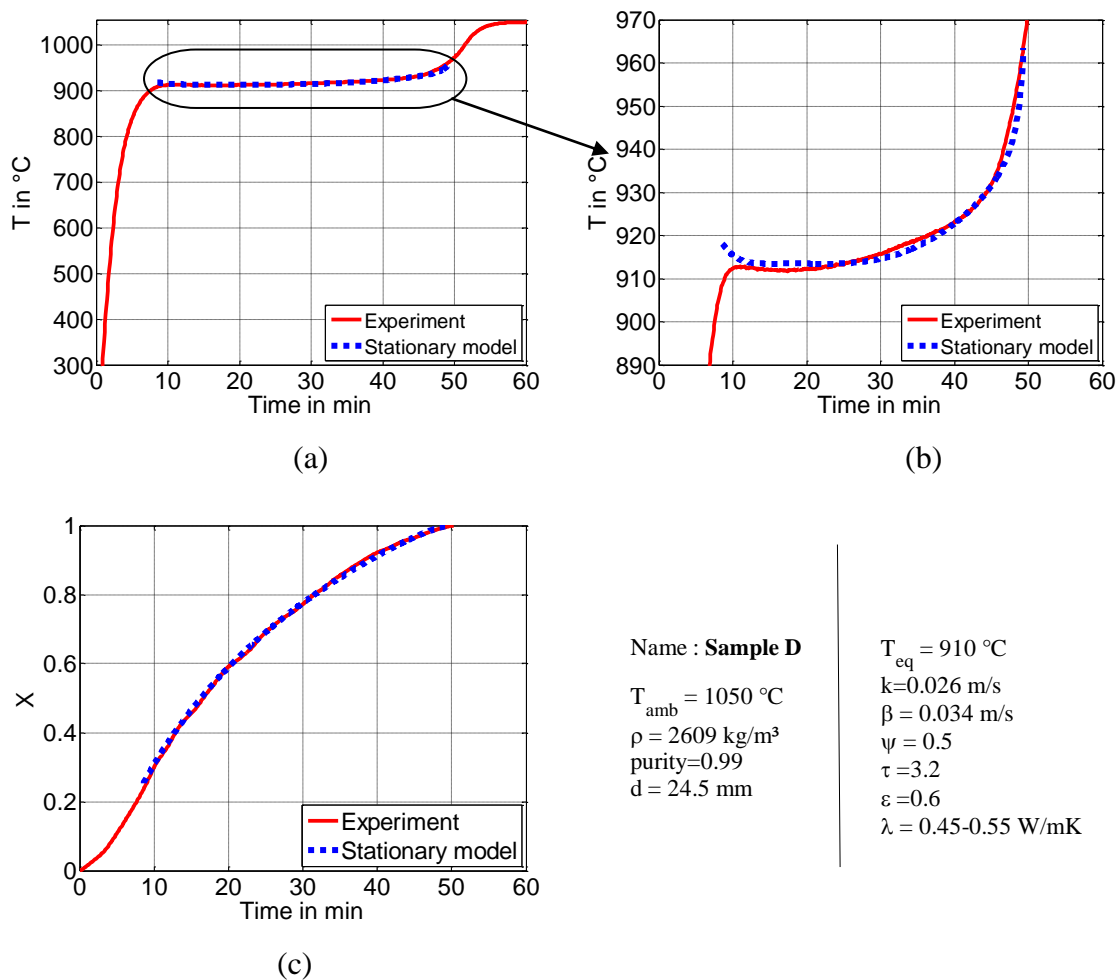


Figure 4-11: Comparison of measured and predicted temperature profiles for Sample D

As the temperature range in the Y-axis is from 300 to 1060°C in the Figure 4-11 (a), the reaction part of the temperature profile looks like a straight line and the measured and

predicted reaction temperature profiles appear to merge to one single line. To perceive the comparison of these two curves more clearly Figure 4-11 (b) has been drawn with Y-axis in the range from 890 to 970°C range. Here it can be clearly seen that the core temperature reaches around 913 °C and then slightly drops and then rises again. The similar behavior has been noticed in the predicted profile as well. The predicted temperature also follows the same trend. The Figure 4-11 (c) shows the measured (solid curve) and predicted (dotted curve) conversion profiles with time for the same sample. The surface of the particle will reach the reaction temperature, before the core of the particle reaches to the reaction temperature. So, certain degree of decomposition gets accomplished during the preheating stage of the core. This initial conversion cannot be predicted by this model, but the degree of this initial conversion can be noticed by comparing the measured temperature and conversion profiles together. For the above sample D, core temperature is reaching the calcination temperature (910°C) at around 8 minutes and corresponding degree of decomposition for 8 min is approximately 20%. So, the pseudo steady state model can predict the conversion degree in the range from 20% to 99.9%. But the extent of initial conversion degree (which can't be determined with this model) varies from stone to stone and it also depends on the corresponding calcination temperature.

The list of properties for this sample is displayed on the right side of Figure 4-11 (c). The diameter of the particle is in mm and all the remaining properties are in S.I units. Thermal conductivity variation with conversion degree is supplied to the program as expression (as determined in the Figure 4-10 (b)). For the sake of space constraint and also to avoid repeatability units are not mentioned in the properties list. The emissivity 0.6 refers to the effective emissivity. Lime emissivity then determined by

$$\epsilon_{\text{lime}} = \frac{1}{\frac{1}{\epsilon_{\text{effective}}} - \frac{A_{\text{stone}}}{A_{\text{furnace}}} \left(\frac{1}{\epsilon_{\text{furnace}}} - 1 \right)} \quad (4.9-1)$$

From the above equation, the lime emissivity calculated as 0.7 for the furnace inner wall emissivity of 0.55, the net effective emissivity predicted by the model 0.6 with best fitting for the measured temperature and conversion profiles.

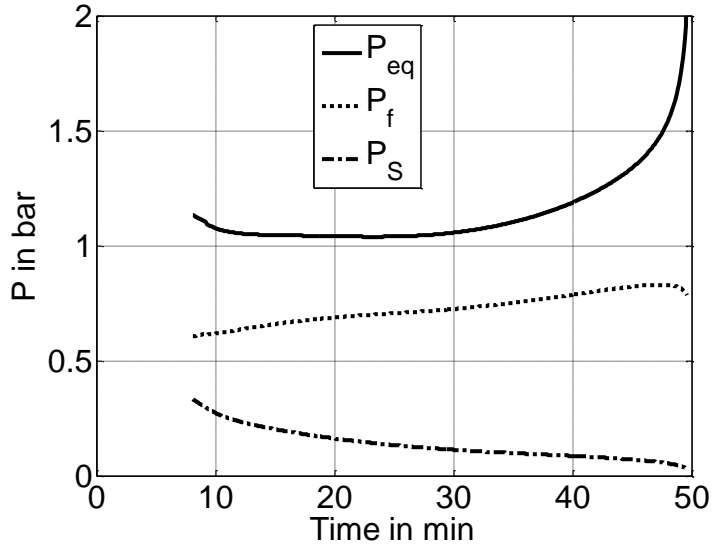
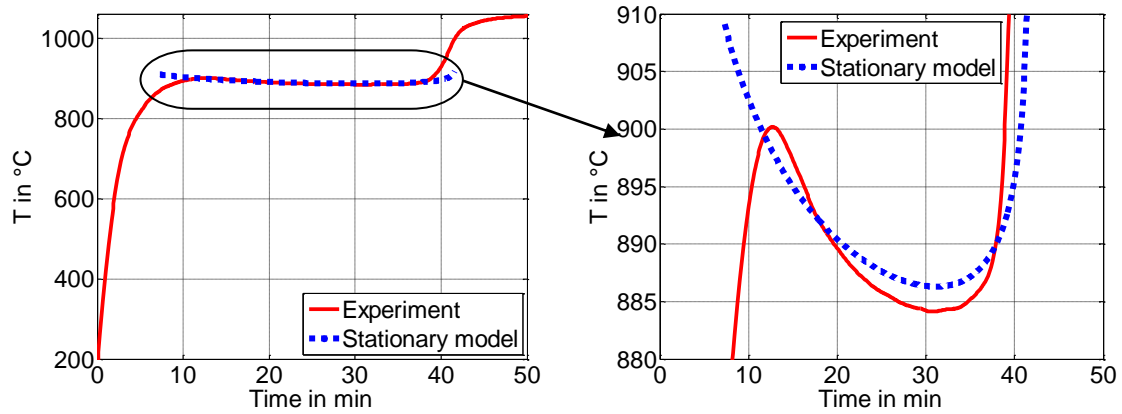


Figure 4-12: P artial pressure profiles for the sample D

The above Figure 4-12 shows the variation of equilibrium pressure P_{eq} and partial pressures of CO_2 at reaction front P_f and the partial pressure at the surface P_s respectively. P_{eq} of 1 bar corresponds to its equilibrium temperature 910 °C; this can be obtained from the equilibrium pressure correlation equation 4.1-4. As the reaction temperature is above 910 °C for most part of the calcination (as can be seen in temperature profile Figure 4-10 (b)), the P_{eq} also more than 1 bar. At the end of the calcination, calcination temperature further increases and hence the P_{eq} increases. Average front pressure P_f is around 0.6-0.7 bar whereas the surface pressure is at much low level, varies between 0.4 in the beginning to 0.02 bar at the end. The difference between the P_f and P_s is the driving force for the diffusion of CO_2 gas deposited at the reaction front of the particle.

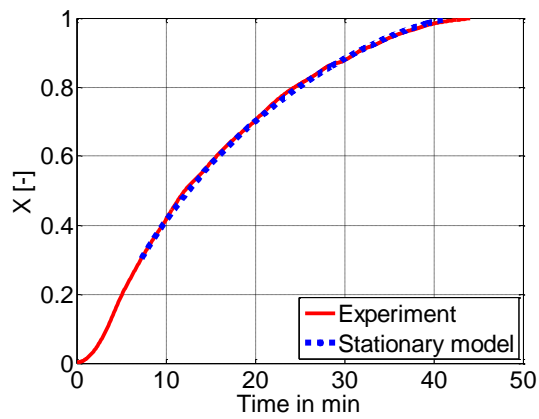
4.9.2 Sample 1mu1

Limestone sample 1mu1 with density 2700 kg m^{-3} and the calcite content (purity 91%) has been decomposed and the quasi stationary model has been applied to predict the temperature and conversion profiles as in the previous sample D.



(a)

(b)

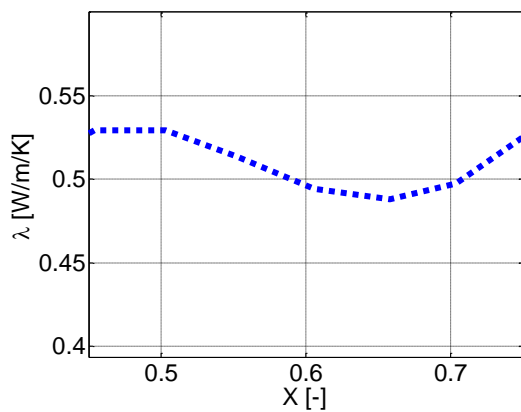


(c)

Name : **1mu1 in air**

$T_{amb} = 1058 \text{ }^\circ\text{C}$
 $\rho = 2700 \text{ kg/m}^3$
 purity=0.9
 $d = 24.5 \text{ mm}$

$k=0.032 \text{ m/s}$
 $T_{eq} = 900^\circ\text{C}$
 $\beta = 0.016 \text{ m/s}$
 $\psi = 0.5$
 $\tau = 1.0$
 $\varepsilon = 0.5$
 $\lambda = 0.52 \text{ W/(mK)}$



(d)

Figure 4-13: Comparison of measured and predicted temperature profiles for the sample 1mu1

Temperature and conversion profile comparisons have shown in Figure 4-13 (a), (b) and (c). The Figures (a) and (c) look similar to the profiles predicted for the previous sample D. However close view temperature profile Figure 4-13 (c) shows the variation of core temperature more clearly for this stone. From the Figure, it can be seen that, the measured core temperature (red curve) reaches to maximum of 900 °C and drops to as low as 885°C before it again rises up. The complete reaction zone is in ‘U’ shape whereas for the previous sample it was continuously increasing trend was observed. Profile predicted by the quasi stationary model (blue dotted curve) predicts slightly high initial temperature of 908°C and it slowly drops and merges with the measured profile. As discussed earlier, this model cannot predict the core temperature profile in the beginning of the calcination process (i.e. during transient phase of core heating). So initially high temperature 908°C predicted by the model can be ignored. Figure 4-13 (d) shows the variation of thermal conductivity with conversion degree. It is determined based on the measured profiles as explained in the previous section 4.7. From this Figure, the average value of conductivity 0.52 has been used for the quasi stationary model.

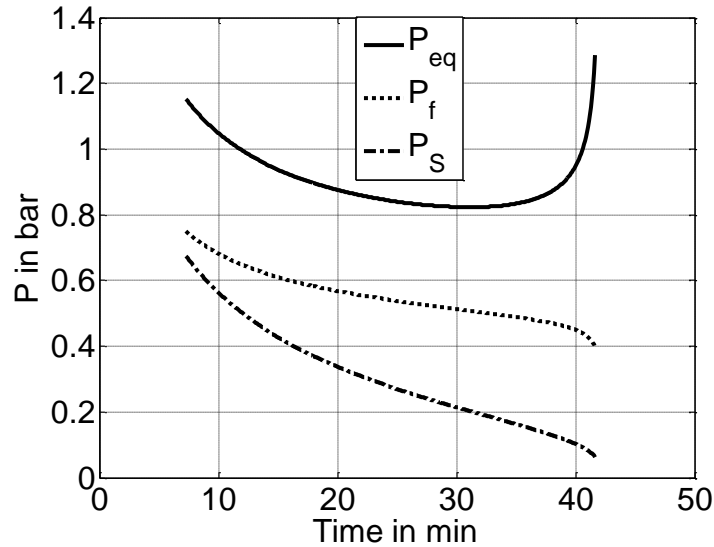


Figure 4-14 : Partial pressure profiles for the sample 1mu1

The above Figure 4-14 shows the equilibrium pressure, front partial pressure and surface partial pressure of CO_2 gas for the sample 1mu1. Equilibrium pressure is maintained around 0.9 to 1bar. The front and the surface pressures decreases with time. The pressure difference between the equilibrium pressure and the front pressure is the driving force for the reaction.

4.10 Transient Model for lime decomposition process

4.10.1 One dimensional approach

In this section, a transient model has been developed which describes the complete calcination process of a particle which undergoes high temperature decomposition process in a shaft kiln. A one dimensional heat conduction equation has been solved numerically with a variable source term. Though the heat of calcination reaction is constant, the source term in the heat equation which is a product of mass rate of CO_2 evolving and heat of reaction is not constant. Mass rate term depends on the surface area of the particle at the reaction front. At the beginning of the calcination, the surface area of the particle is high and maximum amount of CO_2 can be released and at the last stage of calcination, the reaction front moves close to the core of the particle and the surface area of the carbonate region of the particle is very low and hence very low mass of CO_2

evolves from the particle. This way the rate of mass of CO₂ evolution changes from the beginning of the calcination to the end of the calcination.

The top and bottom of the particle is insulated and the length to width ratio of the particle is always maintained to be above 4, so that one dimensional model can be applied where the heat transfer takes place in the axial direction is negligible compared to the heat transfer in radial direction.

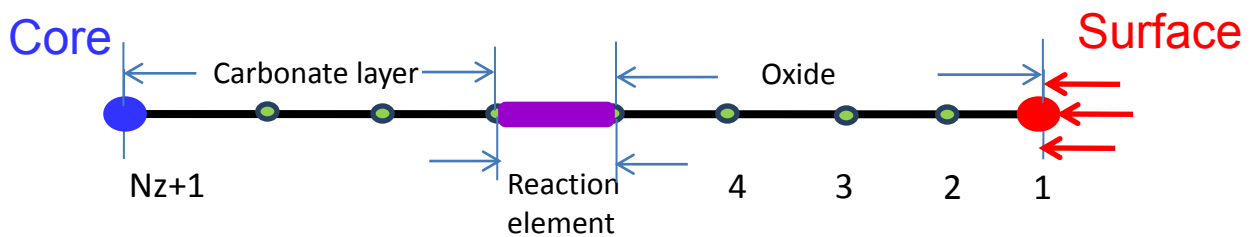


Figure 4-15: One dimensional discretization of spatial domain

4.10.2 Heat conduction equation

Heat equation which describes the calcination process is written in cylindrical coordinates as shown below

$$\frac{\partial T}{\partial t} = \frac{\lambda}{\rho \cdot c_p} \cdot \left(\frac{\partial^2 T}{\partial r^2} + \frac{1}{r} \frac{\partial T}{\partial r} \right) - \frac{\dot{m}_v \cdot \Delta H_R}{\rho \cdot c_p} \quad (4.10-1)$$

where a is the thermal diffusivity in $\text{m}^2 \text{s}^{-1}$

\dot{m}_v is the mass rate of CO₂ per unit volume in $\text{kg s}^{-1} \text{m}^{-3}$

ΔH_R is the enthalpy of reaction in J kg^{-1}

ρ is the density in kg m^{-3}

And c_p is the specific heat capacity $\text{J kg}^{-1} \text{K}^{-1}$.

The above equation in the discretized notation (in Finite Difference Method) can be written as

$$\frac{T_{i,j+1} - T_{i,j}}{\Delta t} = \frac{\lambda / (\rho \cdot c_p)}{r_i \cdot \Delta r} \cdot \left[r_{i+1/2} \left(\frac{T_{i+1,j} - T_{i,j}}{\Delta r} \right) - r_{i-1/2} \left(\frac{T_{i,j} - T_{i-1,j}}{\Delta r} \right) \right] - \frac{(m_v)_i \cdot \Delta H_R}{\rho \cdot c_p} \quad (4.10-2)$$

In the above equation 4.10-2, i and j represent the indices for spatial and time domains respectively.

$$(m_v)_i = \frac{m}{\pi \cdot (r_{i-1}^2 - r_i^2) \cdot h} \quad (4.10-3)$$

m is mass rate of CO₂ in kg s⁻¹, h is the height of the cylinder in m (unity, for one dimensional analysis).

m is obtained by solving the three stationary nonlinear algebraic equations (4.1-5 to 4.1-8) corresponding to the reaction, diffusion and mass transfer resistances described in previous section.

Figure 4-15 shows the one dimensional spatial discretization of the domain with N_Z spatial elements. The right end is the surface element which is exposed to the high temperature (ambient temperature) and the other end is the core which is at room temperature initially. Heat transfers gradually from the surface to the core during the calcination process and at first, surface reaches to the calcination temperature. When the temperature reaches the calcination temperature, the reaction begins at the surface and then slowly reaction progresses towards the core. The entire domain is discretized into N_Z small elements and the reaction front movement is described and modeled in element wise process. In that case, it can be said that the reaction begins at the surface element at first and when the reaction completes at this element, the reaction front moves to the immediate next element towards left. So after certain period of time, when the reaction is occurring at element L, the entire domain left to this element is still unreacted core (carbonate region), while the entire domain right to this element is calcinated part or the product region. In the heat equation the material properties such as density, specific heat and thermal conductivity are taken either for the lime or for the limestone depends on which region the governing heat equation is applied. The properties at the beginning node and at the end node are given by the respective boundary conditions. The natural

boundary condition equation for the radiation heat transfer for the surface node is given by

$$-\lambda \cdot \frac{\partial T}{\partial r} = (\sigma \cdot \epsilon \cdot (T_F^4 - T_S^4) - \alpha_{\text{conv}} \cdot (T_S - T_g)) \cdot 2\pi r_S L \quad (4.10-4)$$

The above differential equation in the finite difference discrete form can be represented as

$$-\lambda \cdot \frac{(T_{S,j} - T_{1,j})}{\Delta r} = (\sigma \cdot \epsilon \cdot (T_F^4 - T_{S,j}^4) - \alpha_{\text{conv}} \cdot (T_{S,j} - T_g)) \cdot 2\pi r_S L \quad (4.10-5)$$

The properties at the other end or the core of the particle are given by the axis symmetry boundary condition.

$$q = 0 \text{ or}$$

$$-\lambda \cdot \frac{\partial T}{\partial r} = 0.$$

The above equation in finite difference form can be simplified to

$$T_{\text{end},j} = T_{\text{end}-1,j} \quad (4.10-6)$$

At the beginning, the temperature at each and every nodal point is constant and it is equal to room temperature in general. The initial condition for the above parabolic differential equation is written as,

when $t=0$,

$$T \text{ (at all nodal points)} = 293 \text{ K.} \quad (4.10-7)$$

With the above boundary and initial conditions (4.10-5 to 4.10-7), the finite difference form of the heat diffusion equation 4.10-2 has been solved with FTCS scheme. FTCS stands for “Forward in Time and Central in Space”. Time derivative has been written in difference form and the new property (temperature at new time step) is computed based on the property value at the previous time step. Hence this is termed as forward in time. For the spatial discretization, central scheme is used where the property at current node is computed based on the property values of its two neighboring nodes on either side. This central difference is second order accurate. FTCS scheme is fully explicit method and the

stability of this method depends on the mesh Fourier number. Mesh Fourier number is defined as

$$\alpha_{\text{Fourier}} = a \cdot \frac{\Delta t}{\Delta r^2}, \quad (4.10-8)$$

where a is thermal diffusivity in m^2s^{-1} ,

Δt is time step size in s,

Δr is element size in m,

α_{Fourier} is mesh Fourier number (dimensionless).

As α_{Fourier} depends on the properties of the material through the thermal diffusivity term, its value needs to be computed for both the carbonate and oxide regions. For the stable solution of the fully explicit FTCS scheme, the mesh Fourier numbers corresponds to both reactant (CaCO_3) zone and the product (CaO) zone must be less than 0.5.

In addition to that, the accuracy of the solution depends on the fineness of spatial and time step sizes. Very fine mesh with very small time step size would attain a most accurate solution, but the computational time and hence the cost would be very high which cannot be usually accommodated. So mesh and time step dependency study has been carried out to obtain optimal size steps both in time and geometrical domains.

4.11 Simulations with transient model

4.11.1 Sample D

A couple of limestone samples considered for describing the application of quasi stationary model to determine the properties and parameters in the previous section, have been again considered to describe the usage of transient model. In this section Sample D has been described.

Below Figure 4-16 shows the comparison between experimentally measured core temperature profile and the core temperature profile predicted by the transient simulation.

Here the set of parameters described for this sample by the stationary model proposed in previous section 4.8 have been again applied. In the previous section, the stationary model has been developed to determine the temperature profile, where it can predict only the reaction part of the total experimentally measured temperature profile. However with the transient model proposed here, the entire temperature profile which includes pre heating and post heating of the particle can also be very well predicted.

From the Figure 4-16 (a), it can be seen that the temperature profile predicted by the transient model (blue dotted curve) is fitted very close with the measured core temperature profile. Curve matching in the reaction zone is clearly seen in the close view Figure 4-16 (b). Figure 4-16 (c) compares the conversion profiles of experiment and the transient model. A good fitting with the measured profile has been attained as shown. List of properties and parameters are given in the right of the Figure 4-16 (c). All properties and parameters are same except that the transient model requires specific heat capacities and thermal conductivities of lime and limestone as well. For limestone these are given as functions of temperature. Lime specific heat capacity near the decomposition temperature can be considered as constant and lime thermal conductivity is given as function of conversion degree which was determined in previous the section 4.7.

The computational details for the transient simulation are listed in the below Table 4.2.

Number of elements	80
Element Size	0.15 mm
Time of experiment	55 min
Number of time steps	180000
Time step size	0.02 s
CPU Time	2 min
$\alpha_{\text{Fourier_CaCO}_3}$	0.4
$\alpha_{\text{Fourier_CaO}}$	0.42

Table 4.3: Computational details of Transient simulation

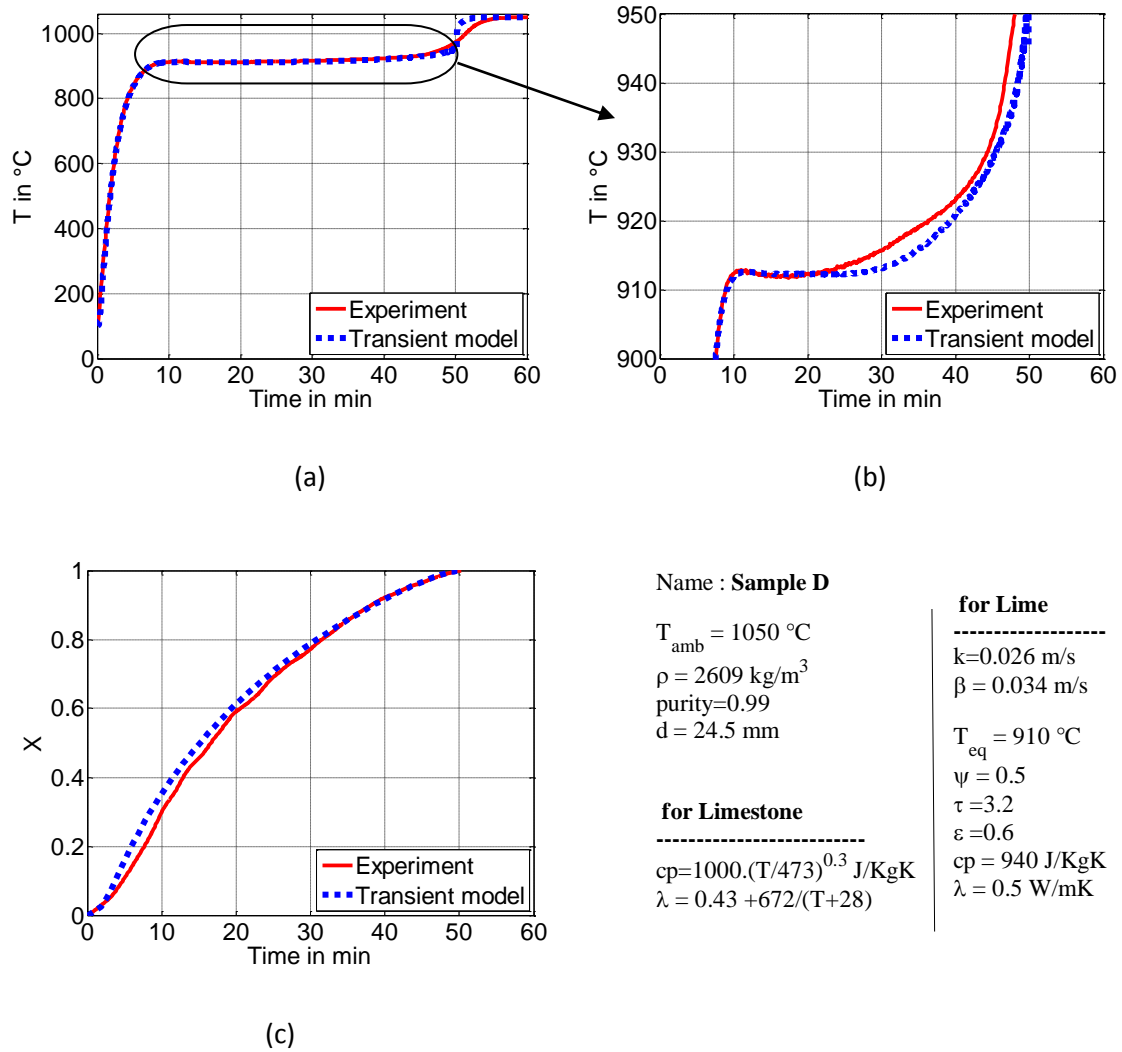


Figure 4-16: Comparison of experimentally measured and predicted temperature (a), (b) and conversion (c) profiles for the sample D

4.11.2 Sample 1mu1

Transient model has been applied to the other sample 1mu1 just as done for the Sample D. Figure 4-17 (a), (b) and (c) show the core temperature and conversion profiles respectively. The explanations of this Figure is same as previous Figure 4-16. In this case, thermal conductivity of lime is given as a constant.

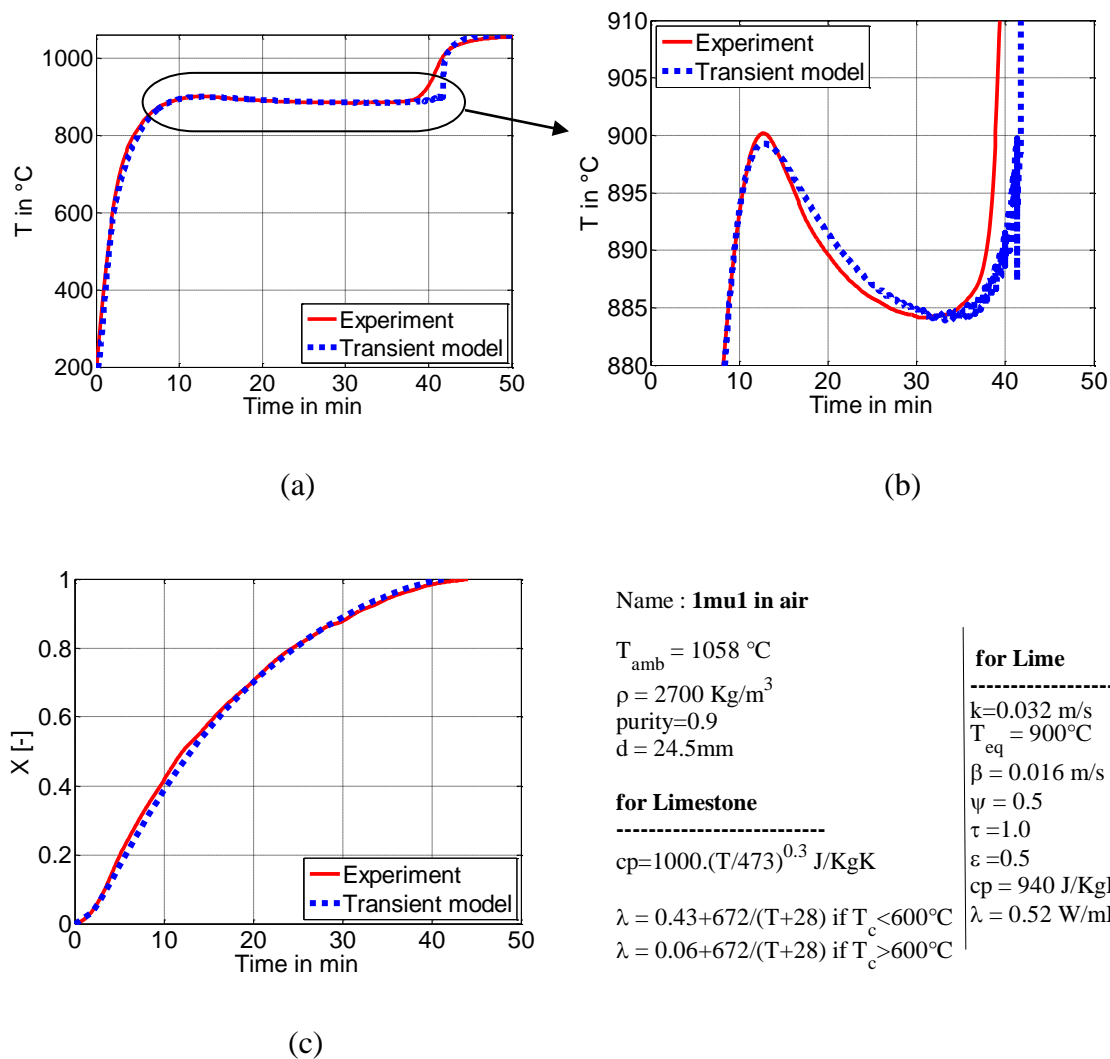


Figure 4-17: Comparison of experimentally measured and predicted temperature profiles for the sample 1mu1

4.12 Comparison between the models with measured profiles

Figure 4-18, compares the temperature profiles predicted by the pseudo stationary and transient models along with the experimentally measured profiles. It is clearly seen that during the reaction phase, temperature profiles of these two methods are almost matching. Similarly conversion profiles predicted by these two methods are compared in Figure 4-18 (c) along with the measured conversion profile. Here also these two methods result in same profile for the same set of parameters used.

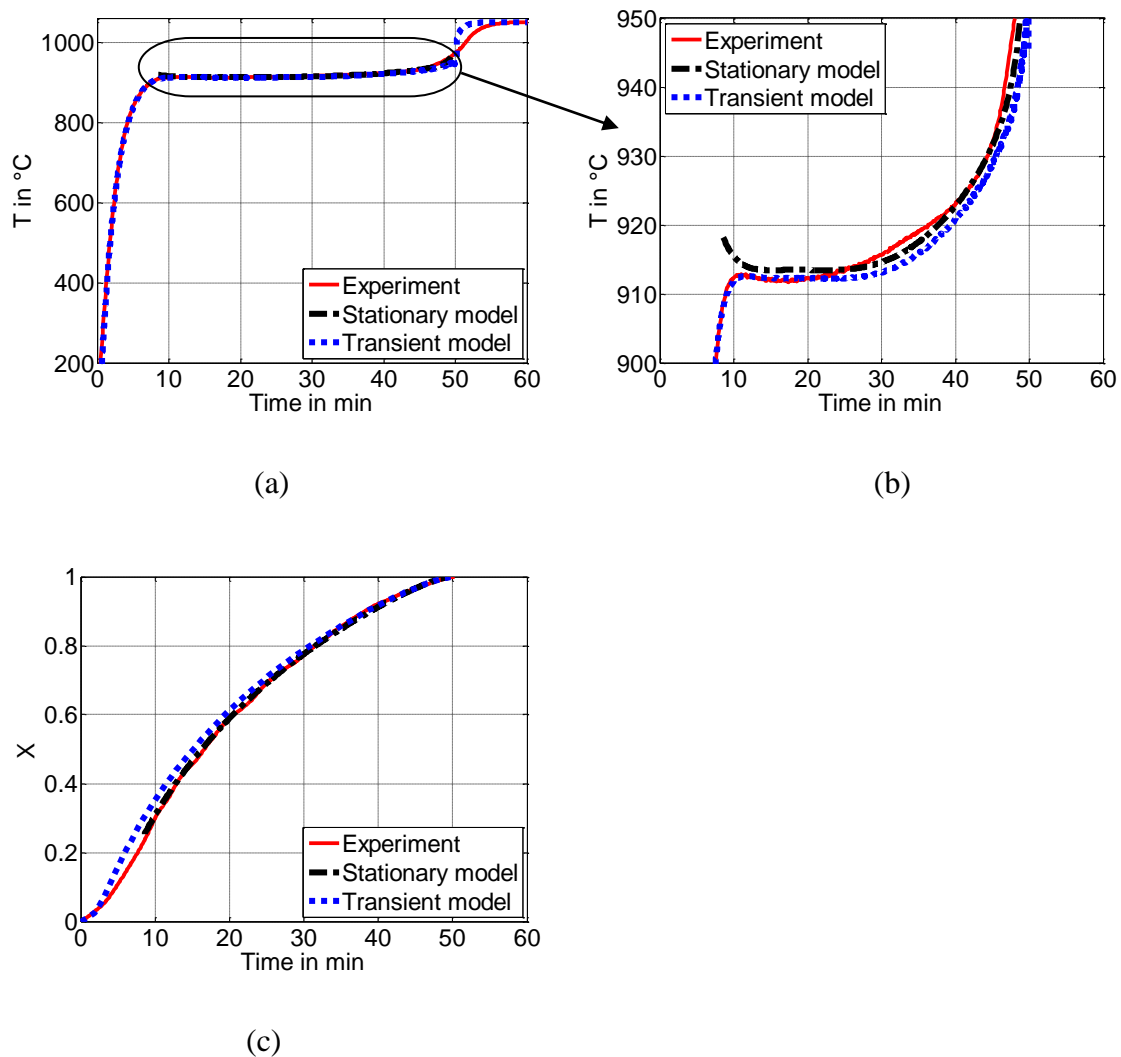


Figure 4-18: Comparison of experimentally measured and predicted temperature profiles (Stationary and Transient models) for the sample D

Figure 4-19 shows the comparison between these two models along with the measured temperature and conversion profiles for the sample 1mu1. Here for both the samples D and 1mu1, the close view of the temperature profile shows completely different core temperature behavior. For sample D, it can be seen that continuously increasing trend is observed whereas for the sample 1mu1 it is seen that sharp decrease in core temperature has been noticed even though the decomposition conditions for both of these specimens are almost the same. This difference in curve behavior explains the variation in properties and parameters for these two samples.

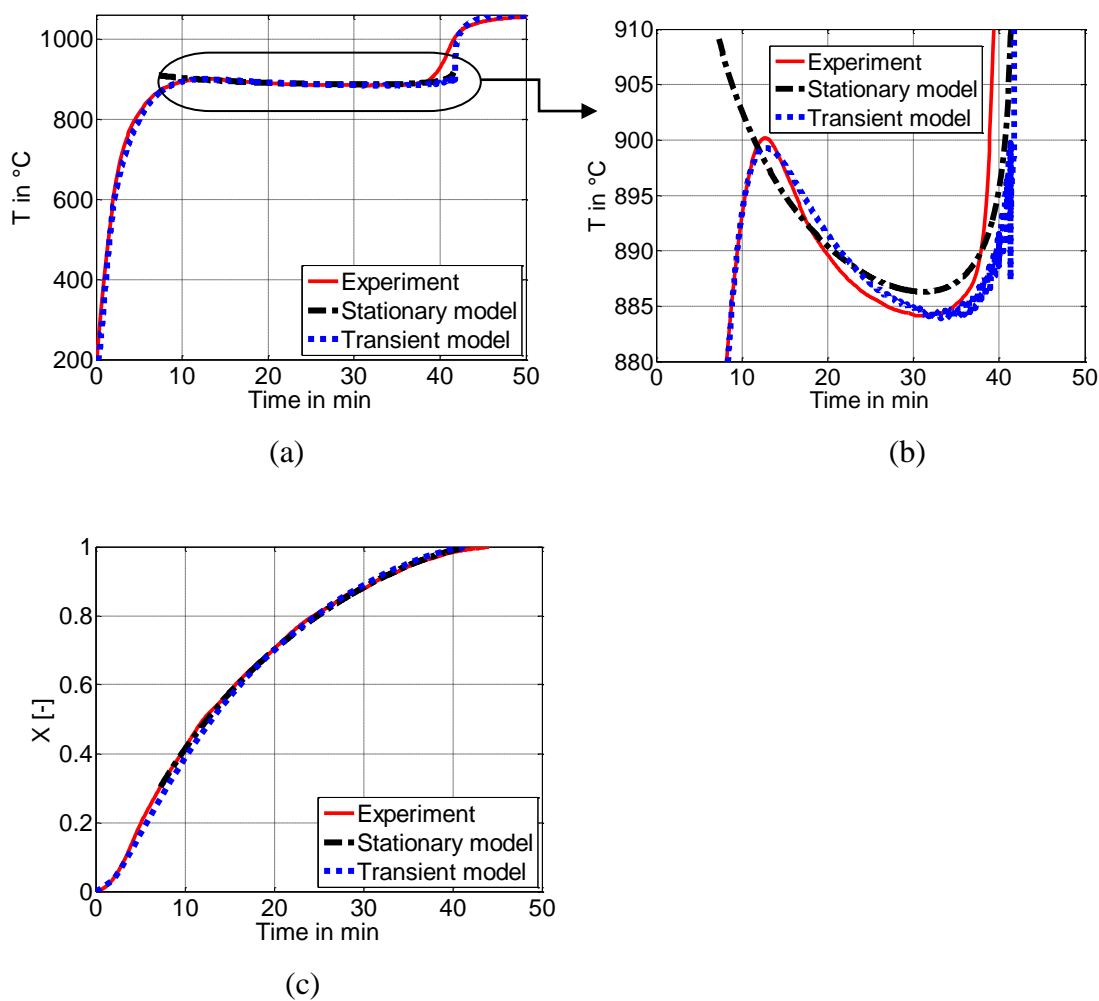


Figure 4-19: Comparison of experimentally measured and predicted temperature profiles (Stationary and Transient models) for the sample 1mu1

4.13 Effect of Gas Temperature on the calcination

4.13.1 Gas Temperature

Air is supplied from the bottom of the furnace at a constant rate with known volume flow. This air takes away the CO₂ gas formed during the reaction and ensures well defined flow conditions around the specimen. The gas enters the furnace bottom at room temperature and gains heat while flowing in the furnace by radiation from the furnace. Practically it is not possible to measure exactly this gas temperature because it increases during the flow inside the tube furnace and also even if the thermocouple is inserted inside the furnace, it also measures the radiation temperature of the furnace. However for few of the decomposition experiments the gas temperature at the exit of the furnace was measured and noticed that the average temperature of the gas inside the furnace is in the range from 300 to 700°C based on the furnace conditions. This gas has relatively lower temperature compared to the surface of the particle undergoing calcination. This temperature difference causes forced convection heat loss of the particle. The temperature of the gas affects the heat transfer process to the particle and hence it influences the calcination. The effect of the air/gas temperature on the calcination process is to be studied.

4.13.2 Furnace Temperature

At the end of the calcination, particle will be heated normally till it attains the ambient (surrounding) temperature. This is called post heating of the particle. Once the particle attains ambient temperature, there is no further heat transfer to the particle and there would be temperature equilibrium where the rate of heat transfer to the particle by radiation is equal to the rate of heat taken away from the particle surface by the air.

$$\sigma \cdot \epsilon \cdot (T_F^4 - T_S^4) = \alpha_{\text{conv}} \cdot (T_S - T_G) \quad (4.13-1)$$

The above equation arrived when the net radiative heat flux described by equation 4-1 is equated to zero. Using the above relation, furnace temperature T_F can be computed at different gas temperatures. For the ambient temperature of 1058 °C which is equal to the

particle surface temperature (T_s) at the end of the calcination, the furnace temperature can be computed and tabulated in the below table for different gas temperatures.

$T_G(^{\circ}\text{C})$	$T_F(^{\circ}\text{C})$	$\alpha [\text{W}/\text{m}^2 \text{K}]$
200	1083	8
400	1082	10
700	1074	12

Table 4.4 Convection heat transfer coefficient at different gas temperatures

The effective emissivity 0.5 has been chosen for the calculations in the above Table.

4.13.3 Effect of Gas Temperature

In order to determine the effect of gas temperature on the calcination, the decomposition experiment for the sample 1mu1, which was analyzed in the previous section has been considered. In the previous case, the gas temperature was taken as 700°C for the analysis. In the current case, quasi stationary model has been applied for two other gas temperatures 200 and 400°C in addition to the previous value of 700°C. As the gas temperature varies, corresponding convective heat transfer coefficient also changes and hence the furnace temperature based on the above relation 4.12-1. There is no influence was observed in the predicted reaction front temperature or conversion profile with the change in gas temperature.

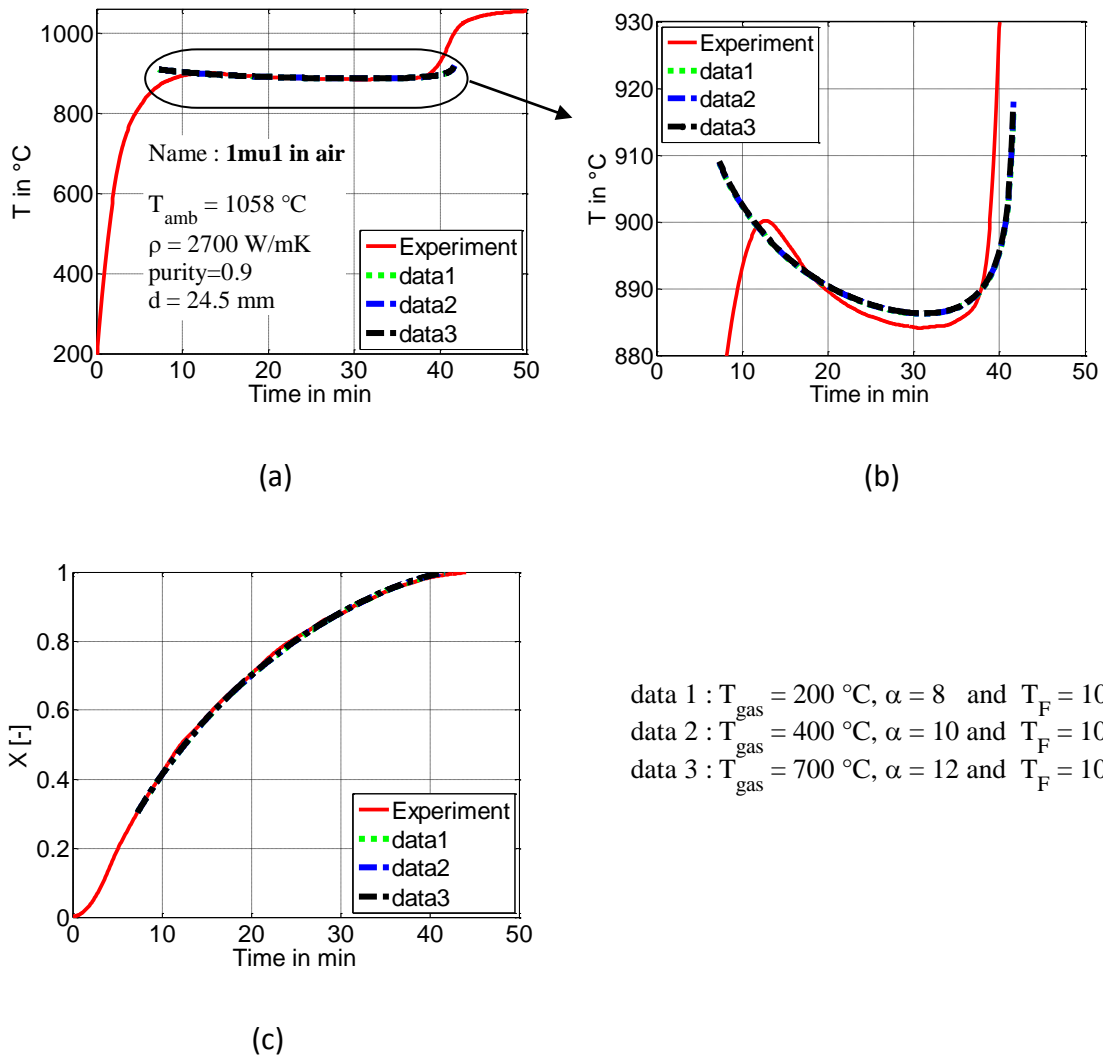


Figure 4-20: Temperature and conversion profiles comparison at different gas temperatures

From the above Figure 4-20, though the gas temperatures changes, corresponding heat transfer coefficient changes and results in new furnace temperature corresponds to the required ambient temperature 1058°C to be maintained. In the above Figure, core temperature profiles determined for three possible gas temperatures 200 , 400 and 600°C would not make any difference in the core temperature profile or conversion profile. The above analysis shows, calcination is nearly independent of gas temperature because the change in gas temperature is compensated by change in furnace temperature.

4.14 Determination of decomposition temperature

Thermogravimetric experiments have been conducted with several samples from various origins. Transient or stationary models have been used to reproduce the measured temperature and conversion profiles in order to determine the material properties and other calcination parameters. Silva [1] conducted several experiments with various varieties of limestone to study the decomposition temperature. For the present work, it is considered to use the average of measured values from Silva. However for few of limestone decomposed in the current study, it was observed that the core temperature is much higher than 910°C irrespective of the ambient temperature used for the decomposition experiment. For these samples, the decomposition temperature has been measured using the Simultaneous Setaram TG-DTA 92 apparatus. The apparatus and the method used to determine the decomposition temperature is same as Silva [1]. Below table 4-4 lists the sample name and the decomposition temperature measured.

Sample	Decomposition temperature in °C
BL0607	920
SZ	920

Table 4.5: Measured decomposition temperature

From the above results, the equilibrium temperatures for these samples have been considered as 920°C.

Influence of the parameters on calcination

5.1 Introduction

Calcination behavior is influenced by the origin of the stone as discussed in the previous chapters. Variation in heat capacities of Lime and Lime stone of different origins [1] result in change in enthalpy of reaction of calcination process. Generally, thermophysical properties of limestone of different origins also varies, hence its influence on decomposition process must be studied [55]. Reaction coefficient, thermal conductivity and pore diffusion (tortuosity) are the significant parameters which can make significant difference to the calcination behavior.

In this chapter the influence of these parameters on the calcination process has been studied. The sample 1mu1 decomposed at 1050 °C, for which the temperature profiles and conversion profiles plotted in the previous chapter (Figure 4-13) has been considered here again to show the effect of the calcination parameters. To understand the influence of these parameters, each parameter is doubled and then reduced to half from the value predicted by the model. In these two cases effect of calcination behavior on increasing or decreasing the parameter to two folds is studied. In addition to this, the calcination behavior for the extreme variation in the properties has also been studied. In order to have a reference in analysis, the temperature variation corresponds to calcination time of 20 min has been considered, because total calcination time for this sample is 40 minutes.

This analysis gives us the insight about a particular parameter influence on the temperature profiles. In the following sections, influence of each one of these parameter is discussed with appropriate temperature and conversion profiles.

5.2 Influence of thermal conductivity

Figure 5-1 (a), (b) shows the core temperature and conversion profiles measured (continuous red curves) and predicted by the stationary model (blue dotted curves) for the sample 1mu1 which was described in chapter 4. In order to study the influence of thermal conductivity (λ), quasi stationary process has been simulated at different thermal conductivities. When conductivity increases, the temperature difference between the front and the surface of the particle must be reduced for the given heat flux hence the front temperature increases.

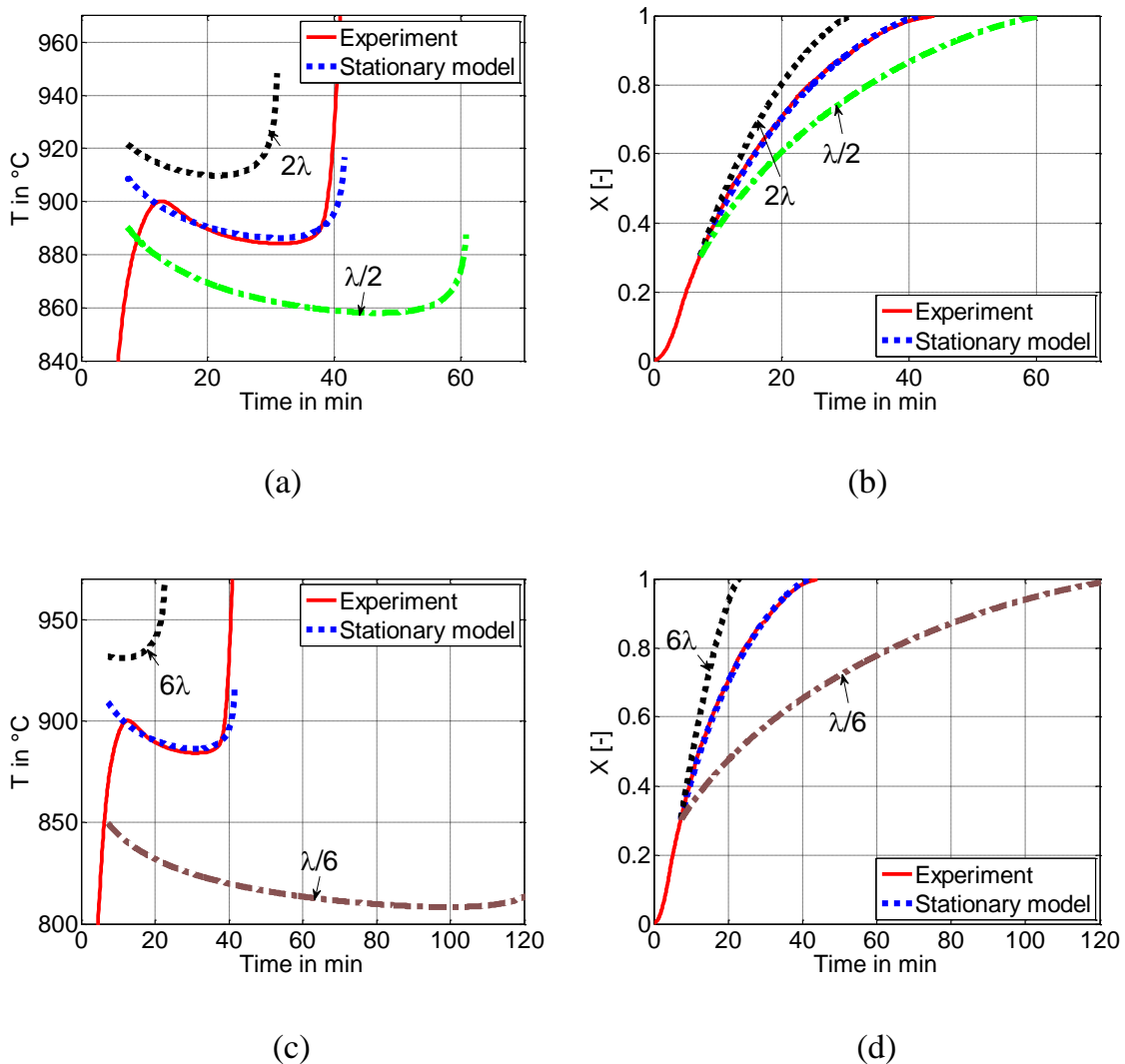


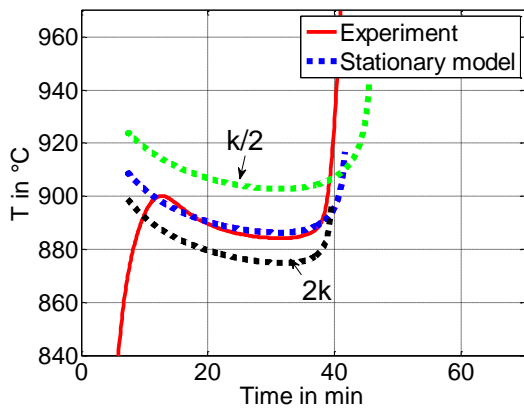
Figure 5-1: Comparison of temperature (a), (c) and conversion (b), (d) profiles for the sample 1mu1 with stationary model at different thermal conductivities

When λ is doubled, calcination temperature increases from 890°C to 910°C and the reaction time decreases from 42 min to 31 min i.e. decreased by 26%. Whereas when λ is reduced to half, calcination temperature decreases from 890°C to 869°C and the time of calcination increases from 42 min to 70 min i.e. increased by 67%. Both the core temperature as well as calcination time are significantly influenced with change in thermal conductivity. Figure 5-1 (c), (d) depicts the temperature profile trends at extreme variations in thermal conductivities. From Figure 5-1 (c) it is also observed that higher thermal conductivity (6λ) results in a continuously increasing core temperature profile, whereas lower conductivity ($\lambda/6$) results in a temperature profile which decreases steeply and then slowly rises again at the end. In other words, it can be said that a "U" shaped profile is the outcome for lower thermal conductivities. It can also be noted that, decomposition needs extremely longer time 120 minutes when the conductivity is reduced by 6 folds.

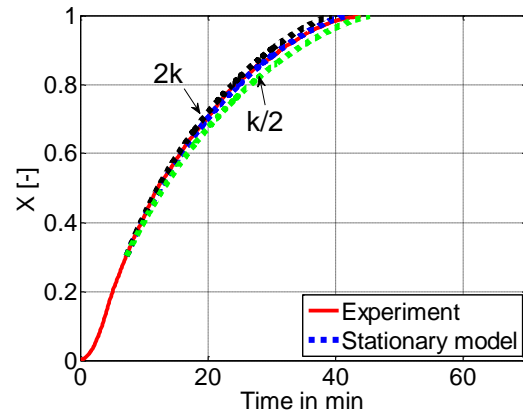
5.3 Influence of reaction coefficient

In this section the above analysis have been applied to study the influence of reaction coefficient. Figure 5-2 (a), (c) show the core temperature profiles and Figure 5-2 (b), (d) show the conversion profiles for the same sample 1mu1. In this Figure, the effect of variation of reaction coefficient (k) on temperature and conversion profiles can be viewed.

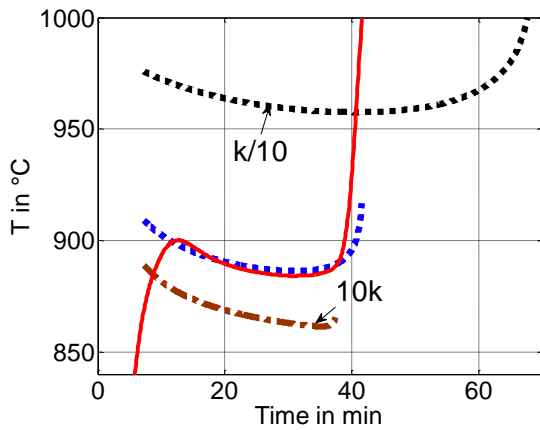
When reaction coefficient (k) increases, the difference of equilibrium and front pressure of CO₂ must be decreased for the given mass flux. This in turn results in decrease in equilibrium pressure and hence the decomposition temperature. From the Figure 5-2 (a), it can be observed that when k is doubled, calcination temperature decreases from 890°C to 880°C and the reaction time decreases from 42 min to 40 min. Whereas when k is reduced to half, calcination temperature increases from 890°C to 907°C and the time of calcination increases from 42 min to 45.4 min.



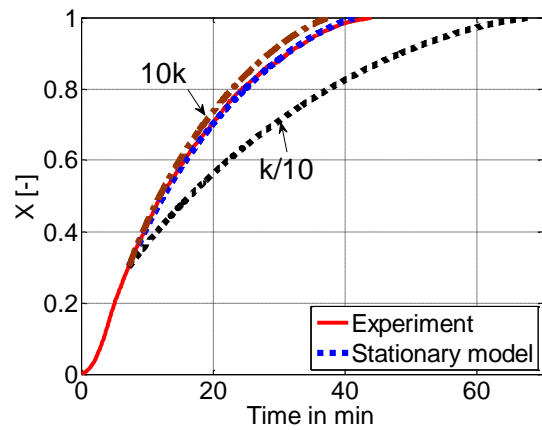
(a)



(b)



(c)



(d)

Figure 5-2: Comparison of temperature (a), (c) and conversion (b), (d) profiles for the sample 1mu1 with stationary model at at different reaction coefficients

The reaction coefficient is varied ten folds in the Figure 5-2 (c) and (d). It can be depicted that, when it is rised to 10 folds, a reduction in front temperature has been noticed, however there is no considerable change in calcination time is observed. But when it is reduced to ten folds, the temperature raies to 960°C and the time increases to 70 minutes.

5.4 Influence of tortuosity

Figure 5-3 shows the influence of tortuosity on the core temperature and conversion profiles. Higher tortuosity results in lower diffusivity and thereby higher front pressure and temperatures.

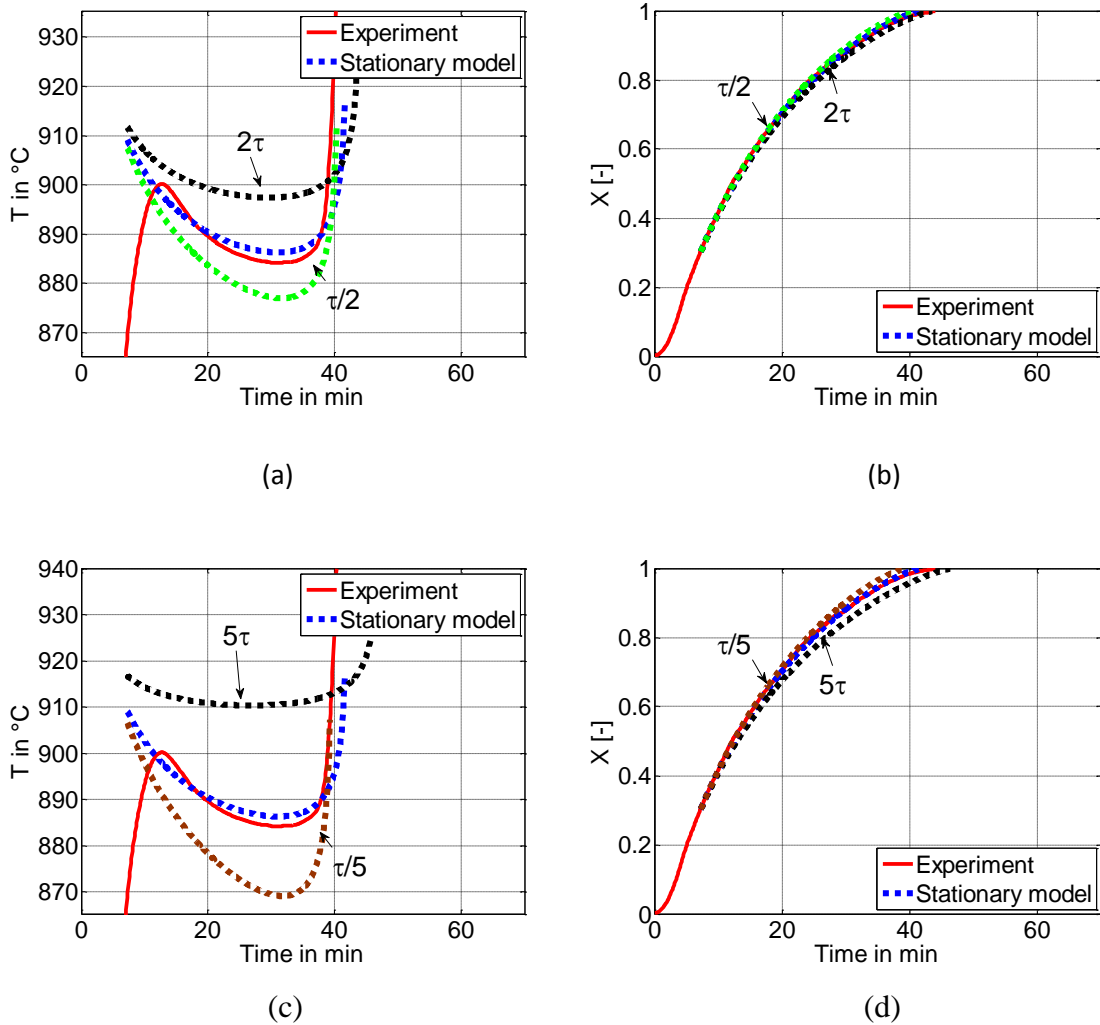


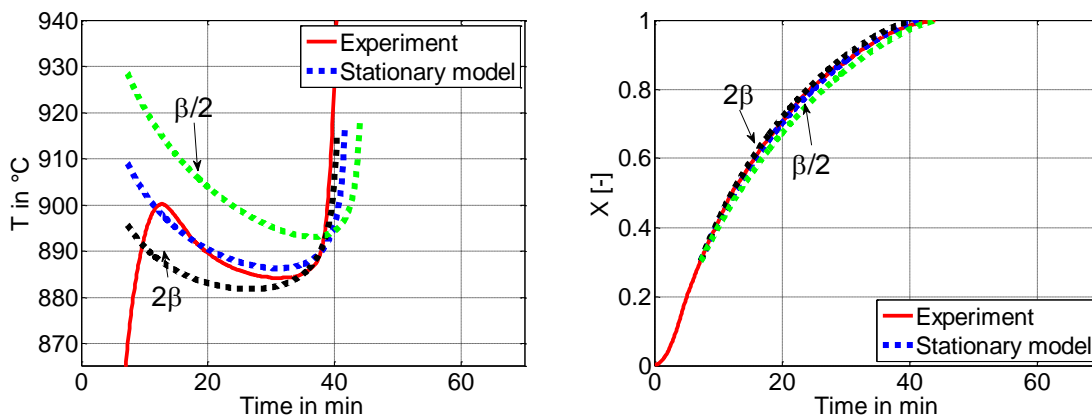
Figure 5-3: Comparison of temperature (a), (c) and conversion (b), (d) profiles for the sample 1mu1 with stationary model at at different tortuosities

When tortuosity is doubled, calcination temperature increases from 890°C to 899°C and the reaction time increases from 42 min to 44 min. Whereas when tortuosity is reduced to half, calcination temperature decrease from 890°C to 884°C and the time of calcination decrease from 42 min to 40 min.

At lower tortuosities, the core temperature profile is in “U” shape whereas at higher values it looks like a continuously increasing trend. This effect is clearly seen in the Figure 5-3 (c). Though the property is five folds varied, there is no significant change in calcination time is noticed.

5.5 Influence of mass transfer coefficient

Figure 5-4 shows the influence of mass transfer coefficient (β) on the calcination process. When β is doubled, calcination temperature decreases from 890°C to 884°C and the reaction time decreases by a minute. Whereas when β is reduced to half, calcination temperature increases from 890°C to 904°C and the time of calcination increases by 2 min. Lower values of β results in higher initial temperatures and the temperature drops gradually. From the Figure 5-4 (c) it can be observed that when β is raised by ten folds, initially very high temperature has been predicted, but slowly drops with time, whereas at very high values of β results in continuously increasing temperature profile. However there is no significant change in calcination time has been observed even it is ten folds raised.



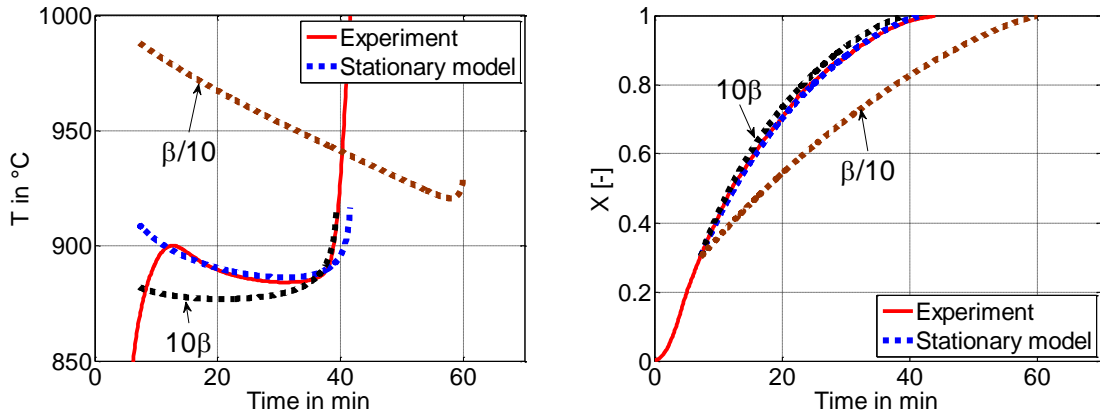


Figure 5-4: Comparison of temperature (a), (c) and conversion (b), (d) profiles for the sample 1mu1 with stationary model at different mass transfer coefficients

5.6 Equilibrium Temperature

In order to study the influence of equilibrium temperature on calcination, the simulation has been carried out at two different possible equilibrium temperatures 920°C and 880 °C. From the Figure 5-5 it can be noticed that higher equilibrium temperatures result in higher core temperatures. It is also noticed that the curve behavior is not affected with variation in equilibrium temperature. There is no discernable change in the calcination time has been noticed.

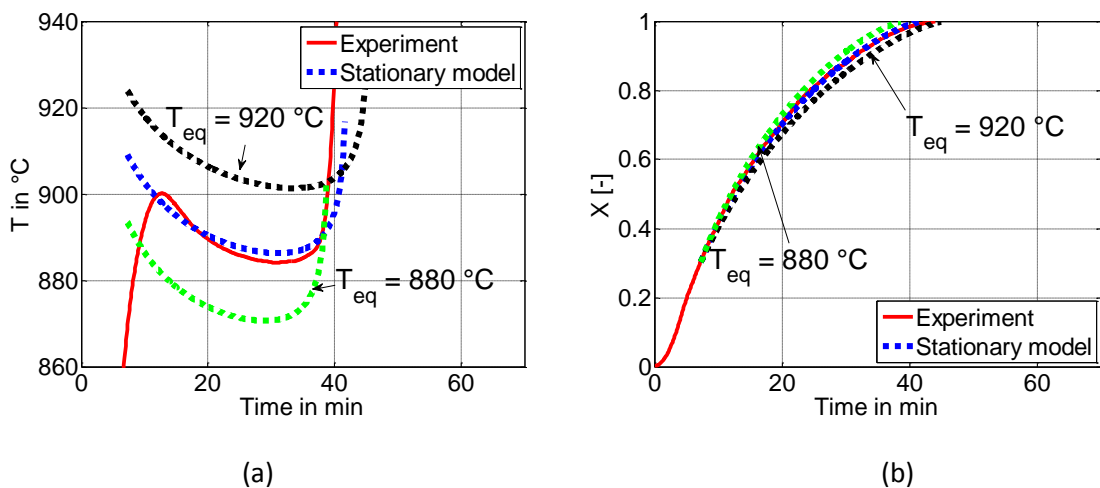
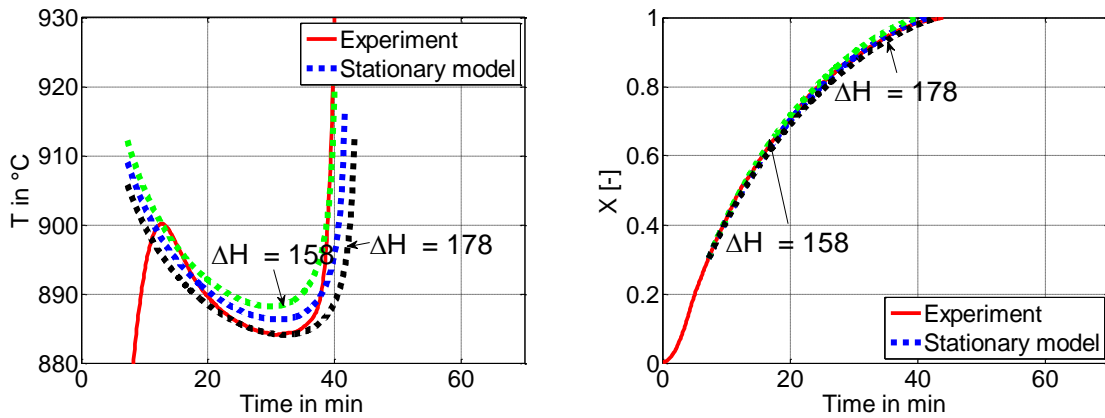


Figure 5-5: Comparison of temperature (a) and conversion (b) profiles for the sample 1mu1 with stationary model at different equilibrium temperatures

5.7 Enthalpy of reaction

Enthalpy of reaction has been varied from 168 kJ/mole to 158 and 178 kJ/mole and the stationary simulation has been applied to verify its influence on the calcination. Higher enthalpy shows slightly lower temperature profile. However the variation of calcination temperature or time is not significant. Below Figure 5-6 shows the variation of enthalpy of reaction.



(b)

Figure 5-6: Comparison of temperature (a) and conversion (b) profiles for the sample 1mu1 with stationary model at different enthalpies of reaction.

5.8 Conclusions

Thermal conductivity shows significant influence in the calcination process, compared to other parameters. Next to conductivity reaction coefficient also exhibits strong effect on the calcination process. Reaction coefficient shows noticeable variation of core temperature and calcination time. Tortuosity influences the shape of the core temperature profile. At higher tortuosity, temperature profile is a continuously increasing curve, whereas for the low tortuosity, it decreases first to a lowest temperature and then gradually increases forming a “U” shaped curve. Similar behaviour is observed for the thermal conductivity as well. Mass transfer coefficient exhibits lowest influence both in terms of core temperature variation as well as in the calcination time. Though there is a little difference in core temperatures observed in the beginning of the calcination, but later almost no difference has been found in

the core temperature upon changing the mass transfer coefficient. A 20 K change of equilibrium temperature results in approximately 10 K change in the predicted core temperature profiles, but the shape of the profile is not influenced. Enthalpy of reaction shows no considerable influence on the calcination process.

Sensitivity of parameters in industrial shaft kilns

6.1 Introduction

In this chapter, influence of process parameters on the calcination of limestone particles undergoing decomposition in an Industrial shaft kiln has been analyzed. Industrial shaft kiln is assumed as a packed bed of spherical particles with bed porosity of 0.4 for the determination of heat and mass transfer coefficients. The typical gas flow rate of 11960 m³/hr has been considered with the excess air number 1.3 [56],[57],[58] for all the calculations.

The system of quasi stationary equations which describe the calcination in a shaft kiln has been solved simultaneously to predict the calcination temperature and conversion profiles. Later these predicted profiles have been used to analyze the sensitivity to calcination for various parameters which control the calcination mechanism. Definition of the term sensitivity in the current context is described in the section 6.3 of this chapter. Typical material properties of the particle and parameters have been chosen to simulate the calcination behavior are described in the below Table 6.1.

Parameter	Value
Thermal conductivity	0.6 Wm ⁻¹ K ⁻¹
Reaction coefficient	0.03 ms ⁻¹
Tortuosity	2
Porosity	0.5
Density	2700 kgm ⁻³
Purity	0.99
Enthalpy of reaction	168 kJmol ⁻¹
Equilibrium Temperature	910 °C
Partial pressure of CO ₂ gas in the kiln	0.3 bar
Excess air number	1.3
Combustion air	5770 m ³ /h
Cooling air	5330 m ³ /h
Fuel	860 m ³ /h
Superficial velocity of gas	0.7 m/s
Kiln diameter	2.5 m

Table 6.1 : Calcination Parameters and material Properties

6.2 Determination of heat and mass transfer coefficients for the kiln

The heat transfer in a shaft kiln (packed bed) is dominated by convection. One approach to estimate the convective heat transfer coefficient (α) in a packed bed is given by Jeschar et al.[25, 26,[51]] in which a packed bed can be described as a bundle of parallel pipes. The Nusselt correlation in the packed bed is given as:

$$\text{Nu}_{\text{bed}} = 2 + 1.12 \cdot (\text{Re})^{(1/2)} \cdot (\text{Pr})^{(1/3)} \cdot \left(\frac{1-\psi}{\psi} \right)^{(1/2)} + 0.005 \cdot (\text{Re}) \quad (6.2-1)$$

where ψ is the void fraction of the packed bed.

The Nusselt number is defined as:

$$\text{Nu}_{\text{bed}} = \frac{\alpha \cdot d}{\lambda_g} \quad (6.2-2)$$

where d is the size of the particle and λ_g is the gas thermal conductivity.

The Reynolds number is given by:

$$\text{Re} = \frac{w \cdot d}{v \cdot \psi} \quad (6.2-3)$$

where v is gas kinematic viscosity and w is the empty tube velocity that is called as superficial velocity, if no packing were present in the bed. This velocity is determined by:

$$w = w_{\text{STP}} \cdot \frac{\rho_{\text{STP}}}{\rho} \quad (6.2-4)$$

where w_{STP} is the velocity at STP (standard temperature and pressure) condition, ρ and ρ_{STP} are the density at temperature T and at STP. The velocity w_{STP} is given as:

$$w_{\text{STP}} = \frac{\dot{V}_{\text{STP}}}{A_F} \quad (6.2-5)$$

Here \dot{V}_{STP} is the gas volume flow at STP and A_F is the cross-section area of the kiln.

The Prandtl number is defined as:

$$\text{Pr} = \frac{v \cdot \rho \cdot c_p}{\lambda_g} \quad (6.2-6)$$

In the simulation of limestone decomposition, the convective mass transfer of the produced CO_2 into the gaseous ambience must be calculated. With analogy to heat transfer, the mass transfer coefficient of CO_2 from the limestone surface to the gas, β , can be calculated from the Sherwood function.

$$\text{Sh} = 2 + 1.12 \cdot (\text{Re})^{(1/2)} \cdot (\text{Sc})^{(1/3)} \cdot \left(\frac{1 - \psi}{\psi} \right)^{(1/2)} + 0.005 \cdot (\text{Re})$$

The Sherwood function is defined as:

$$Sh = \frac{\beta \cdot d}{D_{CO_2-air}}$$

Where D_{CO_2-Air} is the binary diffusivity of CO_2 in air, which will be determined in the next section.

The Schmidt number Sc is defined as:

$$Sc = \frac{v}{D_{CO_2-air}}$$

6.3 Gas properties

To calculate the Nusselt and the Reynolds numbers, the material property values have to be calculated at the gas temperature T because the temperature difference is significant. The material property values are calculated with the following equations given by Specht [51]:

$$\lambda = \lambda_o \cdot \left(\frac{T}{T_o}\right)^{n_\lambda}, \quad \mu = \mu_o \cdot \left(\frac{T}{T_o}\right)^{n_\mu}, \quad a = a_o \cdot \left(\frac{T}{T_o}\right)^{n_\mu+1-n_c}, \quad \rho = \rho_o \cdot \left(\frac{T}{T_o}\right)^{-1}, \quad c_p = c_{po} \cdot \left(\frac{T}{T_o}\right)^{n_c}$$

$$v = v_o \cdot \left(\frac{T}{T_o}\right)^{n_\mu+1} \quad \text{and} \quad D = D_o \cdot \left(\frac{T}{T_o}\right)^{n_D+1}$$

The diffusivity of the CO_2 in air, D_{CO_2-Air} can be approximated with $D_o = 0.16 \cdot 10^{-4} \text{ m}^2/\text{s}$ and $n_D = 1.77$. In the above equations, T_o is the reference temperature taken as 273 K. The material properties of gas components at the temperature T_o are gathered in Table 6-2.

Gas	M	ρ_o	c_{po}	n_c	λ_o	n_λ	μ_o	n_μ
unit	kg/kmol	kg/m ³	J/kg/K	-	W/m/K	-	mg/m/s	-
N ₂	28	1.26	1000	0.11	0.024	0.76	16.8	0.67
CO	28	1.26	1000	0.12	0.024	0.78	16.8	0.67
Air	29	1.29	1000	0.10	0.025	0.76	17.4	0.67
O ₂	32	1.44	900	0.15	0.025	0.80	19.7	0.67
CO ₂	44	1.98	840	0.30	0.017	1.04	14.4	0.77
H ₂ O	18	0.81	1750	0.20	0.016	1.42	8.7	1.13

Table 6.2: Material properties of gases at $T_o = 273$ K

The properties of gas mixtures can be calculated with the following formulas:

$$\rho_M = \sum \rho_i \cdot \tilde{x}_i \quad (6.3-1)$$

$$\lambda_M \approx \sum \lambda_i \cdot \tilde{x}_i \quad (6.3-2)$$

$$c_{pM} = \sum c_{pi} \cdot x_i = \frac{1}{\rho_M} \sum c_{pi} \cdot \tilde{x}_i \cdot \rho_i \quad (6.3-3)$$

Where \tilde{x}_i is the molar or volume fraction of component i in a gas mixture and x_i the mass fraction of component i in a gas mixture.

Assuming the constant temperature inside the kiln and 30 volume % CO₂ gas and 70% air, heat and mass transfer coefficients in the kiln for two different temperatures have been determined and plotted. Figure 6-1 presents the variation of convective heat transfer coefficient with respect to particle size for two different kiln gas temperatures. These heat transfer coefficients are computed using the Nusselt number correlation (6.2-1). From this figure it can be observed that for small particles of size 20 mm, the heat transfer coefficient is high of 200 W/m²/K. When the particle size increases heat transfer coefficient gradually decreases and reaches to 90 W/m²/K for the large particles of size 120 mm. Heat transfer coefficients for the higher gas temperatures are slightly higher compared to the heat transfer coefficients calculated at 900°C. However no significant difference is observed.

Figure 6-2 shows the variation of mass transfer coefficient with respect to diameter of the particle computed using the equation (6.3-2). Similar to the heat transfer coefficient, mass

transfer coefficient also decreases with increase in diameter of the particle. At high gas temperature, the mass transfer coefficient is higher compared to that of the lower temperature for the same diameter. Mass transfer coefficient varies in the range of 0.7 to 0.35 ms^{-1} for 1200 °C decomposition, whereas it varies between 0.5 to 0.25 ms^{-1} for the calcination carried out at 900°C.

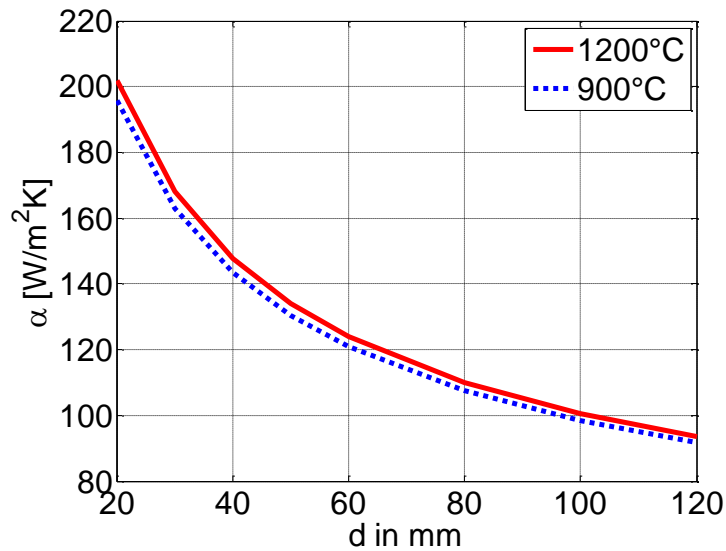


Figure 6-1: Variation of heat transfer coefficient of the bed with particle diameter for different temperatures

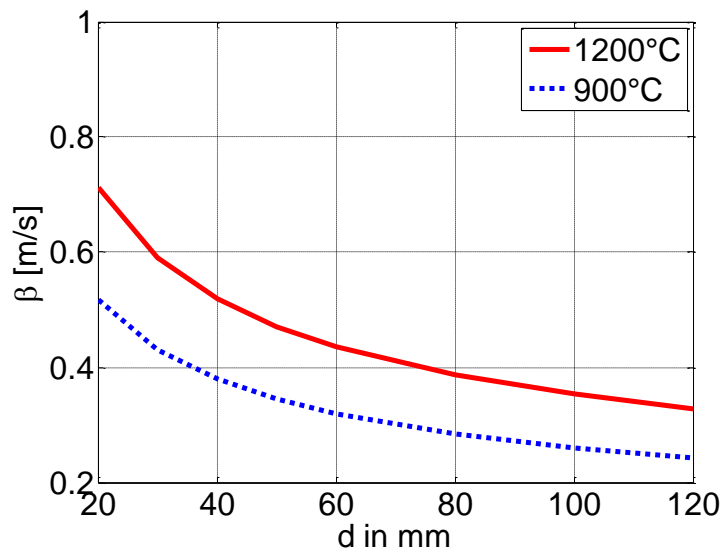


Figure 6-2: Variation of mass transfer coefficient of the bed with particle diameter for different temperatures

6.4 System of equations

System of stationary equations have been formulated and solved simultaneously to determine the temperature and conversion profiles for the limestone calcination. The equations used are same as the set of equations described in chapter 4, except the heat transfer equation where convection heat transfer is used here in this case instead of radiation heat transfer, because major heat transfer takes place by convection mechanism in a shaft kiln.

$$\dot{Q} = \alpha(T_{\text{gas}} - T_{\text{solid}}) \cdot A \quad (6.4-1)$$

Where α is the convection heat transfer coefficient, A is the surface area of the particle. Figure 6-3 and Figure 6-4 show the core temperature profiles for the decomposition at 1200 °C and 900 °C respectively for the particle diameters ranging from 20 to 120 mm. It can be seen from both the Figures that as the particle size increases core temperature decreases. For higher temperature decomposition, the average core temperature ranging between 960 °C to 915 °C for the particles of smallest to largest sizes. However for the lower temperature decomposition, the range of core temperature variation is not so significant and it is in the range of 865 to 860 °C for the smallest to largest size particles respectively.

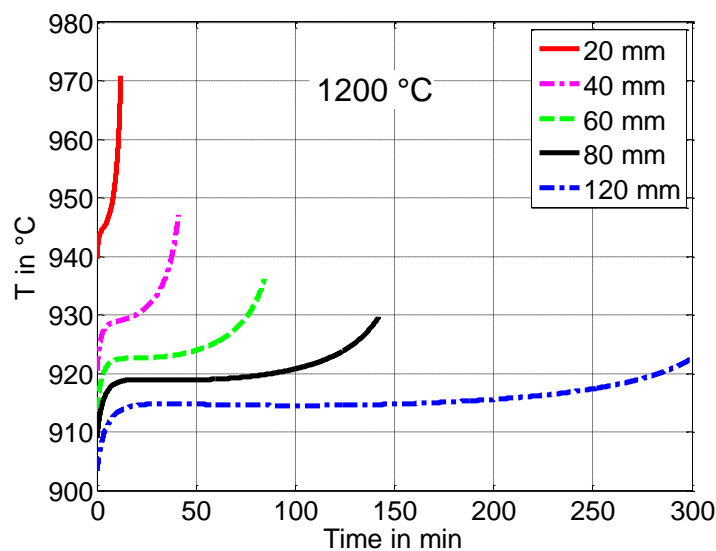


Figure 6-3: Predicted core temperature profiles of limestone samples decomposed at 1200 °C

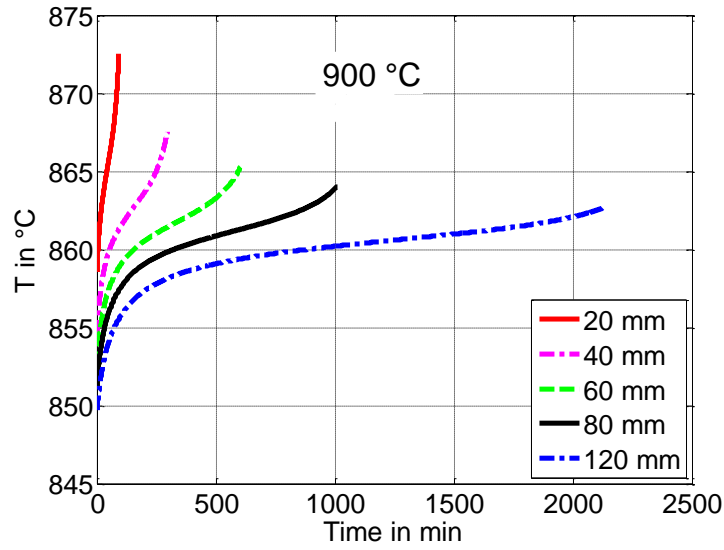


Figure 6-4: Predicted core temperature profiles of limestone samples decomposed at 900 °C

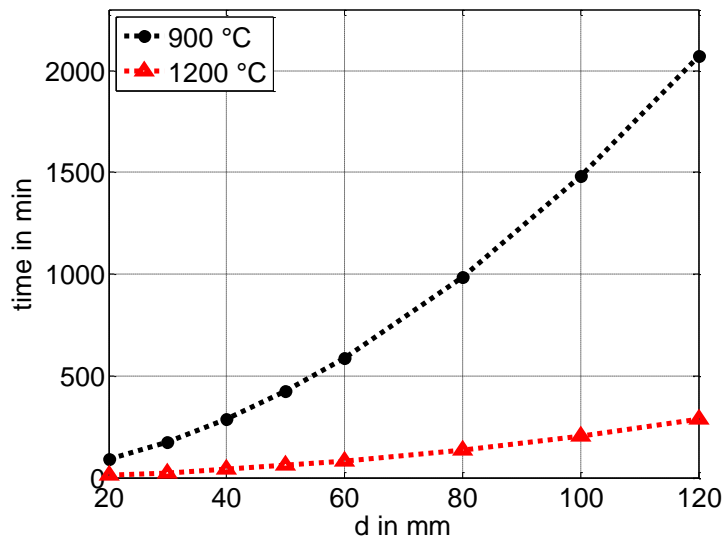


Figure 6-5: Predicted calcination time with the diameter of the particle

The above Figure 6-5 shows the required calcination time for different particle diameters. As the particle diameter increases calcination time increases exponentially for the lower decomposition temperature and the difference between the calcination times for these two temperatures is very high for the larger particles. For the complete decomposition of 120 mm particles, it requires more than 2000 minutes when the kiln gas temperature is 900°C where as it needs only 300 minutes if the gas temperature is maintained at 1200 °C.

6.5 Definition of Sensitivity

Sensitivity to calcination is defined as the extent of influence caused by each of the resistances on the time of calcination. It is formulated as

Sensitivity $\Omega_{\phi} = \frac{(t_{\phi_2} - t_{\phi_1}) / t_{\phi_2}}{(\phi_2 - \phi_1) / \phi_2}$ where Ω_{ϕ} is the sensitivity with respect to the parameter ϕ .

t_{ϕ_2} is the time required for complete calcination when the property is ϕ_2 and t_{ϕ_1} is the time required for complete calcination when the property is ϕ_1 . In the below sections the property ϕ is varied 5% i.e. $(\phi_2 - \phi_1) / \phi_2 \cdot 100 = 5$ and influence of this change on the calcination time is computed and discussed for the calcination at two different gas temperatures 900°C and 1200°C.

6.6 Sensitivity of various parameters

6.6.1 Heat transfer coefficient

Figure 6-6 shows the variation of sensitivity to heat transfer coefficient with respect to the diameter of the particle for the shaft kilns which are operated at gas temperatures 900 and 1200°C. The kiln operating at high temperature 1200°C exhibits higher sensitivity to heat transfer coefficient at lower diameters and the sensitivity decreases gradually with increase in size of the particle. Similar trends are observed for the sensitivities determined for other lower kiln temperature 900°C as well. The maximum sensitivity is determined as 32% for the high temperature calcination and for lower diameter particles and the lowest sensitivity of 14% was found for lower temperature decomposition at 120 mm particles.

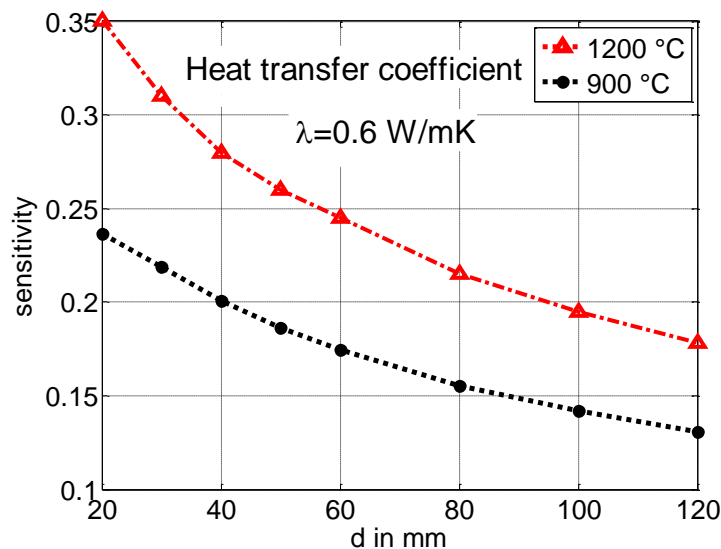


Figure 6-6: Variation of sensitivity to heat transfer coefficient with particle size

The above analysis is conducted at thermal conductivity of $0.6 \text{ Wm}^{-1}\text{K}^{-1}$. However conductivity of various limestones varies in the range from 0.4 to $0.8 \text{ Wm}^{-1}\text{K}^{-1}$. So the sensitivity analysis has been carried out for heat transfer coefficient at these possible boundary values of conductivity. Figure 6-7 (a) describes the sensitivity of heat transfer coefficient at kiln gas temperature 900 °C for three thermal conductivities 0.4, 0.6 and $0.8 \text{ Wm}^{-1}\text{K}^{-1}$. From this Figure it can be said that based on the conductivity, the sensitivity ranges in between 0.2 and 0.26 for 20 mm size and between 0.1 and 0.15 for the large particle size. Similarly Figure 6-7 (b) describes the same at 1200 °C. From this Figure it can

be observed that the sensitivity is in the range from 0.28-0.4 for smaller particles and it is in between 0.18 and 0.22 for the big particles.

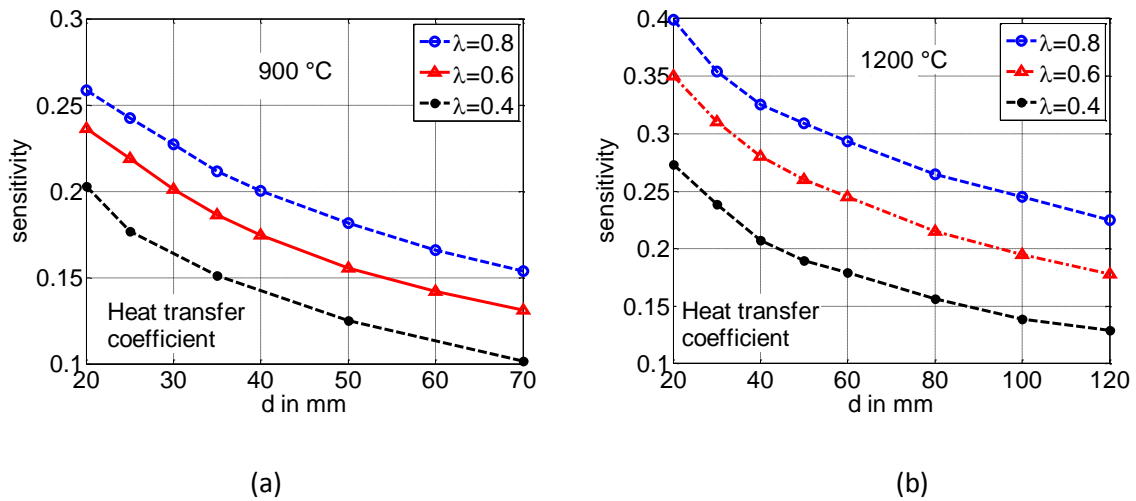


Figure 6-7: Variation of sensitivity to heat transfer coefficient with particle size for different thermal conductivities.

6.6.2 Thermal conductivity

Figure 6-8 presents the variation of sensitivity with respect to the diameter of the particle for the shaft kilns with the same ambient temperatures 900 and 1200°C. Sensitivity to thermal conductivity increases with increase in particle size at both of these kiln conditions. At high temperature, influence of thermal conductivity is found to be much higher when compared to the decomposition at lower kiln temperatures. The highest sensitivity found to be 78% for the high temperature calcination and for large particles. From this Figure it can be inferred that for the particles above 30 mm in size, that is most common particle size in industrial kilns, thermal conductivity controls the time of calcination from 40 to 80%.

It can also be understood that the thermal conductivity contributes to the major controlling factor for the limestone decomposition for the industrial kilns where the expected particle size ranges between 60-120 mm in size.

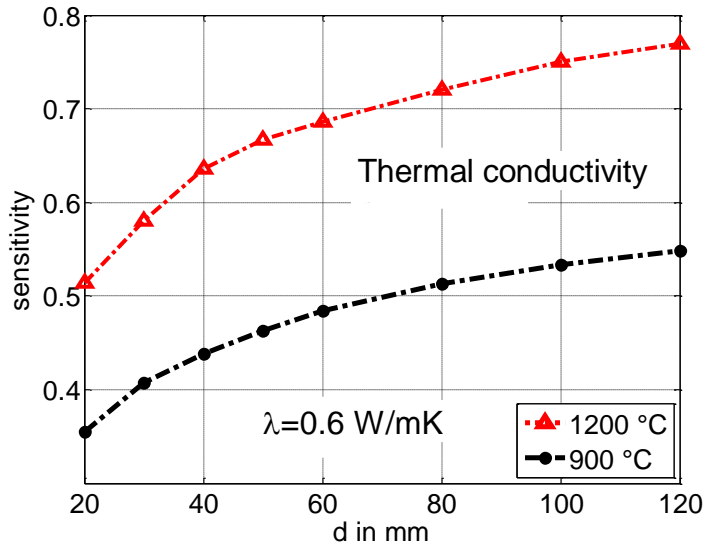


Figure 6-8: Variation of sensitivity to thermal conductivity with spherical particle size

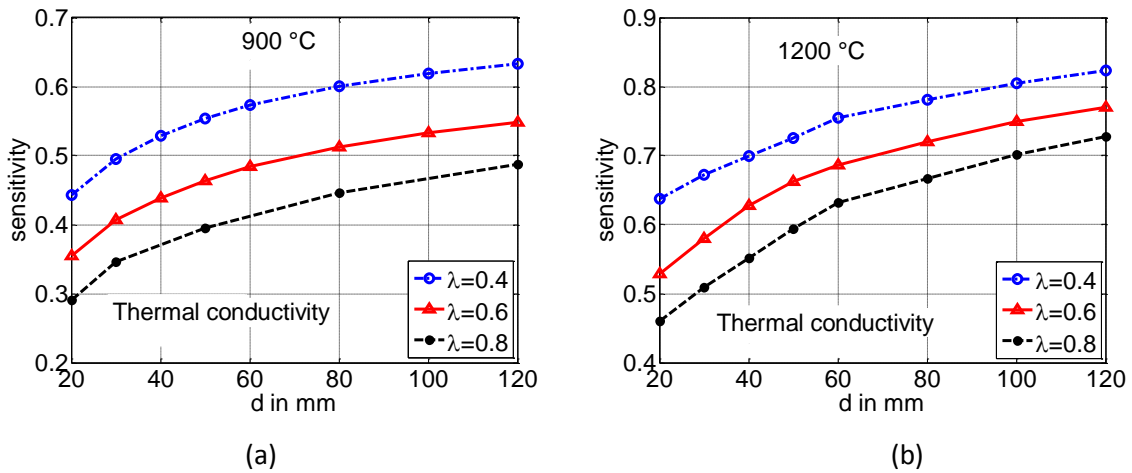


Figure 6-9: Variation of sensitivity to thermal conductivity with particle size for different thermal conductivities.

Figures 6-9 (a) and (b) describes the influence of boundary values of conductivity at 900 and 1200 °C respectively. From the Figure 6-9 (a) it can be observed that the range of sensitivity to conductivity is in between 0.3 and 0.45 for smaller particles whereas it is in between 0.5 and 0.62 for larger particles. Similarly from the Figure 6-9 (b), it can be noted that maximum sensitivity of 0.8 has been found for larger particles with very low thermal conductivity.

6.6.3 Reaction coefficient

Figure 6-10 depicts the variation of sensitivity of reaction coefficient with respect to the diameter of the particle for the shaft kilns which are at gas temperatures 900 and 1200°C respectively. For both of these temperatures, the sensitivity to reaction coefficient decreases with increase in particle diameter. Sensitivity varies between 27 to 7% when the gas temperature is 900 °C and it varies from 11 to 5% for higher gas temperatures. From this analysis, it can be inferred that, reaction coefficient is important parameter for lower temperature calcination process and for lower particle sizes. Irrespective of the kiln gas temperature the sensitivity of reaction coefficient on calcination drops to below 10% when the particles are bigger than 80 mm.

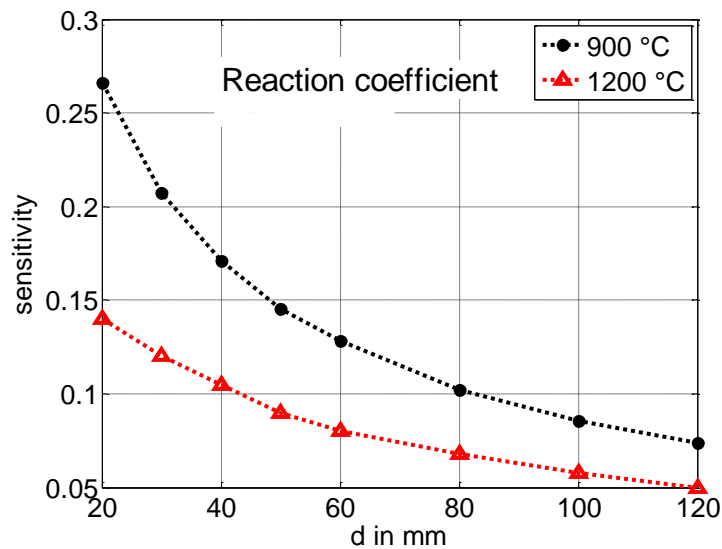


Figure 6-10: Variation of sensitivity to reaction coefficient with spherical particle size

6.6.4 Diffusion coefficient

Figure 6-11 describes the variation of sensitivity to diffusion coefficient with respect to the diameter of the particle for the shaft kilns which are operated at two gas temperatures. For the kiln operating at high temperature 1200°C shows lowest sensitivity to diffusion coefficient at lower diameters and the sensitivity increases very slowly with increase in size of the particle. The increase in sensitivity is 4 to 5% when the particle size increases from 30 to 120 mm in diameter. This shows very low sensitivity values found for the high kiln gas temperature. However for the kiln gas temperature of 900°C, sensitivity increases with diameter gradually from 20 to 30% when the particle size increases from 20 to 120 mm.

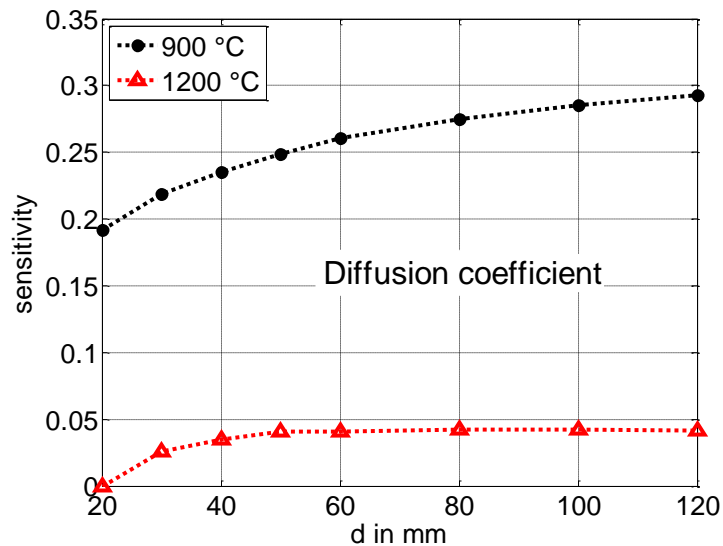


Figure 6-11: Variation of sensitivity to diffusion coefficient with particle size

Diffusion resistance is important when the decomposition occurs at lower temperatures and especially with bigger sizes.

6.7 Mass transfer coefficient

Mass transfer coefficient exhibits nearly no influence on calcination. At low temperature calcination the sensitivity is found to be around 0.7% maximum and at higher temperatures the influence is almost zero. The influence can be seen in the below Figure 6-12.

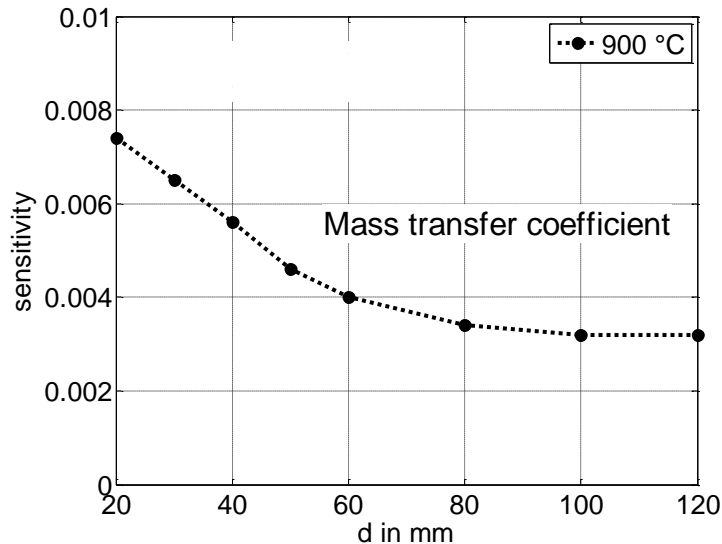


Figure 6-12: Variation of sensitivity to mass transfer coefficient with particle size

6.8 Analysis and discussion

From the above analysis it is evident that the decomposition is highly sensitive to thermal conductivity. Thermal conductivity causes up to 80% sensitive at larger particles and with higher temperature calcination process. Heat transfer coefficient contributes to 30% sensitivity for smaller particles. Diffusion coefficient shows up to 30% sensitivity for low temperature calcination and reaction coefficient shows minimum sensitivity compared to other parameters. Mass transfer coefficient didn't show any considerable influence on the decomposition time.

While considering the resistances due to heat transfer, conduction, chemical reaction, diffusion and mass transfer the sum of sensitivities of all these parameters should be summed up to 100% (around). This can be verified by considering the sensitivities at a particular diameter and at particular gas temperature. In the below table 6.3, the sensitivity is

considered at particle size 60 mm. At both the temperatures 1200 and 900 °C, the sum of all the sensitivities are summed up to 104 and 103 respectively. 3-4% error could be result of numerical errors.

Parameter	percentage sensitivity	
	1200 °C	900 °C
Heat transfer coefficient	24	16
Thermal conductivity	68	49
Reaction coefficient	8	13
Diffusion coefficient	4	26
Mass transfer coefficient	0	0
Total	104	103

Table 6.3: List of sensitivities of calcination paramters at particle size 60 mm and at the gas temperature of 1200°C

Chapter 7

Lime decomposition in CO₂ atmosphere

7.1 Introduction

In this chapter, Lime decomposition in the pure CO₂ environment has been described. Calcination experiments have been conducted with the limestone samples as described in Chapter 4. All the experimental setup and the experimental procedure is the same as that described in the earlier chapter except CO₂ gas is supplied to the tube furnace instead of air was sent in the earlier case.

Quasi stationary model and transient model have been developed for the decomposition in CO₂ environment as well as that in the previous case (decomposition in air). Heat transfer modeling part is same as in the previous case. However, the mass transfer mechanism varies because, the CO₂ pressure of 1 bar (approximately) is maintained around the specimen and hence the equilibrium pressure and the front pressure must be greater than one bar for the necessary driving force for the solid decomposition reaction to be established. The pressure difference between front and the surface results in bulk flow of gas in the oxide layer. The resistance to the bulk flow is negligible compared to the resistance of the diffusion process that occurs in the oxide layer when the particle is decomposed in the air environment. In this case, decomposition reaction is mainly controlled by heat transfer mechanism as the mass transfer resistances are negligible. The decomposition mechanism for such a system is more sensitive to chemical reaction

resistance and heat transfer resistance. So it could be possible to determine the thermal conductivity more accurately.

The system of algebraic equations described in Chapter 4 along with the below equation 7.1-1 have been solved simultaneously for the unknown parameters (T_f , T_s , X , r_f , \dot{M}_{CO_2} and \dot{Q}). The bulk flow of CO_2 gas in the oxide layer can be described by the Darcy's flow in a porous medium and hence the following equation describes the mass flow of CO_2 gas.

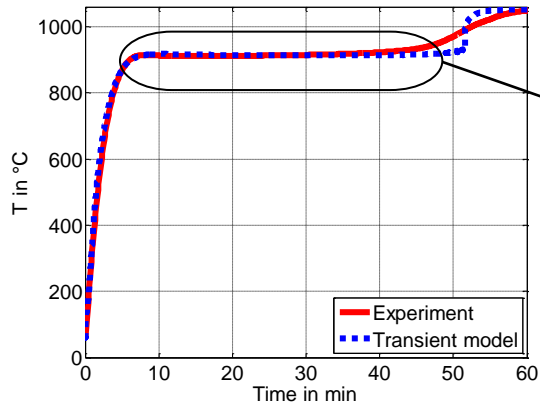
$$\dot{M}_{CO_2} = \frac{2\pi L}{\ln\left(\frac{r_s}{r_f}\right)} \cdot \frac{\kappa}{\mu} \cdot \rho \cdot (p_f - p_\infty) \quad (7.1-1)$$

In the above equation $\kappa [m^2]$ is permeability of oxide layer and μ is the dynamic viscosity of CO_2 gas. p_f and p_s are the partial pressures of CO_2 gas at the reaction front and at the ambient environment respectively. The new parameter κ is added for the analysis of these experiments because of Darcy flow model and the tortuosity (parameter with diffusion model) and mass transfer coefficient are excluded from the analysis.

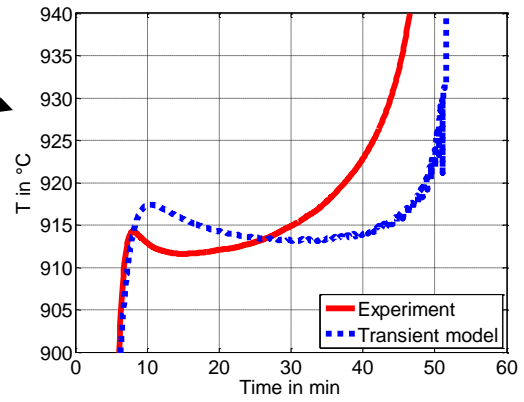
7.2 Determination of properties

7.2.1 Sample T

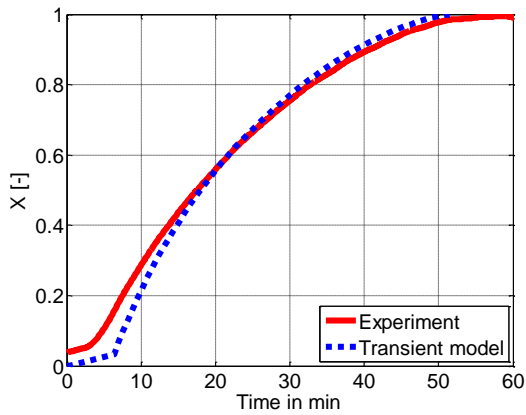
The cylindrical limestone sample T with density 2630 kg m^{-3} and diameter 24.5 mm has been decomposed in the CO_2 environment at 1050°C . The calcination time needed for this sample under these conditions is 50 minutes. Figure 7-1 (a), compares the complete core temperature profile whereas Figure 7-1 (b) shows the close view of the core temperature profile. Comparison of measured and predicted conversion profiles have been compared as shown in the Figure 7-1 (c). The list of parameters and properties are listed on the right side of the Figure 7-1 (c). The parameters and units are already described in the previous chapter, however here additional parameters permeability (m^2) (κ) and partial pressure of CO_2 (p_{amb}) have been included. Partial pressure listed here is in bars.



(a)



(b)



(c)

Name : **Sample T in CO₂ gas**

$$T_{\text{amb}} = 1052 \text{ }^{\circ}\text{C}$$

$$\rho = 2635 \text{ kg/m}^3$$

$$\text{purity} = 0.99$$

$$d = 24.5 \text{ mm}$$

for Limestone

$$c_p = 1000 \cdot (T/473)^{0.3}$$

$$\lambda = 0.53 + 672 / (T + 28) \text{ if } T_c < 600^{\circ}\text{C}$$

$$\lambda = 0.83 + 672 / (T + 28) \text{ if } T_c > 600^{\circ}\text{C}$$

for Lime

$$k = 0.038 \text{ m/s}$$

$$T_{\text{eq}} = 910^{\circ}\text{C}$$

$$\kappa = 1 \cdot 10^{-12} \text{ m}^2$$

$$p_{\text{amb}} = 0.85 \text{ bar}$$

$$\text{epsilon} = 0.5$$

$$c_p = 940 \text{ J/kgK}$$

$$\lambda = 0.7 \text{ W/mk}$$

Figure 7-1: Comparison of measured and predicted temperature (a), (b) and conversion (c) profiles for the sample T in CO₂ environment

7.2.2 Sample F2-IV

Sample F2 - IV which is a relatively very low density (2090 kgm^{-3}) sample with diameter 25 mm also decomposed in CO_2 environment at very high temperature $1190 \text{ }^\circ\text{C}$. The calcination time is only 30 minutes under these conditions. The measured and predicted temperature and conversion profiles have been compared as shown in the Figure 7-2.

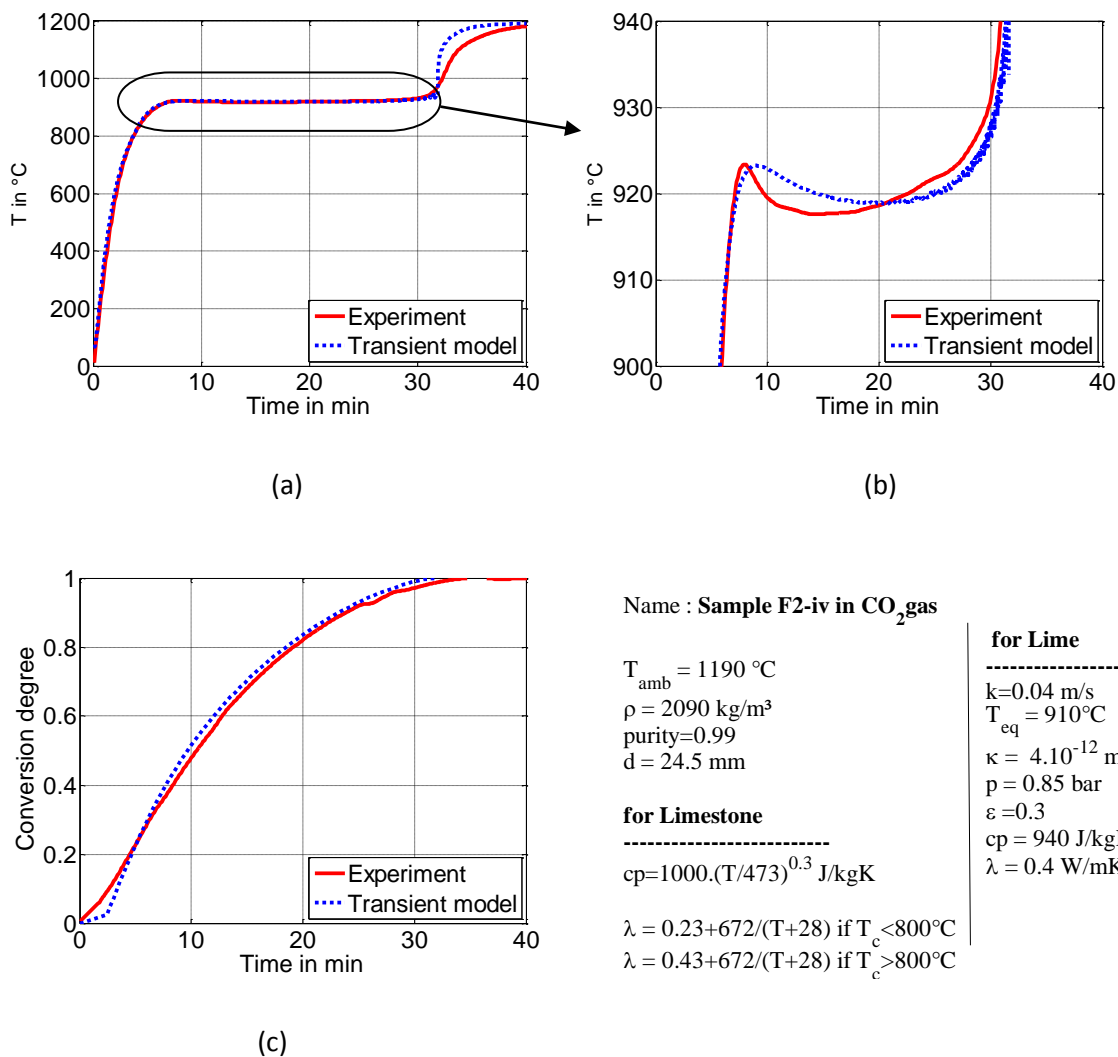


Figure 7-2: Comparison of measured and predicted temperature (a), (b) and conversion (c) profiles for the sample F2-IV in CO_2 environment

7.3 Summary

Decomposition experiments have been conducted in the CO₂ environment. The process of decomposition has been modeled and the temperature and conversion profiles predicted are compared with the measured profiles. Below Table 7-1 compares the thermal conductivity determined for the sample T and sample F2- IV when the experiments are conducted at different ambient temperatures in these two different environments. For the sample T, the thermal conductivity is in the range 0.7-0.73 W/m/K whereas for the sample F-IV it is in the range of 0.35-0.44.

Sample Name	T_{amb} (°C)	Decomposed environment	Thermal conductivity (W/m/K)
T	1058	air	0.73
	1164	air	0.7
	1052	CO ₂	0.7
F2- IV	965	air	0.4
	1042	air	0.44
	1126	air	0.35
	1045	CO ₂	0.44
	1190	CO ₂	0.4

Table 7.1 : Comparison of thermal conductivity determined by experiments conducted in air and CO₂ environments

Chapter 8

Recarbonation of lime

8.1 Introduction

During this Industrial era, usage of fossil fuels is very much increased. Due to this, CO₂ emissions have been increased rapidly. This in turn causes the global warming. It became a challenging task to remove the CO₂ gas from the industrial flue gases to protect the environment. Thus it takes interest to investigate the ways to reduce the CO₂ emissions. One of the ways to remove the CO₂ is by using the recarbonation reaction. Several researchers studied the recarbonation behavior of lime. This chapter focuses on the methods of recarbonation experiments conducted in our laboratory and also the influence of temperature and type of lime on the recarbonation reaction. It is also discussed the effect of recarbonation after several cycles of carbonation-decomposition.

8.2 Historical background and Literature review

One of the ways of separation and storage of CO₂ is by making it reacts with lime (CaO(s) + CO₂ (g) ↔ CaCO₃(S)). This reaction is called carbonation and in the opposite direction the calcination process occurs which produces a concentrated stream of CO₂ gas. The first investigation of this separation of CO₂ in 1867 was done by DuMotay and Marechal. They had the first patent for the use of lime to aid the gasification of carbon by steam [59].

To meet high energy demands, fossil fuels usage have been increased which in turn results in high CO₂ emissions. Before the industrial revolution the concentration of CO₂ in the environment was around 280 ppm. Later in the year 1950, CO₂ concentration has been raised to 315 ppmv but in 1990 it is in levels of 355 ppmv [60]. This increase in the CO₂ provokes the half of the greenhouse effect that causes global warming. The IPPC (Intergovernmental Panel on Climate Change) has the opinion that “the balance of evidence suggests a discernible human influence on the global climate ” [60]. This means

it is necessary to create a cost-effective system to slow down the CO₂ emissions. Research has been amplified in the recent past in this regard. Several methods and techniques have been proposed by various authors across the globe for the carbonation of lime to separate CO₂ from flue gases in which CaO is used as sorbent. Mackenzie et al. concluded that CO₂ separation with the calcium based sorbents (CaO) is one of the economically attractive way [61]. Hence it is also important to study the influence of carbonation efficiency with number of cycles of calcination and carbonation of CaO. Jia et al. [62] studied the influence of number of cycles on the carbonation and mentioned that the efficiency of repeated carbonation reaction varies with origin of limestone. Abanades [63] reviewed and collected several series of experimental data on the decay of maximum lime carbonation degree with respect to number of cycles. The loss of efficiency with number of cycles of carbonation is due to loss in porosity of the small pores and the reaction is limited by increasing the thickness of the product layer on the surface of the particle [59]. Cultrone et al. [64] studied the carbonation behavior of lime based mortars in presence of additives and CO₂ rich environment and later compared the results with naturally carbonated mortars. It was found that under natural conditions the carbonation is pretty slower and suggested that extent of carbonation depends on amount of CO₂ used. Capture and storage of CO₂ is one of the major parts in power industry. Carbonation loop is used for post combustion absorption of CO₂ by lime as shown in the Figure 8-1. In Carbonate looping process, lime reacts with CO₂ in the flue gas from the power plant. This reaction takes place in a chamber called carbonator which is maintained at 650°C. Due to high temperatures, the specific surface area of the sorbent reduces. It results in lower CO₂ capture in the carbonate loop [65]. Nikulshina [66] studied the carbonation behavior with lime and lime milk and observed that intra particle diffusion is controlling mechanism for the carbonation with lime particles whereas lime milk carbonation is less hindered by diffusion and catalyzed by water. Experiments and modelling of successive calcination-carbonation cycles have been carried out by Eric Bouquet et al. [67]. Based on their model, voids present between the micro grains will be filled up when the critical thickness of the carbonate layer reaches to 43 nm. In this situation, the carbonation is controlled by the diffusion coefficient which falls from 2×10^{-12} to 6.5×10^{-14} at 650 °C. This change in diffusivity is responsible for drastic change in carbonation rate. In another study Fennel et al. [68] studied that the loss of CO₂ carrying capacity after n cycles is because of the reduction in void space narrower than 150 nm.

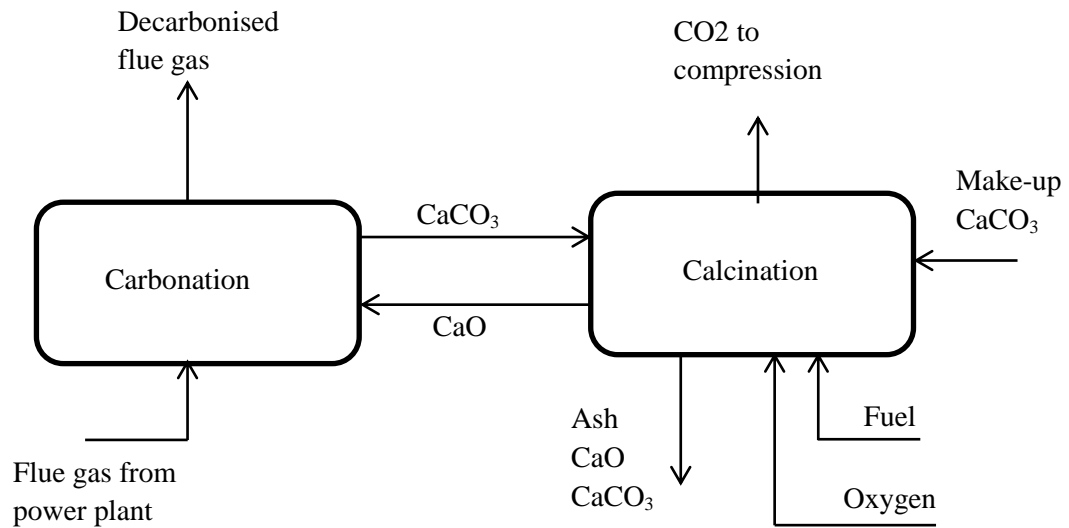


Figure 8-1: Principle of the carbonate looping process [70]

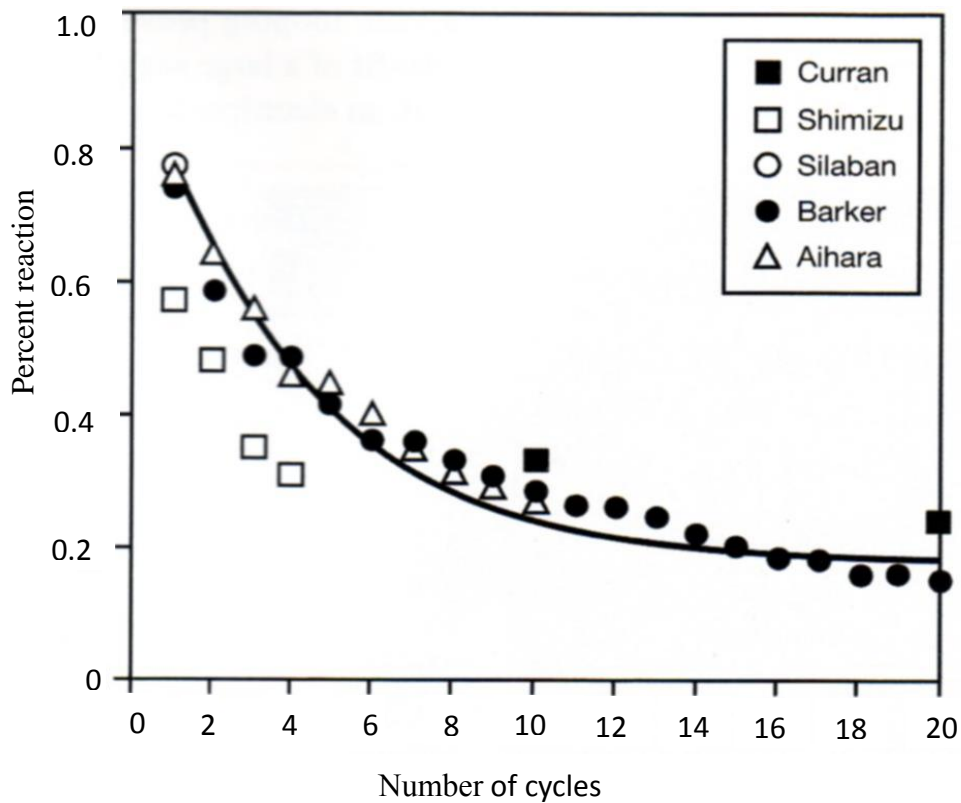


Figure 8-2 Decay of maximum carbonation degree with number of cycles [63]

Current study focuses mainly to understand the best conditions for the carbonation reactions and the influence of repeated cycles on carbonation. The effect of particle size and the temperature for the limestone of different origins have also been studied on the recarbonation reaction.

8.3 Experimental setup

The experimental setup for conducting the recarbonation experiments is shown schematically in the Figure 8-3. The experimental set up and methodology is same as described in chapter 3 which is used for decomposition experiments. However in the latter case, lime particles are supported in a perforated plate and the CO₂ gas has been supplied from the bottom of the furnace. The ceramic particle bed at the bottom of the tube furnace ensures the uniform flow field to be established to have perfect contact with lime particles. Perforated plate with lime particles is hanged to a weight balance which records the increase in weight during recarbonation process. Furnace has been heated and maintained at different constant temperatures and the recarbonation behavior has been studied at different temperatures.

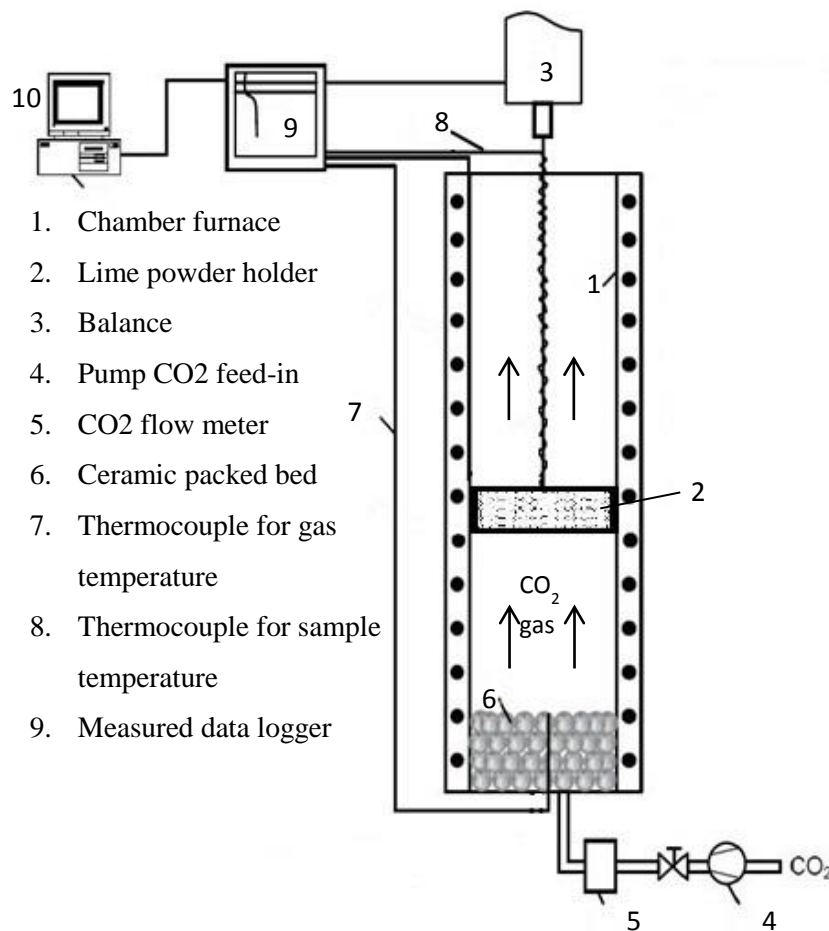


Figure 8-3: Schematic diagram of the experimental setup for carbonization

8.3.1 Reaction with lime particles

Lime particles with size around 3-4 mm are deposited on a porous plate holder as shown in the Figure 8-2 and CO₂ gas is passed through this perforated holder. This perforated holder ensures the CO₂ gas flow is in contact with the lime particles. The holder is inserted in a tube furnace as shown in the Figure 8-1 and it is hanged to a balance which is connected to the computer. The mass change of the perforated plate holder has been recorded which shows the progress of the carbonation reaction.



Figure 8-4: Porous ceramic holder with lime particles

Initially the experiments are conducted with lime particles at room temperature and no increase in mass of the sample has been observed even after several minutes. As a first step, the sample of weight 5.65 g (with particle size 2-4 mm) is continuously exposed to flow of CO₂ gas at 2 m³/hr for 120 minutes. However no change in mass has been noticed even after couple of hours. This shows no carbonation reaction took place at room temperature.

8.3.2 Reaction with Lime milk

Lime is mixed with water to make lime milk as shown in the Figure 8-4.



Formation of $\text{Ca}(\text{OH})_2$ is an exothermic reaction. Lime milk is applied to the ceramic porous plate as shown in the Figure 8-5. The holder is allowed to dry and ensured the pores are not blocked with lime milk. This is important because CO_2 gas must penetrate through the porous plate in order to have contact with lime milk. Now the holder is placed in the tube furnace and subjected to the flow of CO_2 gas as in the previous case. The weight of the lime milk associated with the ceramic holder is recorded as before. As the time progress there is no change in weight is recorded. The experiment is continued for couple of hours with continuous flow of gas, but no reaction has been achieved.

From the above two experiments (lime particles or lime milk) lime could not react with CO_2 to give carbonate. This shows that the carbonation is almost negligible at room temperature irrespective of the form of the reactant lime.



Figure 8-5: Lime milk



Figure 8-6: Ceramic porous plate with lime milk

8.4 Carbonation at higher temperatures

As it was found no reaction at the room temperature, carbonation experiments at higher temperatures have been carried out. A special perforated steel holder has been made with 0.5 mm size perforations as shown in the Figure 8 -5 below.



Figure 8-7: Perforated steel holder with lime particles

Experiments are conducted at different temperatures 300, 400,600 and 800°C and lime particles of different size range 0.75 mm, 2 mm and 3.5 mm. Lime is sieved in to these three different size ranges for the carbonation experiments.

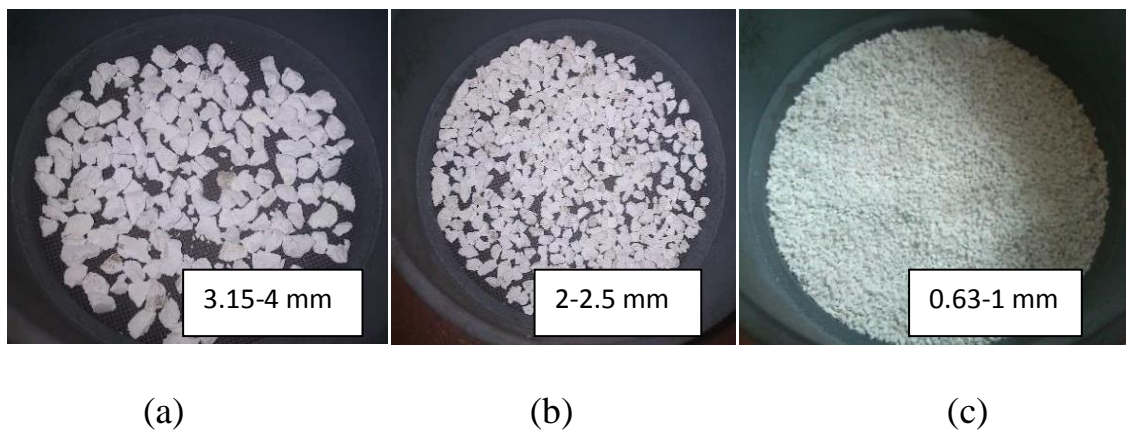


Figure 8-8: Lime particles of different size distribution

8.5 Influence of Temperature

Furnace is maintained at a constant uniform temperature at which experiment is going to be conducted and the continuous supply of CO₂ gas has been maintained from the bottom of the furnace as described in the Figure 8-1. For this study lime obtained from the two different limestones has been taken. One sample is named as F2-IV which is low density limestone and the other one is high density limestone B. At first lime from F2-IV has been tested for carbonation reaction at different constant ambient temperatures 300, 400 and 600°C. In each of these experiments, the increase of mass of lime is recorded with time. From the stoichiometry,

$$\text{Percent reaction at time } t = \frac{m_t}{(0.44/0.56) \cdot m_{\text{total}}} \cdot 100 \quad (8.5-1)$$

where m_t is the mass gained due to reaction at time t and m_{total} is the total initial mass of the lime sample. Figure 8-7 shows the percent of carbonation reaction with respect to time for the lime F2_IV at two different temperatures 400 and 600 °C. At 200 and 300°C experiments were conducted as well. However there is no significant progression of the reaction has been observed. At 400°C, the reaction is found to be less than 5% even after 60 minutes. But at 600°C a significant percent of reaction has been achieved. In 80 minutes the reaction has been progressed up to 32 percent and maintained almost at constant value further with respect to time.

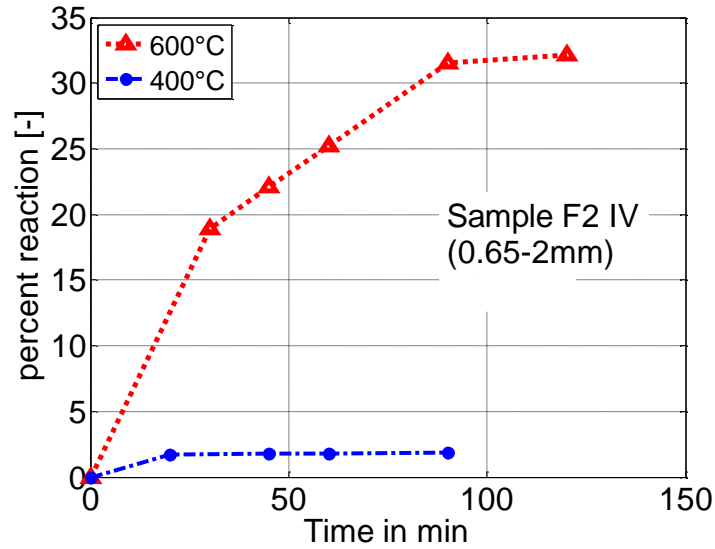


Figure 8-9: Carbonation of Sample F2_iv at 400 and 600°C

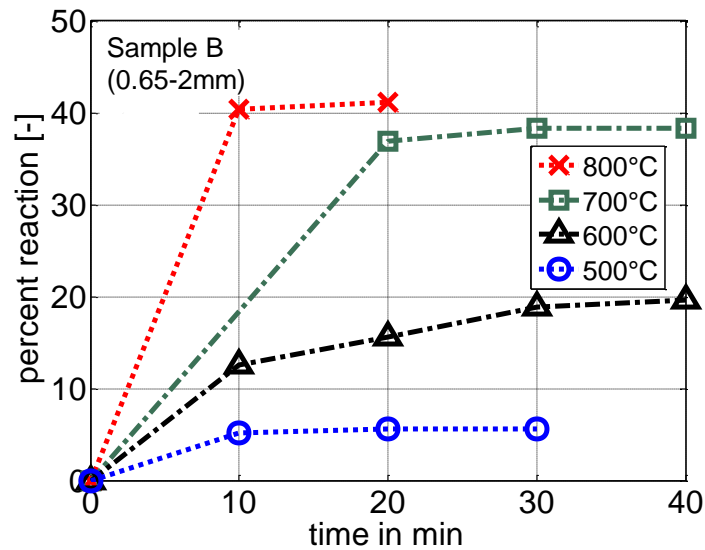


Figure 8-10: Carbonation of Sample B at different temperatures.

Figure 8-8: shows the percent of reaction versus time for the lime B at four different temperatures 500, 600, 700 and 800°C respectively. From this Figure it can be clearly seen that 5% of the recarbonation is attained in 10 minutes when experiment is conducted at 500°C whereas at higher temperatures much better carbonation reaction occurred. For the sample at 600°C attains 20% conversion in 30 minutes, sample carbonized at 700°C

attains 37% conversion in 20 minutes and the sample carbonized at 800°C attains 40% recarbonation just in 10 minutes.

8.5.1 Influence of particle size

In order to study the influence of particle size on recarbonation reaction, three different lime size distributions have been used for the carbonation reaction at 800°C with the Lime B.

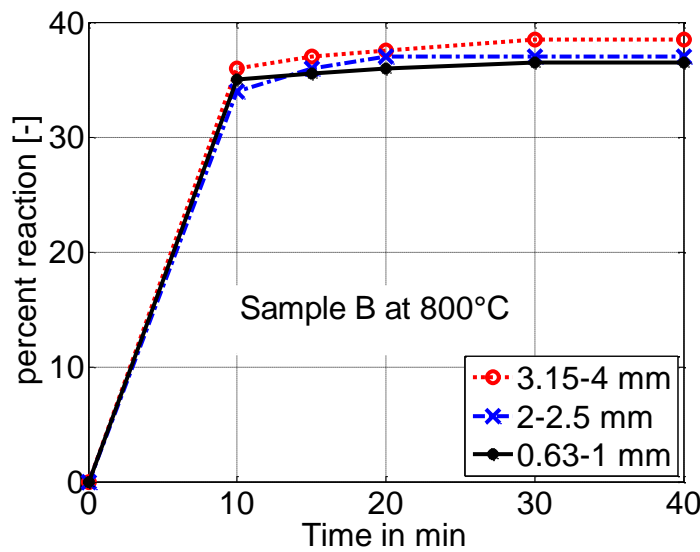


Figure 8-11: Carbonation of Lime B at 800°C with different particle sizes

Above Figure 8-9 shows the percent reaction obtained with three different particle size distributions 3.15-4 mm, 2-2.5 mm and 0.63-1 mm respectively. At 800°C, all these samples reach around 35% of the carbonation in 10 minutes and then found a very slow progression of the reaction. It is expected that the smaller particles with large surface area for carbonation reaction should attain higher reaction degree. However bigger particles show 2-3% higher degree of carbonation compared to smaller particles. This may be due to the reversible reaction of limestone decomposition which is also favoured at this temperature and smaller particles would under go faster decomposition and hence smaller particles could attain slightly lesser carbonation.

8.5.2 Influence of number of cycles

It is very important to study the influence of recarbonation with number of cycles. Lime B is allowed for carbonation at 800°C and after 20 minutes when it reaches to maximum carbonation of 30%, it is decomposed at higher temperatures fully to lime again. This lime again subjected to carbonation reaction. This cycle has been repeated several times to study the influence of carbonation after few of the cycles.

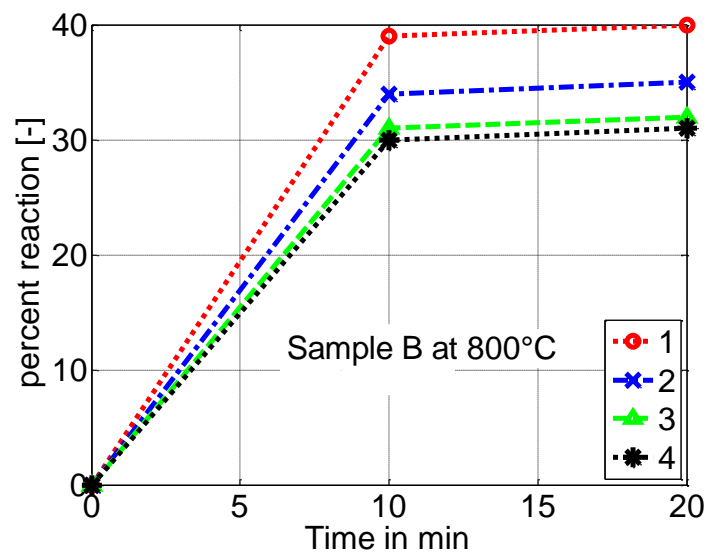


Figure 8-12: Sample B recarbonation cycles at 800°C

Figure 8-10: shows the influence of carbonation reaction of the lime B for 4 cycles. For the first time, when the lime B is carbonized it attains 40% of the reaction. This is showed in the red dotted line in the figure. This lime is decomposed and recarbonized 2nd , 3rd and 4th time. Blue, green and black dotted lines show these recarbonizations behaviors respectively. It is clearly seen that the recycling of lime would result in loss of carbonation efficiency. However after three cycles, the loss is around 20%. The same analysis has been done for the other sample F2_IV at the same conditions as shown in the Figure 8-11. For this sample it can be observed that the percent reaction has been dropped from 61% for the first cycle to 55% for the 4th cycle. Here the efficiency of recarbonation has been dropped just around 10%.

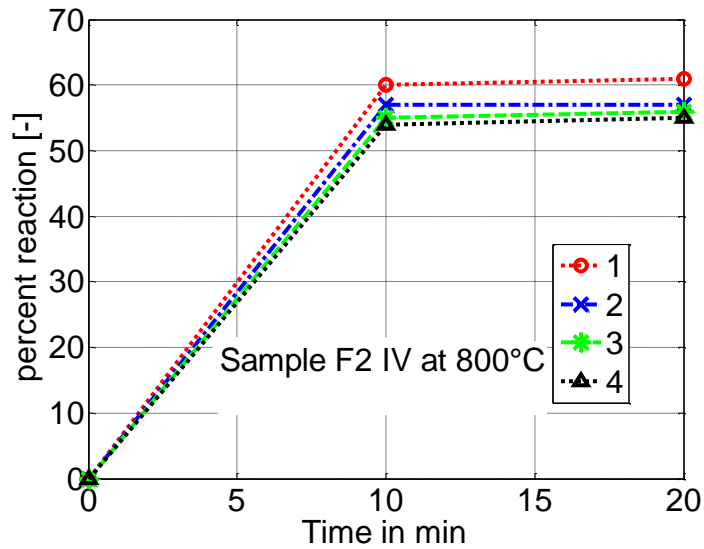


Figure 8-13: Sample F2_IV recarbonation cycles at 800°C

8.6 Summary

From the above observations, it can be concluded that, recarbonation is favored at higher temperatures. At 300 °C the degree of carbonation reaction is around 2 - 5% and it increases with temperature. At 800°C, the degree of reaction is in the range of 30 - 60% depending on the type of lime. Particles are used in the size range from 0.6 mm to 4 mm. In this size range, no significant change in degree of reaction has been noticed. Recarbonation reaction has been conducted for two lime samples up to 4 cycles. The efficiency drop for each of the cycles is around 2 - 5% was observed and after 4 cycles the total efficiency loss was observed between 10 - 20% depending on the type of lime.

Chapter 9

Material properties

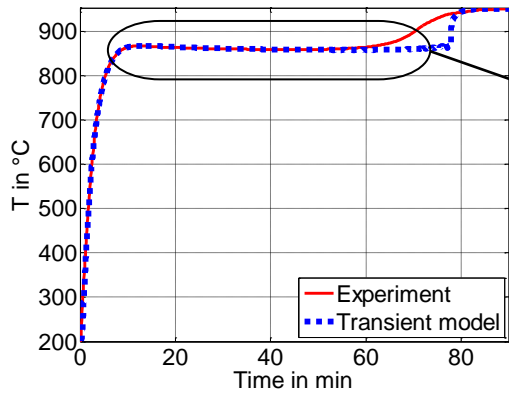
9.1 Introduction

In this chapter material properties and process parameters of limestone at different temperatures, sizes, experimental conditions for limestones of different origins have been discussed. In the below sections, each of the figure has 3 sub figures (a), (b) and (c). Subfigures (a) and (b) compares the core temperature profile in full and closed view respectively. Subfigure (c) compares the conversion degree. The properties predicted by the transient model have been listed along with experimental measurements on the right side of subfigure (c).

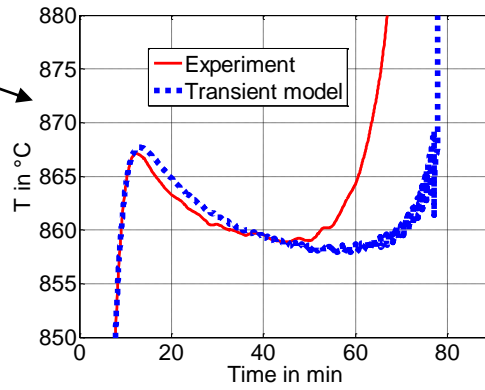
9.2 Experiments at different temperatures

9.2.1 Sample 1mu1 decomposed at (950°C)

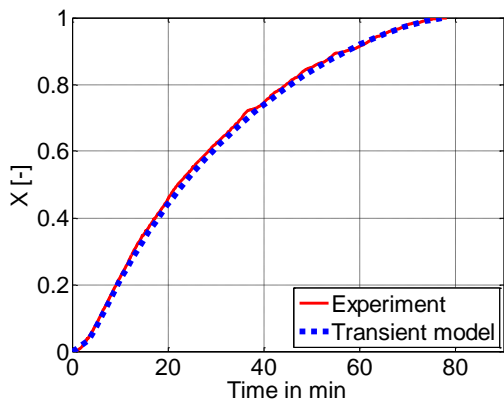
Figure 9-1 compares the measured and profiles predicted by the transient model for the limestone 1mu1 which was decomposed at 950°C. Similarly Figure 9-2 compares the same for the same limestone but decomposed at 1050 °C. From these two Figures it can be observed that the way transient model has been used to predict the temperature and conversion profiles in these two cases.



(a)



(b)



(c)

Name : **1mu1 in air**

$T_{amb} = 951 \text{ } ^\circ\text{C}$

$\rho = 2700 \text{ Kg/m}^3$

purity=0.9

$d = 24.5 \text{ mm}$

for Limestone

 $c_p = 1000 \cdot (T/473)^{0.3}$

$\lambda = 0.43 + 672/(T+28)$ if $T_c < 600^\circ\text{C}$

$\lambda = 0.38 + 672/(T+28)$ if $T_c > 600^\circ\text{C}$

for Lime

 $k = 0.03 \text{ m/s}$

$T_{eq} = 900^\circ\text{C}$

$\beta = 0.018 \text{ m/s}$

$\psi = 0.5$

$\tau = 1.5$

$\varepsilon = 0.5$

$c_p = 940 \text{ J/KgK}$

$\lambda = 0.52 \text{ W/mK}$

Figure 9-1: Comparison of measured and predicted temperature (a), (b) and conversion (c) profiles for the sample 1mu1 in air environment at 950 °C

9.2.2 Sample 1mu1 at 1050 °C

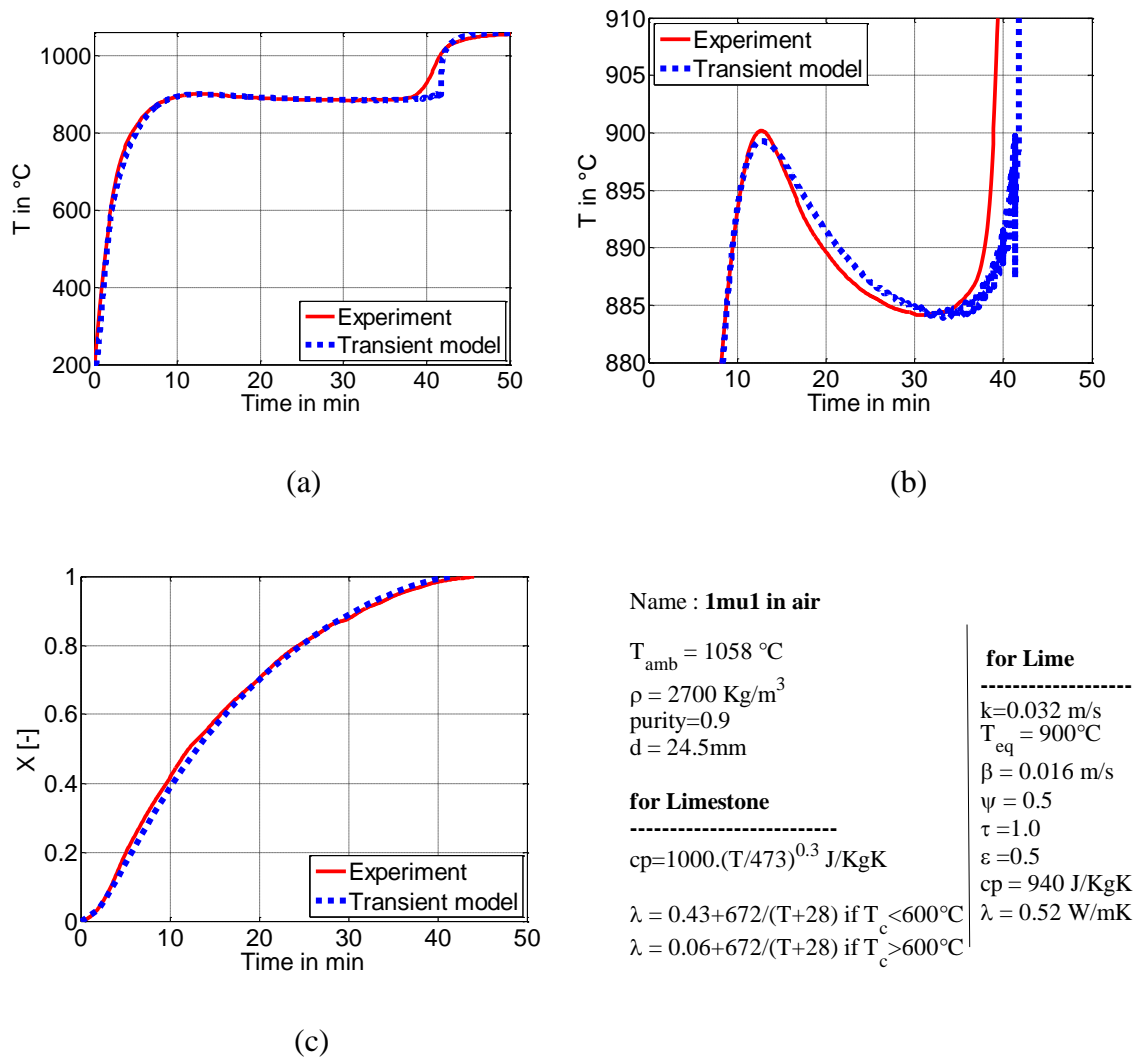


Figure 9-2: Comparison of measured and predicted temperature (a), (b) and conversion (c) profiles for the sample 1mu1 in air environment at 1058 °C

In the above section, Limestone sample 1mu1 decomposed at two different ambient temperatures has been compared. Table 9.1 describes the list of best fitting parameters of Transient model in these two cases. Thermal conductivity is found to be 0.52 in both the cases and reaction coefficient is found to be slightly higher when the decomposition taken place at higher temperature. Tortuosity predicted by the model is 1.5 and 1.0 for the experiment at both of these temperatures 950°C and 1050°C respectively. This can be because the sample cut from the real stone at different locations may have slightly

different internal structures which resulted in slight variation in tortuosity factor. A difference of 10% is found in the mass transfer coefficient in both of these cases. As mass transfer coefficient is calculated based the correlation for this case and it is known that the correlations cannot predict the heat and mass transfer coefficients so accurately hence this small difference in mass transfer coefficient in this case is not so important to be noted.

Sample 1mu1	950°C	1050°C
Thermal conductivity	0.52	0.52
Reaction coefficient	0.03	0.032
Tortuosity	1.5	1.0
Mass transfer coefficient	0.018	0.016
Effective emissivity	0.5	0.5

Table 9.1: Comparison of properties for the sample 1mu1 at two ambient temperatures.

9.3 Experiments with different particle sizes

Limestone sample KN1 with three different diameters 14.4 mm, 24.5 mm and 32.2 mm have been decomposed at the same kiln conditions and at 1050 °C temperature. For better readability the particle with 14.4 mm diameter is referred as small particle, particle with 24.5 mm diameter as medium particle and the one with 32.2 mm as the big particle in further discussion. Figure 9-3 shows the measured temperature and conversion profiles for these three samples. From this Figure, the calcination time can be noted as 80, 60 and 25 minutes for the big, medium and small size particles respectively. The product layer begins to sinter in the case of larger particles due to prolonged calcination times and hence reduces the porosity [69]. This in turn results in increase in diffusion resistance. In the current analysis, porosity has been considered constant irrespective of the particle size. The decrease in porosity in the case of larger particles is compensated by slightly increase in tortuosity value.

In the next section, transient model has been used to simulate the temperature and conversion profiles for these three experiments and the best set of parameters and properties have been listed.

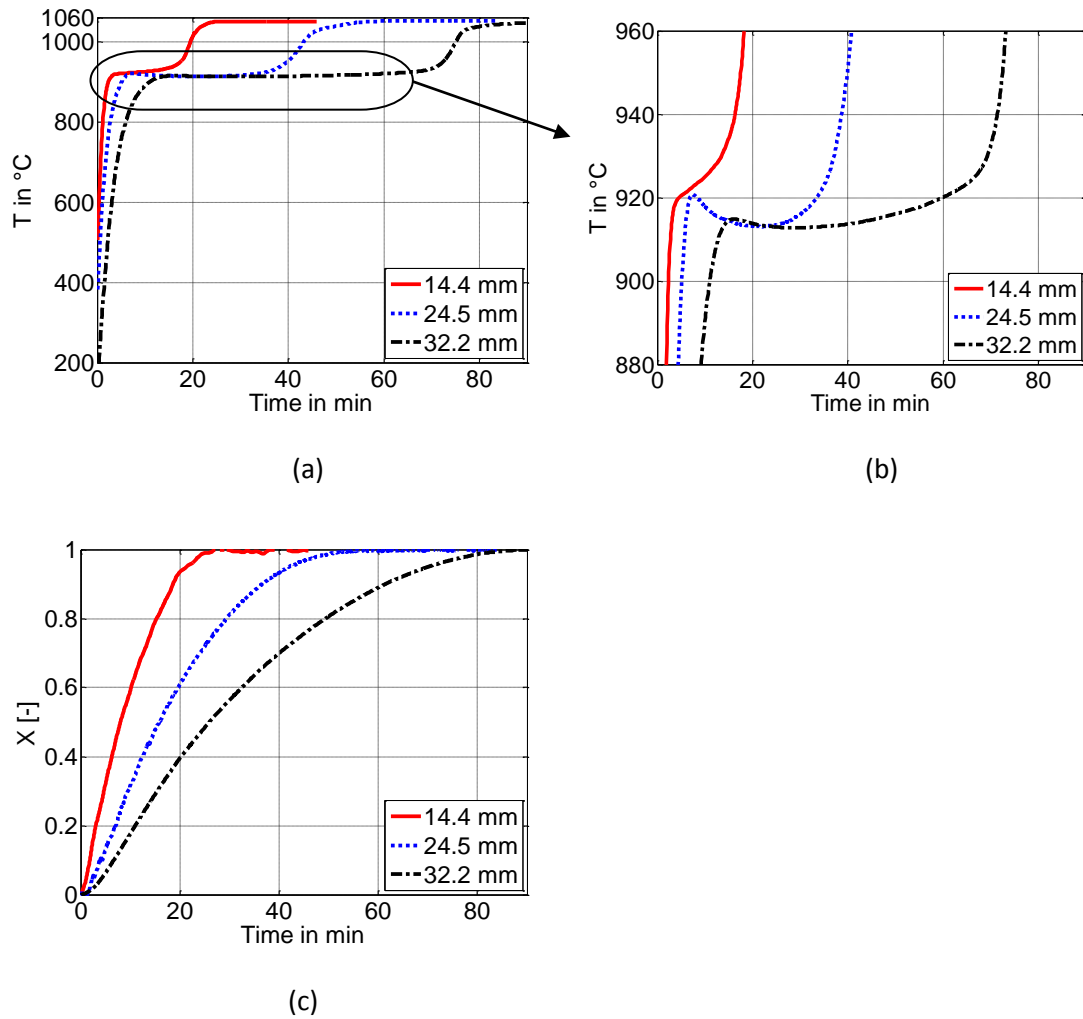


Figure 9-3: Comparison of experimentally measured temperature (a), (b) and conversion (c) profiles for the sample KN1 in air environment at 1050 $^{\circ}\text{C}$ at different particle sizes

9.4 Simulations and comparisons for the sample KN1

9.4.1 Sample KN1 with 14.4 mm (Small particle)

Figure 9-4 shows the measured and predicted profiles for the small particle. Figure 9-4 (a) compares the core temperature profile, while Figure 9-3 (b) shows the same but at close view. Figure 9-3 (c) compares the conversion profile. The set of parameters are given on the right side of Figure 9-3 (C). Similarly in the below subsections 9.4.2 and 9.4.3, the analysis has been done for medium and big particles respectively.

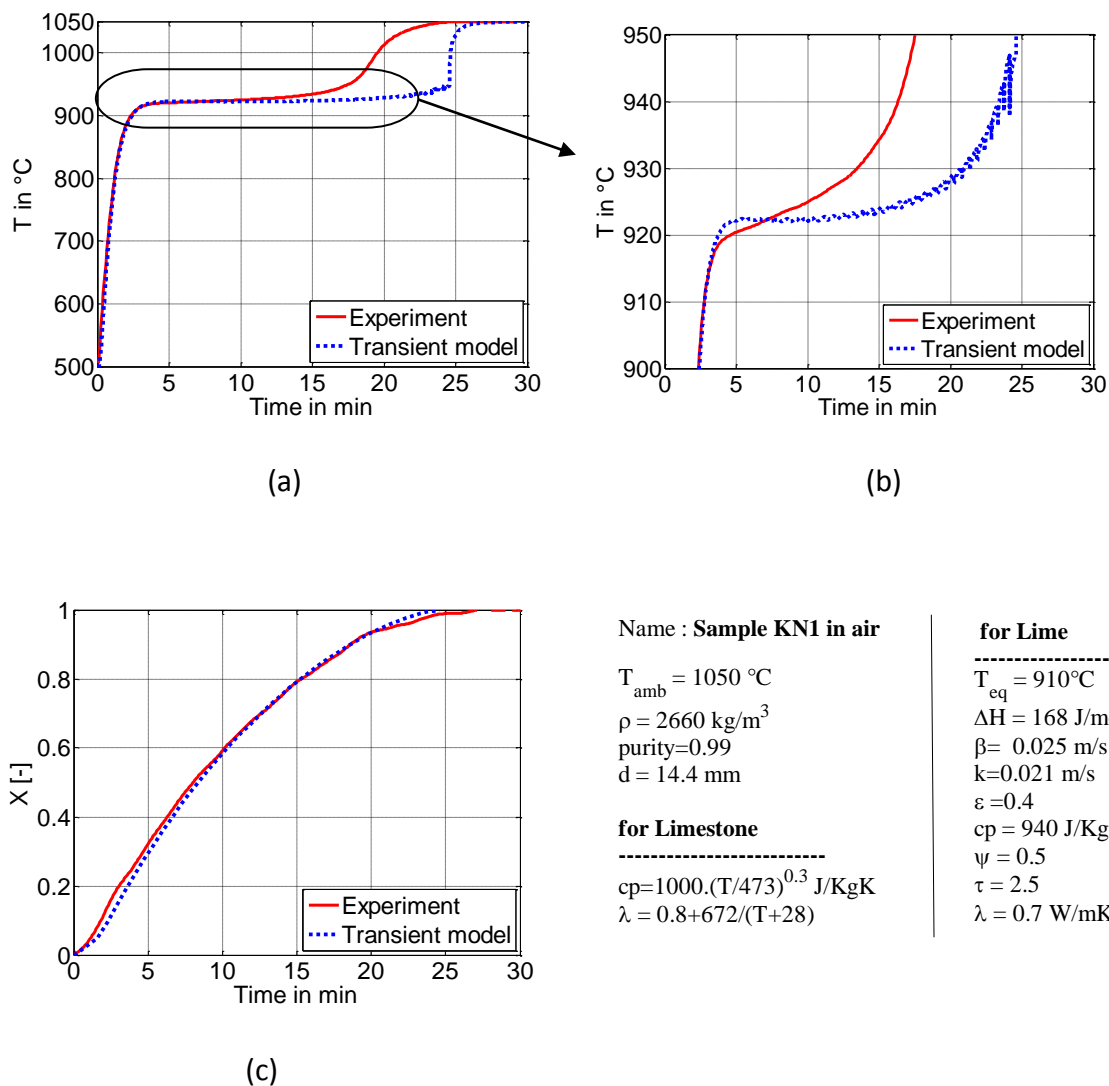


Figure 9-4: Comparison of measured and predicted temperature (a), (b) and conversion (c) profiles for the sample KN1 with particle size 14.4 mm

9.4.2 Sample KN1 with 24.5 mm (Medium particle)

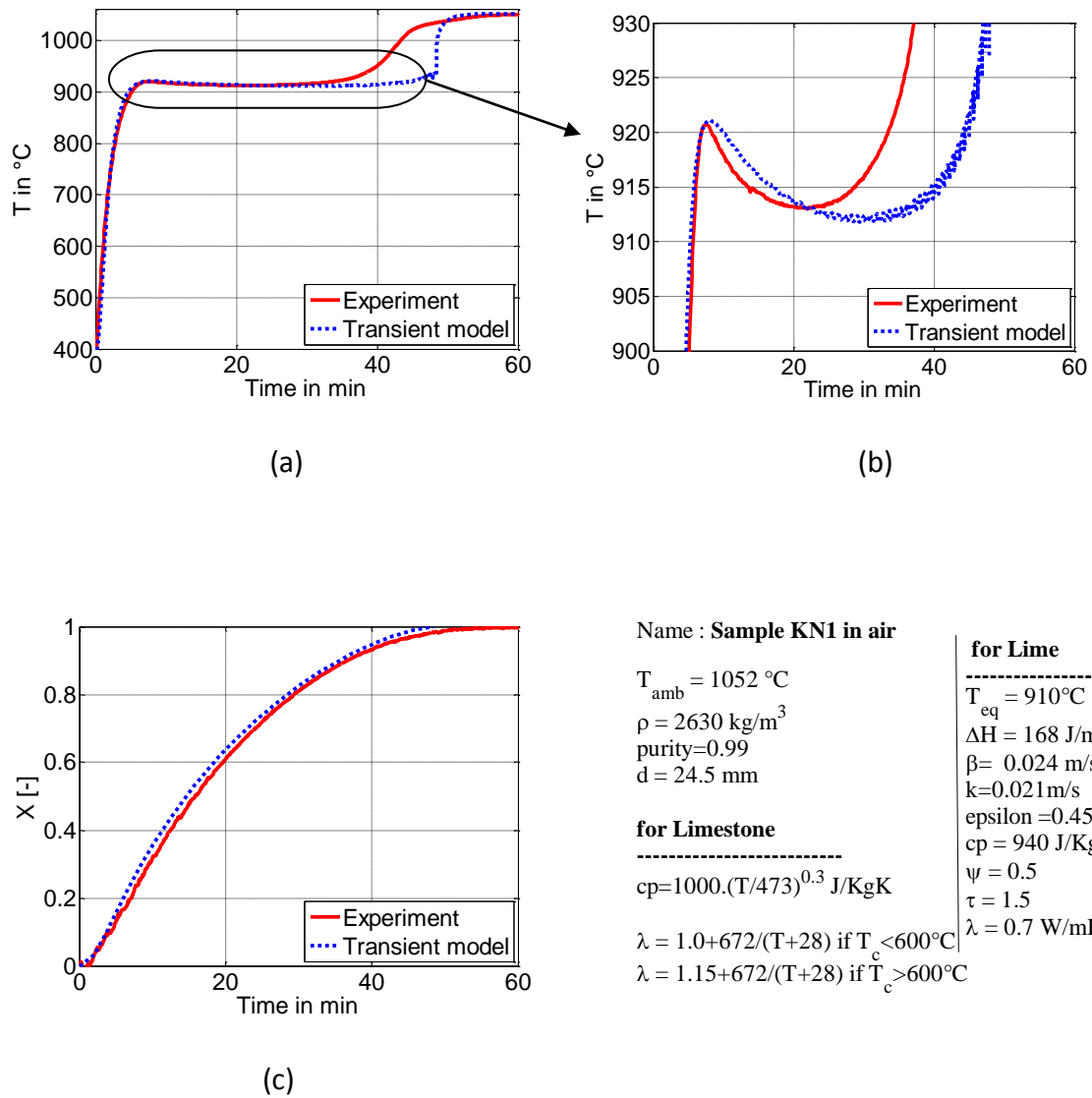


Figure 9-5: Comparison of measured and predicted temperature (a), (b) and conversion (c) profiles for the sample KN1 with particle size 24.5 mm

9.4.3 Sample KN1 with 32.2 mm (Big particle)

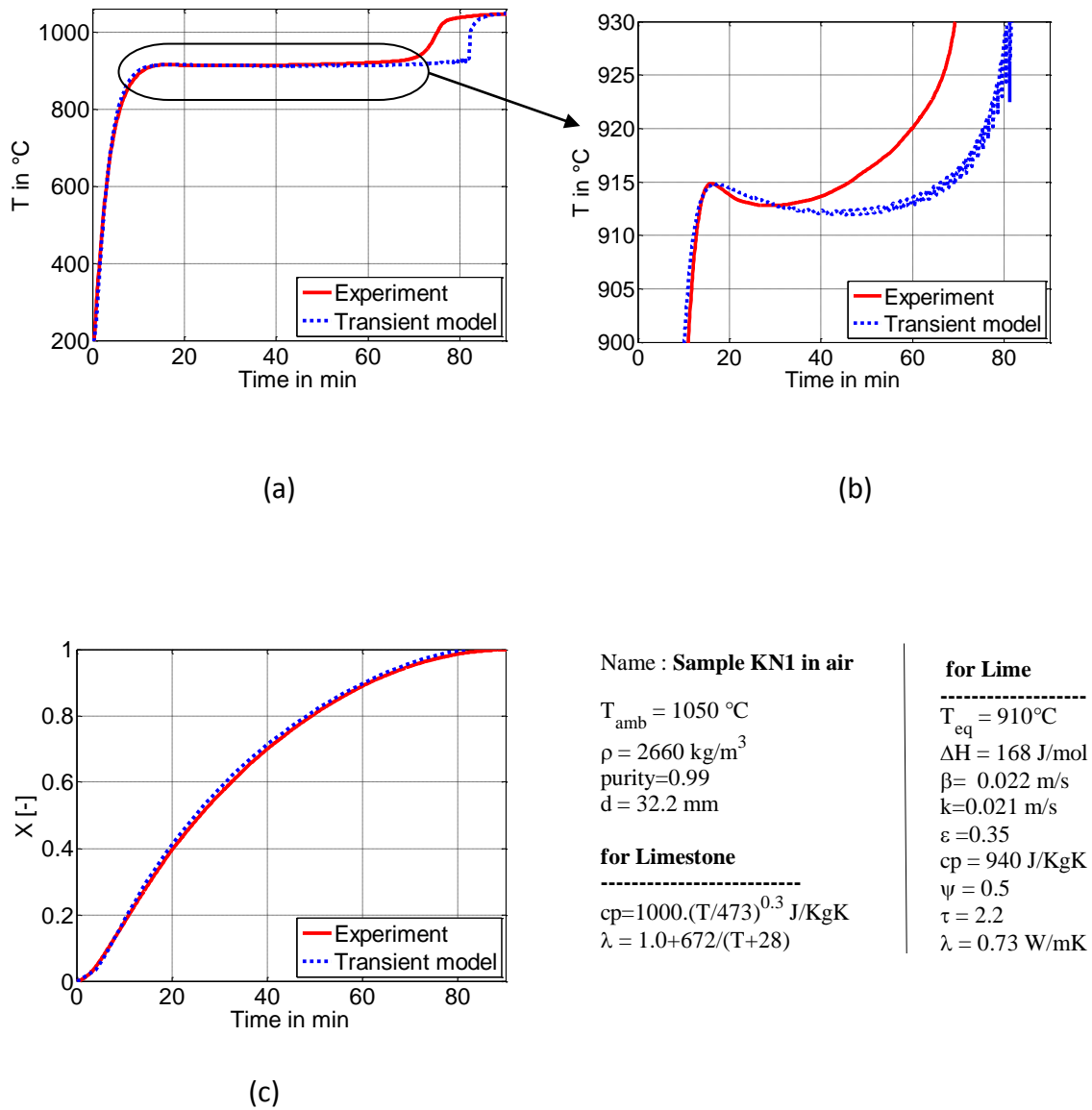


Figure 9-6: Comparison of measured and predicted temperature (a), (b) and conversion (c) profiles for the sample KN1 with particle size 32.2 mm

In the above section 9.4, the calcination behavior of the sample KN1 at three different sizes has been compared with the transient model. The important parameters are tabulated as shown in the below Table 9.2. From this table it can be noted that the conductivity is

predicted by the model is 0.7 for the medium size particle and 0.73 for other two size particles. Irrespective of the particle size reaction coefficient is predicted as 0.021 for all the particle sizes. Tortuosity is varied from 1.5 to 2.2 for these three particles and also slight variation in mass transfer coefficient can be noticed. Effective emissivity of the big particle is 0.35, which is the lowest value compared to the other two particle sizes. This low value is explained based on the smaller annular area (because of bigger particle size) in the tube furnace resulting in lower view angle for the radiation heat transfer from the furnace inner wall to the particle surface.

Sample KN1	14 mm	24 mm	32 mm
Thermal conductivity	0.73	0.7	0.73
Reaction coefficient	0.021	0.021	0.021
Tortuosity	2.0	1.5	2.2
Mass Transfer coefficient	0.025	0.024	0.022
Effective emissivity	0.4	0.45	0.35

Table 9.2: Comparison of properties for the sample KN1 at three particle sizes

9.5 Material properties and parameters for various Limestone

In order to determine the material properties and parameters, several limestone samples from different origins (locations) have been chosen. Properties determined with transient model along with experimental measurements have been listed in the below tables. For better readability, the samples have been classified into four groups and each group (with similar properties) has been tabulated distinctly. All the column headers are listed with respective units and the full forms of the property names are given in the nomenclature. The samples decomposed are either in air or in CO₂ environment. Samples decomposed in CO₂ environment are mentioned in the sample name column.

Column ‘purity’ stands for percent of calcium carbonate in the limestone.

Column ‘time’ - time required for complete calcination.

Column 'T (°C)' - core temperature when conversion is 50%.

Column 'time50' - time required for 50% calcination.

Table 9.3 summarizes the list of group -1 samples with diameter 24.5 mm and all are decomposed in air environment. From this table it can be noticed that each of the limestone of same type is decomposed at two different temperatures (this field is in bold font) and the properties are compared. The purity of the samples has been varied from 0.9 to 0.99 and the density from 1900 to 2700 kgm⁻³. Model predicts equilibrium temperature of 900°C for the first sample 1mu1 whereas 910°C for all other samples. The emissivities of these samples are in the range from 0.5 and 0.6.

Table 9.4 lists the low density samples (group-2). These samples have density in the range from 2000-2200 kgm⁻³, but with high purity 0.99. Model predicts the low thermal conductivities and low emissivities for these samples as shown in the table. Few of the samples from this group have also been decomposed in CO₂ gas environment. For decomposition in CO₂ gas, Darcy flow model has been used and the permeability coefficient is predicted as 10⁻¹² m². Tortuosity and Mass transfer coefficients are not applicable in this case.

Table 9.5 describes another list named as group-3 samples. These samples are found to have relatively higher thermal conductivities up to 0.75 Wm⁻¹K⁻¹. In addition to the properties at different temperature and different environments (air and CO₂), different particle sizes (24.5 mm and 32.4 mm) are also compared for a sample in this list.

Table 9.6 lists the samples from the smallest size 14 mm to the biggest size 47.5 mm in diameter from different origins. For big particle, the effective emissivity is predicted as smaller compared to the small particle. This is because of lower annular area in the furnace when the particle diameter is bigger. Lower annular area results in lower effective emissivity because of lower view angle of radiation. BL0107 shows the highest thermal conductivity 0.8 Wm⁻¹ K⁻¹ and sample SZ shows the highest tortuosity 4.5.

For all the samples analyzed and listed in the following tables, enthalpy of reaction is considered as 168 kJ/mol. Thermal conductivity and specific heat capacity of limestones are considered as functions of temperatures. These functions are taken based on the

values reported in the literature [1]. On an average, tortuosity is around 1.5 to 2 for most varieties of limestones; however some limestones have higher tortuosity. Reaction coefficient of limestone from different origins varies in the range from 0.01 to 0.065 ms⁻¹. It can be observed that for many of the samples it increases with the increase in ambient temperature. Mass transfer coefficient listed in the table is independent of type of limestone; it only depends on the furnace temperature. It can be noted that for the sample B (listed in Table 9.5), tortuosity is predicted as 4.5. Such high values induce high diffusion resistance. When the same sample decomposed in CO₂ environment, very lower permeability 5.10⁻¹⁴ m² is predicted. Lower permeability again induces high diffusion resistance. From this observation it can be inferred that higher diffusion resistance is depicted for this sample in both of these experimental and modelling methods. Emissivity of the lime at the decomposition temperature is in the range from 0.3 to 0.6 for the samples analyzed. Equilibrium dissociation temperature varied between 900 °C to 920°C. The profiles corresponding to the values reported in these tables are given in Appendix.

Experimental measurements									Predicted Properties						
Experiment Number	Lime sample	d	T _{amb}	ρ	purity	time	T(°C)	time50	ΔH	T _{eq}	k	λ	β	τ	ε
	[-]	mm	[°C]	[kg/m ³]	[-]	[min]		[min]	[kJ/mol]	[°C]	[m/s]	[W/(m K)]	[m/s]	[-]	
1	1mu1	24.5	951	2742	0.92	74	865	23	168	900	0.03	0.52	0.018	1.5	0.5
2	1mu1	24.5	1058	2700	0.91	40	896	12	168	900	0.032	0.52	0.016	1	0.5
3	8mu2	24.5	955	2651	0.97	108	880	30	168	910	0.015	0.52	0.02	1.5	0.55
4	8mu2	24.5	1040	2750	0.96	55	895	17	168	910	0.028	0.52	0.024	1	0.55
5	17X	24.5	913	2050	0.98	120	852	36	168	910	0.015	0.4	0.029	1.5	0.55
6	17X	24.5	1048	2400	0.99	53	890	16	168	910	0.034	0.4	0.029	1.5	0.55
7	3T1	24.5	951	1914	0.98	73	862	23	168	910	0.022	0.4	0.029	1.5	0.6
8	3T1	24.5	1057	2150	0.99	40	882	12	168	910	0.055	0.4	0.035	1.4	0.6
9	13mu3	24.5	1057	2770	0.99	60	898	19	168	910	0.021	0.4	0.029	1	0.55

Table 9.3: Parameters and properties for the list of group -1 samples

Experiment Number	Experimental measurements								Predicted properties						
	Lime sample	d	T _{amb}	ρ	purity	time	T(°C)	time50	T _{eq}	k	λ	β	τ	κ	ε
	[-]	mm	[°C]	[kg/m ³]	[-]	[min]		[min]	[°C]	[m/s]	[W/(m K)]	[m/s]	[-]	[m ²]	
1	F2-IV	24.5	851	2098	0.99	250	806	76	910	0.015	0.35	0.016	1	[-]	0.35
2	F2-IV	24.5	965	2080	0.99	93	872	28	910	0.022	0.4	0.02	2	[-]	0.35
3	F2-IV	24.5	1042	2080	0.99	55	893	19	910	0.032	0.44	0.029	2.5	[-]	0.35
4	F2-IV in CO2	24.5	1045	2170	0.99	56	910	20	910	0.035	0.44	[-]	[-]	1.10 ⁻¹²	0.35
5	F2-IV	24.5	1126	2133	0.99	40	904	14	910	0.032	0.35	0.025	1.5	[-]	0.27
6	F2-IV in CO2	24.5	1190	2090	0.99	33	919	11	910	0.04	0.4	[-]	[-]	1.10 ⁻¹²	0.3
7	F1-iii	24.5	909	2200	0.98	180	860	51	910	0.011	0.44	0.013	2.5	[-]	0.3
8	F1-iii	24.5	955	2212	0.99	118	879	36	910	0.013	0.44	0.013	2.5	[-]	0.3
9	F1-iii	24.5	1062	2214	0.99	58	913	19	910	0.016	0.44	0.025	2.5	[-]	0.3
10	F1-i	24.5	1012	2200	0.99	60	896	18	910	0.02	0.55	0.025	1.5	[-]	0.4

Table 9.4: Parameters and properties for the list of group -2 samples

Expt Nr.	Experimental measurements								Predicted properties						
	Lime sample	d	T _{amb}	ρ	purity	time1	T(°C)	Time50	T _{eq}	k	λ	β	τ	κ	ε
	[-]	mm	[°C]	[kg/m ³]	[-]	[min]		[min]	[°C]	[m/s]	[W/(m K)]	[m/s]	[-]	[m ²]	
1	A	24.5	1032	2657	0.96	44	896	15	910	0.029	0.65	0.029	1	[-]	0.6
2	B	24.5	1044	2740	0.99	55	926	20	910	0.02	0.75	0.028	4.5	[-]	0.45
3	B in CO2 gas	24.5	1040	2738	0.99	48	925	14.6	910	0.038	0.75	[-]	[-]	5.10 ⁻¹⁴	0.5
4	T	24.5	1164	2625	0.99	28	920	8.8	910	0.05	0.7	0.034	2	[-]	0.45
5	T in CO2	24.5	1052	2625	0.99	53	911	17	910	0.038	0.7	[-]	[-]	1.10 ⁻¹²	0.45
6	D	24.5	1050	2609	0.998	50	915	17	910	0.026	0.5	0.034	3.2	[-]	0.6
7	D	32.4	1050	2350	0.998	80	913	26	910	0.024	0.55	0.029	3.8	[-]	0.45

Table 9.5: Parameters and properties for the list of group -3 samples

Expt. Nr.	Experimental measurements								Predicted Properties						
	Lime sample	d	T amb	ρ	purity	time1	T(°C)	time2	ΔH	Teq	k	λ	β	τ	ε
	[-]	mm	[°C]	[kg/m ³]	[-]	[min]		[min]	[kJ/mol]	[°C]	[m/s]	[W/(m K)]	[m/s]	[-]	
1	BL0107	24.5	1090	2666	0.98	39	927	15	168	920	0.032	0.8	0.032	2	0.4
2	BL0107	47.5	1090	2675	0.99	118	918	41	168	920	0.032	0.8	0.032	2	0.3
3	BL0607	24.5	1165	2685	0.99	30	926	11	168	920	0.065	0.7	0.038	2	0.4
4	BL0607	47.5	1165	2681	0.99	90	920	32	168	920	0.055	0.75	0.038	2	0.3
5	SZ	14.4	1040	2330	0.99	60	925	19	168	920	0.022	0.65	0.025	3	0.45
6	SZ	24.5	1040	2470	0.99	30	940	10	168	920	0.015	0.65	0.025	4.5	0.45
7	KN1	14.4	1050	2660	0.99	25	923	8	168	910	0.021	0.7	0.025	2.5	0.4
8	KN1	24.5	1050	2630	0.99	50	914	16	168	910	0.021	0.7	0.024	1.5	0.45
9	KN1	32.4	1050	2660	0.99	84	913	26	168	910	0.021	0.73	0.022	2.2	0.35

Table 9.6: Parameters and properties for the list of group - 4 samples

References

- [1] M. Silva, “Experimental investigation of the thermophysical properties of new and representative materials from room temperature up to 1300 ° C,” Otto-von-Guericke-Universität, Magdeburg, Germany, 2009.
- [2] “The Processing and Major Uses of Limestone Ground Calcium Carbonate,” *Longcliffe Quarries Ltd.* [Online]. Available: <http://www.longcliffe.co.uk/>.
- [3] A. Bes, “Dynamic process simulation of limestone calcination in normal shaft kilns,” Otto-von-Guericke-Universität, Magdeburg, Germany, 2006.
- [4] C. Cheng, “Thermal Process Simulation of Reactive Particles on Moving Grates,” Otto-von-Guericke-Universität, Magdeburg, Germany, 2007.
- [5] *U.S. Geological Survey, 2015, Mineral commodity summaries 2015: 2015.*
- [6] “International Lime Association (ILA).” [Online]. Available: <http://www.internationallime.org/world-lime-production>.
- [7] D. Hai Do, “Simulation of Lime Calcination in Normal Shaft and Parallel Flow Regenerative Kilns,” Otto-von-Guericke-Universität, Magdeburg, Germany, 2012.
- [8] T. Schwertmann, “Untersuchung des Optimierungspotentials des Ringschachtofens zum Brennen von karbonitischem Gestein,” 2006.
- [9] A. Wolter, S. Luger, and G. Schaefer, “Zur Kinetik der Hydratation von Branntkalk,” *Zement-Kalk-Gips Int.*, vol. 57, no. 8, pp. 60–68, 2004.
- [10] H. Kainer, E. Specht, and R. Jeschar, “Reaction, Pore diffusion and Thermal conduction Coefficients of Various Magnesites and their influence on the Decomposition Time,” *Zement Kalk Gips*, vol. 39, no. 7, pp. 214–219, 1986.
- [11] E. T. Turkdogan, R. G. Olsson, H. A. Wriedt, and L. . Darken, *Calcination of Limestone*, vol. 254. Society of Mining Engineers, 1973.
- [12] W. A. Gilkey, “Calcination Rates of Limestone,” *Ind. Eng. Chem.*, pp. 727–728, 1926.
- [13] C. C. Furnace, “The Rate of Calcination of Limestone,” *Ind. Eng. Chem.*, vol. 23, no. 5, pp. 534–538, 1931.
- [14] F. R. Campbell, A. W. D. Hills, and A. Paulin, “Transport properties of porous lime and their influence on the decomposition of porous compacts of calcium carbonate,” *Chem. Eng. Sci.*, vol. 25, no. 6, pp. 929–942, Jan. 1970.
- [15] F. Garcã, A. Abad, L. F. De Diego, P. Gayã, and J. Adã, “Calcination of calcium-

- based sorbents at pressure in a broad range of CO₂ concentrations,” *Chem. Eng. Sci.*, vol. 57, no. 13, pp. 2381–2393, 2002.
- [16] K. Patil, S. Jain, R. K. Gandhi, and H. S. Shankar, “Calcium Carbonate decomposition under External Pressure Pulsations,” in *AIChE Annual Meeting, Conference Proceedings*, 2004, no. 1, pp. 3943 – 3962.
- [17] P. C. Okonkwo and S. S. Adefila, “The Kinetics of Calcination of High Calcium Limestone,” *Int. J. Eng. Sci. Technol.*, vol. 4, no. 02, pp. 391–400, 2012.
- [18] M. S. Murthy, “Investigation on the kinetics of thermal decomposition of calcium carbonate,” *Chem. Eng. Sci.*, vol. 49, no. 13, pp. 2198–2204, 1994.
- [19] R. Weise, “Heat Transfer by Free Convection,” *Chem. Abs.*, vol. 55, 1936.
- [20] O. A. Saunders, “The Effect of Pressure Upon Natural Convection in Air,” *Proc. R. Soc. A Math. Phys. Eng. Sci.*, vol. 157, no. 891, pp. 278–291, 1936.
- [21] J. Khinast, G. F. Krammer, C. Brunner, and G. Staudinger, “Decomposition of Limestone: The influence of CO₂ and particle size on the reaction rate,” *Chem. Eng. Sci.*, vol. 51, no. 4, pp. 623–634, 1996.
- [22] A. Irfan and D. Gülsen, “Calcination kinetics of high purity limestones,” *Chem. Eng. J.*, vol. 83, pp. 131–137, 2001.
- [23] K. Muazu, M. Abdullahi, and A. S. Akuso, “Kinetic Study of Calcination of Jakura Limestone Using Power Rate Law Model,” *Niger. J. Basic Appl. Sci.*, vol. 19, pp. 116–120, 2011.
- [24] J. Y. Xie, B. J. Zhong, W. B. Fu, and Y. Shi, “Measurement of Equivalent Diffusivity during the Calcination of Limestone,” *Combust. Flame*, vol. 129, no. 02, pp. 351–355, 2002.
- [25] I. Halikia, L. Zoumpoulakis, E. Christodoulou, and D. Prattis, “Kinetic study of the thermal decomposition of calcium carbonate by isothermal methods of analysis,” *Eur. J. Miner. Process. Environ. Prot.*, vol. 1, no. 2, pp. 89–102, 2001.
- [26] H. Mikulčić, E. Von Berg, M. Vujanović, P. Priesching, R. Tatschl, and N. Duić, “Numerical Modelling of Calcination Reaction Mechanism,” vol. 3, no. 1, pp. 2–6, 2011.
- [27] H. Mikulčić, E. von Berg, M. Vujanović, P. Priesching, L. Perković, R. Tatschl, and N. Duić, “Numerical modelling of calcination reaction mechanism for cement production,” *Chem. Eng. Sci.*, vol. 69, no. 1, pp. 607–615, Feb. 2012.
- [28] K. J. Hill and E. R. S. Winter, “Thermal Dissociation Pressure of Calcium Carbonate,” *J. Phys. Chem.*, 1956.

- [29] E. H. Baker, "The Calcium Oxide-Carbon Dioxide System in the Pressure Range 1-300 Atmospheres," *J. Chem. Soc.*, no. 0, pp. 464–470, 1962.
- [30] M. Silva, E. Specht, and J. Schmidt, "Thermophysical properties of limestone as a function of origin (Part 1): Specific heat capacities," vol. 63, no. 2, pp. 55–62, 2010.
- [31] I. Barin and O. Knacke, *Thermochemical Properties of Inorganic Substances*. Berlin:Springer, 1973.
- [32] Landolt and Börnstein, *Thermodynamic Properties of Inorganic Materials: Pure Substances*, New Series. Berlin: Springer, 2002.
- [33] E. Silva, M. Specht and J. Schmidt, "Thermophysical properties of limestone as a function of origin (Part 2): Calcination enthalpy and equilibrium temperature," *ZKG Int.*, vol. 63, no. 6, pp. 51–57, 2010.
- [34] P. Pott, "Studien über die Dissoziationen von Calcium-Strontium- und Baryum – Karbonat," Freiburg, 1905.
- [35] H. Riesenfeld, "La décomposition de carbonate de chaux," *Chim. Phys.*, vol. 7, p. 561, 1909.
- [36] J. Johnston, "The Thermal Dissociation of Calcium Carbonate," *Journal of the American Chemical Society*, vol. 32, no. 8, pp. 938–946, 1910.
- [37] Marc and Simek, "Zeitschrift für anorganische Chemie." *Anor Chem.* 82, 1913.
- [38] J. C. Southard and P. H. Royster, "The Thermal Dissociation of Calcium Carbonate," *J. Phys. Chem.*, vol. 40, no. 4, pp. 435–438, 1936.
- [39] R. S. Boynton, *Chemistry and Technology of lime and Limestone*, ISBN: 978-. New York John Wiley & Sons Inc, 1980.
- [40] C. Cheng and E. Specht, "Reaction rate coefficients in decomposition of lumpy limestone of different origin," *Thermochim. Acta*, vol. 449, no. 1–2, pp. 8–15, Oct. 2006.
- [41] S. Hogewoning, "Zur Relation von Kalksteineigenschaften und Branntkalkreaktivität," Technische Universität Clausthal, Germany, 2008.
- [42] K. Hild and K. Mitt, "Thermophysical Properties of Matter, Thermal Radiative Properties, Nonmetallic Solids," *Wilhelm-Inst. Eisenforsch. Düsseld.*, 1932.
- [43] A. W. D. Hills, "The mechanism of the thermal decomposition of calcium carbonate," *Chem. Eng. Sci.*, vol. 23, pp. 297–320, 1968.
- [44] W. Lipinski and A. Steinfeld, "Heterogeneous thermochemical decomposition under direct irradiation," *Int. J. Heat Mass Transf.*, vol. 47, no. 8–9, pp. 1907–1916, Apr. 2004.

- [45] W. Bauer, “Bauer_wolfgang,” Universität Duisburg - Essen.
- [46] T. Rajeswararao, “Effective Diffusivities in Calcium carbonate and Calcium oxide Solid Pellets,” *Chem. Eng. Commun.*, vol. 35, pp. 203–209, 1984.
- [47] C. N. Saiterfield and T. K. Sherwood, *Role of Diffusion in Catalysis*. Addison-Wesley, 1963.
- [48] G. Radilla, M. Kacem, J. M. Lombard, and M. Fourar, “Transport properties of lavoux limestone at various stages of CO₂-like acid-rock alteration,” *Oil Gas Sci. Technol.*, vol. 65, no. 4, pp. 557–563, 2010.
- [49] S. Takkinen, S. Jaakko, and H. Timo, “Heat and Mass Transfer in Calcination of Limestone Particles,” *AIChE J.*, vol. 00, no. 0, pp. 1–10, 2011.
- [50] R. Lech, “Thermal decomposition of limestone: Part 4—permeability of product layer,” *Silic. Ind.*, vol. 72, pp. 45–52, 2007.
- [51] E. Specht, *Wärme- und Stoffübertragung in der Thermoprozesstechnik-Grundlagen, Berechnungen, Prozesse*. Essen: Vulkan-Verlag, 2014.
- [52] F. P. Incropera and D. P. DeWitt, *Introduction to Heat Transfer*. 2011.
- [53] “http://www.engineeringtoolbox.com/dry-air-properties-d_973.html” .
- [54] “http://www.engineeringtoolbox.com/air-properties-d_156.html” .
- [55] C. Cheng, E. Specht, and G. Kehse, “Influence of origin and material property of limestone upon its decomposition behaviour in shaft kilns,” *ZKG Int.*, vol. 60, no. 1, pp. 51–61, 2007.
- [56] B. Hallak, E. Specht, R. Gröpler, and G. Warnecke, “Simulation of limestone calcination in -normal shaft kilns – mathematical model,” *ZKG Int.*, vol. 68, no. 9, pp. 66–71, 2015.
- [57] B. Hallak, F. Herz, E. Specht, and G. Kehse, “Energy consumption and CO₂ content in the flue gas of normal shaft kilns. Part 1: Influence of the air excess number,” *ZKG Int.*, vol. 67, no. 11, pp. 60–66, 2014.
- [58] B. Hallak, F. Herz, E. Specht, and G. Kehse, “Energy consumption and CO₂ content in the flue gas of normal shaft kilns. Part 2: Influence of the limestone quality and the process parameters,” *ZKG Int.*, vol. 67, no. 12, pp. 38–41, 2014.
- [59] J. C. Abanades and D. Alvarez, “Conversion limits in the reaction of CO₂ with lime,” *Energy and Fuels*, vol. 17, no. 2, pp. 308–315, 2003.

- [60] J. T. Houghton, L. G. Meira Filho, B. A. Callander, N. Harris, A. Kattenberg, and K. Maskell, "Climate Change 1995: The Science of Climate Change, Contribution of Working Group I to the Second Assessment Report of the Intergovernmental Panel on Climate Change," *The supplementary report to the IPCC Scientific Assessment*. Cambridge University Press: Cambridge, U.K., 1996.
- [61] a MacKenzie, D. L. Granatstein, E. J. Anthony, and J. C. Abanades, "Economics of CO₂ capture using the calcium cycle with a pressurized fluidized bed combustor," *Energy & Fuels*, vol. 21, no. 2, pp. 920–926, 2007.
- [62] L. Jia, R. Hughes, D. Lu, E. J. Anthony, I. Lau, N. R. Canada, and A. Criteria, "Attrition of Calcining Limestones in Circulating Fluidized-Bed Systems," *Ind. Eng. Chem. Res.*, vol. 46, pp. 5199–5209, 2007.
- [63] J. C. Abanades, "The maximum capture efficiency of CO₂ using a carbonation / calcination cycle of CaO / CaCO₃," *Chem. Eng. J.*, vol. 90, no. 3, pp. 303–306, 2002.
- [64] G. Cultrone, E. Sebastián, and M. O. Huertas, "Forced and natural carbonation of lime-based mortars with and without additives: Mineralogical and textural changes," *Cem. Concr. Res.*, vol. 35, no. 12, pp. 2278–2289, 2005.
- [65] B. Schüppel, "Impact of Improved Sorbents on the Performance of the Carbonate Looping Process," Technical University Darmstadt, Darmstadt, Germany, 2012.
- [66] V. Nikulshina, M. E. Gálvez, and a. Steinfeld, "Kinetic analysis of the carbonation reactions for the capture of CO₂ from air via the Ca(OH)₂–CaCO₃–CaO solar thermochemical cycle," *Chem. Eng. J.*, vol. 129, no. 1–3, pp. 75–83, May 2007.
- [67] E. Bouquet, G. Leysens, C. Schönnenbeck, and P. Gilot, "The decrease of carbonation efficiency of CaO along calcination-carbonation cycles: Experiments and modelling," *Chem. Eng. Sci.*, vol. 64, no. 9, pp. 2136–2146, 2009.
- [68] P. S. Fennell, R. Pacciani, J. S. Dennis, J. F. Davidson, and A. N. Hayhurst, "The Effects of Repeated Cycles of Calcination and Carbonation on a Variety of Different Limestones , as Measured in a Hot Fluidized Bed of Sand," *Energy & Fuels*, vol. 21, no. 1, pp. 2072–2081, 2007.
- [69] J.-T. Lee, C. T. Keener, and M. Knoderer, "Thermal decomposition of limestone in a large scale thermogravimetric analyzer," *Thermochim. Acta*, pp. 223–240, 1993.
- [70] E. Bernd and S. Jochen, "CO₂ Capture based on Chemical and Carbonate looping," *VGB Power Tech*, no. 11, 2008.

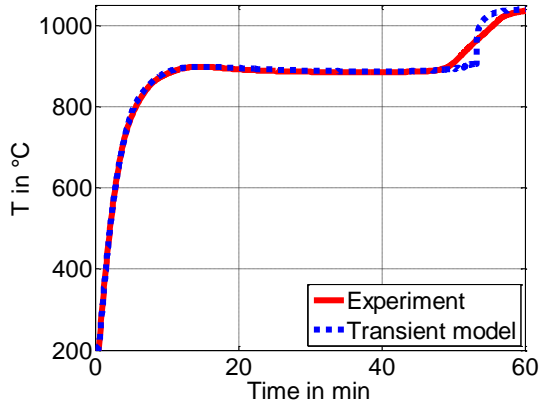
Appendix

The measured and predicted temperature profiles for the samples listed in the tables 9.3 to 9.6 have been shown in the following figures. Figure under each header is sub divided in to Figures (a), (b), (c), (d) and (e). In all the following Figures, (a) represents measured and predicted temperature profiles, (b) shows the same in the close view. Figure (c) demonstrates the measured and predicted conversion profiles. On the right of the Figure (c), the list of parameters is given. In all the Figures (d), represents the thermal conductivity variation with respect to the conversion degree for different effective emissivity values. Figure (e) shows the measured core temperature with respect to the measured conversion degree. In this Figure core temperature behavior can be clearly seen the way it varies from sample to sample.

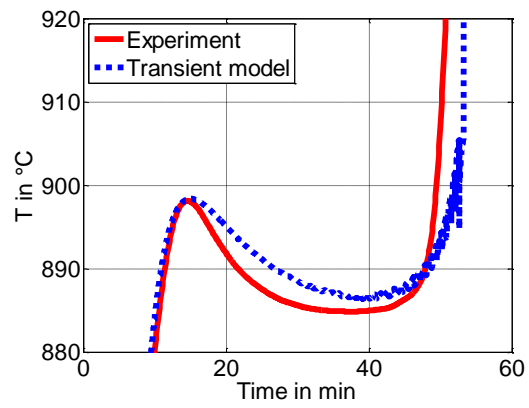
As the header of each of the following sections describes the details about the Figure, titles (captions) are not separately mentioned for each of these Figures.

Group 1

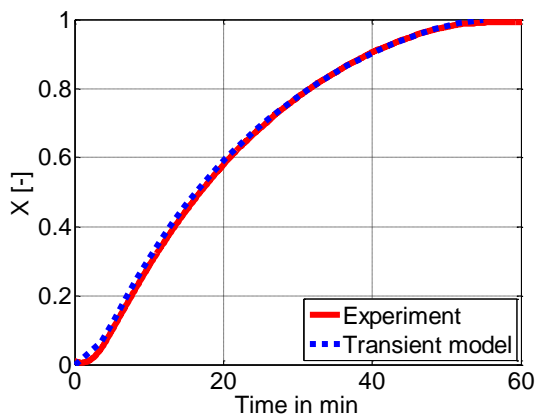
1. Sample 8mu2 (24.5 mm) in air at 1040 °C



(a)



(b)



(c)

Name : **Sample 8mu2 in air**

$$T_{amb} = 1040 \text{ } ^\circ\text{C}$$

$$\rho = 2750$$

$$\text{purity} = 0.96$$

$$d = 24.5$$

for Limestone

$$cp = 1000 \cdot (T/473)^{0.3}$$

$$\lambda = 0.23 + 672 / (T + 28) \text{ if } T_c < 800^\circ\text{C}$$

$$\lambda = 0.03 + 672 / (T + 28) \text{ if } T_c > 800^\circ\text{C}$$

for Lime

$$k = 0.028$$

$$T_{eq} = 910^\circ\text{C}$$

$$\beta = 0.024$$

$$\Delta H = 168$$

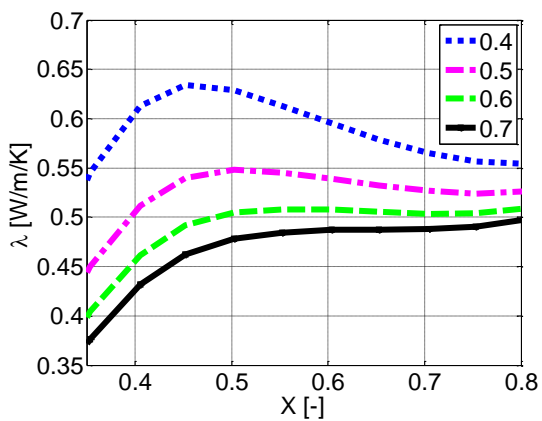
$$\psi = 0.5$$

$$\tau = 1.0$$

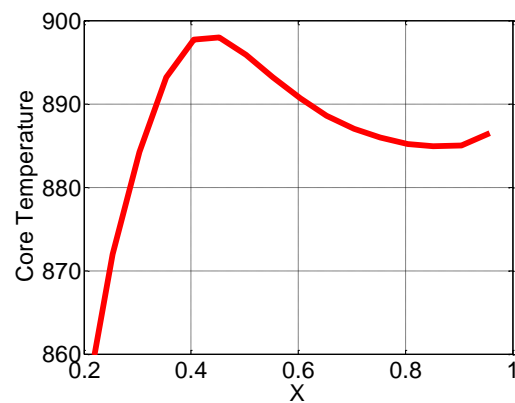
$$\varepsilon = 0.55$$

$$cp = 940$$

$$\lambda = 0.52$$

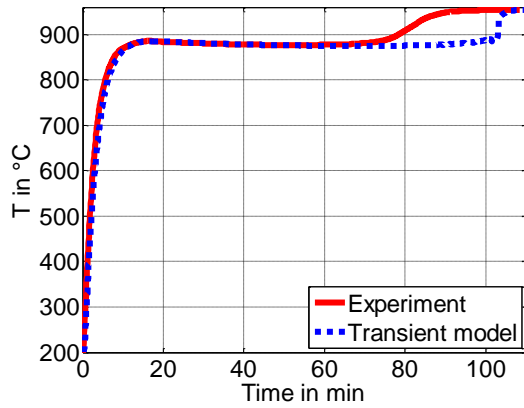


(d)

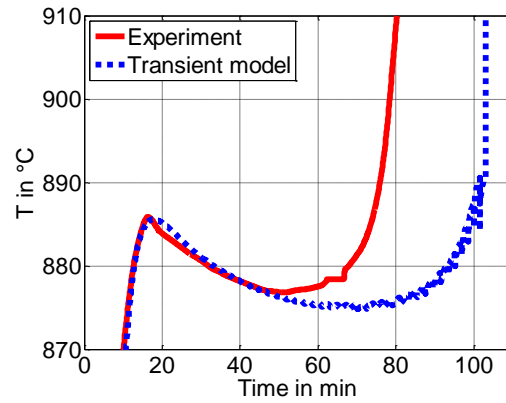


(e)

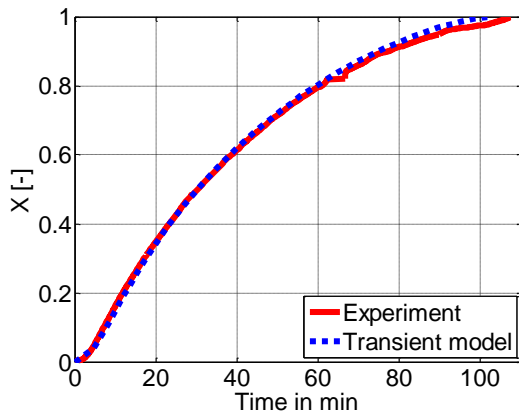
2. Sample 8mu2 (24.5 mm) in air at 955 °C



(a)



(b)



(c)

Name : **Sample 8mu2 in air**

$T_{amb} = 955 \text{ }^\circ\text{C}$

$\rho = 2650$

purity=0.97

$d = 24.5$

for Limestone

$cp = 1000 \cdot (T/473)^{0.3}$

$\lambda = 0.23 + 672/(T+28)$ if $T_c < 800 \text{ }^\circ\text{C}$

$\lambda = 0.13 + 672/(T+28)$ if $T_c > 800 \text{ }^\circ\text{C}$

for Lime

$k = 0.015$

$T_{eq} = 910 \text{ }^\circ\text{C}$

$\beta = 0.02$

$\Delta H = 168$

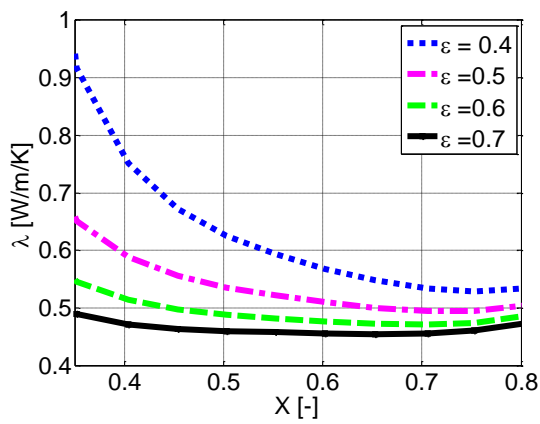
$\psi = 0.5$

$\tau = 1.5$

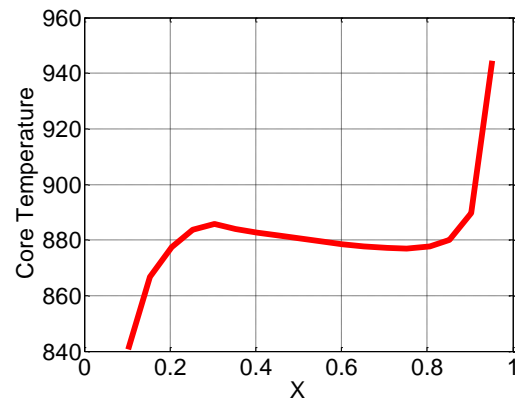
$\varepsilon = 0.55$

$cp = 940$

$\lambda = 0.52$

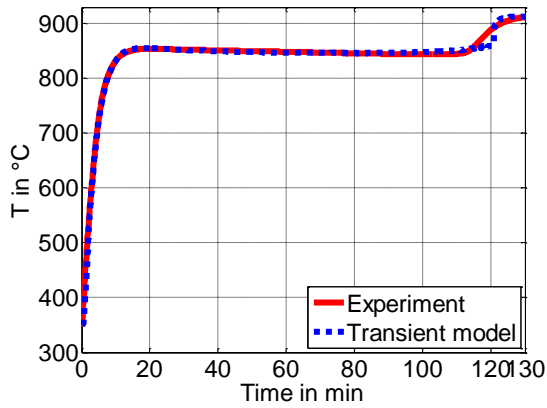


(d)

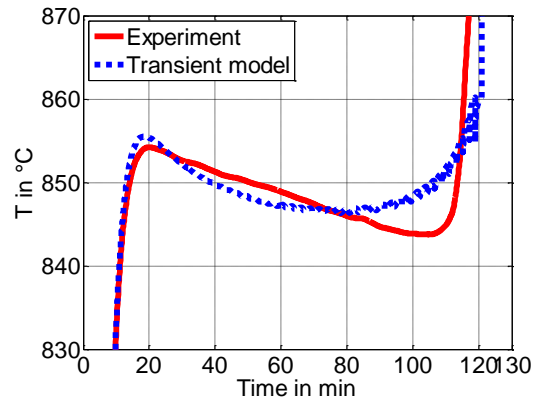


(e)

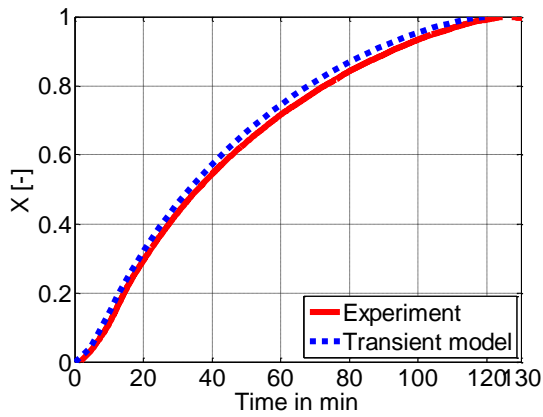
3. Sample17X (24.5 mm) in air at 913 °C



(a)



(b)



(c)

Name : **Sample 17X in air**

$T_{amb} = 913 \text{ } ^\circ\text{C}$

$\rho = 2050$

purity=0.98

$d = 24.5$

for Limestone

$c_p = 1350 \cdot (T/473)^{0.3}$
 $\lambda = 0.13 + 672/(T+28)$ if T_c

for Lime

$k = 0.015$

$T_{eq} = 910 \text{ } ^\circ\text{C}$

$\beta = 0.029$

$\Delta H = 168$

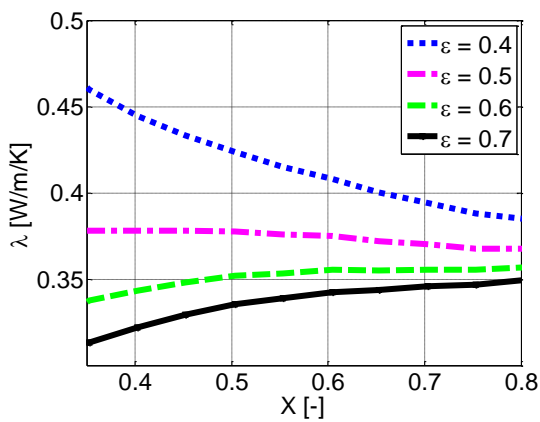
$\psi = 0.5$

$\tau = 1.5$

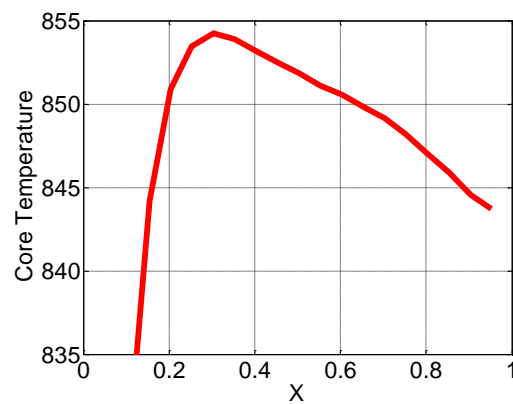
$\epsilon = 0.55$

$c_p = 940$

$\lambda = 0.4$

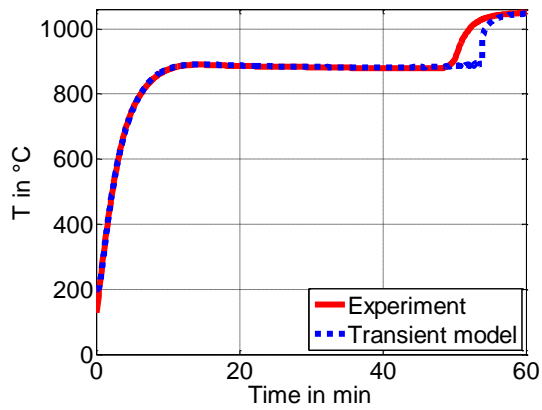


(d)

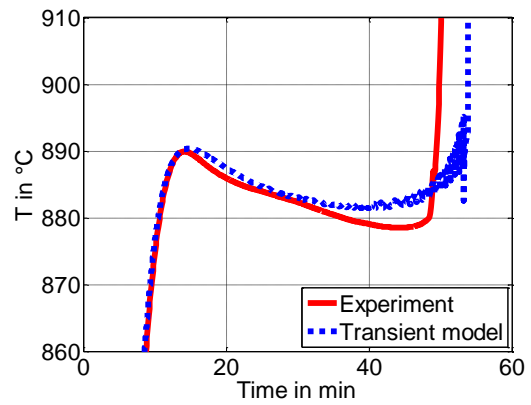


(e)

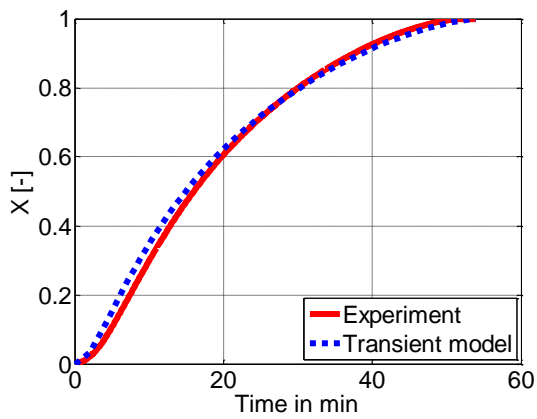
4. Sample17X (24.5 mm) in air at 1048 °C



(a)



(b)



(c)

Name : **Sample 17X in air**

$T_{amb} = 1048 \text{ }^\circ\text{C}$

$\rho = 2400$

purity=0.99

$d = 24.5$

for Limestone

$cp = 1200 \cdot (T/473)^{0.3}$

$\lambda = 0.13 + 672/(T+28)$ if T_c

for Lime

$k = 0.034$

$T_{eq} = 910 \text{ }^\circ\text{C}$

$\beta = 0.029$

$\Delta H = 168$

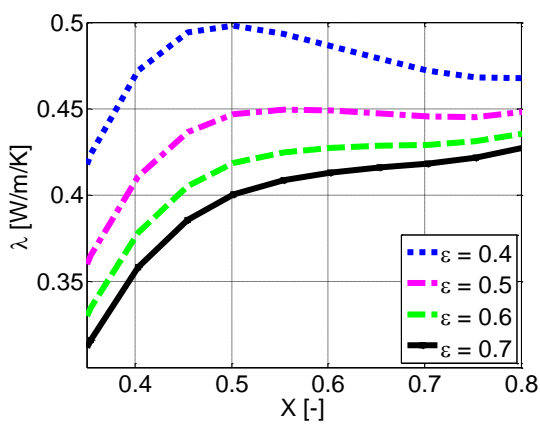
$\psi = 0.5$

$\tau = 1.5$

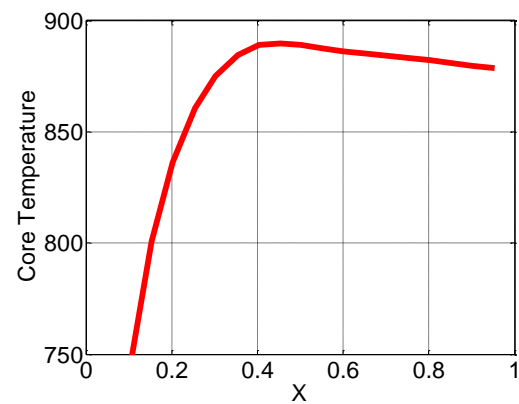
$\varepsilon = 0.55$

$cp = 940$

$\lambda = 0.4$

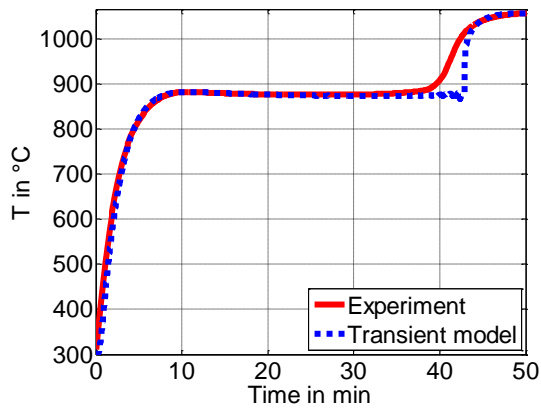


(d)

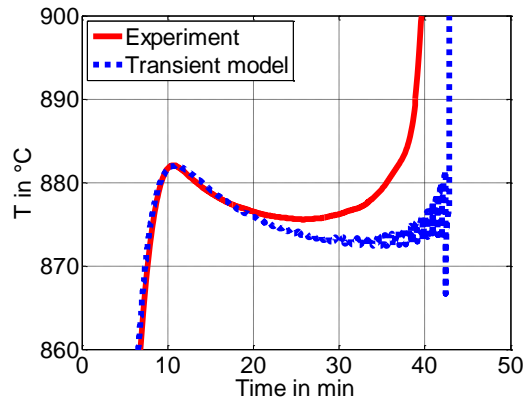


(e)

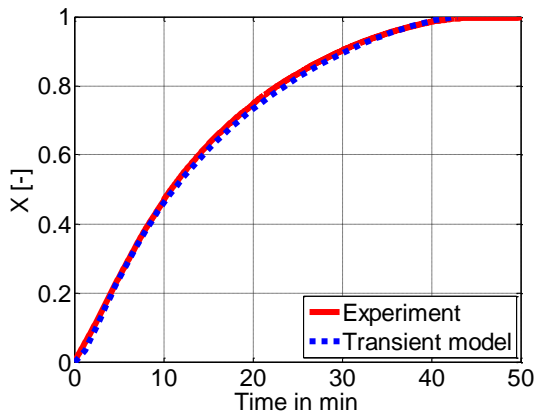
5. Sample 3T1 (24.5 mm) in air at 1057 °C



(a)



(b)



(c)

Name : **Sample 3T1 in air**

$T_{amb} = 1057 \text{ }^\circ\text{C}$

$\rho = 2150$

purity=0.99

$d = 24.5$

for Limestone

$cp = 1000 \cdot (T/473)^{0.3}$

$\lambda = 0.13 + 672 / (T + 28)$ if $T_c < 800 \text{ }^\circ\text{C}$

$\lambda = 0.10 + 672 / (T + 28)$ if $T_c > 800 \text{ }^\circ\text{C}$

for Lime

$k = 0.055$

$T_{eq} = 910 \text{ }^\circ\text{C}$

$\beta = 0.035$

$\Delta H = 168$

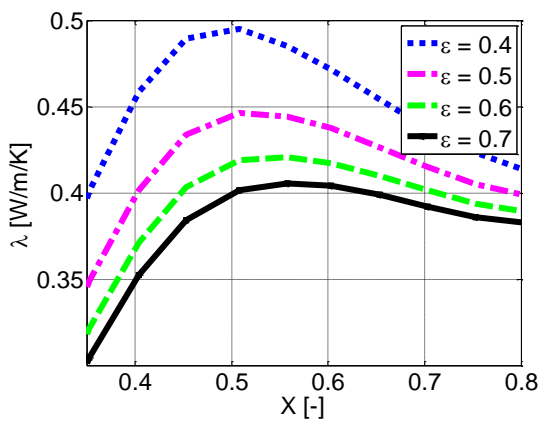
$\psi = 0.5$

$\tau = 1.3$

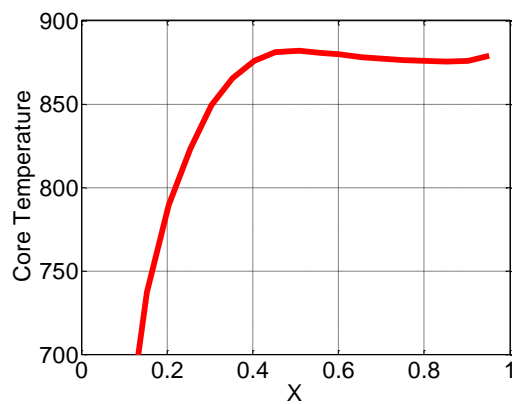
$\varepsilon = 0.6$

$cp = 940$

$\lambda = 0.4$

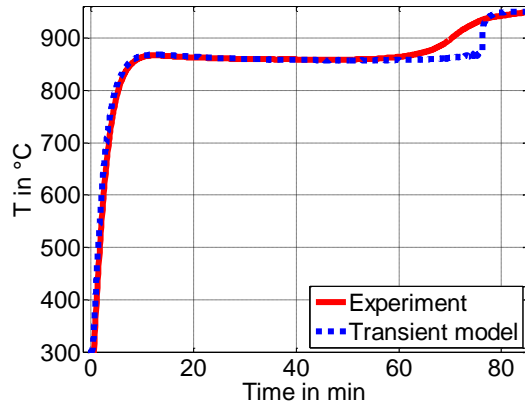


(d)

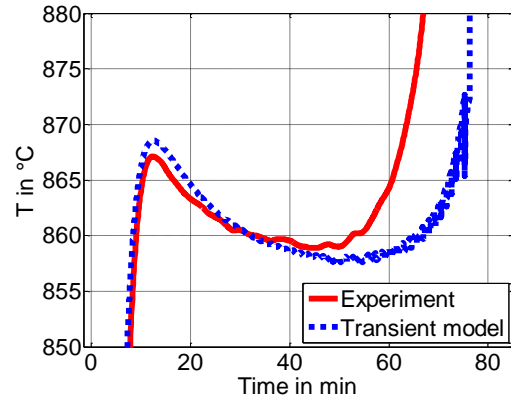


(e)

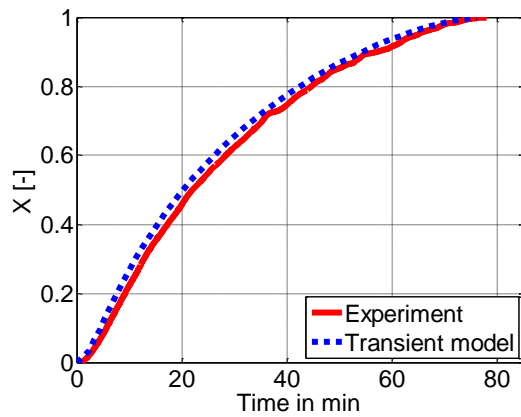
6. Sample 3T1 (24.5 mm) in air at 951 °C



(a)



(b)



(c)

Name : **Sample 3T1 in air**

$T_{amb} = 950 \text{ } ^\circ\text{C}$

$\rho = 1914$

purity=0.98

$d = 24.5$

for Limestone

 $c_p = 1000 \cdot (T/473)^{0.3}$

$\lambda = 0.13 + 672 / (T + 28)$ if $T_c < 800 \text{ } ^\circ\text{C}$

$\lambda = 0.04 + 672 / (T + 28)$ if $T_c > 800 \text{ } ^\circ\text{C}$

for Lime

 $k = 0.022$

$T_{eq} = 910 \text{ } ^\circ\text{C}$

$\beta = 0.029$

$\Delta H = 168$

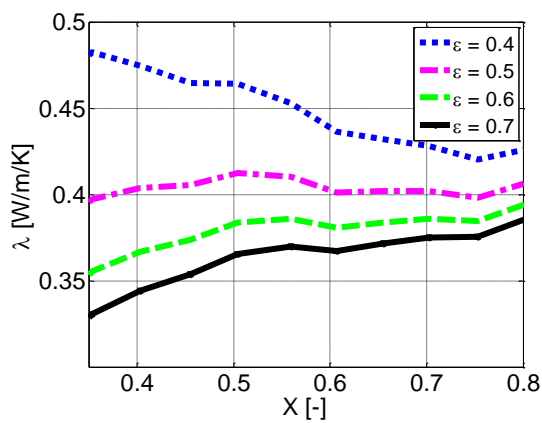
$\psi = 0.5$

$\tau = 1.5$

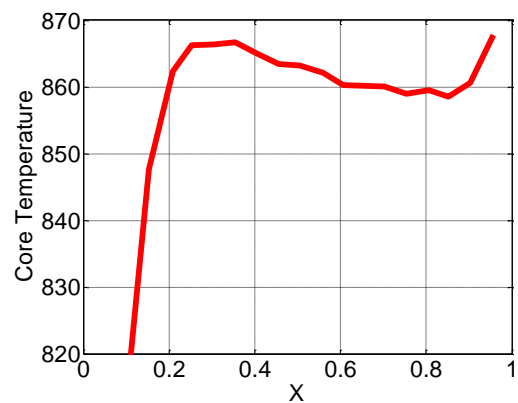
$\varepsilon = 0.6$

$c_p = 940$

$\lambda = 0.4$

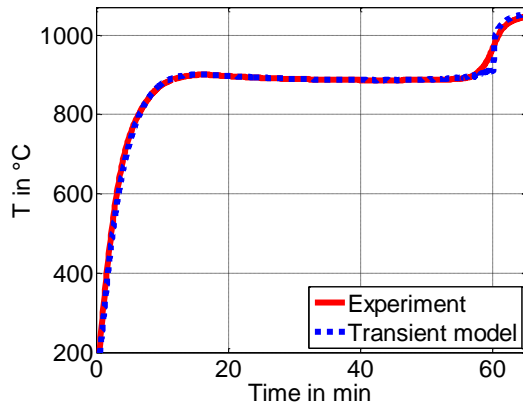


(d)

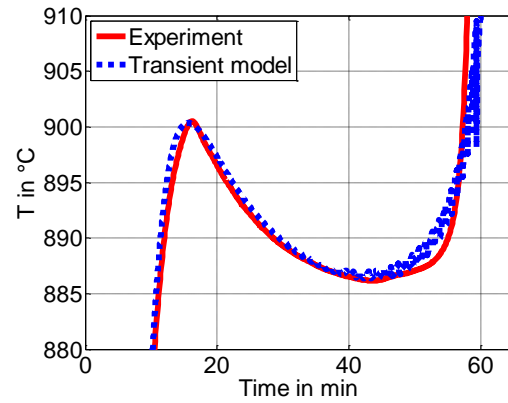


(e)

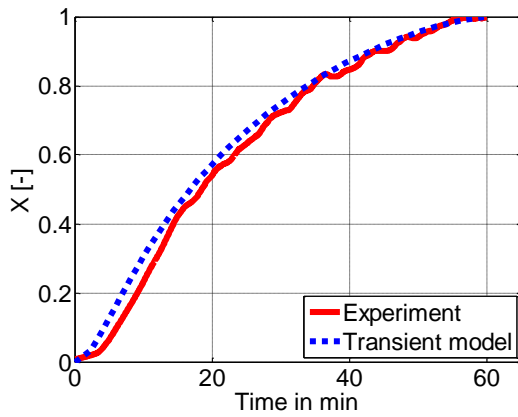
7. Sample13mu3 (24.5 mm) in air at 1057 °C



(a)



(b)



(c)

Name : **Sample 13mu3 in air**

$T_{amb} = 1057 \text{ °C}$

$\rho = 2770$

purity=0.99

$d = 24.5$

for Limestone

$cp = 1150 \cdot (T/473)^{0.3}$
 $\lambda = 0.13 + 672/(T+28)$ if T_c

for Lime

$k = 0.021$

$T_{eq} = 910 \text{ °C}$

$\beta = 0.029$

$\Delta H = 168$

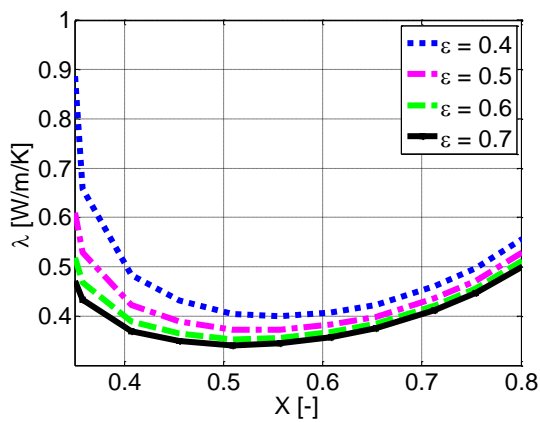
$\psi = 0.5$

$\tau = 1.0$

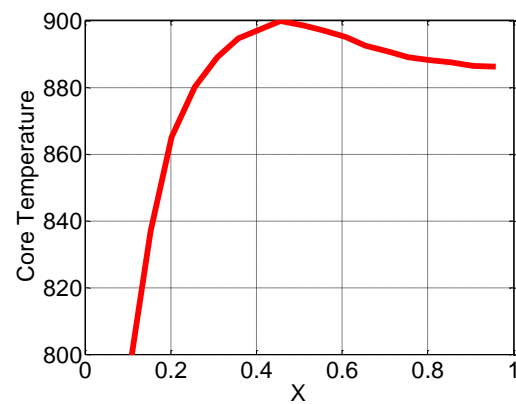
$\varepsilon = 0.55$

$cp = 940$

$\lambda = 0.4$



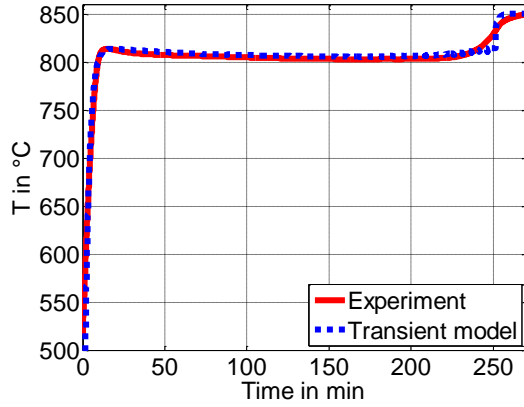
(d)



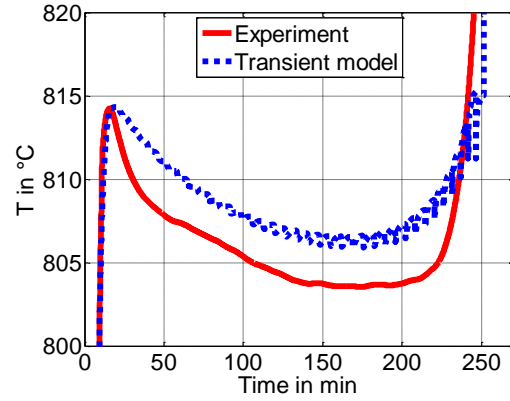
(e)

Group 2

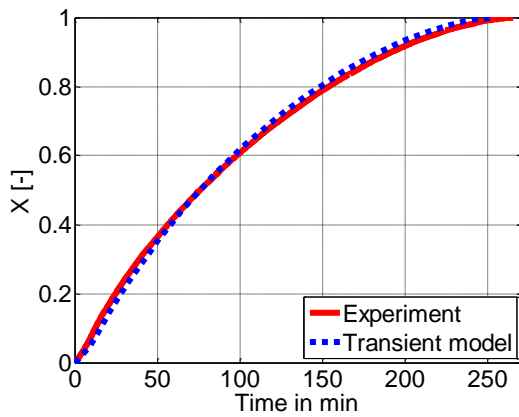
1. Sample F2-IV (24.5 mm) in air at 851°C



(a)



(b)



(c)

Name : **Sample F2-IV in air**

$T_{amb} = 851 \text{ } ^\circ\text{C}$

$\rho = 2098$

purity=0.99

$d = 24.5$

for Limestone

$c_p = 1000 \cdot (T/473)^{0.3}$

$\lambda = 0.23 + 672 / (T + 28)$

for Lime

$k = 0.015$

$T_{eq} = 910 \text{ } ^\circ\text{C}$

$\beta = 0.016$

$\Delta H = 168$

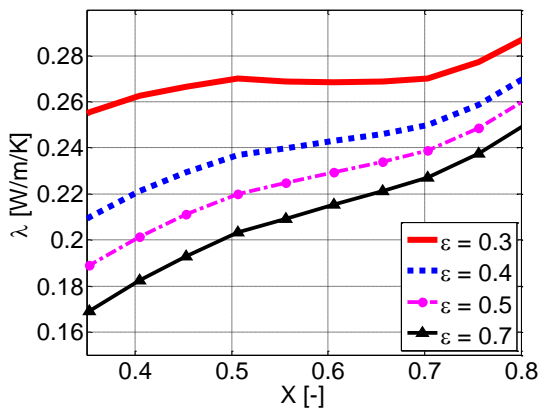
$\psi = 0.5$

$\tau = 1.0$

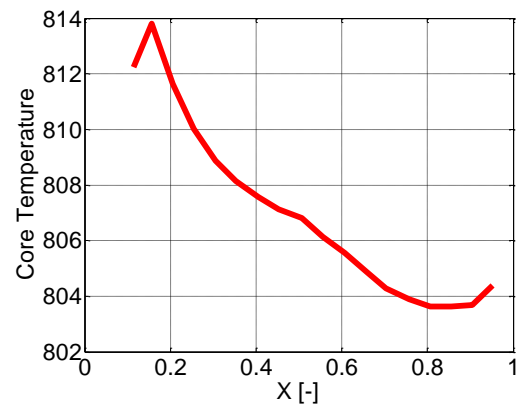
$\varepsilon = 0.3$

$c_p = 940$

$\lambda = 0.35$

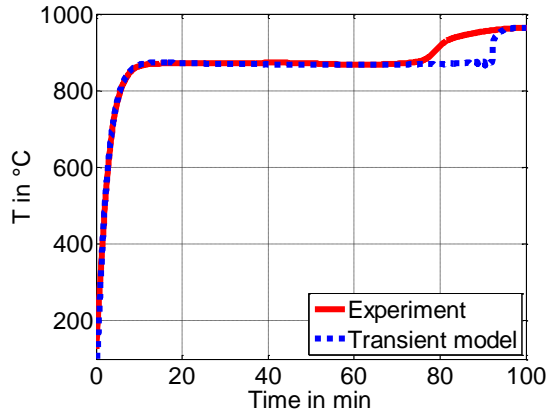


(d)

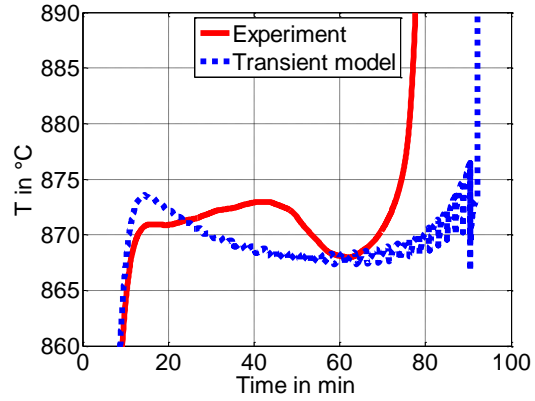


(e)

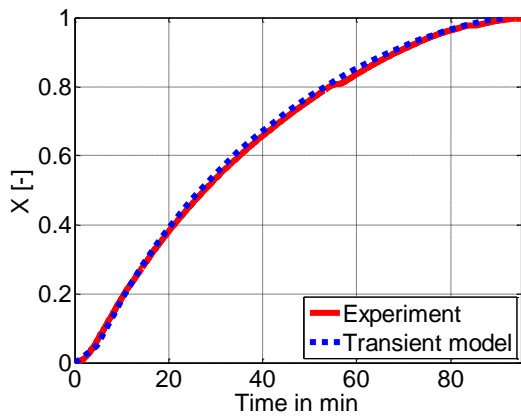
2. Sample F2-IV (24.5 mm) in air at 965 °C



(a)



(b)



(c)

Name : **Sample F2-IV in air**

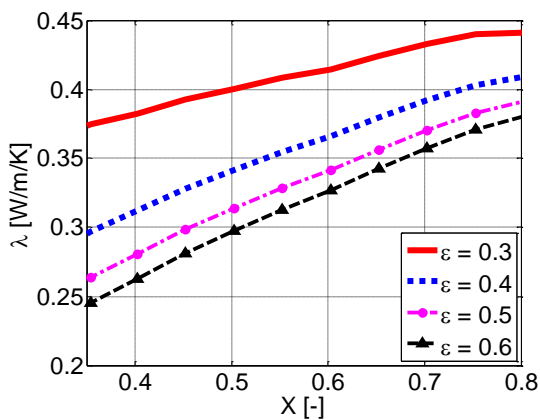
$T_{amb} = 965 \text{ }^\circ\text{C}$
 $\rho = 2080$
 purity=0.99
 $d = 24.5$

for Limestone

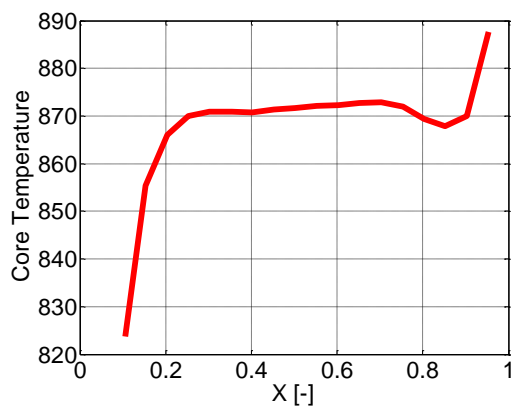
$cp = 1000 \cdot (T/473)^{0.3}$
 $\lambda = 0.23 + 672/(T+28)$

for Lime

$k = 0.022$
 $T_{eq} = 910 \text{ }^\circ\text{C}$
 $\beta = 0.02$
 $\Delta H = 168$
 $\psi = 0.5$
 $\tau = 2.0$
 $\varepsilon = 0.35$
 $cp = 940$
 $\lambda = 0.4$

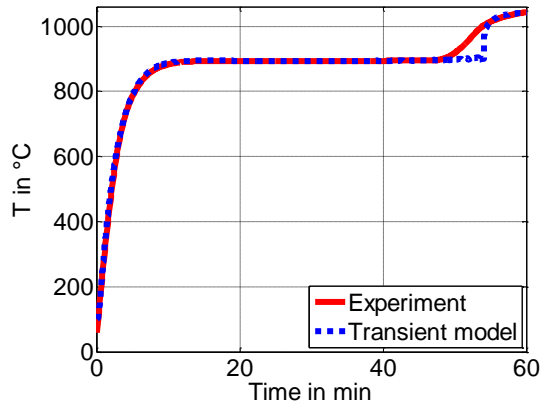


(d)

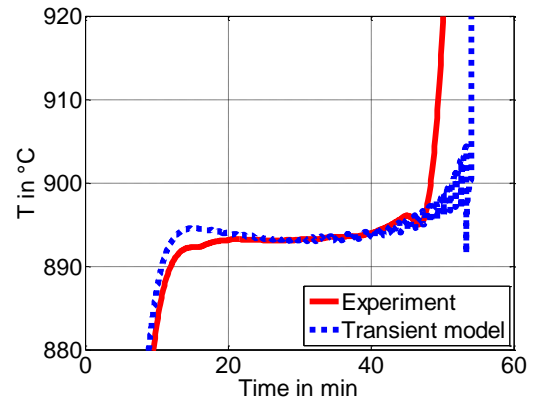


(e)

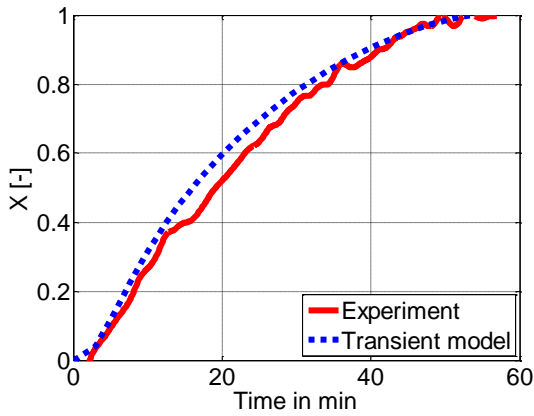
3. Sample F2-IV (24.5 mm) in air at 1042 °C



(a)



(b)



(c)

Name : **Sample F2-IV in air**

$T_{amb} = 1042 \text{ }^\circ\text{C}$

$\rho = 2083$

purity=0.99

$d = 24.5$

for Limestone

$cp = 1000 \cdot (T/473)^{0.3}$

$\lambda = 0.15 + 672 / (T + 28)$

for Lime

$k = 0.032$

$T_{eq} = 910 \text{ }^\circ\text{C}$

$\beta = 0.029$

$\Delta H = 168$

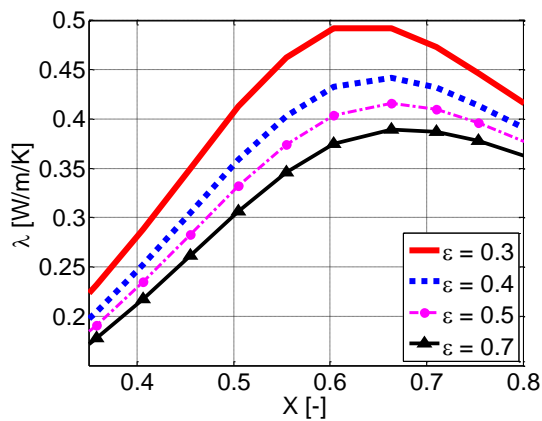
$\psi = 0.5$

$\tau = 2.5$

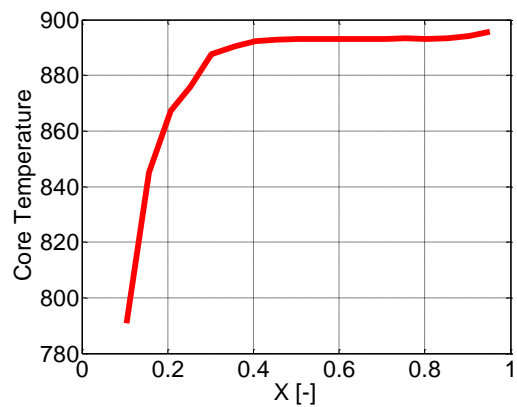
$\varepsilon = 0.35$

$cp = 940$

$\lambda = 0.44$

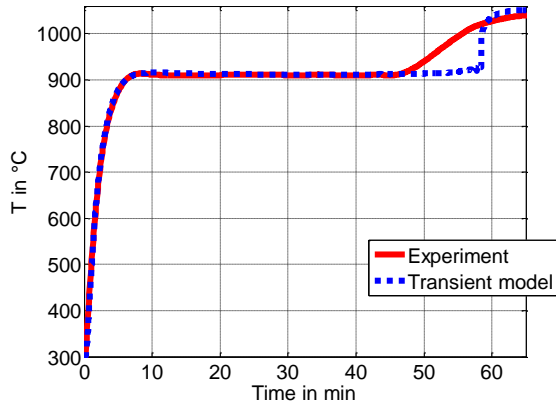


(d)

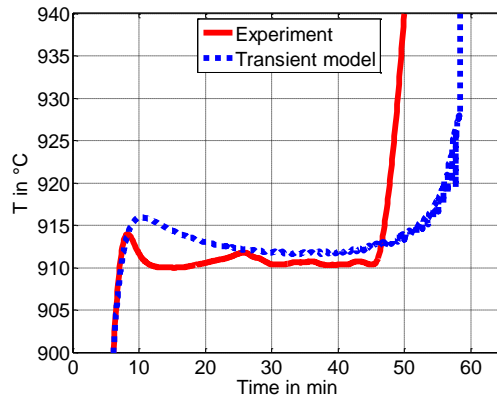


(e)

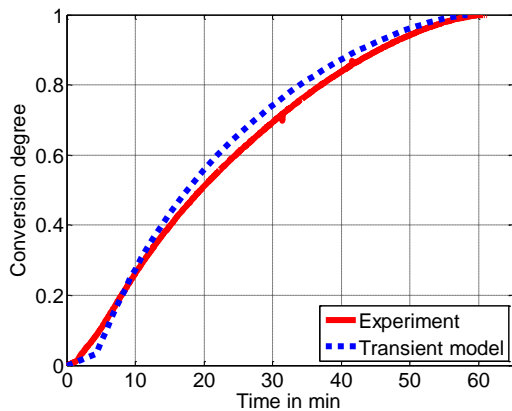
4. Sample F2-IV (24.5 mm) in CO₂ at 1045 °C



(a)



(b)



(c)

Name : Sample F2-IV in CO₂ gas

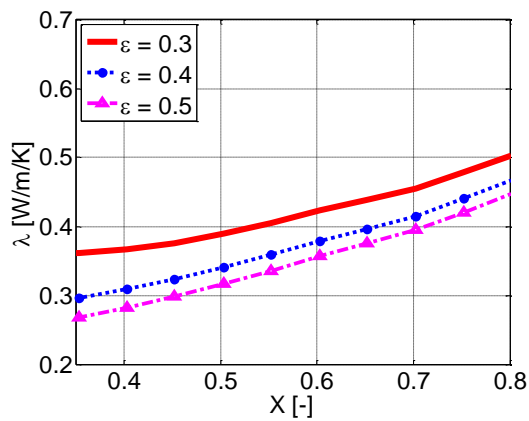
$T_{amb} = 1045 \text{ } ^\circ\text{C}$
 $\rho = 2133$
 purity=0.99
 $d = 24.5$

for Limestone

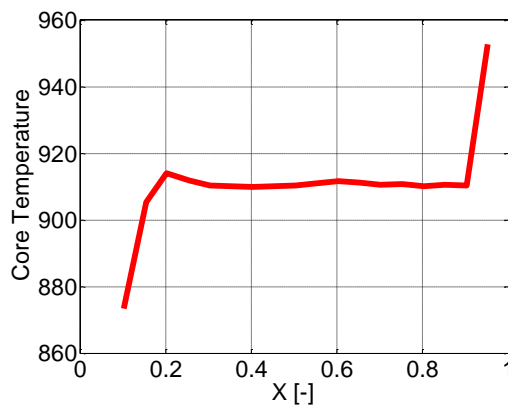
 $cp = 1000 \cdot (T/473)^{0.3}$
 $\lambda = 0.33 + 672/(T+28)$ if $T_c < 800^\circ\text{C}$
 $\lambda = 0.43 + 672/(T+28)$ if $T_c > 800^\circ\text{C}$

for Lime

 $k = 0.038$
 $T_{eq} = 910^\circ\text{C}$
 $\kappa = 1 \cdot 10^{-12}$
 $p = 0.85 \text{ bar}$
 epsilon=0.35
 $cp = 940$
 $\lambda = 0.44$

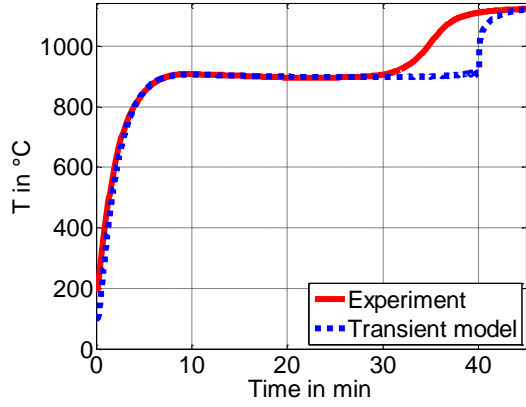


(d)

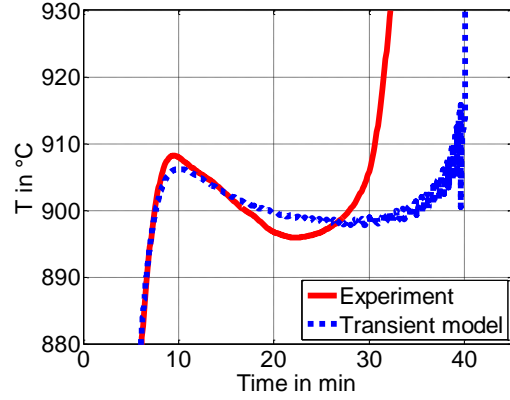


(e)

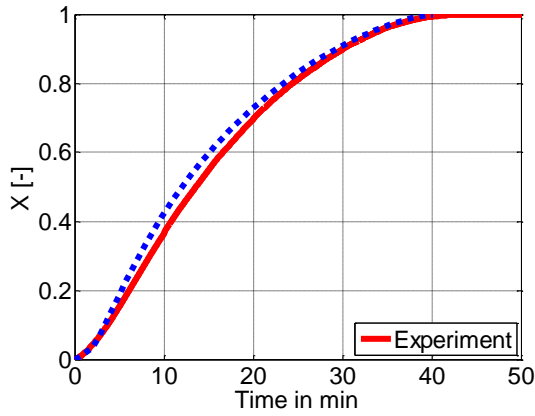
5. Sample F2-IV (24.5 mm) in air at 1126 °C



(a)



(b)



(c)

Name : **Sample F2-IV in air**

$T_{amb} = 1126 \text{ }^\circ\text{C}$

$\rho = 2133$

purity=0.99

$d = 24.5$

for Limestone

$cp = 1000 \cdot (T/473)^{0.3}$
 $\lambda = 0.33 + 672/(T+28)$

for Lime

$k = 0.032$

$T_{eq} = 910 \text{ }^\circ\text{C}$

$\beta = 0.025$

$\Delta H = 168$

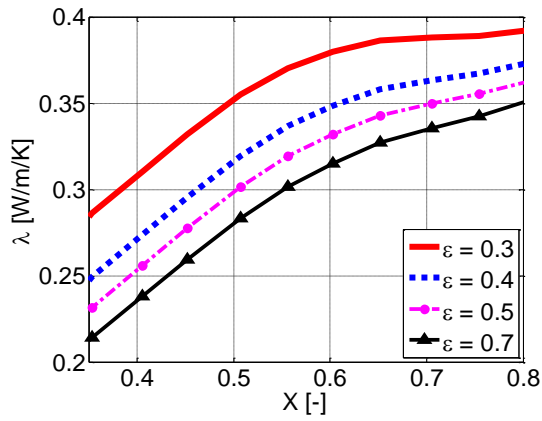
$\psi = 0.5$

$\tau = 1.5$

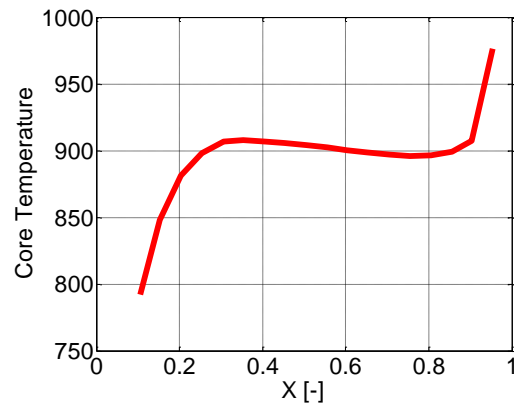
$\epsilon = 0.27$

$cp = 940$

$\lambda = 0.35$

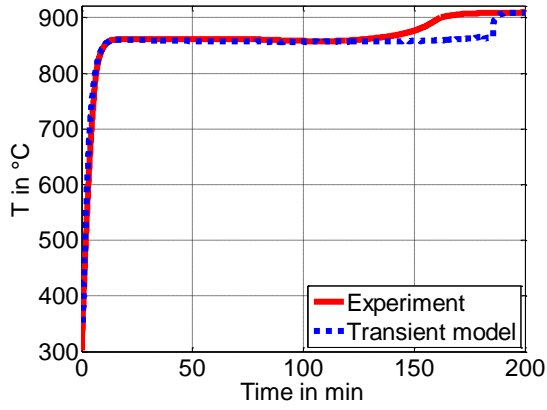


(d)

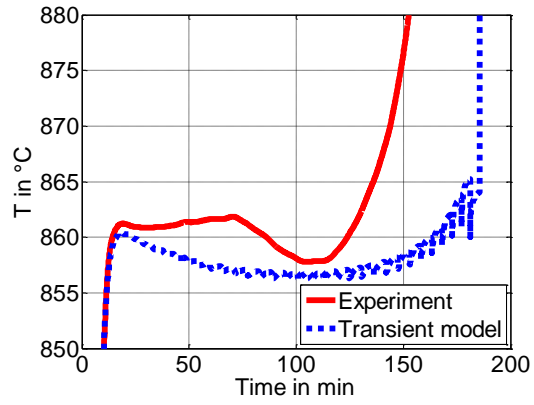


(e)

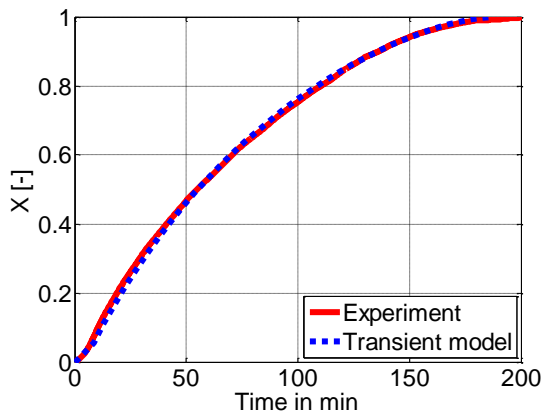
6. Sample F1-iii (24.5 mm) in air at 909 °C



(a)



(b)



(c)

Name : **Sample F1-iii in air**

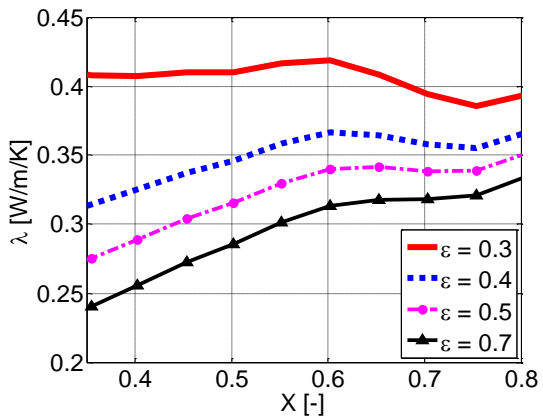
$T_{amb} = 909 \text{ }^\circ\text{C}$
 $\rho = 2200$
 purity=0.98
 $d = 24.5$

for Limestone

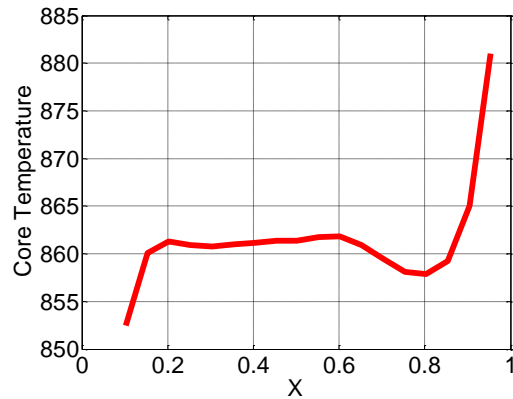
$c_p = 1000 \cdot (T/473)^{0.3}$
 $\lambda = 0.33 + 672 / (T + 28)$

for Lime

$k = 0.011$
 $T_{eq} = 910 \text{ }^\circ\text{C}$
 $\beta = 0.013$
 $\Delta H = 168$
 $\psi = 0.5$
 $\tau = 2.5$
 $\varepsilon = 0.3$
 $c_p = 940$
 $\lambda = 0.44$

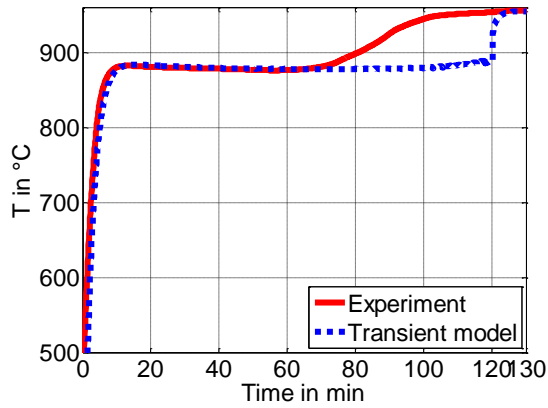


(d)

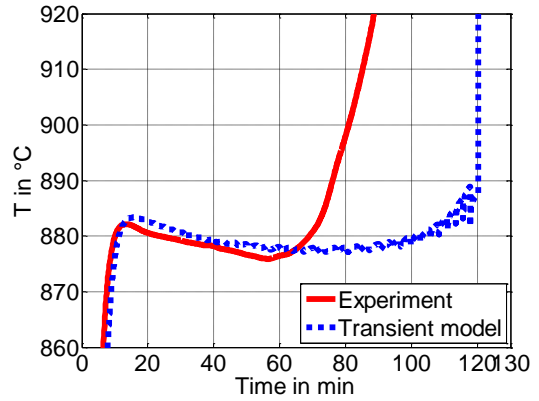


(e)

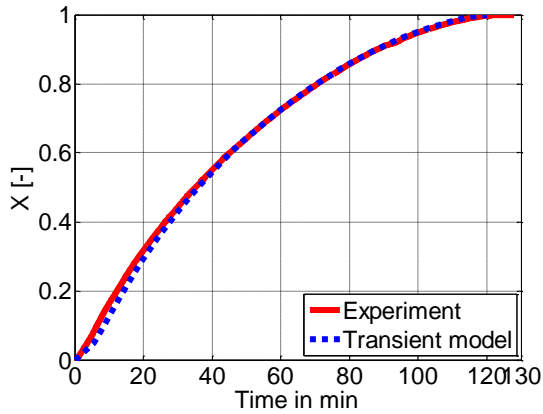
7. Sample F1-iii (24.5 mm) in air at 955 °C



(a)



(b)



(c)

Name : **Sample F1-iii in air**

$T_{amb} = 955 \text{ } ^\circ\text{C}$

$\rho = 2212$

purity=0.99

$d = 24.5$

for Limestone

$cp = 1000 \cdot (T/473)^{0.3}$

$\lambda = 0.33 + 672 / (T + 28)$

for Lime

$k = 0.013$

$T_{eq} = 910 \text{ } ^\circ\text{C}$

$\beta = 0.013$

$\Delta H = 168$

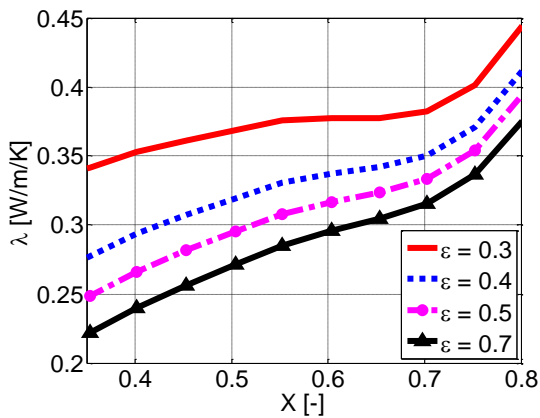
$\psi = 0.5$

$\tau = 2.5$

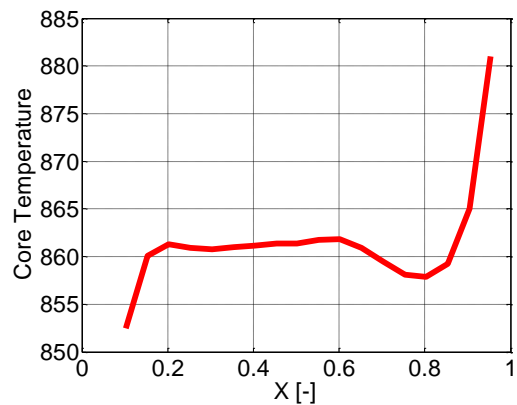
$\epsilon = 0.3$

$cp = 940$

$\lambda = 0.44$

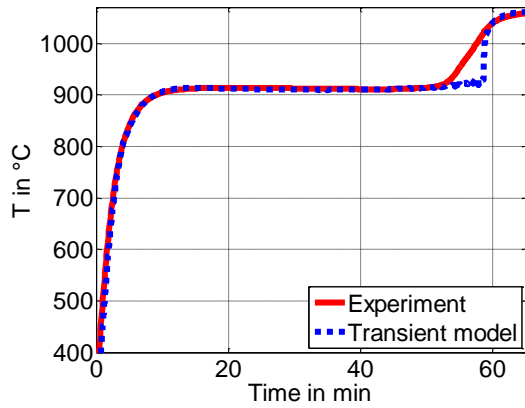


(d)

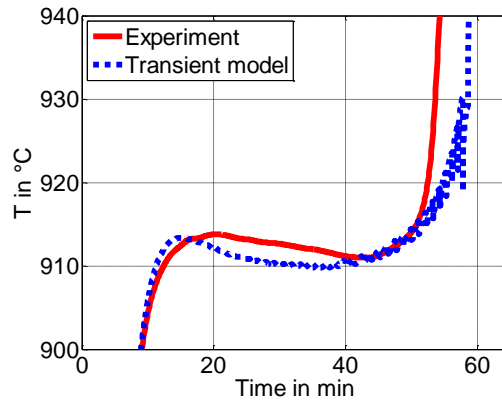


(e)

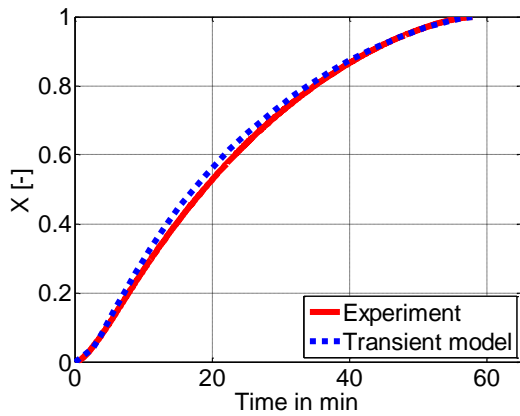
8. Sample F1-iii (24.5 mm) in air at 1062 °C



(a)



(b)



(c)

Name : **Sample F1-iii in air**

$T_{amb} = 1062 \text{ } ^\circ\text{C}$

$\rho = 2214$

purity=0.99

$d = 24.5$

for Limestone

$cp = 1000 \cdot (T/473)^{0.3}$

$\lambda = 0.33 + 672 / (T + 28) < 800 \text{ } ^\circ\text{C}$

$\lambda = 0.08 + 672 / (T + 28) < 800 \text{ } ^\circ\text{C}$

for Lime

$k = 0.016$

$T_{eq} = 910 \text{ } ^\circ\text{C}$

$\beta = 0.025$

$\Delta H = 168$

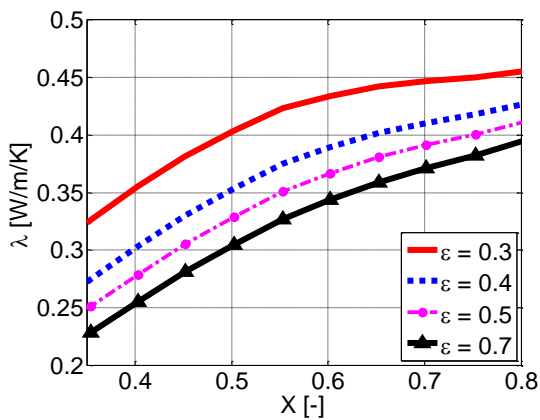
$\psi = 0.5$

$\tau = 2.5$

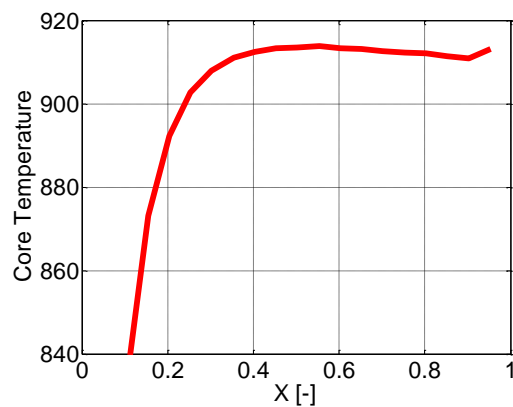
$\varepsilon = 0.3$

$cp = 940$

$\lambda = 0.44$

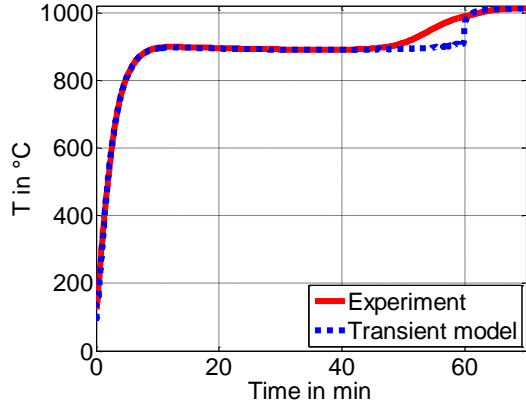


(d)

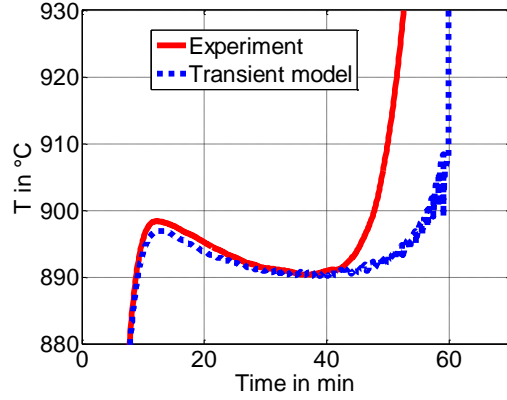


(e)

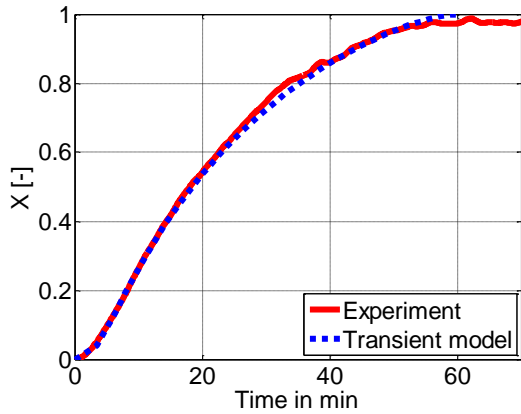
9. Sample F1-i (24.5 mm) in air at 1012 °C



(a)



(b)



(c)

Name : **Sample F1-1 in air**

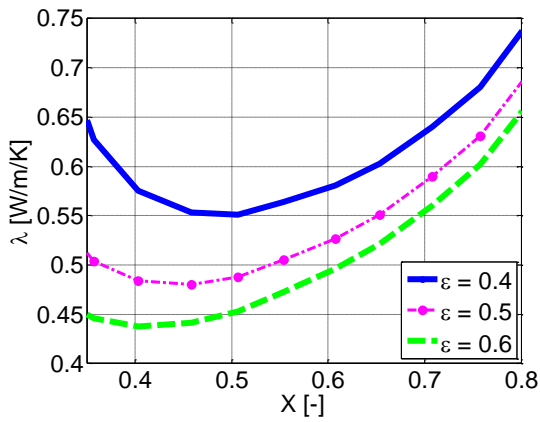
$T_{amb} = 1012 \text{ }^\circ\text{C}$
 $\rho = 2200$
 purity=0.99
 $d = 24.5$

for Limestone

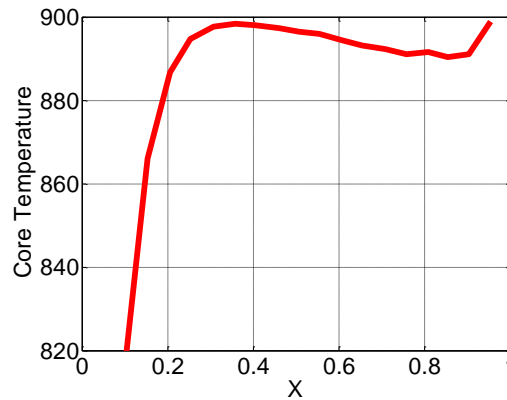
$cp = 1000 \cdot (T/473)^{0.3}$
 $\lambda = 0.33 + 672/(T+28)$

for Lime

$k = 0.02$
 $T_{eq} = 910 \text{ }^\circ\text{C}$
 $\beta = 0.025$
 $\Delta H = 168$
 $\psi = 0.5$
 $\tau = 1.5$
 $\varepsilon = 0.4$
 $cp = 940$
 $\lambda = 0.55$



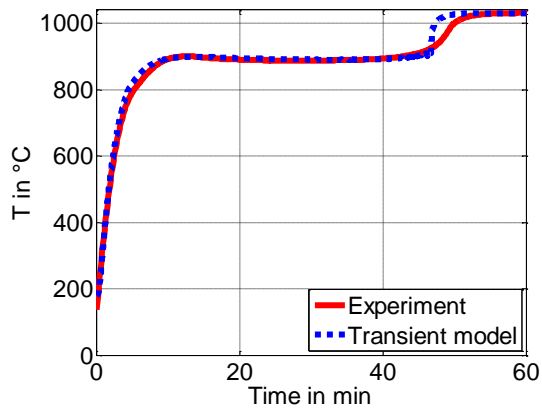
(d)



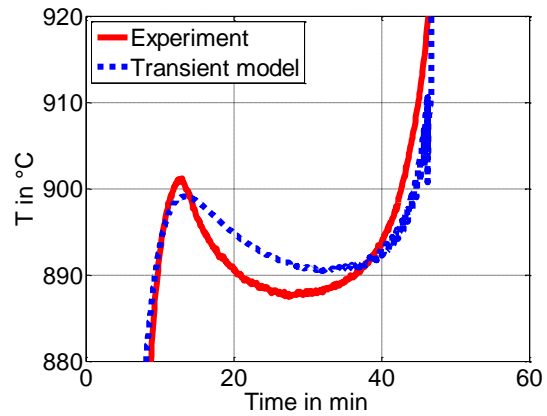
(e)

Group 3

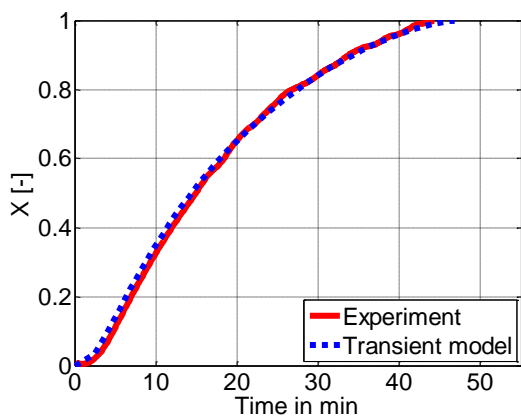
1. Sample A (24.5 mm) in air at 1030 °C



(a)



(b)



(c)

Name : **Sample A in air**

$T_{amb} = 1030 \text{ }^\circ\text{C}$

$\rho = 2657$

purity=0.96

$d = 24.5$

for Limestone

$cp = 1000 \cdot (T/473)^{0.3}$

$\lambda = 0.43 + 672/(T+28)$ if $T_c < 800^\circ\text{C}$

$\lambda = 0.13 + 672/(T+28)$ if $T_c > 800^\circ\text{C}$

for Lime

$k = 0.029$

$T_{eq} = 910^\circ\text{C}$

$\beta = 0.029$

$\Delta H = 168$

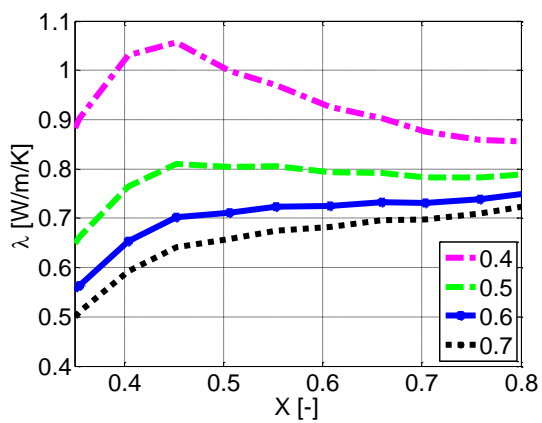
$\psi = 0.5$

$\tau = 1.0$

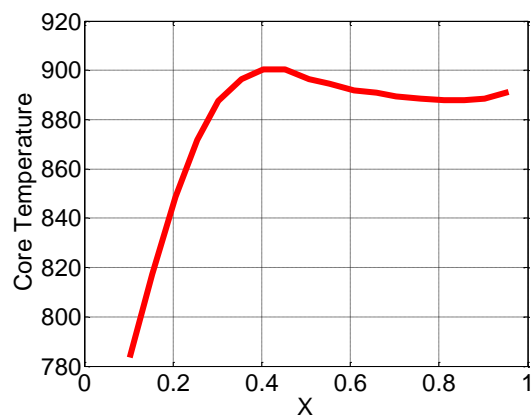
$\varepsilon = 0.6$

$cp = 940$

$\lambda = 0.65$

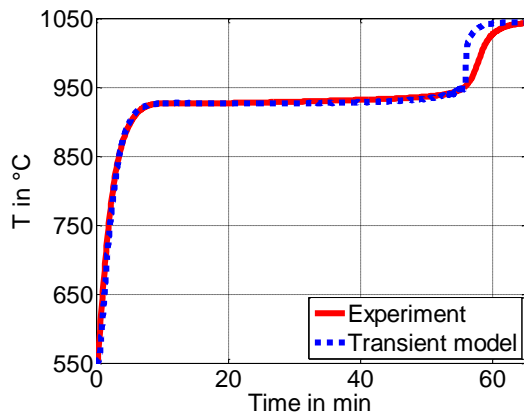


(d)

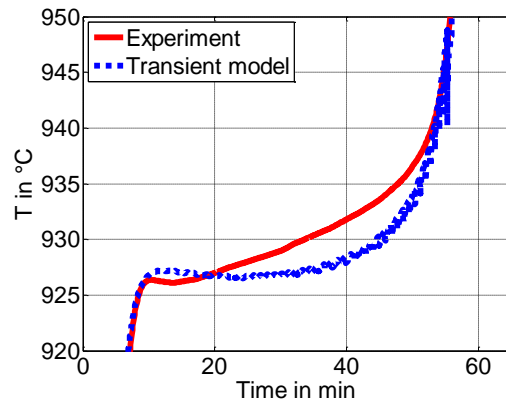


(e)

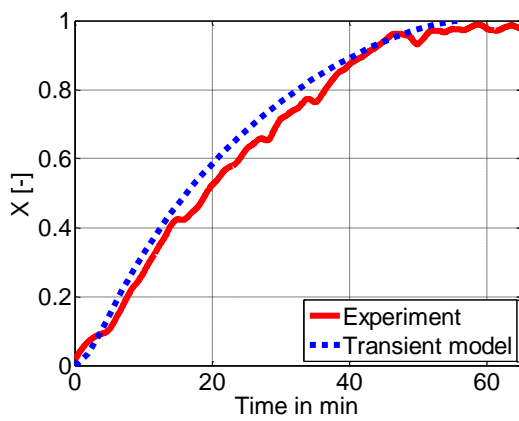
2. Sample B (24.5 mm) in air at 1044 °C



(a)



(b)



(c)

Name : **Sample B in air**

$T_{amb} = 1044 \text{ } ^\circ\text{C}$

$\rho = 2744$

purity=0.99

$d = 24.5$

for Limestone

$cp = 1000 \cdot (T/473)^{0.3}$

$\lambda = 0.83 + 672/(T+28)$ if $T_c < 800^\circ\text{C}$

$\lambda = 1.0 + 672/(T+28)$ if $T_c > 800^\circ\text{C}$

for Lime

$k = 0.02$

$T_{eq} = 910^\circ\text{C}$

$\beta = 0.028$

$\Delta H = 168$

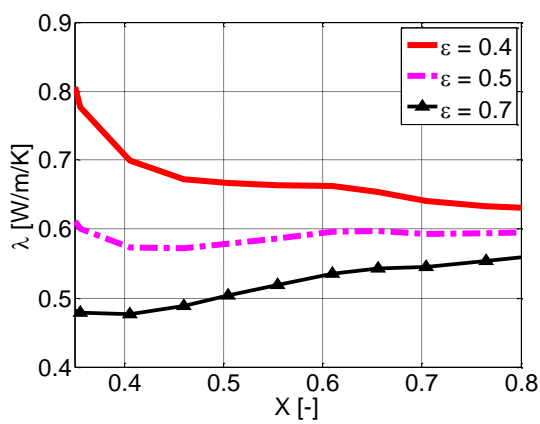
$\psi = 0.5$

$\tau = 4.5$

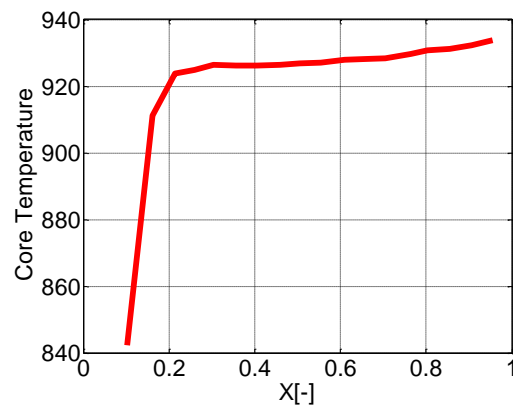
$\varepsilon = 0.45$

$cp = 940$

$\lambda = 0.75$

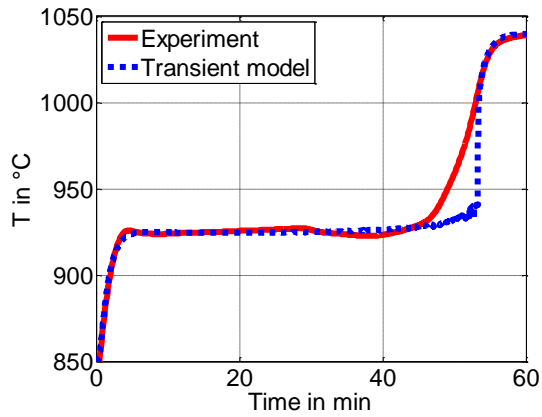


(d)

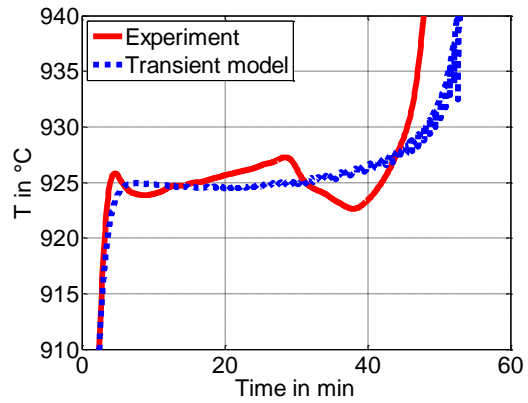


(e)

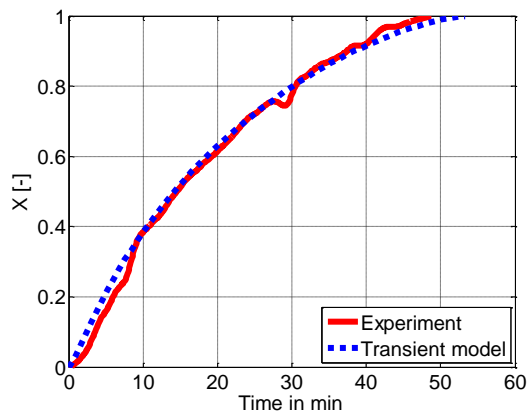
3. Sample B (24.5 mm) in CO₂ at 1040 °C



(a)



(b)



(c)

Name : **Sample B in CO₂ gas**

$T_{amb} = 1040 \text{ °C}$
 $\rho = 2738$
 purity=0.99
 $d = 24.5$

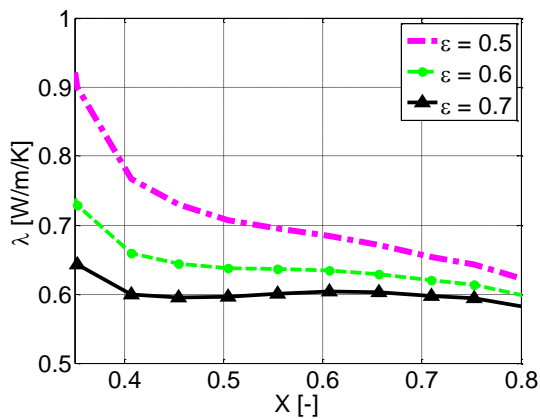
for Limestone

 $cp = 1000 \cdot (T/473)^{0.3}$

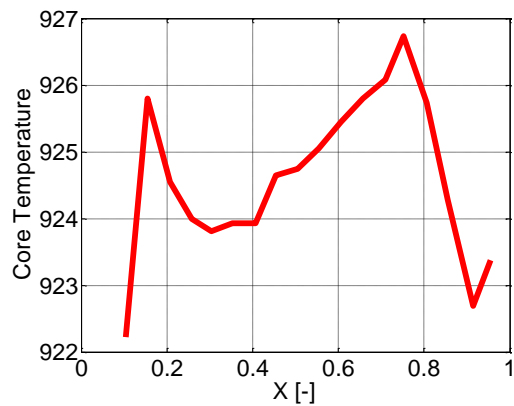
$\lambda = 0.83 + 672/(T+28)$ if $T_c < 800 \text{ °C}$
 $\lambda = 1.2 + 672/(T+28)$ if $T_c > 800 \text{ °C}$

for Lime

 $k = 0.038$
 $T_{eq} = 910 \text{ °C}$
 $\kappa = 5 \cdot 10^{-14}$
 $p = 0.85 \text{ bar}$
 $\epsilon = 0.5$
 $cp = 940$
 $\lambda = 0.75$

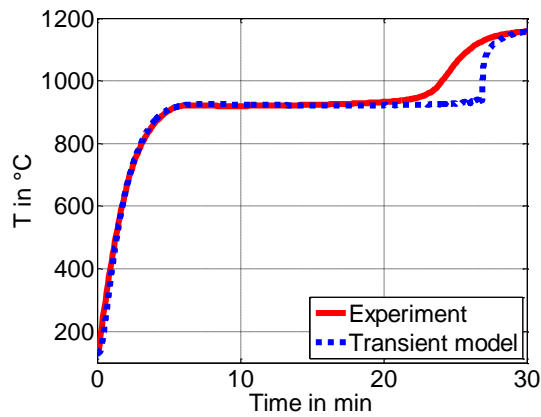


(d)

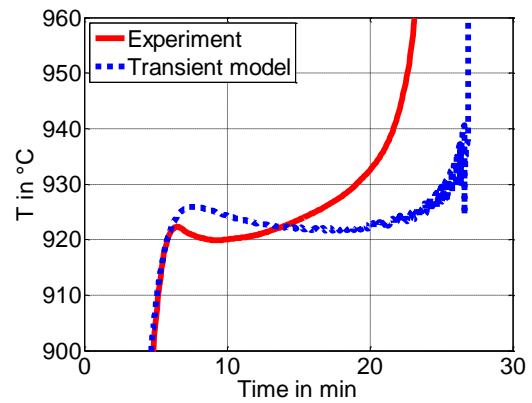


(e)

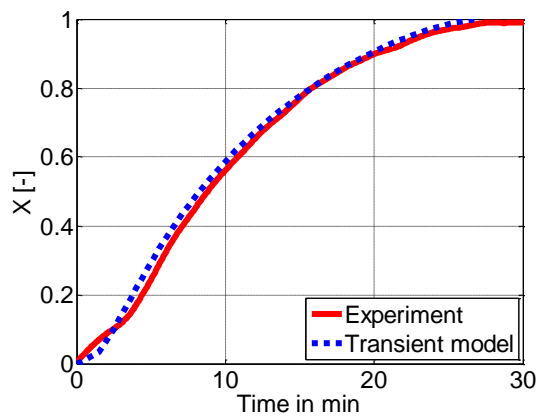
4. Sample T (24.5 mm) in air at 1164 °C



(a)



(b)



(c)

Name : **Sample T in air**

$T_{amb} = 1164 \text{ } ^\circ\text{C}$

$\rho = 2625$

purity=0.99

$d = 24.5$

for Limestone

$cp = 1000 \cdot (T/473)^{0.3}$

$\lambda = 0.83 + 672/(T+28)$ if $T_c < 800^\circ\text{C}$

$\lambda = 1.0 + 672/(T+28)$ if $T_c > 800^\circ\text{C}$

for Lime

$k = 0.05$

$T_{eq} = 910^\circ\text{C}$

$\beta = 0.034$

$\Delta H = 168$

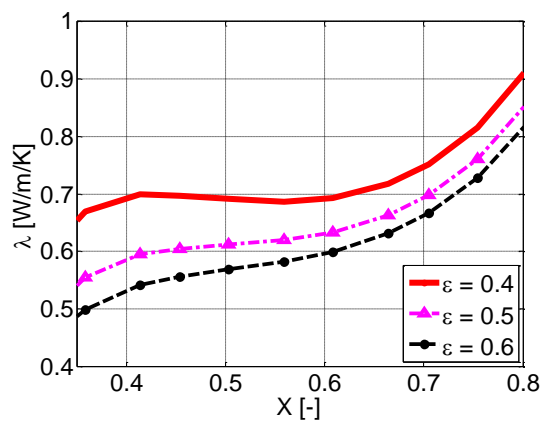
$\psi = 0.5$

$\tau = 2.0$

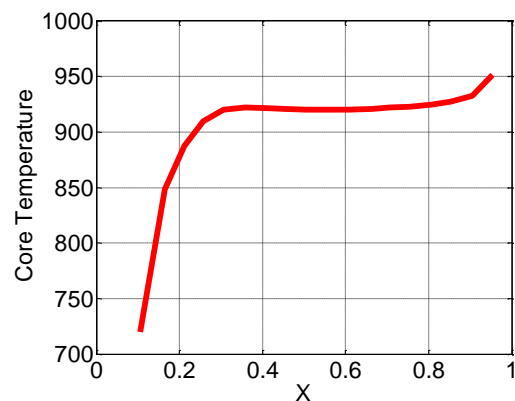
$\varepsilon = 0.45$

$cp = 940$

$\lambda = 0.7$

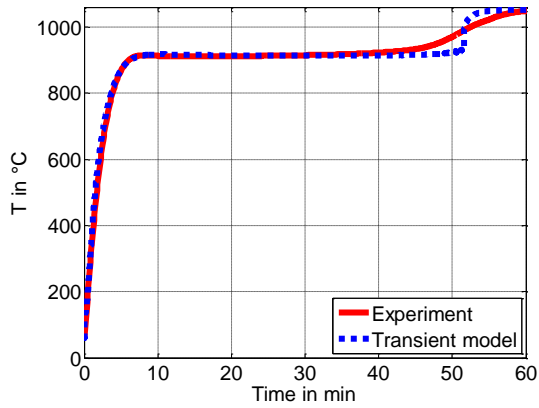


(d)

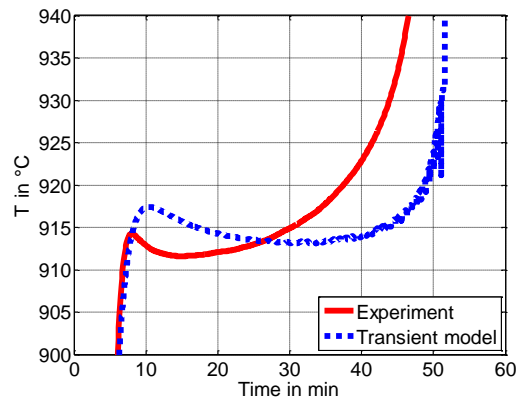


(e)

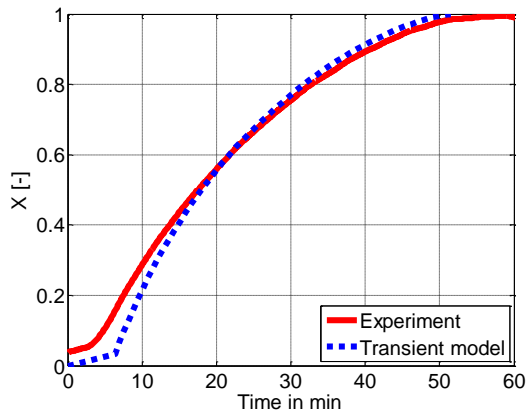
5. Sample T (24.5 mm) in CO₂ at 1052 °C



(a)



(b)



(c)

Name : Sample T in CO₂ gas

$T_{amb} = 1052 \text{ °C}$

$\rho = 2635$

purity=0.99

$d = 24.5$

for Limestone

$cp = 1000 \cdot (T/473)^{0.3}$

$\lambda = 0.53 + 672/(T+28)$ if $T_c < 800 \text{ °C}$

$\lambda = 0.83 + 672/(T+28)$ if $T_c > 800 \text{ °C}$

for Lime

$k = 0.038$

$T_{eq} = 910 \text{ °C}$

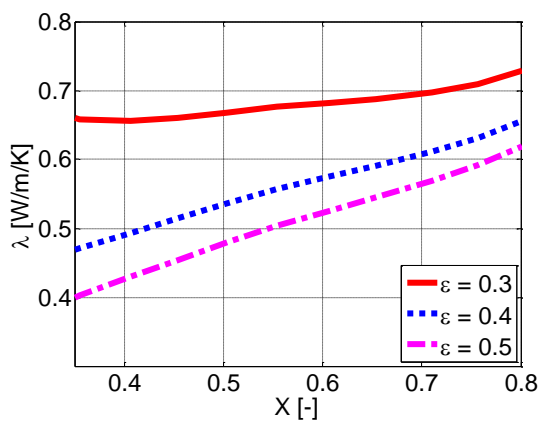
$\kappa = 10^{-12}$

$p = 0.85 \text{ bar}$

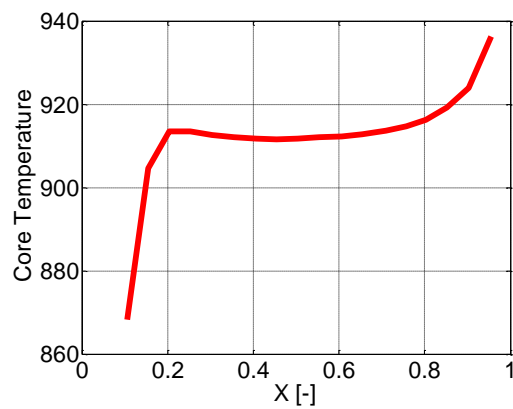
epsilon=0.45

$cp = 940$

$\lambda = 0.7$

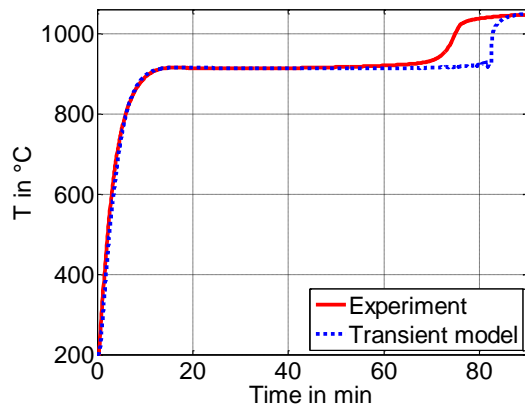


(d)

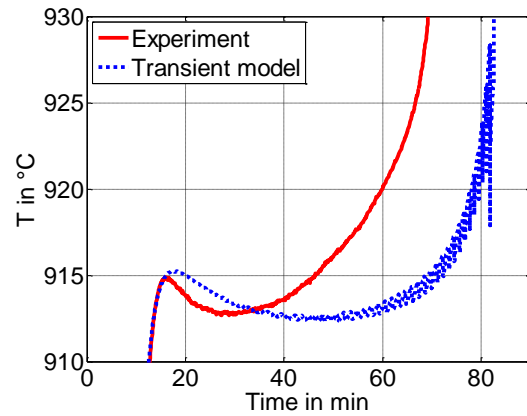


(e)

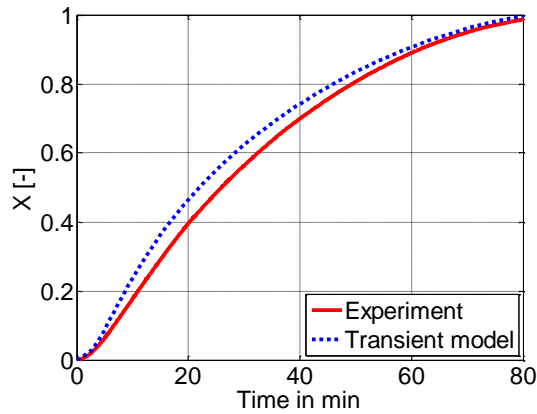
6. Sample D (32.4 mm) at 1050 °C



(a)



(b)



(c)

Name : **Sample D in air**

$T_{amb} = 1050 \text{ } ^\circ\text{C}$

$\rho = 2700$

purity=0.9

$d = 32.4$

for Limestone

$cp = 1000 \cdot (T/473)^{0.3}$

$\lambda = 0.43 + 672/(T+28)$ if $T_c < 600^\circ\text{C}$

$\lambda = 0.63 + 672/(T+28)$ if $T_c > 600^\circ\text{C}$

for Lime

$k = 0.024$

$T_{eq} = 910^\circ\text{C}$

$\beta = 0.029$

$\Delta H = 168$

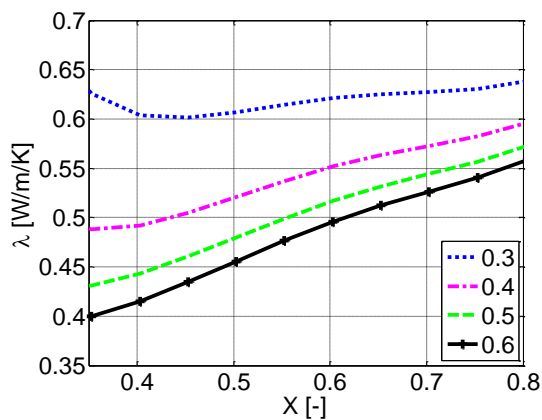
$\psi = 0.5$

$\tau = 3.8$

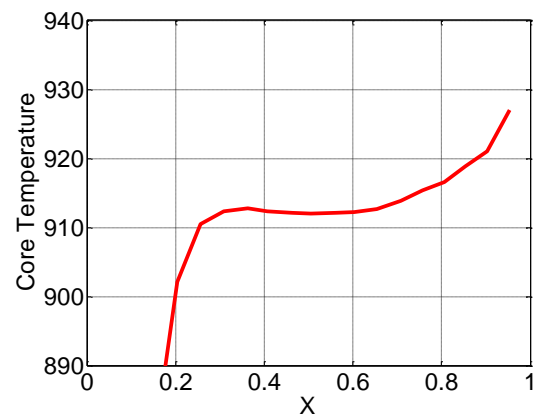
$\varepsilon = 0.45$

$cp = 940$

$\lambda = 0.55$



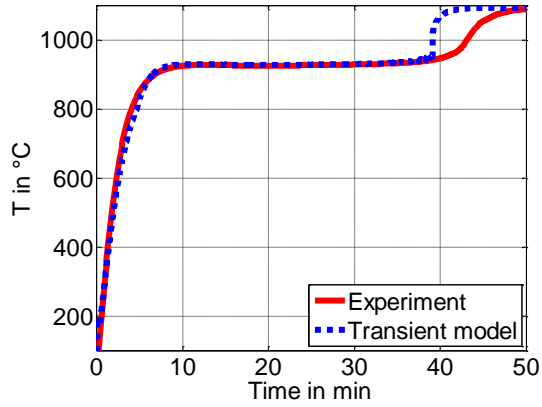
(d)



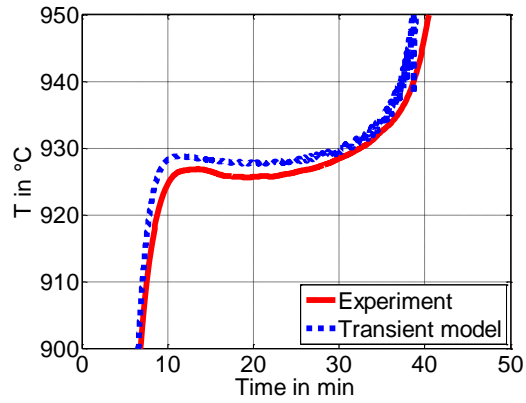
(e)

Group 4

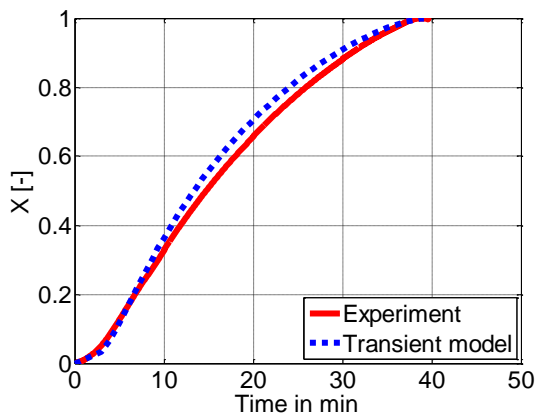
1. Sample BL0107 (24.5 mm) in air at 1095 °C



(a)



(b)



(c)

Name : **Sample BL0107 in air**

$T_{amb} = 1095 \text{ }^\circ\text{C}$

$\rho = 2666$

purity=0.98

$d = 24.5$

for Limestone

$cp = 1000 \cdot (T/473)^{0.3}$

$\lambda = 0.5 + 672/(T+28)$ if $T_c < 800^\circ\text{C}$

$\lambda = 1.1 + 672/(T+28)$ if $T_c > 800^\circ\text{C}$

for Lime

$k = 0.032$

$T_{eq} = 920^\circ\text{C}$

$\beta = 0.032$

$\Delta H = 168$

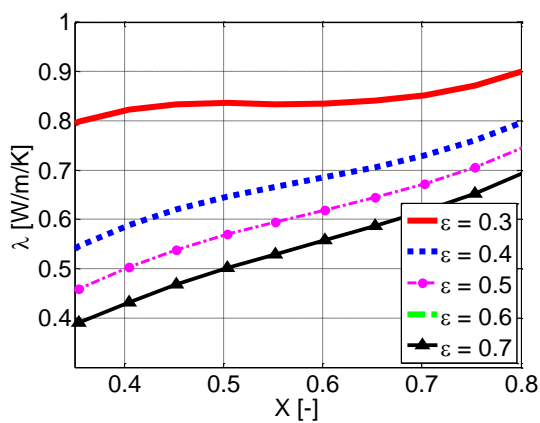
$\psi = 0.5$

$\tau = 2.0$

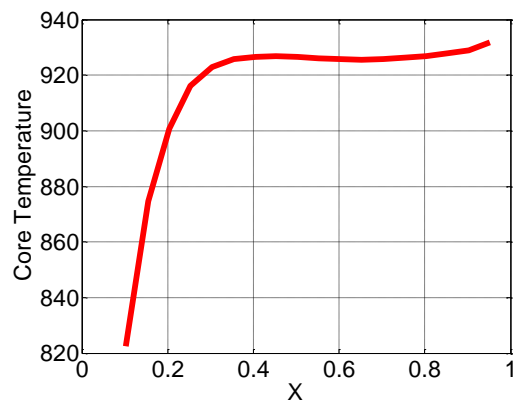
$\epsilon = 0.4$

$cp = 940$

$\lambda = 0.8$

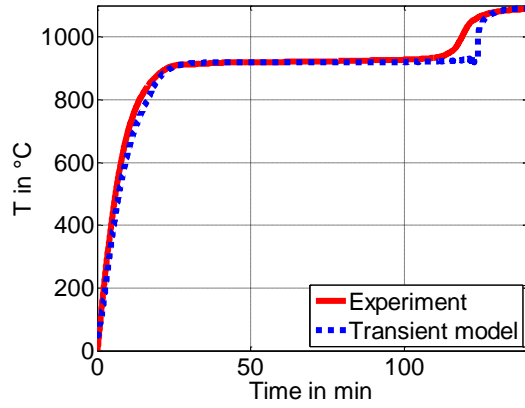


(d)

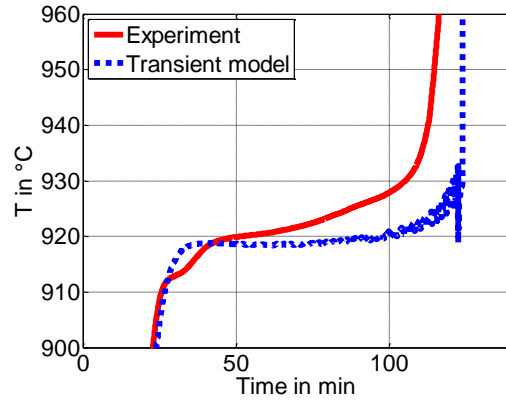


(e)

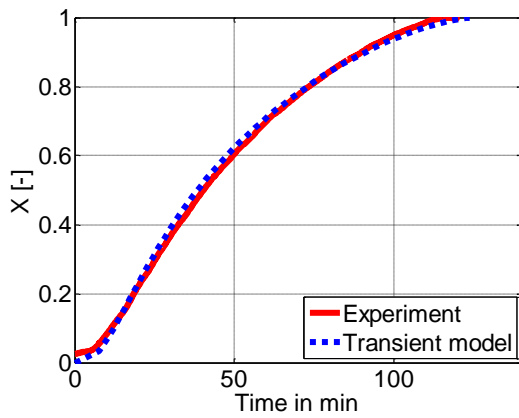
2. Sample BL0107 (47.5 mm) in air at 1092 °C



(a)



(b)



(c)

Name : **Sample BL0107 in air**

$T_{amb} = 1092 \text{ °C}$

$\rho = 2675$

purity=0.98

$d = 47.5$

for Limestone

$cp = 1000 \cdot (T/473)^{0.3}$

$\lambda = 0.5 + 672/(T+28)$ if $T_c < 800 \text{ °C}$

$\lambda = 1.1 + 672/(T+28)$ if $T_c > 800 \text{ °C}$

for Lime

$k = 0.032$

$T_{eq} = 920 \text{ °C}$

$\beta = 0.032$

$\Delta H = 168$

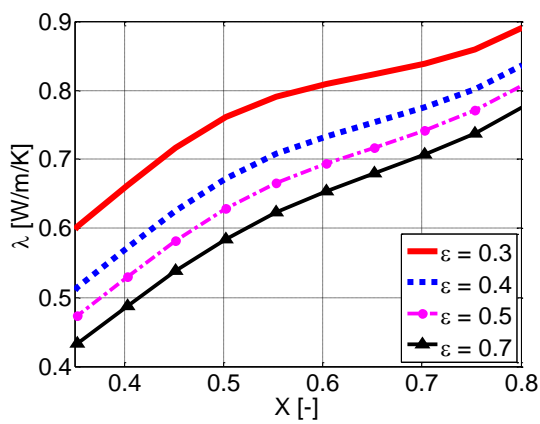
$\psi = 0.5$

$\tau = 2.0$

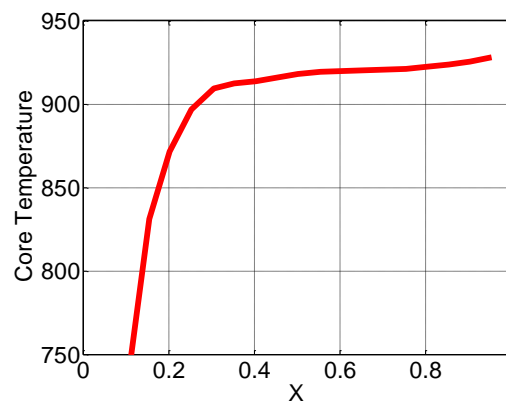
$\varepsilon = 0.3$

$cp = 940$

$\lambda = 0.8$

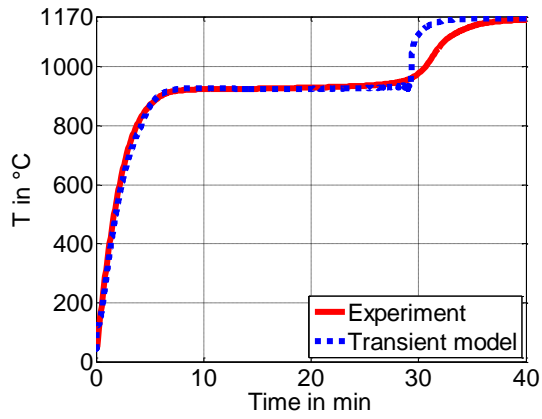


(d)

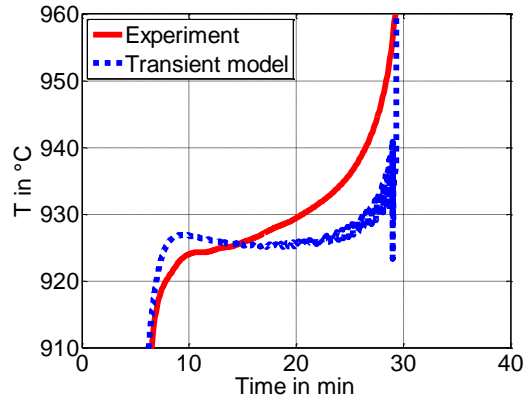


(e)

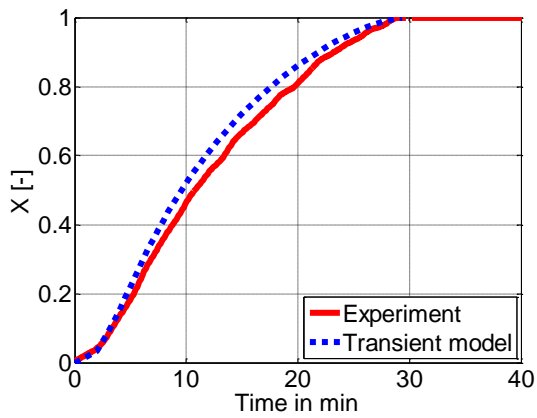
3. Sample BL0607 (24.5 mm) in air at 1164 °C



(a)



(b)



(c)

Name : **Sample BL0607 in air**

$T_{amb} = 1164 \text{ °C}$

$\rho = 2685$

purity=0.99

$d = 24.5$

for Limestone

$c_p = 1000 \cdot (T/473)^{0.3}$

$\lambda = 0.5 + 672/(T+28)$ if $T_c < 800 \text{ °C}$

$\lambda = 1.1 + 672/(T+28)$ if $T_c > 800 \text{ °C}$

for Lime

$k = 0.065$

$T_{eq} = 920 \text{ °C}$

$\beta = 0.038$

$\Delta H = 168$

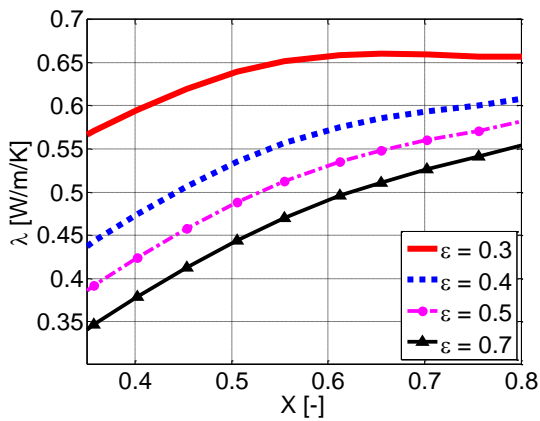
$\psi = 0.5$

$\tau = 2.0$

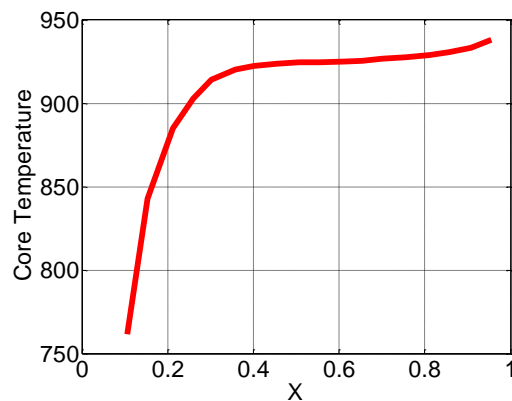
$\varepsilon = 0.4$

$c_p = 940$

$\lambda = 0.7$

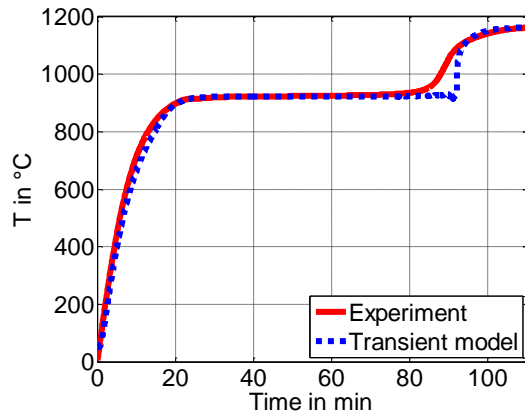


(d)

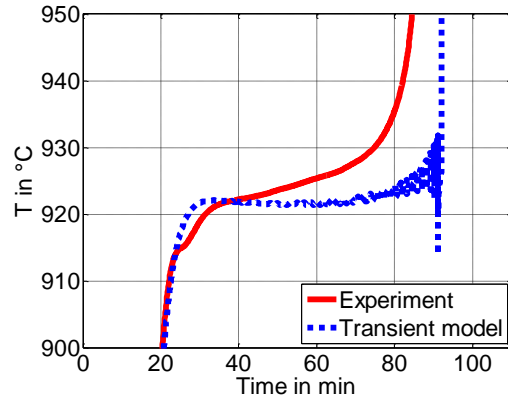


(e)

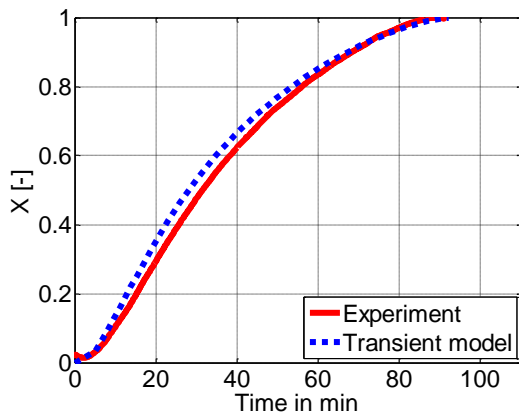
4. Sample BL0607 (47.5 mm) in air at 1164 °C



(a)



(b)



(c)

Name : **Sample BL0607 in air**

$T_{amb} = 1164 \text{ } ^\circ\text{C}$

$\rho = 2681$

purity=0.99

$d = 47.5$

for Limestone

$cp = 1000 \cdot (T/473)^{0.3}$

$\lambda = 0.5 + 672/(T+28)$ if $T_c < 800^\circ\text{C}$

$\lambda = 1.1 + 672/(T+28)$ if $T_c > 800^\circ\text{C}$

for Lime

$k = 0.055$

$T_{eq} = 920^\circ\text{C}$

$\beta = 0.038$

$\Delta H = 168$

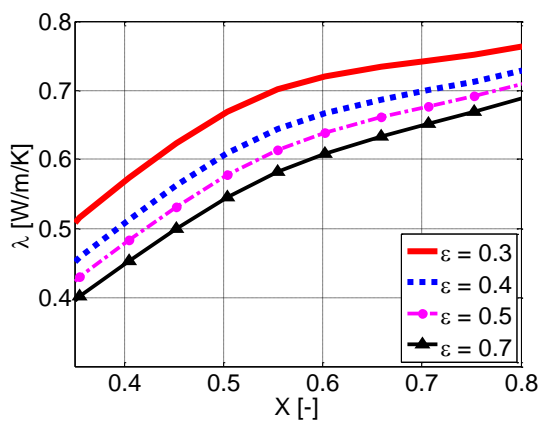
$\psi = 0.5$

$\tau = 2.0$

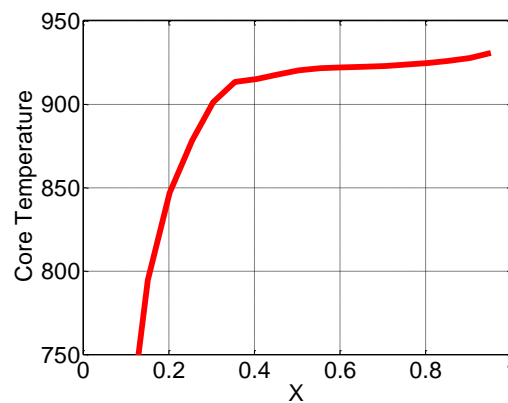
$\varepsilon = 0.3$

$cp = 940$

$\lambda = 0.75$

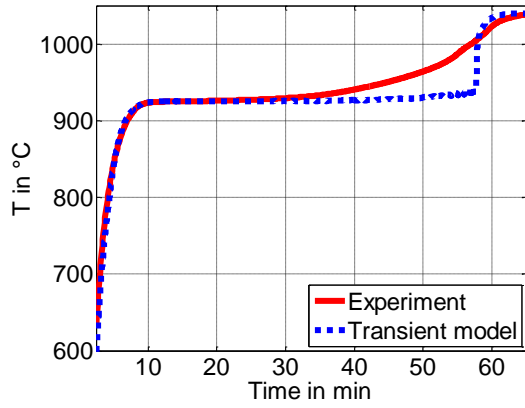


(d)

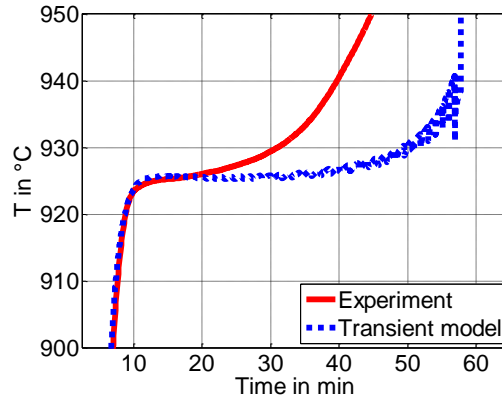


(e)

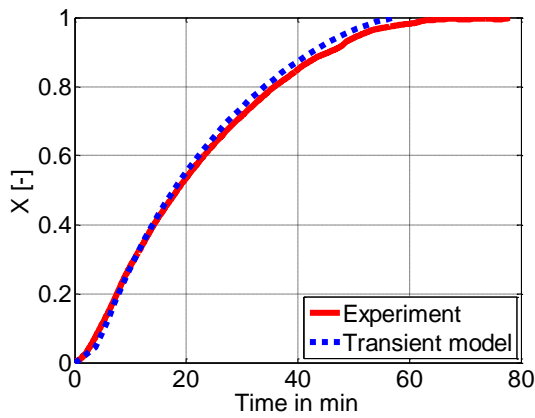
5. Sample SZ (24.5 mm) in air at 1040 °C



(a)



(b)



(c)

Name : **Sample SZ in air**

$T_{amb} = 1040 \text{ } ^\circ\text{C}$

$\rho = 2681$

purity=0.99

$d = 24.5$

for Limestone

$cp = 1000 \cdot (T/473)^{0.3}$

$\lambda = 0.5 + 672/(T+28)$ if $T_c < 800^\circ\text{C}$

$\lambda = 0.8 + 672/(T+28)$ if $T_c > 800^\circ\text{C}$

for Lime

$k = 0.022$

$T_{eq} = 920^\circ\text{C}$

$\beta = 0.025$

$\Delta H = 168$

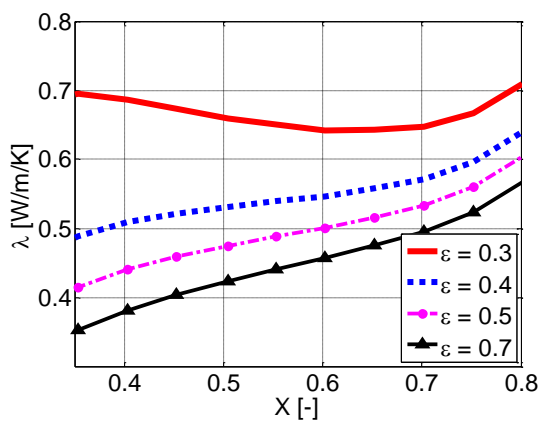
$\psi = 0.5$

$\tau = 3.0$

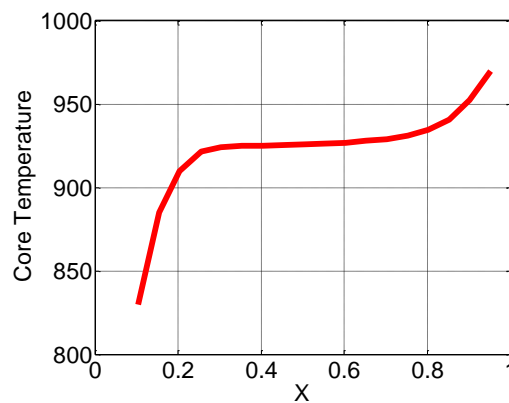
$\varepsilon = 0.4$

$cp = 940$

$\lambda = 0.65$

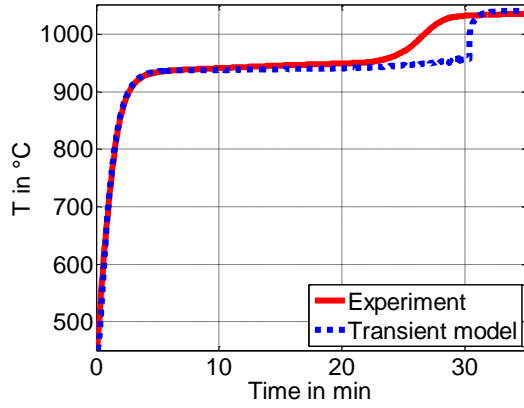


(d)

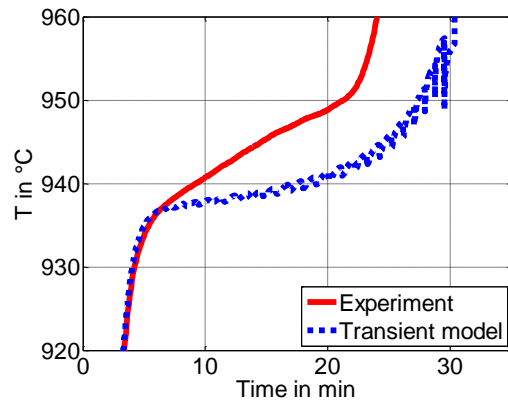


(e)

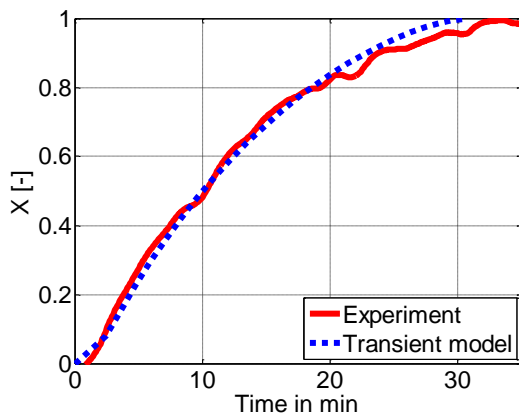
6. Sample SZ (14.4 mm) in air at 1040 °C



(a)



(b)



(c)

Name : **Sample SZ in air**

$T_{amb} = 1040 \text{ }^\circ\text{C}$

$\rho = 2470$

purity=0.99

$d = 14.4$

for Limestone

$cp = 1000 \cdot (T/473)^{0.3}$

$\lambda = 0.5 + 672 / (T + 28)$

for Lime

$k = 0.015$

$T_{eq} = 920 \text{ }^\circ\text{C}$

$\beta = 0.025$

$\Delta H = 168$

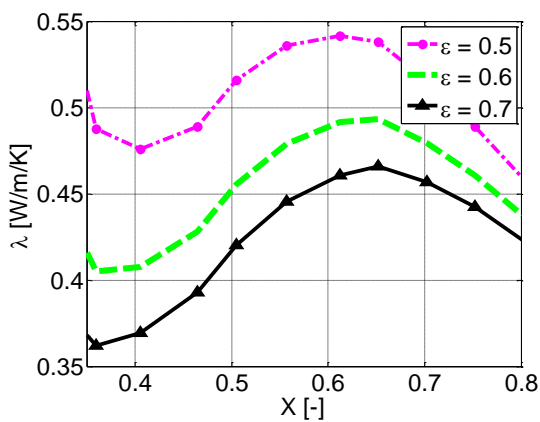
$\psi = 0.5$

$\tau = 4.5$

$\varepsilon = 0.4$

$cp = 940$

$\lambda = 0.65$



(d)


List of Publications

- Technical paper titled “Finite Element Analysis of Reaction Front Tracking in Lime Calcination” has been published in ASME conference proceedings.
Details: Paper no. AJTEC2011-4457pp.T10130-T10130-6,ISBN:978-0-7918-3892-1, <http://dx.doi.org/10.1115/AJTEC2011-44572>.
- Presented paper titled “Modeling and Experiments of Lime calcination” in “ECCOMAS Special Interest Conference, Numerical Heat Transfer 2012, held in 4–6 September 2012, Gliwice–Wroclaw, Poland

List of Master Thesis Supervised

- [1] Yu Guo, *Determination of thermophysical properties of limestone of different origins*, Master Thesis, Otto-von-Guericke-Universität Magdeburg, 2013.
- [2] Oscar Fernandez, *Measurement of recarbonisation behaviour of lime to absorb CO₂*, Master Thesis, Otto-von-Guericke-Universität Magdeburg, 2013.
- [3] JiangPing, *Influence of parameters on calcination behavior of lime at different temperatures and also in the pure CO₂ environment*, Otto-von-Guericke-Universität Magdeburg, 2014.
- [4] Leping Zheng, *Study of limestone decomposition process with different particle sizes*, Master Thesis, Otto-von-Guericke-Universität Magdeburg, 2014.
- [5] Xin Xu, *Study of limestone decomposition process with real stones (irregular shapes)*, Master Thesis, Otto-von-Guericke-Universität Magdeburg, 2015.
- [6] Diyu Wu, *Simulation of Refractory Wall Drying during Heating up of Industrial Kilns to prevent Cracking*, Master Thesis, Otto-von-Guericke-Universität Magdeburg, 2015.

Curriculum Vitae

First name	Gourisankar	
Family name	Sandaka	
Nationality	Indian	
Date of birth	15-06-1981	
Place of birth	Ichapuram, Andhra Pradesh, India.	
Parents	S. Krishna Rao and S. Lakshmi	
Marital status	Married	
Email	s.gourisankar@gmail.com	
1999 - 2003	Bachelor of Technology in Chemical Engineering, Andhra University College of Engineering, AP, India.	
2004 - 2006	Master of Technology in Chemical Engineering, Indian Institute of Technology Madras, Chennai, TN, India.	
2006 - 2009	Programmer Analyst in Cognizant Technology Solutions, Chennai, India.	
2009 july– 2015	Ph.D study, ISUT, Otto von Guericke University, Magdeburg, Germany. under the guidance of Prof. Dr.-Ing. E. Specht .	

